Analysis of the performance impact of component aging in a hybrid energy PV-diesel-battery rural microgrid : modeling, control, and energy management

Khadim Ullah Jan

université PARIS-SACLAY

Analysis of the Performance Impact of Component Aging in Hybrid Energy PV-Diesel-Battery Rural Microgrid: Modeling, Control, and Energy Management

Analyse de l'impact du vieillissement des composants sur les performances d'un micro-réseau rural à énergie hybride PV-diesel-batterie : modélisation, contrôle et gestion de l'énergie

Thèse de doctorat de l'Université Paris-Saclay
École doctorale n°575, Electrical, Optical, Bio-physics and Engineering (EOBE)
Spécialité de doctorat : Génie Électrique
Graduate School : Sciences de l'ingénierie et des systèmes. Référent : **CentraleSupélec**

Thèse préparée dans l'unité de recherche **Laboratoire de Génie Electrique et Electronique de Paris (Université Paris-Saclay, CentraleSupélec, CNRS)**, sous la direction de **Anne MIGAN-DUBOIS**,
Professeure des universités, Université Paris-Saclay et la co-direction de **Demba DIALLO**,
Professeur des universités, Université Paris-Saclay

Thèse soutenue à CentraleSupélec, Paris-Saclay, le 15 décembre 2022, par

Khadim Ullah JAN

Composition du Jury

Membres du jury avec voix délibérative

Marc PETIT Professeur des universités, GeePs, CentraleSupélec	Président
Manuela SECHILARIU Professeure des universités, AVENUE UTC - Université de technologie de Compiègne	Rapporteure & Examinatrice
Fei GAO Professeur des universités, Femto-ST, UTBM - Université de technologie de Belfort-Montbéliard	Rapporteur & Examinateur
Ghjuvan Antone FAGGIANELLI Maître de conférences, SPE UMR 6134, Université de Corse	Examinateur

THÈSE DE DOCTORAT
NNT: 2022UPAST184

Analysis of the Performance Impact of Component Aging in Hybrid Energy PV-Diesel-Battery Rural Microgrid: Modeling, Control, and Energy Management

Dissertation submitted
for the award of the degree of

DOCTOR OF PHILOSOPHY

in
ELECTRICAL ENGINEERING

in the
EOBE DOCTORAL SCHOOL

of the

UNIVERSITÉ PARIS-SACLAY

by

KHADIM ULLAH JAN

Page intentionally left blank

Project Description

The proposition of an affordable legacy rural microgrid considering local conditions

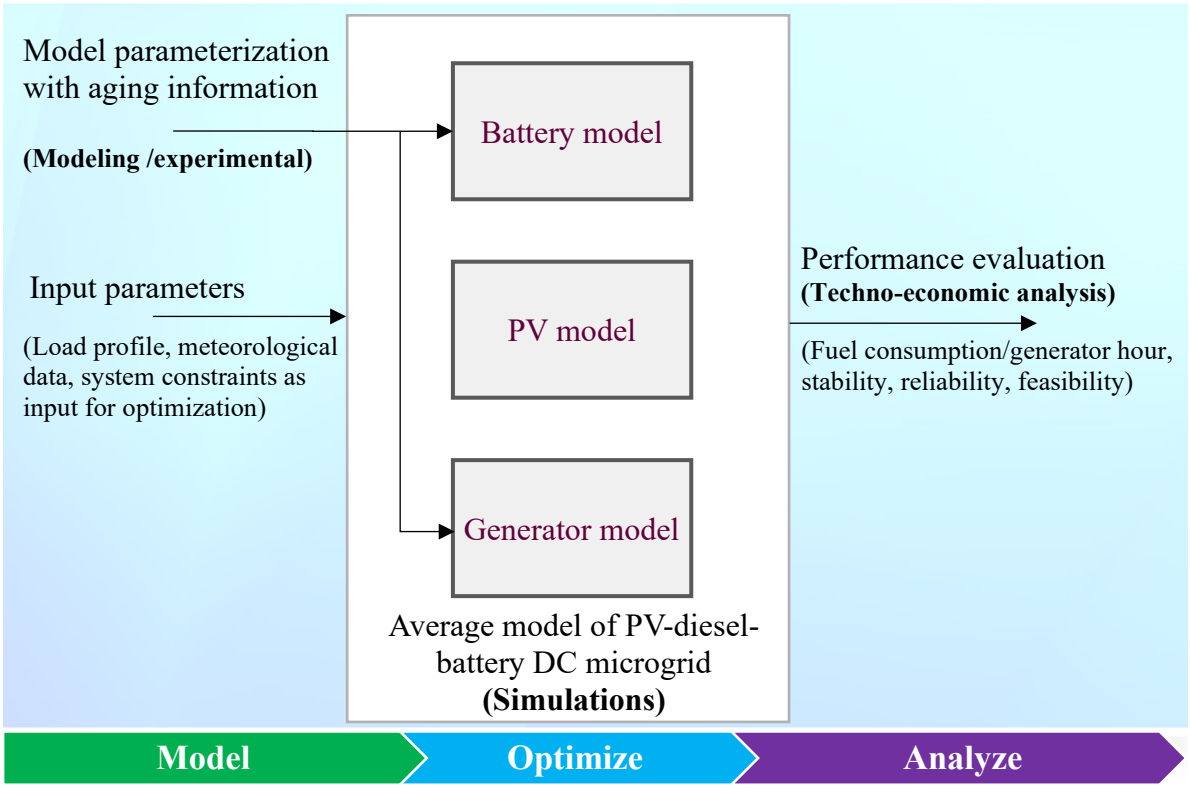

96V_{DC}/30kW PV-diesel-battery DC microgrid for a rural base case of 125 households of 1100 inhabitants with a net consumption of 500kWh/day in GOGMA, BURKINA FASO.

— *Design, optimize, and simulate a 30kW microgrid with PV-diesel-battery as a base case*[1]

— *Simulate the cost-optimal system with degraded mode operation of DG and batteries*[2]

— *Analyze the net performance impact in the degraded mode*[3]

The study motivation is about proposing a second-life hypothesis for cost reduction to increase the social acceptance of the rural microgrids. PV is excluded from degradation impact as it has considerable lifetime compared to legacy batteries and diesel generator. We have assumed PV useful life of 20 years that also equals project lifetime.

[1] The yearly performance analysis is simulated at one-hour time-step. The base case simulations have no degradation.
[2] The degradation impact of batteries and DG is included and the system is optimized for the best cost. PV degradation is not considered.
[3] Techno-economic analysis of the second-life proposition and a conclusion is drawn for the project feasibility and its economic gains.

Abstract

Islanded microgrids, a power generation scheme at the local level, are gaining interest to electrify the bottom of the social pyramid. However, such systems are financially risky for grid managers due to less return on investment. Therefore, affordable energy access will continue to remain a pressing issue for more than 8% of the world's population, of which 90% are residents of rural areas. The thesis proposes a three-step methodology to model, optimize, and analyze the affordable integration of retired batteries in a DC rural microgrid. A PV-diesel-battery microgrid that is more suitable to the local conditions of BURKINA FASO is proposed to test the technical and economic viability of our second-life hypothesis for cost reduction.

The study objectives are achieved based on an approach driven by measurements and simulations. The central portion of the experiments covers the parametric analysis and aging of lead-acid batteries using a test bench developed in the laboratory. We propose two battery tests to estimate remaining capacity and sorting in different groups. We also applied a modified technique to recover battery capacity using heavy cycling. Finally, two scenarios of the proposed average microgrid model are annually simulated to determine the net aging impact of batteries and diesel generators. The energy flow is controlled using rule-based energy management due to the ease of its implementation in the rural context. A hybrid optimization technique called particle swarm optimization-genetic algorithm (hybrid PSO-GA) is used to determine optimal sizing and best annual cost. The Levelized cost of energy (LCOE) from the final design in the degraded mode is \$0.18/kWh, the same as the domestic tariff in BURKINA FASO. Compared to \$0.23/kWh in the base case with no degradation, the resulting LCOE in the degraded mode is 23.2% cheaper and environment-friendly due to delaying battery recycling. We also found that batteries below 60% roundtrip efficiencies may lead to an uneconomical and less technically viable battery operation in the microgrid. Ultimately, a techno-economic optimum second-life microgrid design is then proposed. The geographic and economic conditions of the study site can be used to apply the thesis outcomes in similar energy-deprived communities.

Keywords: PV-diesel-battery microgrid; legacy battery; optimal system; energy management; degradation impact; rural electrification; techno-economic analysis.

Résumé en Français

Les micro-réseaux insulaires, un système de production d'électricité au niveau local, suscitent un intérêt croissant pour électrifier le bas de la pyramide sociale. Cependant, ces systèmes sont financièrement risqués pour les gestionnaires de réseaux en raison de la baisse des revenus. Par conséquent, l'accès à une énergie abordable restera un problème pressant pour plus de 8% de la population mondiale, dont 90% sont des résidents des zones rurales. Cette thèse propose une méthodologie en trois étapes pour modéliser, optimiser et analyser l'intégration abordable de batteries hors d'usage dans un micro-réseau rural à courant continu. Un micro-réseau PV-diesel-batterie plus adapté aux conditions locales du BURKINA FASO est proposé pour tester la viabilité technique et économique de notre hypothèse de deuxième vie.

Les objectifs de l'étude sont atteints grâce à une approche basée sur des mesures et des simulations. La partie centrale des expériences porte sur l'analyse paramétrique et le vieillissement des batteries au plomb à l'aide d'un banc d'essai développé au laboratoire. Nous proposons deux tests de batterie pour estimer la capacité restante et le tri dans différents groupes. Nous avons également appliqué une technique modifiée pour récupérer la capacité des batteries en cas de cyclage lourd.

Enfin, deux scénarios du modèle de micro-réseau moyen proposé sont simulés annuellement pour déterminer l'impact net du vieillissement des batteries et des générateurs diesel. Le flux d'énergie est contrôlé à l'aide d'une gestion de l'énergie basée sur des règles en raison de la facilité de sa mise en œuvre dans le contexte rural. Une technique d'optimisation hybride appelée optimisation par essaims de particules - algorithme génétique (PSO-GA hybride) est utilisée pour déterminer le dimensionnement optimal et le meilleur coût annuel. Le LCOE du design final en mode dégradé est de 0,18 $/kWh, soit le même que le tarif domestique au BURKINA FASO. Comparé à 0,23 $/kWh dans le cas de base sans dégradation, le LCOE résultant dans le mode dégradé est 23,2% moins cher et respectueux de l'environnement en raison du report du recyclage des batteries. Nous avons également constaté que les batteries dont charge-décharge est inférieure à 60 % peuvent conduire à une exploitation non rentable et moins techniquement viable des batteries dans le micro-réseau. En fin de compte, une conception technico-économique optimale du micro-réseau de seconde vie est alors proposée. Les conditions géographiques et économiques du site d'étude peuvent être utilisées pour appliquer les résultats de la thèse à des communautés similaires en manque d'énergie.

Mots clés : micro-réseau PV-diesel-batterie ; batterie de deuxième vie ; système optimal ; gestion de l'énergie ; impact de la dégradation ; électrification rurale ; analyse technico-économique.

Acknowledgments

This doctoral research has been prepared full-time at the Group of electrical engineering Paris Laboratory (GEEPS), UNIVERSITÉ PARIS-SACLAY, with the funding support by the ISLAMIC DEVELOPMENT BANK (ISDB) under Grant No. 600036563-ENERGY, and in part, by the University of Engineering and Technology, Mardan, PAKISTAN. The reported results in this work would not have been achieved without the support of many people. The authors gratefully acknowledge many groups and individuals who have contributed to and helped us develop our thinking about energy and sustainability. I appreciate the full cooperation from LAKDHAR M. KADKADI, NAZAR EL-HILALI, MAHMUD AMAN from the ISDB side, PROF. DR. IMRAN KHAN, ex-Vice Chancellor and PROF. DR. SHAHID KHATTAK, the current Vice-Chancellor from the home institution side, and all the directly concerned at the UNIVERSITÉ PARIS-SACLAY.

My special recognition, high appreciation, and sincere thanks go to my research supervisors PROF. ANNE MIGAN-DUBOIS and PROF. DEMBA DIALLO. Their timely feedback on simulations/ experimental outcomes/ articles/ scientific presentations and careful editing of this manuscript contributed much to the timely completion of this work. I cannot forget their moral support and encouragement during the rise and fall and the COVID-19 period. These factors were the main drive that gave me the courage and momentum to keep going. I remember all the insightful scientific arguments, consistent hard work, whiteboards full of explanations and new ideas, and challenging questions in each progress meeting that enabled me to be more oriented towards achieving the Ph.D. goals.

Thanks to all members of the jury, MANUELA SECHILARIU, FEI GAO, MARC PETIT, and GHJUVAN ANTONE FAGGIANELLI, for agreeing to evaluate this manuscript and examining quality of the work done and candidate's confidence and command on the subject. Your detailed observations, critical proofreading, and consistent suggestions had improved this work and enriched my understanding of the topic. Your efforts had allowed me to take a step back in my work and understand the operational stakes of the problem and make it easier or the readers to follow. A big thankyou to all of you for the great discussion during the defense. A special thanks to the EOBE doctoral school internal thesis monitoring committee, PHILLIPE DESSANTE, JEAN-CHRISTOPHE GINEFRI, and FRÉDÉRIC MAZALEYRAT. Thanks to MME EMILIA DAVODEAU for helping in many administrative procedures with the EOBE doctoral school.

Life abroad was a unique and wonderful experience to work in a mixed culture environment under a single roof. GEEPS, a very welcoming lab, was like a second home to me. I lived these three years in the best conditions. I developed myself both autonomously and as a team member to work in a multicultural environment without any problems with interpersonal relations, opinions,

or cultural differences. I am particularly thinking of the tremendous administrative support from the Lab director PROF. CLAUDE MARCHAND, the administrative team; SÉVERINE, NATHALIÉ, SYLVIÉ, and CHRISTINE, prompt support from the IT team, OLIVIER and ANTHONY, and on the technical part ÉRIC BERTHELOT, AURORÉ, and RICHARD. All the unforgettable moments with my colleagues will be remembered and missed. I am thankful to all of the GEEPS family for giving me the life-learning experiences, the best moments, discussions, fun, and gatherings in POINT K. Thanks to CHARLES, SANDRA, PAUL, YAO, YOUSRA, LUNA, MOHSEN, TANBIR, CYRIL, CHUANYONG, KOKOUVI, GUILLAUME, MAHERY, ANTOINE, LEONARDO, FANEVA, SUN-JEI, SLEIMANE, DAVIDE, QIHAO, BAOJI, TOM, NICOLAS, MATTIA, JULIEN, ALEKSANDRA, MONIKA, and KOFFI, for making every moment beautiful and thank you for your great support during the defense. Thanks to everyone I met in many international/national conferences, summer schools, travel, field visits, or lab work for the great discussion and support. I am honored and happy to bring back to my home institution in PAKISTAN such a unique culture, experiences of rewarding discussions on many academic and non-academic matters, and the practical knowledge learned during my life at the UNIVERSITÉ PARIS-SACLAY.

Finally, last but not least, I am thankful to all the seven incredible women in my life, my five daughters, JAVERIA (late), LAILMA, AIMAN, HAREEM, and AAYMA, my wife ASIYA, and my kind mother for their unconditional support, understanding, and love at every problematic stage in this journey. These beautiful souls make my every day an opportunity to get many achievements. You have been quite brave for these three-year. I could not see my daughters growing in their golden period of the lovely childhood that I consider an unrecoverable loss during this period. However, their love and sweet thoughts made the distance separating PAKISTAN from FRANCE feel non-existent. The end of year 2022 has been very special by the arrival of my lovely family in FRANCE, who made the evening of December 15 so beautiful with their presence during the Ph.D. oral defense and the reception after with the delicious traditional food. It was wonderful for them to discover the University, the culture, the people, and the environment where I worked.

In the end, I hope the presented material in this manuscript and their arrangements in various chapters/sections will make it sound, accessible, and attractive to the readers.

Ph.D. is a story full of rising and fall where you are the main character to your depth and soul—the story of perseverance that brings you strength, dignity, beauty, and purposeful life.

KHADIM ULLAH JAN

PARIS, DECEMBER 2022

All glory and praises to the Almighty God for the blessings bestowed upon me and for giving me the strength to complete this work.

***

Analysis of the Performance Impact of Component Aging in Hybrid Energy PV-Diesel-Battery Rural Microgrid: Modeling, Control, and Energy Management

Khadim Ullah Jan

University Paris-Saclay
GeePs Laboratory| 11 rue Joliot Curie, 91192 Gif-sur-Yvette, Paris, France

To the loving memory of my father

who left this world for his heavenly abode on April 26, 2006 (1954-2006) and could not see any of my successes. His loving spirit sustains me still and stable. May his soul rest in peace, and may God give him the highest rank in Jannat-ul-Firdous.

Contents

Figures

Tables

Symbols and Notations

γ: power temperature coefficient, 49
θ_c: individual PV cell temperature in $°K$, 49
θ_r: reference temperature in $°K$, 50
r_1 r_2: uniformly distributed numbers between $[0\ 1]$, 133
R_{20}, A_{21}, A_{22}: constants in battery equations, 57
$T_{1ss} - T_{2ss}$: time slots with sunshine, 72
$V_1(t), V_2(t)$: voltage drop accross capacitors, 62
\$: United States dollar, 71
$\Delta P_{L,lp}$: low-priority load cut, 73
$\Delta P_{L,t}$: change in load power, 75
ΔP_B: admissible battery power variation, 73
ΔP_{Gen}: change in generated power, 75
ΔP_L: load power deficit, 73
ΔP_{PV}: PV power deficit, 73
ΔP_t: net power difference in microgrid, 75
$\Delta W(t)$: effective corrosion layer thickness, 92
ΔW_{limit}: absolute limit of corrosion layer, 92
$°K$: Kelvin degree, 49
$A_{s,PV}$: PV module surface in m^2, 51
A_0: constant in battery equations, 57
B: damping coefficient of engine, 116
$C_{B,bank}$: aggregated battery bank capacity, 136
$C_{B,corr}$: capacity loss due to corrosion, 91
$C_{B,deg(limit)}$: battery degradation limit, 91
$C_{B,deg}$: capacity loss due to degradation, 91
$C_{B,e}$: total extracted battery capacity in Ah, 106, 193
$C_{B,f}$: battery capacity fade, 90
$C_{B,max}$: battery maximum capacity, 77
$C_{B,min}$: minimum battery capacity, 77
$C_{B,n}$: nominal battery capacity, 57
$C_{B,n(0)}$: nominal capacity during commissioning, 65, 91
$C_{B,n}$: nominal battery capacity, 90
$C_{B,r(y)}$: battery remaining capacity in years, 65
$C_{B,r}$: battery remaining capacity in Ah, 54, 91
$C_{B,t}$: battery total capacity in Ah, 54
c_1, c_2: constants (cognitive and social parameters), 133
C_B: individual battery capacity in Ah, 136
C_{10} : C-rate at 10A, 57
$CC_{0,pv}$: initial capital cost of PV, 72
CC_0: total initial capital cost of equipment, 70
D^n: d-dimensional rectangular search space, 132
E_{Bi}: battery absorbed energy in kWh, 139
E_{Bo}: battery discharged energy in kWh, 139
E_D: defficient energy in kWh, 139
E_{GO}: the bandgap energy ($1.12eV$), 51
E_m: voltage source in battery electrical model, 55
E_{m0}: battery cell voltage at full charge, 57
E_p: parasitic branch voltage, 56
F:feasible part of the search space, 133
$F(t)$: fuel consumption function, 69
$f(\bar{x})$: real-valued objective function, 132
$F_{B,life}$: battery float lifetime, 93
$F_{h,l}$: lower heating value of fuels, 115
F_0: fuel curve intercept of function $F(t)$, 70
$f_1(I_B, n_{bc})$: factor for I_B and bad charges, 92
$f_{acid}(t)$: battery acid stratification, 92
f_{SoC}: SoC impact on degradation, 92
f_{str}: acid stratification function, 93
G: solar global in-plane irradiation in Wm^{-2}, 51
g_{best}: global best particle, 133
$g_i(\bar{x})$: set of constraints, 132
GE_t: total generated energy in kWh, 70
$I_{0,D}$: reverse saturation current of the diode, 51
$I_{B,10}$: battery discharge current at 10-hr rate, 92
$I_{B,n}$: nominal battery current, 110
$I_{c,sh}$: shunt leakage current in a solar cell, 50
$i_{\tau,e}$: current that produce electric torque, 116
I_B: battery charge-discharge current, 54, 90
I_B^*: nominal battery current at nominal capacity, 57
I_c: solar cell output current, 51
I_D: diode leakage current, 50
I_m: RC branch current in battery equivalent-circuits, 57
I_{MPP}: PV panel current at MPP, 52
I_{or}: solar cell saturation current at θ_r, 51
I_{ph}: photo-generated current in a PV cell, 49
I_{SC}: the short-circuit current at STC, 51
J: damping coefficient of rotational inertia, 116
$J(\omega_m)$: dynamic torque of DG system, 116
k: discrete time index, 62
$K_{SoC,0}, K_{SoC,min}$: constants relating SoC_{min} to SoC_0, 92
K_B: Boltzmann constant $1.38 \times 10^{-31}\ JK^{-1}$, 50
K_E: a constant in battery equations ($volts/°C$), 57
K_I: short-circuit current temperature coefficient, 51
kW: kilowatt, 69
$L_{B,th}$: battery lifetime throughput, 71
l_a: asset lifetime, 70
l_b: lower bound, 133
L_{DG}: DG lifetime in hours, 70
$LCOE_B$: Levelized cost of energy for battery, 71
$LCOE_{PV}$: Levelized cost of energy for PV, 72
$M_{B,rep}$: battery replacement cost, 71
$M_{B,w}$: battery wear cost, 71
$M_{DG,fix}$: generator fixed cost, 69

$M_{DG,o\&m}$: DG operation and maintenance expenses, 70
$M_{DG,rep}$: DG replacement cost, 70
$M_{fuel,eff}$: effective cost of fuels, 70
$M_{PV,o\&m(y)}$: yearly O&M cost of PV, 71
$M_{t,o\&m(y)}$: total yearly O&M cost, 70
$n_{B,c}$: series-connected battery cells, 54
$N_{B,opt}$: total number of batteries from optimization, 136
$N_{B,s}$: number of batteries in a series string, 136
$N_{c,PV}$: number of PV cells, 49
N_B: total number of batteries, 71
n_{bc}: the number of bad charges beyond 90% SoC, 92
n_D: ideality factor of the diode, 50
N_{DG}: number of diesel generators, 69
n_{en}: engine speed, 115
n_p: number of poles in the machine, 116
N_{PV}: number of PV panels in the array, 51
P: number of particles, 133
$P_{B,d}$: battery power loss due to degradation, 74
$P_{DG,d}$: DG power loss due to degradation, 74
$P_{DG,r}$: DG rated power in kW, 69
$P_{L,peak}$: maximum microgrid load power, 69
$P_{PV,0}$: PV power at STC during installation, 51, 52
$P_{PV,MPP}$: maximum PV power at MPP, 49
$P_{PV,s}$: PV power loss due to partial shading, 74
$P_{PV,y}$: the PV output power in years, 51
P_B: battery power, 69, 73
p_{best}: best previous position of particle, 133
P_{Con}: consumed power, 73
P_{DG}: diesel generator power, 69
P_{Gen}: available power in the system (net generation), 75
P_L: load power, 69
Pb: negative lead electrode, 88
PbO_2: positive lead oxide electrode, 88
PS-S: physical system to Simulink, 59
q: electron charge, which equals $1.6X10^{-19}C$, 50
$Q_{B,e}$: extracted battery charge, 57
$Q_{B,f}$: battery charge loss due to capacity fading, 91
$Q_{B,init}$: initial stored charge in the battery, 58
r: interest rate, 70
$R_{c,s}$: series resistance of a solar cell, 50
$R_{c,sh}$: shunt resistance of a solar cell, 50
R_0: battery terminal resistance, 55
R_{00}: the value of battery R_0 at SoC=1, 57
R_1C_1: RC branch resistance/capacitance, 55
R_2: battery internal resistance, 55
r_{ff}: fuel flow rate, 115
R_{int}: battery internal resistance, 53
R_p: parasitic branch resistance, 56, 64
S: search space, 132
$S_{B,limit}$: speed factor for capacity loss, 93
SoC_0: initial SoC at t=0, 90
SoC_{max}: maximum SoC, 137
SoC_{min}: minimum SoC, 92
S-PS: Simulink to physical system, 59
t: time interval, 75
$T_{2(tr)}$: transient intermittency period, 73
T_B: battery temperature, 57, 89
t_i, t_f: drift intervals, 90
T_s: sampling period, 62
u_b: upper bound, 133
u_ω: control signal for governor, 69
$V_{B,n}$: nominal battery voltage, 110
$V_{c,L}$: load voltage of the PV cell, 50
$V_{oc,c}$: solar cell voltage at open-circuit, 50
$V_{R1||C1}$: voltage drop at RC branch, 57
V_B: battery terminal voltage, 54
V_c: individual solar cell voltage, 51
v_i^{k+1}: particle new velocity after an update, 133
v_i^k: particle's previous velocity, 133
V_{int}: internal source voltage, 54
V_{MPP}: PV panel voltage at MPP, 52
V_T: solar cell thermal voltage, 51
w: inertia weight factor, 133
X, Y: coefficients for parameter extraction, 61
x_i^{k+1}: new particle's position after an update, 133
x_i^k: current particle's position, 133
x_j: decision variable, 132
y: years, 51
Z_{IEC}: expected number of useful lifecycles, 91
Z_W: weighted number of cycles, 91
Δk: discharge interval in hours, 90
$\eta_{B,rt}$: battery roundtrip efficiency, 71
η_{MPP}: PV panel array efficiency at MPP, 51
η_c: Coulombic efficiency, 62
η_{conv}: converter efficiency, 75
η_{PV}: PV panel array efficiency, 51
η_T: thermal efficiency, 115
θ_p: battery parameter vector, 64
λ_m: machine field flux, 116
ρ_{corr}: resistance of corrosion layer, 92
$\sigma_{B,s}$: battery self-discharge rate, 75
$\sigma_{B,y}$: battery yearly degradation rate, 65
$\sigma_{B,z}$: constant for battery degradation, 91
$\sigma_{PV,y}$: PV system yearly degradation rate, 52, 72
τ: RC time-constant, 56
$\tau_{en,avg}$: average engine torque, 115
$\tau_{g,e}$: electrical torque component of generator part, 116
τ_d: transport delay for generator voltage, 69
τ_{en}: engine torque, 115
τ_l: load torque, 116
τ_m: mechanical torque, 69, 116
$\varphi'(k)$: vector of Regressors, 64
ω_m: DG rotational speed, 116

Abbreviations

All the relevant abbreviations are included on the title pages of the respective chapters. The following quick links can be used to go to the corresponding pages.

Key Definitions

The following terms and definitions are given in their simplest form to understand this document. The readers may refer to the **Bibliography** or the "*IEEE Standards Dictionary: Glossary of Terms & Definitions"* to better understand some of these terms.

Modular: all the DC devices are modular, which means that they can be reorganized to get the desired configuration. Batteries are an example of modular devices. They can be grouped in series or parallel to get a certain voltage level. Nevertheless, it can affect the cost of a microgrid system.

PV shedding: in case the PV power generation is over the consumption of the microgrid.

Constraint: a condition that system configurations must satisfy. For example, batteries must return to 50% state-of-charge (SoC) by the end of a day.

LCOE: cost of energy per kWh, a performance indicator.

Deferrable load: an electrical load that can be turned ON anytime when electricity is available. Water pumps, ice makers, and battery-charging stations are a few examples.

Dispatchable source: on-demand energy production, such as diesel generators (DG).

Intermittent: when production fluctuates due to meteorological constraints such as uncontrollable sunshine.

Non-dispatchable source: the energy cannot be ensured on demand, such as PV.

Energy resources: any renewable or non-renewable power generation unit that can source energy in the microgrid.

Cycle charging: An energy dispatch strategy in which if DG is ON, it operates at full capacity to supply load and charge batteries.

Legacy: anything which is not new, whose life and use history is not known or even difficult to estimate.

Load factor: a criterion to determine generator efficiency and fuel consumption.

Custom-made battery charger: consists of a transformer and rectifier that rely slightly on overcharge. This battery charger is not microprocessor-based and has little intelligence.

Sulfation: The abnormal growth of acid crystals on lead-acid battery plate.

Lifecycle: different stages of the microgrid system components from installation to the decommissioning and final replacement.

Calendar aging: The reduction in battery capacity with time, mainly due to self-discharge when kept off-shelf ($I_B = 0$) for a longer time.

Cycle aging: is related to the battery charge-discharge, mainly degradation of the active material during the process.

State-of-health: Practically, a battery's state-of-health (SoH) is 100% at the time of installation, and it decreases proportionally, reaching below 70% within the ten years of mission profile and in safe operational limits.

Vented lead-acid batteries (open): hydrogen and oxygen are vented to the open air through small holes in the vent plugs. To top up water from time to time.

VRLA batteries (sealed): hydrogen and oxygen are converted into the water using a pre-inserted catalyzer. These batteries are maintenance-free.

C-rate: It is a per unit (p.u.) battery discharge rate: C_{10} of a 100Ah battery means a discharge in 10 hours with a 10A load.

Speed governor: an electromechanical structure used for speed regulation of an engine by adjusting the fuel intake.

Wet-stacking: The condition in which unburned fuel particles cause increased wear and tear to the generator parts.

Constraints: In optimization, the system constraint is a condition that must be satisfied in the decision.

Chapter-I: Introduction and Scope

Key Terms

Rural electrification, second-life batteries, social acceptance of energy technologies, microgrid cost reduction, renewable energies, energy-poverty mitigation, PV-diesel-battery microgrid.

Acronyms

AGM Absorbed glass mat
ARE Alliance for rural electrification
EMS Energy management system IEA International energy agency
LCOE Levelized cost of energy
SDG Sustainable development goals
SoC State-of-charge
SHS Solar home system
VRLA Valve-regulated lead-acid

Chapter Highlights

This chapter serves as a warmup to the topic and an introduction to the current art. Important notions for the understanding of this study are defined, and different relevant study areas are briefly introduced.

Contents

CHAPTER 1

INTRODUCTION AND SCOPE: TOWARDS LOW-COST DC MICROGRIDS

This chapter discusses the reason for developing low-cost rural electrification systems in simple terms. Definitions, theories, and general information on electrification trends are included to understand the topic theme and context. A DC microgrid that is more suitable to the local conditions in isolated regions is proposed. Discussion of the main issues related to energy access with a bibliographic review of the state of the art highlights the significance of this project to society, the developing world, and concerned energy-related communities. The chapter concludes with the rest of the manuscript structure.

1.1 General Introduction

(1) Motivation: In the 21st century and on a dark planet? The underdeveloped world still struggles with keeping its electrification coverage. Currently, 14% of the global population lives without access to cheap and reliable electrification services [1], [2]. The situation is more catastrophic in rural areas as the grid extension or transmission and power distribution is quite costly due to population dispersion, rugged terrain, or both. Even if there is a grid, it is not stable due to overloaded feeders and poor power quality.

In today's world, electricity is the driving force behind all social and economic progress. Many developing countries have tremendous technological advancements in every field of life, but not really in the energy sector. As shown in Figure 1.1 [2], the most affected part of the energy-poor population lives in developing ASIA and AFRICA. According to the *International Energy Agency* (IEA) and *World Watch Institute*, 2 out of 10 people in developing ASIA and 7 out of 10 in SUB-SAHARAN AFRICA have no reliable grid [2]. Though some countries are quickly progressing to achieve a 100% electrification rate by 2030, part of SUB-SAHARAN AFRICA and developing ASIA are far behind the race.

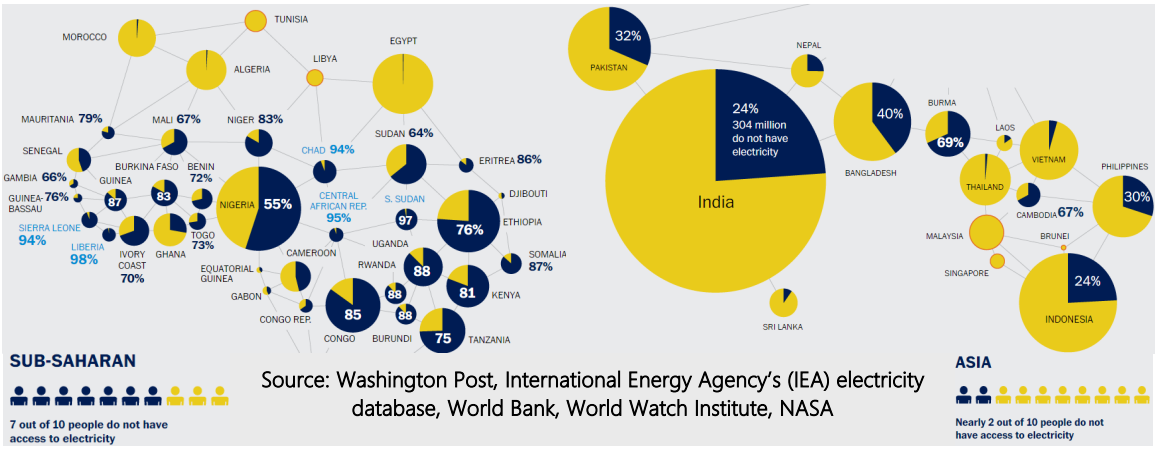

Figure 1.1 – Global electrification rate [2]

As shown in Figure 1.2 [2], it is expected that by 2030, around 674 million people (8% of the world population) will have no access to electricity at affordable costs, 90% of which will be in the rural areas [2].

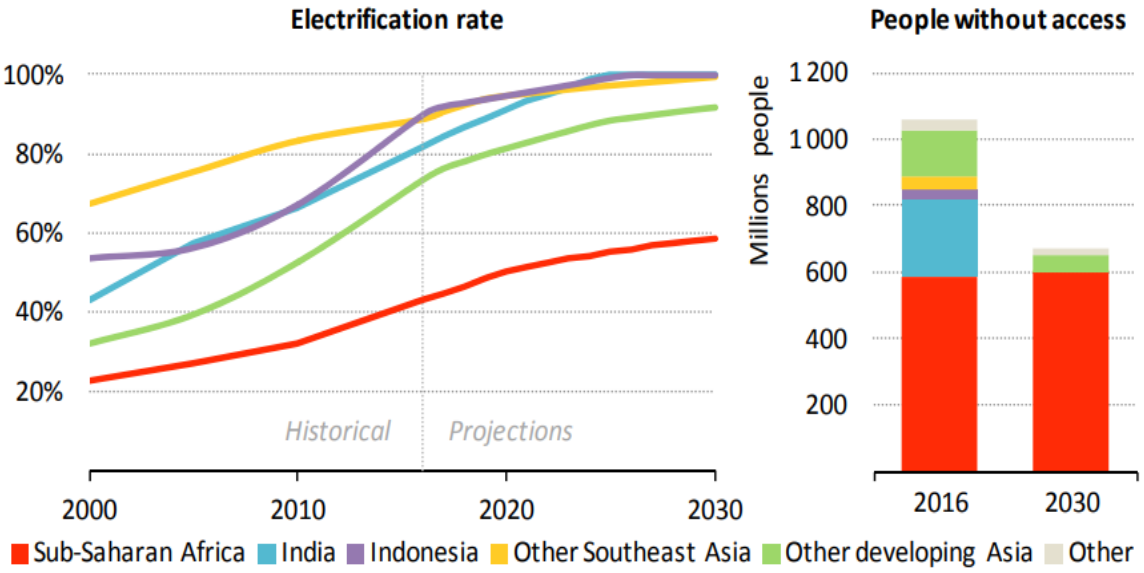

Figure 1.2 – Projected electrification rate and population without electricity[1] [2]

The global population rate shapes the basic living needs of societies. Affordable energy access will be the first and most affected target. According to the "*UN World Population Prospects 2019*" report, the global population will reach 9.7 billion in 2050 and ~10.9 billion in 2100 (Figure 1.3, adapted from "*World Population Prospects 2019*" [3]).

By contrast, many populous and wealthy economies will touch the peak and slightly bend to decline by 2050. The least developed top populous countries such as PAKISTAN, TANZANIA, part of INDIA, NIGERIA, ETHIOPIA, CONGO, and the rest of the small countries

[1] Other includes rest of the least developed countries in Latin America, Middle East, and North Africa.

in SUB-SAHARAN AFRICA, *i.e.*, (BURKINA FASO, SIERRA LEONNE, LIBERIA, CHAD, TOGO, SUDAN, and MALI) will continue to hike. These regions contribute to more than half of the projected increase in population (demographic data obtained from [3]). These countries are already facing issues providing reliable electricity to rural people, which would worsen with time. This study is mainly carried out for GOGMA village in BURKINA FASO, due to the feasibility of the project to the local climatic and economic conditions. The justification of this case study is further detailed in SUBSECTION 4.1.1. In addition, similar projects could be easily implemented in the rest of SUB-SAHARAN AFRICA or another part of the developing world with similar local conditions.

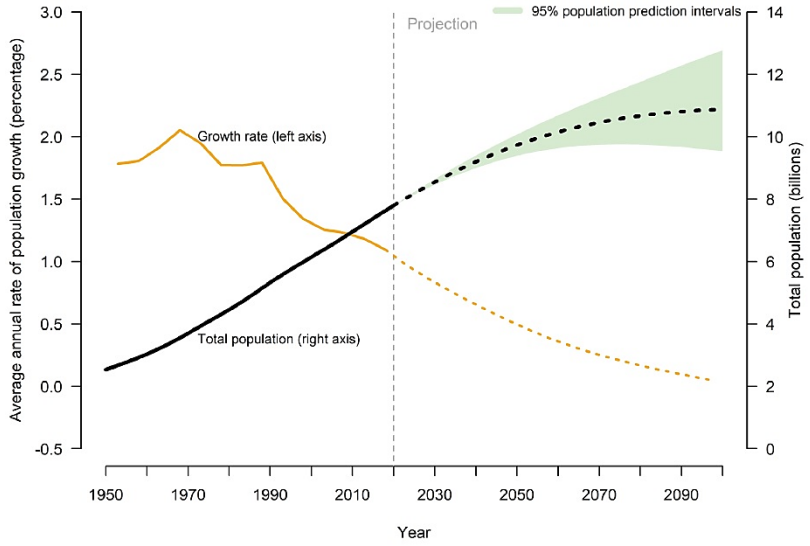

Figure 1.3 – World population growth projections [3]

The projected electrification access rate increases to achieve "*Universal Access to Electricity by Everyone by 2030*". Achieving this target is feasible for a few countries but still a challenge for least developed economies, especially in remote areas. Further details about energy access projections are enlisted using Table 1.1 (information adapted from [2]). Given these projections, rural electrification has become a humanitarian challenge.

Table 1.1— World population without access to electricity [2]

	2000		2016		Projected by 2030	
	million	%	million	%	million	%
AFRICA	532	66%	588	48%	602	36%
North Africa	14	10%	0	0%	0	0%
Central Africa	73	90%	98	75%	122	63%
East Africa	164	90%	172	61%	135	34%

	2000		2016		Projected by 2030	
	million	%	million	%	million	%
South Africa	15	34%	8	14%	1	1%
Other Southern Africa	108	86%	135	69%	156	55%
West Africa	158	67%	175	48%	188	36%
DEVELOPING ASIA	1059	33%	439	11%	54	1%
China	18	1%	0	0%	0	0%
India	600	57%	239	18%	0	0%
Indonesia	99	47%	23	9%	0	0%
Other Southeast Asia	100	33%	42	11%	2	<1%
Other Developing Asia	242	68%	135	27%	52	9%
CENTRAL AND SOUTH AMERICA	56	13%	17	3%	4	1%
MIDDLE EAST	15	9%	17	7%	14	5%
World	**1672**	**27%**	**1060**	**14%**	**674**	**8%**

90% of the remaining 8% of world population without electricity by 2030 will be rural people OR 9 out of 10 people who have no access to electricity will be residents of the far-flung areas [2].

(2) Energy Access Overview: Energy access is not only about the prosperity of the local people, development of their small-scale businesses, and utilization of the indigenous resources, but also has an impact on the global security and peace, as everyone wants equal opportunities, education, health, safety, and to improve their living standards. Electricity also means women's empowerment and the creation of local jobs. Thus meeting energy demands safely, reliably, and economically while minimizing climatic impacts is not easy and remains a global challenge [4], [5].

(3) Conventional Grids Vs Microgrids: Electricity grid is one of the largest systems spanning over continents. As shown in Figure 1.4, most of the power is generated from expensive and pollutant resources. Thus, the conventional grid expansion is full of problems such as increased emissions and unaffordable electricity costs. The idea of power generation very close to the consumer end using the indigenous renewable resources, usually called a local microgrid, can solve these issues [6]. Microgrids can

integrate locally generated energy into local distribution networks. If the consumption is local, why not the generation? A local solution, for the local people, with the local resources. However, the poor people lack interest in participating in a locally built microgrid due to the high installation, operational, and maintenance costs.

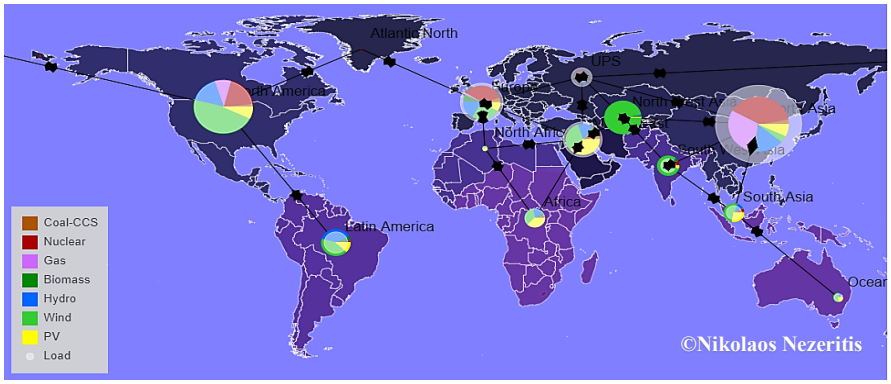

Figure 1.4 – The conventional electricity grid and energy mix (source: theglobalgrid.info)

On the other hand, rural microgrids are not financially viable for business managers due to low revenue collection from poor people. Investors consider any electrification facility in rural areas a financial risk. Thus, a community microgrid like in Figure 1.5 remains a challenge in a rural environment. Electrification in a rural environment brings along many technical and implementation problems [7]. Modeling, analysis, limited finances, and microgrid system architecture still have many challenges [8]. It is impossible to ensure reliable access to the electrification services without a significant cost reduction that mostly comes from storage batteries or diesel generators (DGs). However, it is technically possible to utilize the second-life equipment based on their remaining capabilities. The objective of this study is to technically point out the main issues that limit both the investors and consumers from microgrid installation and participation, respectively.

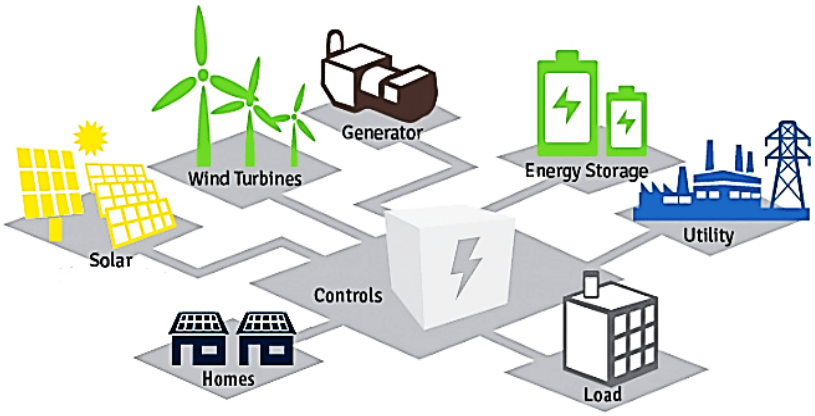

Figure 1.5 – Current community microgrids; a financial risk due to less social acceptance

(4) Global Electrification Trends: In the sustainable electricity scenario, renewable will provide one-third of the global electricity demand by 2040 [1]. The abundance of available surface area for photovoltaic (PV) power generation is a plus in rural areas. Figure 1.7 shows that PV leads to other renewable sources in this energy transition.

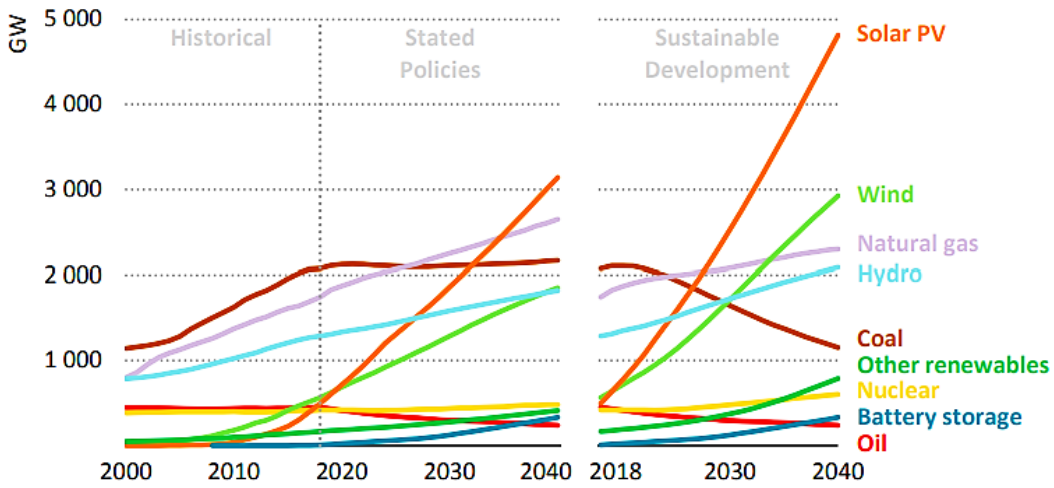

Figure 1.6 – Competitiveness of PV in future power generation mix: Global power generation capacity by source and scenario [1]

Furthermore, as shown in Figure 1.7[2], the people with the lowest electrification rates have the highest solar irradiance and highest PV power production potential [9]. Conclusively, energy sustainability is directly linked to cost, and module cost exponentially decreases for PV power generation. Therefore, a PV-based hybrid energy microgrid is an excellent solution to electrify the people living in distributed geographic locations in the developing world, in particular SUB-SAHARAN AFRICA and SOUTH ASIA [10].

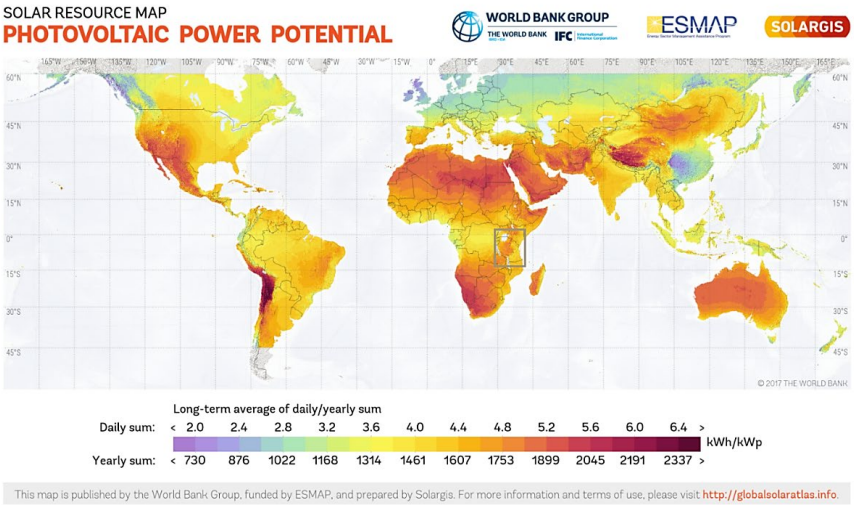

Figure 1.7 – Global solar irradiance and PV power production potential (source: SOLARGIS)

[2] © SolarGIS https://solargis.com/.

(5) Legacy Equipment: Why we need and how it fits in the low-cost microgrids? The term *legacy* has remained practical in many of our daily life scenarios, such as transportation, electronic gadgets, garments, and other utilities. Something that may not fit in one application may still serve better in another. The market entry of Lithium-ion (Li-ion) had decommissioned many lead-acid batteries from cars, small trucks, and sailboats. This battery junk is considered both a challenge and an opportunity. Instead of toxic lead recycling, these batteries could serve better in low-power applications. Thus, it is an eco-friendly contribution to delay recycling. This project aims to propose solutions in energy-deprived rural communities for basic energy access using legacy components [11]. Legacy equipment is not new and comes with an unknown use history and mission profile, *e.g.*, Figure 1.8 (adapted from [12]), old batteries and DG without a datasheet. They are locally available at lower prices and easy shipping to the sites, thus better suit rural microgrids. With a significant cost reduction on initial installation, it is possible to accommodate more consumers, sources, and storage batteries over time and maximize the socio-economic impact of a locally built electrification system.

Figure 1.8 – Legacy batteries, generator, and PV panels [12]

According to reports from GENPACT[3] or TECHNAVIO INC. [13], the global market of electric golf carts is dominated by lead-acid batteries, from around 99% at the beginning of 2010 to about 86% by 2018 [13]. The decreasing market volume indicates the large-scale availability of decommissioned batteries. It will keep growing as Li-ion will continue to replace lead-acid in many applications. For widespread adoption, the legacy technology must meet the expectations of rural people. The second use application must be low-cost, reliable, and sustainable. In this way, it is possible to increase social acceptance of the low-cost legacy technology and accommodate more and more consumers over time. It will ensure consumer engagement and maximize the return on investment on small-scale community microgrids [14].

[3] GENPACT and TECHNAVIO Inc. are technology research companies providing professional services.

1.2 Sustainable Energy—*the Engine of Sustainability and Global Prosperity*

Energy is key to a functioning society and its essential needs. Prosperity, political stability, health, education, safety, women empowerment, climate challenge, and life quality are driven by energy availability and sustainability [15], [16]. Sustainable energy systems have five broad dimensions: technical, economic, social, environmental, and institutional impacts as the critical elements [17]. These influencing factors and twenty-four indicators for rural electrification are detailed in [18].

There are also growing concerns about energy generation and its sustainability [19]. Sustainable and low-cost energy access remains a pressing issue in the developing regions [20], [21]. Low-income people with resource insecurity could bring consequences to achieving the sustainability goals [22]. The basic needs and daily living expenses remain a big challenge for the poor. Also, the regulatory framework is not yet defined for such community-scale electrification. Given these problems, implementing rural electrification projects is not easy due to the risk of low financial return on investments and lack of standards [23]. Thus, it is natural to understand why the energy projects are riskier in financially unstable communities. Therefore, sustainable energy means a financially viable electrification system [24]. For further reading, a vast literature is available on energy for development, electrification, and technology impacts [25].

Energy access and carbon reduction are the two main challenges that must go side by side [26]. Figure 1.10 (adapted from IEA, WEO, 2019 [1]) shows that large electricity grids contribute the most carbon content. Therefore, flexible integration of renewables and distributed generation with indigenous resources will favor the environment.

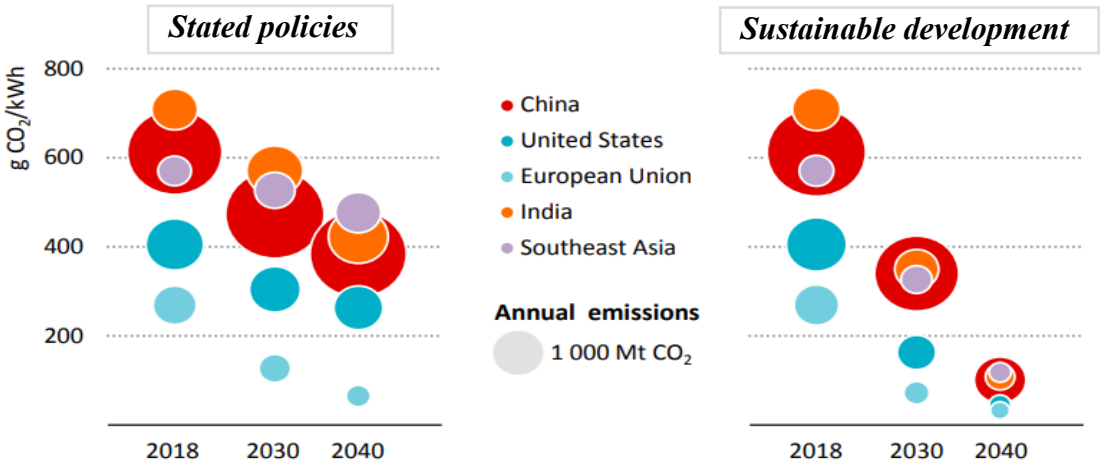

Figure 1.9 – Carbon intensity of electricity generation [1]

1.3 Rural Electrification

Electrification typically begins in urban environments and gradually extends to rural areas; however, this process often runs into obstacles in developing nations where the costly grid extension cannot be materialized, or the grid itself cannot withstand further load [27]. Among other reliability issues, the receiving end voltages drop to an unacceptable value due to distribution losses. Therefore, the rural communities suffer from electricity market failures.

A comparison between the current and future electrification scenarios is shown in Figure 1.10 [2]. These predictions show the required infrastructure and PV generation as a viable solution for off-grid electrification systems. The IEA predicts that rural people will have to rely on decentralized energy sources for 100% electrification [2]. IEA also predicts that to achieve the goal of *Energy Access for All*, even those in hard-to-reach areas, a reasonable portion of the energy sources will come from indigenous renewables such as PV, hydro, and the wind backed up with dispatchable source like a DG [28].

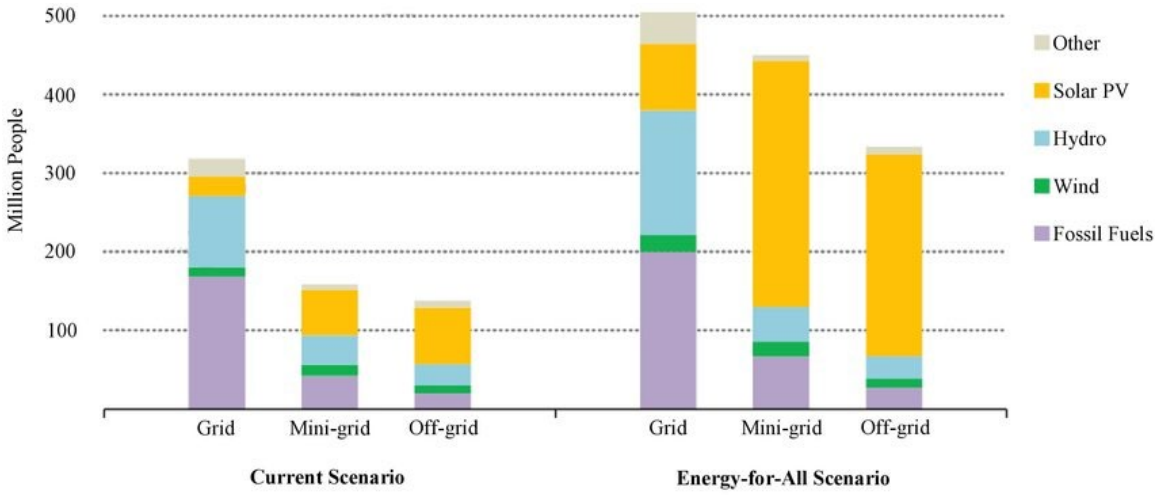

Figure 1.10 – Comparison of the current and future scenarios of energy access through off-grid systems [2]

1.3.1 One Step up the Energy Ladder: Affordable Energy Access for Everyone

(1) General Description: The correlation to interlinking sustainable development goal SDG-7 (affordable and clean energy for all) with other developmental goals is depicted in Figure 1.11 [29]. It shows energy access as a central element to achieve other sustainable goals such as peace, justice, climate action, women empowerment, skills development, and utilization of indigenous resources [30]. Electrification of the local markets has also increased the productivity, creation of local jobs, efficiency, and revenues, as businesses can keep their doors open for extended hours in the late evening.

Figure 1.11 – The impact of SDG-7 on other development goals [29]

In the prior art, techno-economic modeling of the electrification systems have been proposed to achieve social and economic benefits of basic and affordable energy access [31], [32], [33]. Access to local electrification services also means safety by installing street lights. More achievements have been observed, such as more material for the lectures, better test scores, extra teaching hours, and raising the human capital for societal developments.

(2) Consumer's Role: The role of a consumer is vital for the sustainable operation of a microgrid. Among many, four critical factors determine the system sustainability, *i.e.*, awareness of the technology limitations, avoiding unplanned consumption, the knowledge of paying for system maintenance, and on-time payment of the bills [34]. These factors mainly determine if sustainability could be achieved or not in a rural electrification project. A sustainable electrification system must be environmentally friendly and financially viable [35]. Because of these ground circumstances, the second-life proposition and its technological impact is a good balance between environmental protection and cost reduction. While many supportive policies have been put in place, the cost of providing electricity to remote villages remains high. An example is the energy ladder in Figure 1.12. Cost is a missing step while moving from the basic lighting such as burning candles or a LED with a small battery into a more stable and reliable microgrid. Most people with limited finances cannot cross this transition as they need to pay more for the services. Thus, setting up a community microgrid in a rural environment is a potential financial risk and a point of no interest for the investors.

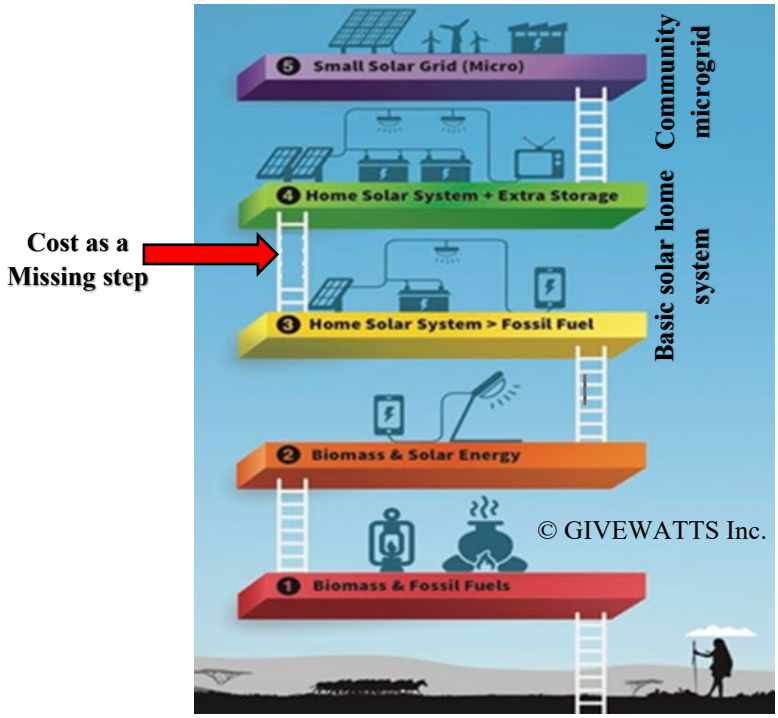

Figure 1.12 – Energy transition: cost as a missing step for the energy-poor communities (source: GIVEWATTS Inc.)

1.3.2 Will Legacy Equipment Solve the Energy Puzzle for the Poor?

Batteries are the most expensive and essential system component. As more and more batteries are being decommissioned, it is the right time to utilize them for other applications, such as PV power smoothening or backup storage. In Figure 1.13, the abundance of legacy batteries at lower prices could address the cost-related issues. This second-use concept could also help favor the environment by delaying battery recycling for two to three years.

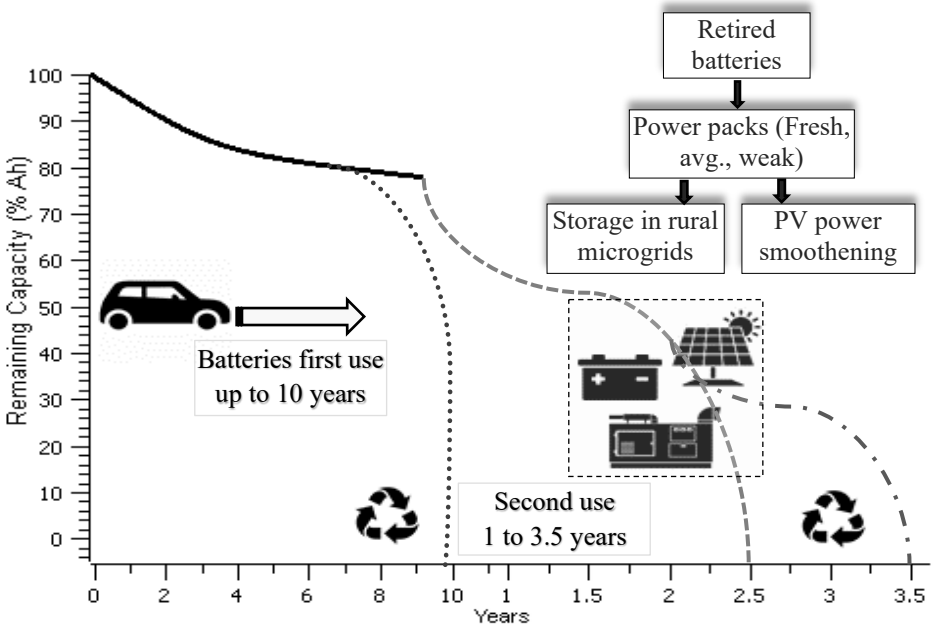

Figure 1.13 – Legacy batteries in electrification services (source: own elaboration)

1.4 Rural Microgrids—*Concept, Structure, and Operation*

(1) Microgrid Layout: Microgrids are a means of providing energy services locally. The concept is rapidly moving from laboratory [36] and pilot demonstration sites into massive global deployment, especially in areas without a possible grid extension [37]. The most practical layout for an islanded rural microgrid is based on local conditions. In rural areas, such microgrids have sufficient surface area for housing the equipment and available rooftop for PV in a secure place [38]. People live in the form of communities of 50 to 100 households in a rural environment. Compared to traditional large grids, small-scale low-voltage DC microgrids could be built faster, cheaper, and at different power and voltage levels. The low-voltage DC microgrids are also suitable for safety and short distance. The architecture shown in Figure 1.14 and its listed specification in Table 1.2 can meet power demands ranging from elemental lightning and entertainment to small-scale community loads. The DC architecture can power most modern DC loads efficiently and at a safer voltage level, which is important for inexperienced local operators/ technicians.

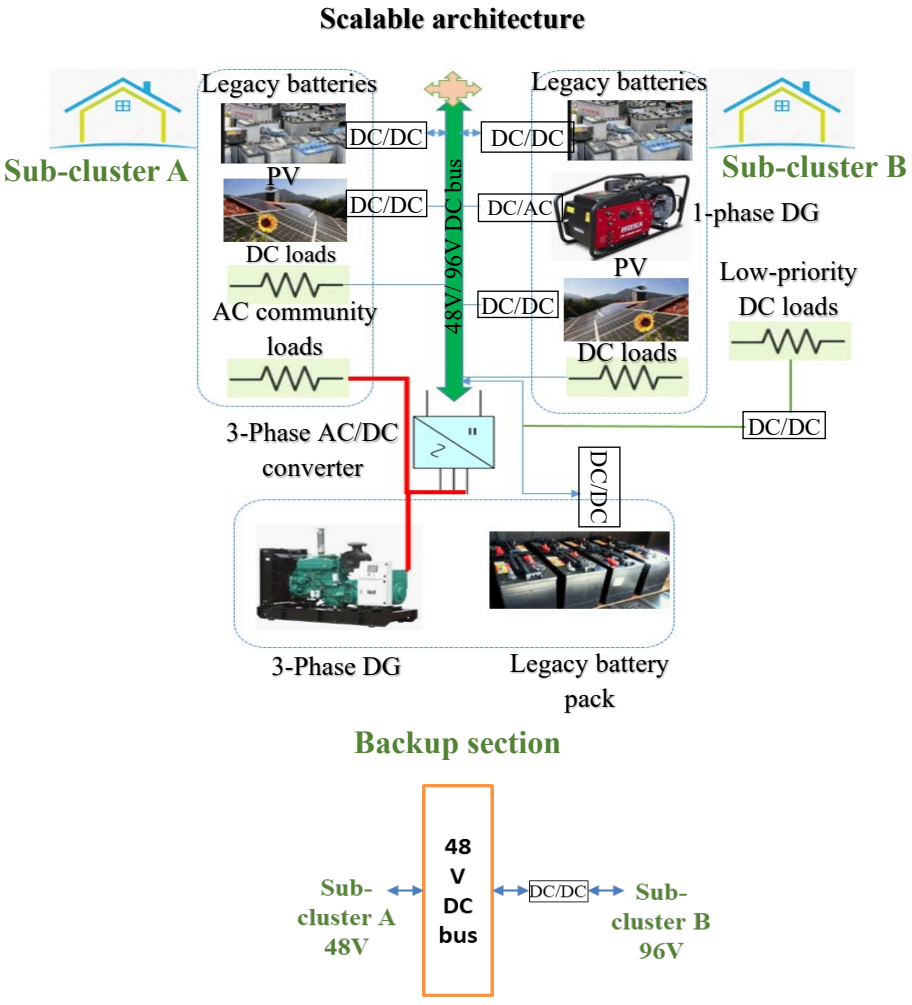

Figure 1.14 – Rural microgrid schematics and system components (*source: own elaboration*)

Table 1.2— System components

Architecture, equipment, and rating of the proposed PV-diesel-battery microgrid

Microgrid type	Rural
Mode	DC/Off-grid
Total microgrid power	30kW
Load type	Residential, low-priority load cut
Battery type/ Nominal voltage	Lead-acid/12V VRLA or flooded
Non-renewable sources	DG
Renewable sources	PV only
Solar PV type and mounting	Flat plate silicon PV panels 325W_p/module
No. of household/ inhabitants	125/ 1100 inhabitants
Configuration	Scalable (could be accommodated with more sources and loads over time)
Ownership	Local community in BURKINA FASO
Domestic load type	Home lighting, entertainment, LED TVs, outdoor lighting, ventilation fans, charging mobile phones, and small electronic gadgets
Community load	Street lights, community shops, healthcare

(2) Lead-acid Batteries: Lead-acid battery is the first developed, proven, and mature secondary (rechargeable) storage technology. The French physicist GASTON PLANTÉ first demonstrated the lead-acid battery in 1859 [39]. Despite of their significant environmental impact, lead batteries are safe, easy to install, low-cost, and abundantly available as legacy for low-power electrification. This battery technology has the shortest payback period. Other characteristics such as plug-and-play, high energy density, fast response, geographical independence, easy handling, and established recycling industry make lead-acid a leading place for the energy storage in microgrids. In contrast, giving such batteries a second-life could further reduce the overall microgrid cost.

The type of batteries used in our work are lead-acid. The batteries are more suitable to cover the low-load period from late night until early morning if the DG operation is on low-priority for cost savings. As described below, they can be either vented lead-acid (VLA: flooded type, battery with a liquid electrolyte) or valve-regulated lead-acid (VRLA: sealed or maintenance-free). More details of other storage options in rural microgrids could be found in further reading of the relevant work in [40], [41].

Unlike primary batteries which are designed to be discharged only one time and then discarded, lead-acid batteries are *rechargeable* and called *secondary batteries*.

— ***VLA (open):*** hydrogen and oxygen are vented to the open air through small holes in the vent plugs. To top up water from time to time.

— ***VRLA (sealed):*** hydrogen and oxygen are converted back into water using a pre-inserted catalyzer. These batteries are maintenance-free.

The factors that can enhance battery performance and remaining life are detailed below [42], [43].

— ***Battery Sizing:*** The battery bank size is directly related to cost, reliability, generator operating hours, maintenance cost, life cycle, level of the depth-of-discharge (DoD), and battery life [44]. In remote microgrids, the battery capacity is designed to feed the system load to cover the PV power deficit.

— ***Charge/discharge:*** Charge control plays a vital role in corrosion of active material due to acid concentration. Therefore, a charge control mechanism must protect the battery from overcharge. On the other hand, the battery should not be discharged below the determined cut-off voltage. It is the voltage below which the battery can no longer accomplish the required task. Typically, this voltage is set at 10.5V for a 12V lead-acid battery. A low-priority load cut may be enabled, or a dispatchable source can be turned ON to handle the load and resume battery charging [45].

— ***Operational Impact:*** The system in which batteries discharge frequently and do not restore to the fully charged state is more likely to reduce the battery lifetime. The battery parameters are continuously monitored in a good control strategy to keep system operation within the desired limits [46]. This parameter-driven control could be easily implemented with rule-based energy management system (EMS) [47], [48]. A comparison of different battery technologies is presented using a Ragone plot in Figure 1.15 (adapted from [49]), and which is further summarized using Table 1.3.

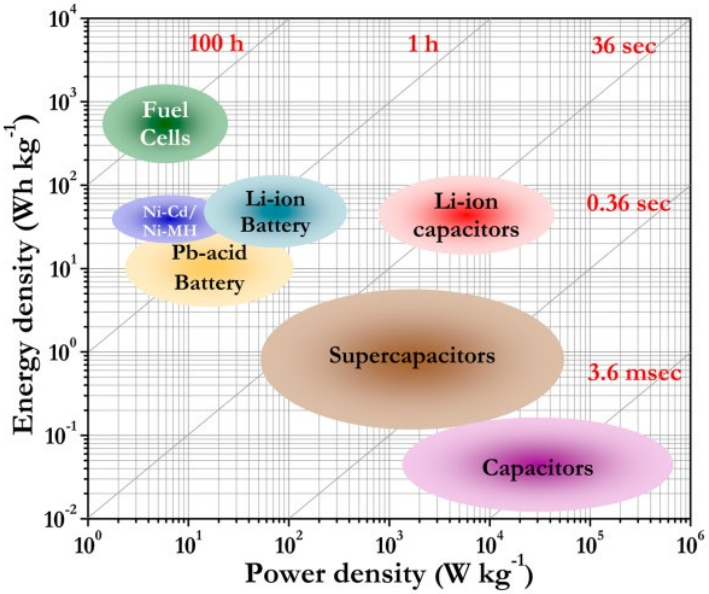

Figure 1.15 – Ragone plot showing the position of lead-acid as a suitable energy storage technology [49]

It is noted that lead-acid batteries have comparatively moderate energy density (needed in low-power applications for long backup) at a relatively lower cost.

Table 1.3— Comparison of different battery technologies [50], [51]

Battery Performance and Cost Comparison

LA: Lead-acid, LI: Li-ion, NAS: Sodium sulfur battery, VRB: Vanadium redox flow battery [50]

Performance parameters	LA	LI	NAS	VRB
Charging efficiency	0.78	0.99	0.89	0.85
Discharge efficiency	0.78	0.99	0.89	0.85
Minimum SoC (SoC_{min})	30%	20%	0%	25%
Maximum SoC (SoC_{max})	100%	100%	100%	100%
Maximum DoD (DoD_{max})	70%	80%	100%	75%
O&M cost (A$/year/kW)	33.4	28.8	68.3	65.2
Number of cycles	1500	2500	2500	12000
The following data is obtained from [51]				
Useful life (years)	10	5–20	15	10–20
Energy cost ($/kWh)	200~400	800~1500	300~500	150~1000
Power density (Wh/kg)	75–300	100–5000	150–230	80–150
Energy density (Wh/kg)	30–50	75–250	150–240	10–75
Operating temperatures (°C)	-20–50	-20–60	300–350	-5–50

Generally, lead-acid batteries have a much lower energy density than Li-ion. However, their low-cost and abundant availability make them an attractive choice for microgrids. On the other hand, lead-acid batteries require more volumetric space due to the lower energy density, which is not a severe issue in rural microgrids. Further information on energy storage, applications, and cost characterization are available in [52], [53]. Researchers are also looking into new promising lead-acid battery hybrids to reduce cost and increase battery power capability, such as the *Ultra battery* (Figure 1.16, proposed by [54], figure adapted from [55]), which is the hybrid of a supercapacitor and battery in the same module.

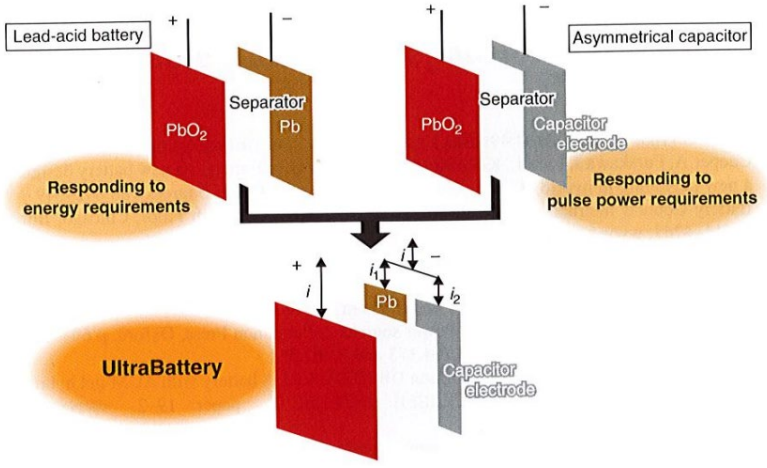

Figure 1.16 – The Ultra battery: supercapacitor and battery in a single module [55]

1.4.1 Low-cost DC Microgrids

Time changes things, so it changed the traditional AC electrical power systems to reshape and perform better in terms of access, efficiency, scalability, and stability. DC microgrids are becoming more attractive with power electronic conversion technology and DC renewable power sources. More than that, batteries, modern low-power DC loads, and the rebirth of DC distribution, all with the natural DC coupling at a comparable efficiency, further increases the technical viability of DC microgrids.

The idea of low-power, low-voltage DC microgrids is not new. Researchers are proposing new distribution architectures, voltage levels, implementation feasibility, and associated challenges for its mass deployment [56]. The grid evolution enabled small-scale microgrids to include more and more energy-efficient and low-cost energy sources and loads. However, it is still too expensive to deploy in rural communities.

(1) DC Microgrids Implementation Feasibility: Today, everything we love and live with are DC operated. Mobile phones, gaming consoles, PC, tablets, network equipment, lighting systems, toys, music players, cameras, electric bikes, and many portable devices are a few examples. DC microgrids are gaining increased interest due to the easy integration of modern low-power DC loads, PV, and storage batteries. It is easier to reduce the number of power converters, allow faster control, and much better efficiency [57]. The following key benefits are the main influencing factors for new energy infrastructures in less developed areas [58]. These exciting benefits also drive consumers to consider a local microgrid as an excellent solution to their evolving energy needs.

Low-cost DC Microgrids: Key Influencing Factors

— ***Efficiency:*** *Low losses due to energy flow in a small distribution circle.*

— ***Reliability:*** *Unlike traditional grid, nearly 100% uptime for critical loads in rural areas. There is no risk of a massive grid catastrophic power loss.*

— ***Security:*** *More secure due to its physical nature and low DC bus voltage.*

— ***Quality:*** *Stable power based on the economical tariffs and usage time.*

— ***Sustainability:*** *Able to utilize more and more indigenous resources.*

— ***On-site power generation:*** *Microgrids can generate power very close to the consumers.*

Microgrids also provide reliable access to electricity at comparatively lower costs [59]. Microgrids can be installed easily anywhere (house, village, hospital, or remote camp) from small-scale to large-scale depending on the available surface and load requirements. Figure 1.20 (adapted from [44]) shows that a reasonable portion of the domestic load could be met at lower costs in community microgrids compared to the standalone basic solar home systems (SHS).

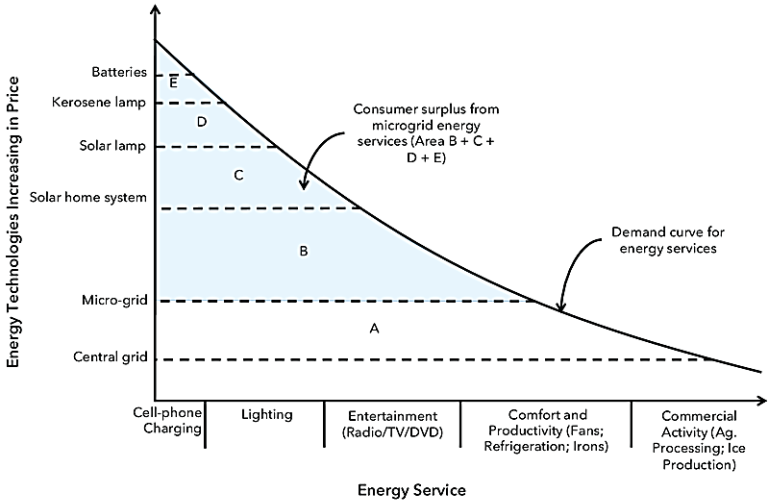

Figure 1.17 – Comparison of cost and energy technologies for electrification services [44]

(2) Declining Prices of PV and Batteries: The declining PV cost using experience curves are depicted in Figure 1.18 [60], [62]. The given cost projections practically make sense as the technology matures and components are produced in bulk, the cost declines [60], [61]. According to [60], each time the cumulative PV production doubles, the price decreases by 25% during the last four decades.

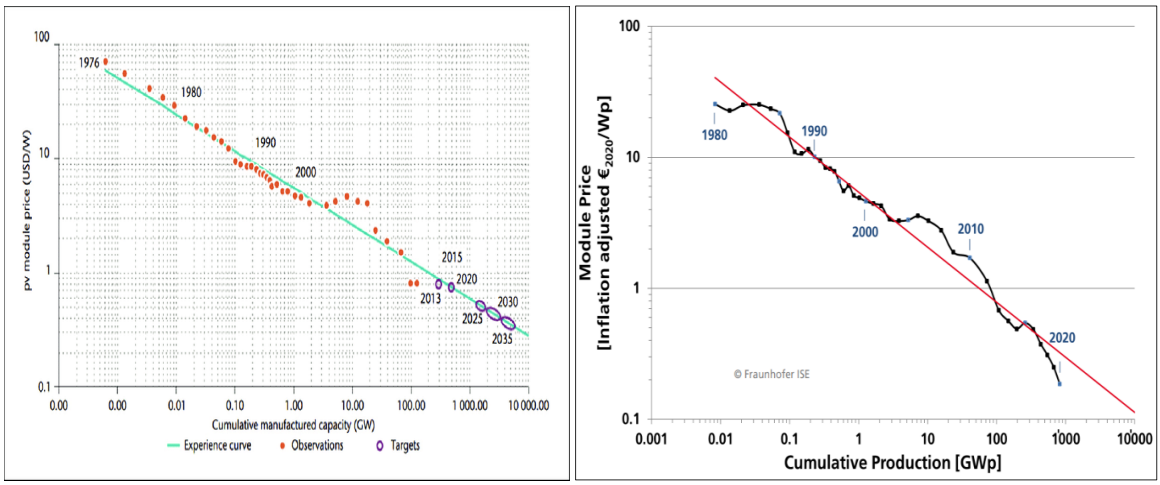

(a) (b)

Figure 1.18 – PV price projections: (a) price in $/W [4][62], (b) inflation-adjusted prices in €/Wp [60]

[4] (a) Orange dots are past prices and purple are future price forecasts (b) price includes all the commercially available PV technologies.

Like PV modules, the battery costs also follow similar downward projections. The use of Li-ion batteries is a current market trend. In the next few years, the lowering price projections could also be directly mapped to the availability of more and more batteries after being decommissioned. In Figure 1.19, following similar PV price trends, when the global battery supply doubles, cost drops by ~19% [63]. In 2020, the average price declines to $137/kWh than $200/kWh in 2017. The prices are estimated to go down $84/kWh in 2025, $57.7 in 2030, nearly a one-third only in a decade [63]. It seems the right time to deploy rural microgrids with the combination of PV and legacy batteries.

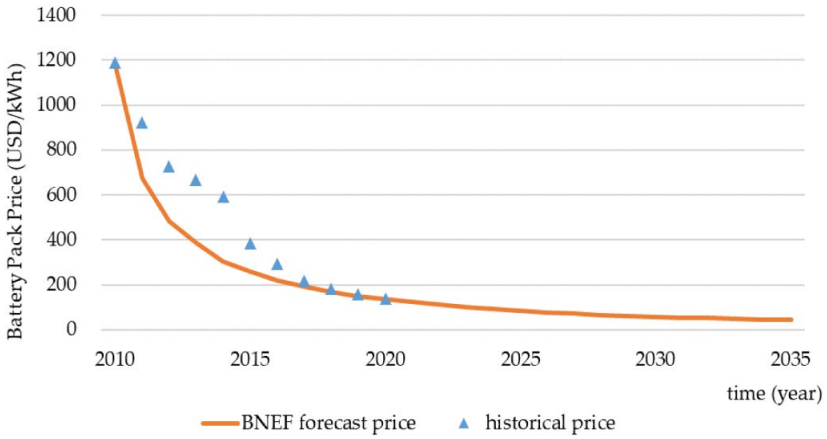

(a) [63]

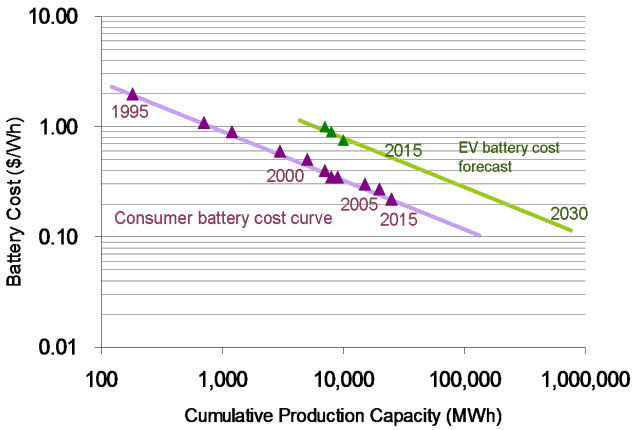

(b) [63]

Figure 1.19 – Experience curve of batteries cost projections [63]: (a) $/kWh (b) $/Wh [5]

1.4.2 PV-Diesel-Battery: An Attractive and Economic Choice

(1) PV-Diesel-Battery Hybrid: Choosing energy sources is central to the system cost, performance, and maintenance [64]. The combination of readily available and indigenous energy sources can supply each home.

[5] Forecasted battery prices: 2025 $96/kWh, 2030 $70/kWh (*source: illustrated by the data from [63]*).

The sources for a low-cost DC microgrid include:

— ***PV*****,** with declining prices and subsidies;

— ***DG*****,** a dispatchable source, available on demand; and

— ***Lead-acid Batteries*****,** their availability in abundance and lower costs, especially in their second-life.

In contrast, the PV system complements DG in large-scale power plants to reduce operational costs. However, in small-scale electrification services, DG can help supply additional energy demand during high loads or extreme weather. The complementary advantages of a hybrid PV-DG-battery system in a remote application are summarized in Table 1.4 [64], [65].

Table 1.4— Feasibility and advantages of a PV-DG-battery microgrid in rural areas [64], [65]

Performance comparison of PV-DG-battery hybrid

Characteristics	*PV*	*Battery*	*DG*	*Hybrid PV-DG-battery*
Reliability *(Social acceptance)*	Highly intermittent nature	Moderate	Highly reliable compromised by fuel availability	Moderate: benefits from both
Size *(Economic aspects)*	The available surface area constrains the size	Suitable for low and mid-range kWh/day	Suitable for high load	Suitable for variable, low, mid, and high range kWh/day
Fuel consumption *(Economic aspects)*	No	No	Proportional to load	Benefits from moderate fuel consumption
Charging cost	Nil	Moderate	Nil	Less constrained
Unit cost/kW	Relatively low	Moderate	Low	Low to moderate
Initial installation cost/kW	Moderate	Low	Low	Low to moderate
Operation cost *(Economic aspects)*	Relatively low	Relatively low	Quite high due to maintenance and fuels	Low to moderate
Maintenance *(Economic aspects)*	Less/infrequent	Less/infrequent	High maintenance at regular intervals	Less burden on the generator, less maintenance
Environmental effects	Nil	Nil in case of delaying recycling	High (emissions concerns due to fuels)	Moderate, could be minimized
Salvage value *(Recycling cost)*	Moderate	Low	Low	Moderate

Performance comparison of PV-DG-battery hybrid				
Loss of load probability *(Reliability)*	High	Moderate	High (depending on fuel availability)	Low, benefits of load handling from one source to another
Nature dependency *(Resilience)*	Highly dependent	Independent	Completely independent	Moderate, could offset one generation source

(2) Key Advantages of the Hybrid Combination: The hybrid generation and storage enhance system maintainability, durability, and reliability. A PV-diesel-battery hybrid is more resilient to weather and operational constraints. The generator is sized to meet cumulative load peaks in a residential or commercial facility[6]. The village can gain several advantages in shifting from individual SHS into a hybrid energy community microgrid [66]. There could be even more environmental and financial gains in powering communal loads and health facilities. Additionally, the microgrid could be put to service in a parameter-driven manner using simple EMS [67], [68] to get an economical and environment bi-objective design [69], [70].

(3) The Ease of Maintenance: A PV-DG-battery architecture enables installers and technicians to decommission or disconnect an energy source for diagnostics, testing, or replacement while other sources could still keep the microgrid up. Compared to other renewable sources such as wind, biomass, and micro-hydro, a PV-diesel-battery hybrid is easier to deploy in any rural environment. However, the technical risks associated with batteries, PV converters, and component failures are frequent and complex.

1.5 Modeling of Legacy Microgrid Components

1.5.1 The Modeling Aspects of System Components

The general architecture of our proposed microgrid model for simulation include PV, DG, and batteries. For the ease of yearly analysis, an average model of the microgrid is simulated using MATLAB®. The optimal operation and best cost are achieved using optimization for the required number of PV, total required batteries, and the size of DG. In off-grid systems, appropriate sizing of PV, DG, and battery is essential for the system's

[6] Refrigeration, water pumping, and purification. Communication apparatus, street lighting, community shops, and power tools could be an additional load in a rural facility.

scalability and adaptability to consumer needs and to minimize annualized cost [71], [72]. In our study, the microgrid has two energy sources (PV and DG), storage batteries (lead-acid), and residential load. We briefly discuss the modeling steps, which are further detailed in CHAPTER-II using mathematical and electrical representation.

(1) PV Modeling: We have used a fixed number of PV panels with no degradation. The project life is same as the PV life, *i.e.*, 20 years. In the average model, PV output power is considered as a function of meteorological condition of the study site.

(2) DG Modeling: The DG is an on-demand dispatchable source that can inject power into the system when renewable sources and storage cannot meet the load demand. The individual parts of a DG could be modeled and sized as per system requirements using SIMULINK®. In [73], additional details are given to model a complete DG for small-scale microgrid applications. In our simulations, we only consider modeling the electrical part of the DG. As a result, fuel consumption and emissions are linked to the total energy produced by the DG using a parametric relationship. In the optimization, we have kept DG on lowest priority to reduce operational cost.

(3) Battery Modeling: The battery can be modeled using electrochemical or equivalent-circuit models. In this work, we focus on the electrical equivalent-circuit models, which are more controllable. The parametric values in electrical circuits can then be used to mathematically model the battery response for simulations in the average microgrid model. The electrical model with 2RC branches in Figure 1.20 is a good compromise between complexity and accuracy. The model can be tuned using the parameters obtained through measurements from our experimental bench in the laboratory.

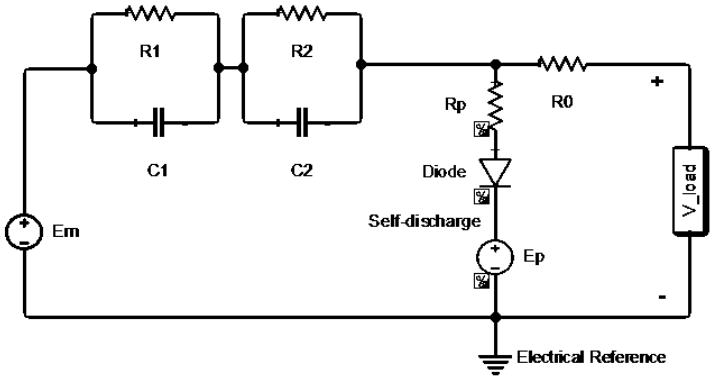

Figure 1.20 – 2RC electrical equivalent-circuit model of a battery cell

The battery parameters are highly non-linear for any change in temperature, open-circuit voltage (V_{oc}), and load current. Therefore, a complex optimization process or curve fitting

could be used to select the best parameters and correlate them to the model. This way, the model could be as realistic as a genuine battery. We have used the degradation impact in the average model of the battery for our microgrid simulations.

(4) Load Modeling: Electricity is not only bringing light to dark places. It also has a significant economic impact on the development of local businesses. Therefore, the rural load becomes a linear sum of domestic and communal/ small-scale commercial loads. In practice, keeping the productive activities, individual needs can emerge, and the corresponding consumption increases. Therefore, a poor load model results in microgrid failure and equipment obsolescence [74]. The computer-based load modeling techniques are a popular way to model the load consumption for any microgrid [75]–[77]. In the case study, we have assumed a yearly load profile for 125 household of 1100 inhabitants with an average total of 500kWh/day consumption by the whole village. The load also accounts for quarterly evolution at an increasing rate of 2.5%.

1.5.2 Design and Simulation Tools for Hybrid PV Systems Modeling

The simulation tools provide the flexibility to quickly analyze the impact of different energy source choices and design configurations [78]. These tools analyze and compare hundreds of possible combinations of conventional sources, renewable sources, battery storage, and loads. The designer can then choose the suitability of a particular design and control scheme to know the behavior of a system before its realization in the pilot demonstration. In general, all simulation tools simplify the design process and run a system before deploying it in the real world. These tools are grouped in the following four categories.

— ***Tools for Component and System Dimensioning:*** Tools such as RETSCREEN®, PVSYST®, and PV*SOL® are used for system sizing. These tools take specific input parameters, such as power consumption, load, degradation, and climatic uncertainty.

— ***Simulation Tools for Modeling Energy Systems:*** These tools can greatly simplify the design process using a few input parameters. It is possible to change the input parameters for an in-depth system performance analysis, *e.g.*, simulating a rural microgrid with component aging using the load profile, battery health, and available PV power. Some of the tools are MATLAB®/SIMULINK®, PSIM®, TRNSYS®, HOMER PRO®, HYBRID2®, and a few more tools detailed in [79], [80].

— ***Research Tools:*** With a high degree of flexibility, such tools are used to simulate a complex system for research purposes. MATLAB® is one such example of a high-standard research tool.

— ***Design Tools:*** Specifically tailored for an application such as planning microgrid layout or designing the distribution architecture. Some tools come with built-in models, while other allow users to design models according to their requirements.

It should be noted that it is not only the quality of the software tool but also the input data and correct simulation mode that determine the accuracy of the results. An executive summary of the software tools is profiled in Table 1.5. The presented tools are not ranked or rated, but their flexibility and features are highlighted. The readers are referred to the IEA report on PV simulation tools for further reading [80].

Table 1.5— Executive summary of the simulation and design tools for hybrid systems

Tool	Features	References
MATLAB®/Simulink *(Research tool)*	*Standard commercial software for detailed research and pre-analysis of a system. Licensed, built-in toolboxes, much more flexible, but learning the software and developing your own models is not easy.*	[79]
RETScreen® PV*SOL® *(Dimensioning tool)*	*Limited available options, used for preliminary study and general dimensioning.*	[79]
HOMER Pro® *(Analysis tool)*	*Apart from technical design and sizing, there are software to analyze the economic impacts, such as HOMER®, which is easy to use, very flexible, and widely used to see the other side of a technically viable system (grave danger of carbon emissions, cost, and life-cycle). A detailed yearly analysis of a hybrid energy system is possible. It is the most popular tool for rapid assessment of the least-cost solution of a clean and reliable power system. Conclusively, HOMER® is more on the economic side of the hybrid microgrids.*	[81]
Hybrid2® *(Simulation tool)*	*EMS and economic analysis functions. Learning the software takes time, but it is best for the design, evaluation, and prediction of hybrid power systems.*	[82]
TRNSYS® (*Simulation tool*)	*Developed by the University of Wisconsin*[7] *mainly for the dynamic simulation of solar systems. This commercial software is highly flexible for solar system design.*	[79]
Additional tools *(Recommended for further reading)*	PYTHON, PVLib, INSEL®, PV-SPS®, PVsyst®	[79]

[7] https://sel.me.wisc.edu/trnsys/features/features.html.

For all the analysis tools in Table 1.5, a hypothetical geographical place is usually one of the input parameters for many tools. For any system modeling, the task is mainly divided into the following three steps.

In the first place, system planners and designers choose a site. It could be any place in the developing world that needs electrification. In our study, this site is a rural village of BURKINA FASO, called GOGMA. In the second step, demand-side requirements and EMS methodologies are estimated. The assessment is done through questionnaires and field surveys or computer tools to generate consumption profiles. For this step, we have assumed a yearly load profile generated using computer tools. Finally, the best option for microgrid design is selected based on the supply-side analysis, available resources, and allocated funds to choose the best economically and technically convenient solution. We have simulated an average model of the overall microgrid system for the ease of yearly simulation and result analysis at a one-hour time-step.

1.5.3 Control and Energy Management

Small electrification systems need proper control as some of the renewable energy sources are intermittent or expensive or both [83]. The supervisory control is designed to have a clear objective to coordinate the energy flow in a multi-energy microgrid [84]. Proper control also minimizes cost and maximizes battery life to operate the system at optimal performance [85], [86]. Poor supervisory control may result in voltage collapse, suboptimal performance, and system failure [87]. Further in-depth analysis of the control schemes could be found in [88], [89]. A supervisory control generally operates on defined rules to ensure reliable and economical microgrid operation. Some of these control characteristics include:

- Economic optimization (optimal operation of the energy sources, reduced maintenance and operational cost);
- Reduce environmental impact;
- Improve supply quality and reliability;
- Prolong battery life; and
- Optimize load sharing and energy exchange.

All such desirable characteristics can be achieved at different control levels. The description of these control stages is as follows.

— ***Local Control:*** is used to control the converter dynamics within a fraction of a second. These control schemes are based on mathematical algorithms to counteract fast disturbances and ensure transient stability. In the decentralized control approach, each component is independently controlled without communication. However, an optimal operation is not possible only with the local parameters. Because of these reasons, most microgrids are controlled using different levels for optimal EMS and power-sharing [90]. A very nice review on different quantification methods and managing intermittent renewable resources is presented in [91].

— ***Primary Control:*** is used to balance the generation and consumption and stabilize the DC bus voltage within the permissible thresholds. Primary control also relies on the local measurements and responds to the disturbances within seconds. Such a control scheme is relatively simple in low-inertia rural microgrids.

— ***Secondary or Supervisory Control:*** Optimizes the generation of all energy sources and storage batteries within their operating limits [92]. It mainly regulates the power flow and keeps the net energy balance within the system [93], [94].

In our study, the supervisory control structure operates on rule-based EMS. Such rules are simple and can be easily implemented for the proposed PV-diesel-battery microgrid, which is more appropriate in a rural context, if the system is to be operated by the local technicians/ operators.

1.6 Chapter Summary

Rural electrification is a point of central discussion in the developing and developed world because of the equal rights to energy access and availability of abundant indigenous resources. After all, *if the consumption is local, why not the generation?* The prime objective of the chapter was a general introduction to enabling energy access using legacy DC microgrids. DC microgrids are believed to be advantageous and economical for electrifying remote areas. The possible future directions in this topic may include an assessment of the community response to such an affordable electrification alternative and knowing the investor confidence in deploying such a small-scale second-life microgrids in the energy-poor countries.

1.7 Motivation and Thesis Objectives

The research questions motivating this study have both technical and social dimensions. Only those electrification systems could be a technological success that can utilize the already available legacies with the rural households to avoid the risk of existing equipment obsolesce. The idea of using legacy batteries and DG is more convincing as they are already being used by the SHS in one or other forms. Otherwise, consumer participation is relatively much more difficult, which is the main cause of microgrid failures in rural areas. This thesis develops a methodological approach to propose legacy batteries and DG for microgrid cost reduction without compromising a certain level of supply reliability.

More precisely, we answer the question: **"*How could the legacy lead-acid batteries and DG be a cost optimal solution for 100% energy access in the rural areas of developing world?*"**. With an in-depth approach to answer the main question, we had focused on the three related questions as the main dissertation goals.

(1): ***"How to operate the rural microgrid within the physical limits of degraded batteries and DG at optimal cost?"***,

(2): ***"What could be compromised for degraded performance?"***, and

(3): ***"At what operational limits and energy cost?"***.

The thesis goals are achieved in a systematic flow from modeling and experimentation to simulating different scenarios and comparison of the obtained results.

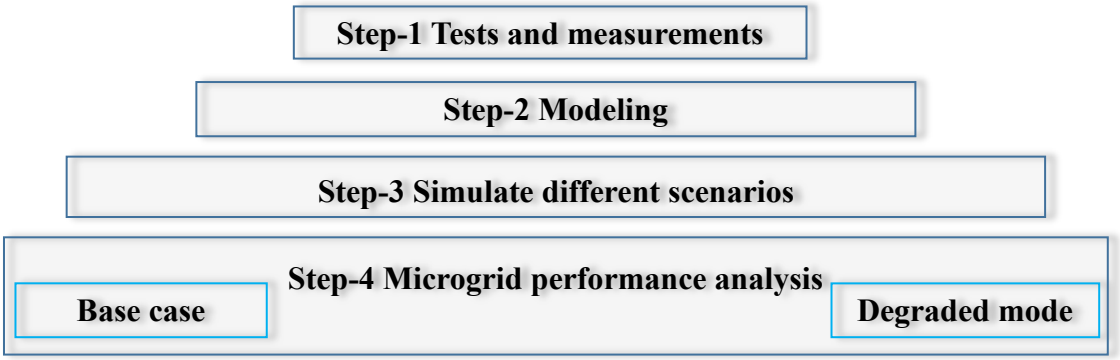

1.8 Thesis Outcomes

The thesis constitutes a step forward in the electrification of rural communities using legacy batteries and DGs. The work involves modeling, measurements, and simulations. The main contributions of the thesis to the existing art are briefly listed as,

- Modified battery physical tests and capacity restoration methods are proposed;
- Two classic battery tests and measurement techniques are proposed for battery health characterization and calculation of actual remaining capacity;
- The validation of second-life hypothesis is done using a modified EMS scheme in a PV-diesel-battery rural microgrid;
- The techno-economic gains of legacy batteries are statistically evaluated; and
- The operational range of the legacy batteries and, in particular, their lowest economical roundtrip efficiencies are analyzed.

1.9 Manuscript Highlights and Organization

This dissertation consists of five chapters in a three-stage approach to model, optimize, and analyze the second-life proposition. The chapters progressively move from introducing the topic, problem formulation, modeling approach, to EMS and performance degradation analysis. The first part of the dissertation is related to the research context including the introduction, problem setting, social aspects of the project, and some propositions. The second portion of the manuscript is more scientific on modeling approach, experimentations, results, and findings.

The dissertation is organized such that each chapter can be read independently with its own bibliographic references, acronyms, and chapter highlights on the respective title pages. We try to deal with the key points and problems discussed above in each chapter. In brief, CHAPTER-I provides a concrete foundation to understand the topic and context, key points and issues related to basic energy access, the technical and scientific stakes of the problem, and the proposed modeling and simulation approach. Then, CHAPTER-II and CHAPTER-III cover modeling and design considerations of the microgrid components. It includes mainly electrical and parametric modeling of microgrid components with and without degradation. CHAPTER-IV is about control, energy management, and aging impact analysis using simulations. The techno-economic data is included to support the presented arguments. Finally, CHAPTER-V concludes the work with a few possible

extensions and suggestions. In a more elaborated form, the chapter highlights are as summarized below.

— **CHAPTER-I: INTRODUCTION AND SCOPE** discusses the reason for developing low-cost electrification systems in simple terms. Discussion of the main issues related to energy access with a bibliographic review of the state of the art highlights the significance of this project to society and the developing world struggling energy access. A DC microgrid architecture that is more suitable to the local conditions is proposed. The chapter also include a brief introduction of the system components and their models.

— **CHAPTER-II: RURAL MICROGRID DESIGN CONSIDERATIONS** provides a well-thought view of electrical modeling and optimal sizing of microgrid components (*PV, DG, battery, and yearly load*). The proposed microgrid architecture and its technical advantages and limitations are introduced.

— **CHAPTER-III: MODELING OF THE AGING DYNAMICS** is about modeling the aging dynamics of batteries and DG. In-depth discussions and related simulations are included to support the validity of used models. The central portion of this chapter covers measurements from our installed battery characterization bench in the laboratory. However, the chapter contains a partial analysis of the individual component. Detailed system operation, energy flow, and performance comparison are in the following chapter.

— **CHAPTER-IV: CONTROL, ENERGY MANAGEMENT, AND AGING IMPACT ANALYSIS** covers comprehensive simulations on the control of an average PV-diesel-battery hybrid model with and without degradation. We have limited our study focus to the degradation of batteries and DG. Further, we analyze and test the overall EMS and control in various operational constraints, system limitations, and meteorological condition. The system is optimally operated at best cost. The chapter concludes with a techno-economic analysis of the degraded mode operation to the base case and the economic gains of the second-life proposition.

— **CHAPTER-V: CONCLUSIONS AND PERSPECTIVES** summarizes the dissertation's framework and provides possible future extensions.

-The end--Chapter-I-*

Bibliography Chapter-I

[1] IEA, IRENA, UNSD, and WEO, "Tracking SDG7: The energy progress report (2019)," May 2019.

[2] IEA, "Energy Access Outlook 2017," IEA, Paris, 2017. Accessed: Nov. 23, 2021. [Online]. Available: https://www.iea.org/reports/energy-access-outlook-2017.

[3] United Nations Report, "World population prospects 2019," UN Population Division, 2019.

[4] USAID and ARE, "Hybrid mini-grids for rural electrification - lessons learned," 2014.

[5] H. Winkler, A. F. Simões, E. L. la Rovere, M. Alam, A. Rahman, and S. Mwakasonda, "Access and affordability of electricity in developing countries," World Development, vol. 39, no. 6, pp. 1037–1050, 2011, doi: https://doi.org/10.1016/j.worlddev.2010.02.021.

[6] A.-K. Gerlach, E. Gaudchau, C. Cader, and V. Wasgindt, "Comprehensive country ranking for renewable energy based mini-grids providing rural off-grid electrification," presented at the 28th EU PVSEC, Sep. 2013, pp. 3806–3817. doi: 10.4229/28thEUPVSEC2013-5DO.13.2.

[7] K. Muralidhar and N. Rajasekar, "A new design and feasible architecture of DC microgrid for rural electrification," International Transactions on Electrical Energy Systems, vol. 31, no. 8, p. e12973, 2021, doi: https://doi.org/10.1002/2050-7038.12973.

[8] DOE, "Summary report: 2012 DOE microgrid workshop," U.S. Dept. Energy:, Washington, DC, USA, Technical report, Jul. 2012.

[9] NASA, "Prediction of worldwide energy resources: Surface meteorology and solar Energy." Accessed: Dec. 20, 2021. [Online]. Available: https://power.larc.nasa.gov/.

[10] L. E. Zubieta, "Are microgrids the future of energy? DC microgrids from concept to demonstration to deployment," in IEEE Electrification Magazine, vol. 4, no. 2, pp. 37–44, 2016, doi: 10.1109/MELE.2016.2544238.

[11] ESMAP, "Mini grids for half a billion people: Market outlook and handbook for decision makers," ESMAP – World Bank, Washington, DC, 014/19 ESMAP, 2019.

[12] J. Dulout and L. F. L. Villa, "Working towards greener golf carts – A study on the second life of lead-acid batteries," in 2019 Fourteenth International Conference on Ecological Vehicles and Renewable Energies (EVER), 2019, pp. 1–5. doi: 10.1109/EVER.2019.8813658.

[13] TECHNAVIO, "Advanced lead-acid battery market by application and geography - Forecast and analysis 2021-2025." https://www.technavio.com/report/advanced-lead-acid-battery-market-size-industry-analysis (accessed Feb. 28, 2022).

[14] D. A. Ghanem and S. Mander, "Designing consumer engagement with the smart grids of the future: bringing active demand technology to everyday life," Technology Analysis & Strategic Management, vol. 26, no. 10, pp. 1163–1175, 2014, doi: 10.1080/09537325.2014.974531.

[15] E. Cecelski, "Enabling equitable access to rural electrification: Current thinking and major activities in energy, poverty and gender," 2002, [Online]. Available: http://hdl.handle.net/11427/22696.

[16] A. H. Hubble and T. S. Ustun, "Composition, placement, and economics of rural microgrids for ensuring sustainable development," Sustainable Energy, Grids and Networks, vol. 13, pp. 1–18, 2018, doi: https://doi.org/10.1016/j.segan.2017.10.001.

[17] A. Kumar, A. R. Singh, Y. Deng, X. He, P. Kumar, and R. C. Bansal, "A novel methodological framework for the design of sustainable rural microgrid for developing nations," IEEE Access, vol. 6, pp. 24925–24951, 2018, doi: 10.1109/ACCESS.2018.2832460.

[18] Md. Mizanur Rahman, "Accomplishing rural electrification for over a billion people: Approaches towards sustainable solutions," Aalto University, Finland, Doctoral dissertation, 2014. [Online]. Available: http://urn.fi/URN:ISBN:978-952-60-5579-4.

[19] F. Barbir and U. Sergio, Sustainable energy production and consumption : benefits, strategies and environmental costing, 1st ed. 2008.

[20] S. C. Bhattacharyya, "Energy access programmes and sustainable development: A critical review and analysis," Energy for Sustainable Development, vol. 16, no. 3, pp. 260–271, 2012, doi: https://doi.org/10.1016/j.esd.2012.05.002.

[21] M. Nasir, H. A. Khan, A. Hussain, L. Mateen, and N. A. Zaffar, "Solar PV-based scalable DC microgrid for rural electrification in developing regions," IEEE Transactions on Sustainable Energy, vol. 9, no. 1, pp. 390–399, 2018, doi: 10.1109/TSTE.2017.2736160.

[22] M. Wackernagel, L. Hanscom, and D. Lin, "Making the sustainable development goals consistent with sustainability," Frontiers in Energy Research, vol. 5, 2017, doi: 10.3389/fenrg.2017.00018.

[23] A. Berizzi, M. Delfanti, D. Falabretti, S. Mandelli, and M. Merlo, "Electrification processes in developing countries: grid expansion, microgrids, and regulatory framework," Proceedings of the IEEE, vol. 107, no. 9, pp. 1981–1994, 2019, doi: 10.1109/JPROC.2019.2934866.

[24] R. Deshmukh, J. Carvallo, and A. Gambhir, Sustainable development of renewable energy mini-grids for energy access: A framework for policy design. LBNL, UC Berkeley, 2016. doi: 10.13140/RG.2.1.3395.5606.

[25] A. N. Zomers, "Rural electrification," University of Twente, Ph.D. thesis, 2001.

[26] IEA, "Global energy & CO2 status report : the latest trend in energy and emissions in 2018," IEA, Paris, France, 2019.

[27] S. Mahapatra and S. Dasappa, "Rural electrification: Optimising the choice between decentralised renewable energy sources and grid extension," Energy for Sustainable Development, vol. 16, no. 2, pp. 146–154, 2012, doi: https://doi.org/10.1016/j.esd.2012.01.006.

[28] IEA, "Cumulative population gaining access to electricity in the Energy for All Case, 2017-2030." IEA, Paris. Accessed: Nov. 22, 2021. [Online]. Available: https://www.iea.org/data-and-statistics/charts/cumulative-population-gaining-access-to-electricity-in-the-energy-for-all-case-2017-2030.

[29] IRENA, "Renewable Energy Statistics 2017," International Renewable Energy Agency, 2017.

[30] T. van der Schoor and B. Scholtens, "Power to the people: Local community initiatives and the transition to sustainable energy," Renewable and Sustainable Energy Reviews, vol. 43, pp. 666–675, 2015, doi: https://doi.org/10.1016/j.rser.2014.10.089.

[31] R. Zahira, D. Lakshmi, G. Ezhilarasi, P. Sivaraman, C. N. Ravi, and C. Sharmeela, "Stand-alone microgrid concept for rural electrification: a review," in Residential Microgrids and Rural Electrifications, S. Padmanaban, C. Sharmeela, P. Sivaraman, and J. B. Holm-Nielsen, Eds. Academic Press, 2022, pp. 109–130. doi: https://doi.org/10.1016/B978-0-323-90177-2.00013-X.

[32] O. Krishan and S. Suhag, "Techno-economic analysis of a hybrid renewable energy system for an energy poor rural community," Journal of Energy Storage, vol. 23, pp. 305–319, Jun. 2019, doi: 10.1016/j.est.2019.04.002.

[33] N. M. Kumar, S. S. Chopra, A. A. Chand, R. M. Elavarasan, and G. M. Shafiullah, "Hybrid renewable energy microgrid for a residential community: A techno-economic and environmental perspective in the context of the SDG7," Sustainability (Basel, Switzerland), vol. 12, no. 10, p. 3944, 2020.

[34] IEA, "Social, economic and organizational framework for sustainable operation of PV hybrid systems within mini-grids," Report IEA-PVPS T11-05:2011, 2011.

[35] O. D. T. Odou, R. Bhandari, and R. Adamou, "Hybrid off-grid renewable power system for sustainable rural electrification in Benin," Renewable energy, vol. 145, pp. 1266–1279, 2020.

[36] Y. Liu, C. Farnell, K. George, H. A. Mantooth, and J. C. Balda, "A scaled-down microgrid laboratory testbed," in 2015 IEEE Energy Conversion Congress and Exposition (ECCE), 2015, pp. 1184–1189. doi: 10.1109/ECCE.2015.7309825.

[37] A. Hirsch, Y. Parag, and J. Guerrero, "Microgrids: A review of technologies, key drivers, and outstanding issues," Renewable and Sustainable Energy Reviews, vol. 90, pp. 402–411, 2018, doi: https://doi.org/10.1016/j.rser.2018.03.040.

[38] L. Mariam, M. Basu, and M. F. Conlon, "Microgrid: Architecture, policy and future trends," Renewable and Sustainable Energy Reviews, vol. 64, pp. 477–489, 2016, doi: https://doi.org/10.1016/j.rser.2016.06.037.

[39] K. R. Bullock, "Lead/acid batteries," Journal of power sources, vol. 51, no. 1–2, pp. 1–17, 1994.

[40] IRENA, "Electricity storage and renewables for island power: A guide for decision makers." IRENA, pp. 1-48, 2012.

[41] S. S. Misra, S. L. Mraz, J. D. Dillon, and D. B. Swanson, "VRLA battery with AGM-gel hybrid for superior performance," in The 25th International Telecommunications Energy Conference, INTELEC '03, 2003, pp. 378–382.

[42] "IEEE Guide for optimizing the performance and life of lead-acid batteries in remote hybrid power systems," IEEE Std 1561-2019 (Revision of IEEE Std 1561-2007), pp. 1–34, Jun. 2019.

[43] "IEEE Guide for selecting, charging, testing, and evaluating lead-acid batteries used in stand-alone photovoltaic (PV) systems," in IEEE Std 1361-2014 (Revision of IEEE Std 1361-2003), pp. 1–39, Jun. 2014.

[44] M. Fantauzzi, D. Lauria, F. Mottola, and A. Scalfati, "Sizing energy storage systems in DC networks: A general methodology based upon power losses minimization," Applied Energy, vol. 187, pp. 862–872, Feb. 2017, doi: 10.1016/j.apenergy.2016.11.044.

[45] N. N. A. Bakar, M. Y. Hassan, M. F. Sulaima, M. N. Mohd Nasir, and A. Khamis, "Microgrid and load shedding scheme during islanded mode: A review," Renewable and Sustainable Energy Reviews, vol. 71, pp. 161–169, May 2017, doi: 10.1016/j.rser.2016.12.049.

[46] G. Chaudhary, J. J. Lamb, O. S. Burheim, and B. Austbø, "Review of energy storage and energy management system control strategies in microgrids," Energies (Basel), vol. 14, no. 16, p. 4929, 2021.

[47] J. J. Martínez, J. A. Padilla-Medina, S. Cano-Andrade, A. Sancen, J. Prado, and A. I. Barranco, "Development and application of a Fuzzy control system for a lead-acid battery bank connected to a DC microgrid," International Journal of Photoenergy, vol. 2018, pp. 1–14, 2018.

[48] R. R. Deshmukh, M. S. Ballal, and H. M. Suryawanshi, "A fuzzy logic based supervisory control for power management in multibus DC microgrid," IEEE Transactions on Industry Applications, vol. 56, no. 6, pp. 6174–6185, 2020, doi: 10.1109/TIA.2020.3012415.

[49] V. Aravindan, J. M. S. Gnanaraj, Y.-S. Lee, and S. Madhavi, "Insertion-type electrodes for nonaqueous Li-ion capacitors.," Chemical reviews, vol. 114 (23), pp. 11619–11635, 2014.

[50] B. Battke, T. S. Schmidt, D. Grosspietsch, and V. H. Hoffmann, "A review and probabilistic model of lifecycle costs of stationary batteries in multiple applications," Renewable and Sustainable Energy Reviews, vol. 25, pp. 240–250, Sep. 2013, doi: 10.1016/j.rser.2013.04.023.

[51] H. L. Ferreira, R. Garde, G. Fulli, W. Kling, and J. P. Lopes, "Characterisation of electrical energy storage technologies," Energy, vol. 53, pp. 288–298, May 2013, doi: 10.1016/j.energy.2013.02.037.

[52] I. Hadjipaschalis, A. Poullikkas, and V. Efthimiou, "Overview of current and future energy storage technologies for electric power applications," Renewable and Sustainable Energy Reviews, vol. 13, no. 6, pp. 1513–1522, Aug. 2009, doi: 10.1016/j.rser.2008.09.028.

[53] K. Mongird, et al., "Energy storage technology and cost characterization report." US Department of Energy, Jul. 2019.

[54] A. Cooper, J. Furakawa, L. Lam, and M. Kellaway, "The UltraBattery—A new battery design for a new beginning in hybrid electric vehicle energy storage," Journal of Power Sources, vol. 188, no. 2, pp. 642–649, 2009.

[55] R. J. Brodd, Batteries for sustainability: selected entries from the Encyclopedia of sustainability science and technology. New York: Springer, 2013.

[56] A. T. Elsayed, A. A. Mohamed, and O. A. Mohammed, "DC microgrids and distribution systems: An overview," Electric Power Systems Research, vol. 119, pp. 407–417, Feb. 2015, doi: 10.1016/j.epsr.2014.10.017.

[57] L. E. Zubieta, "DC microgrids from concept to demonstration to deployment," in IEEE Electrification Magazine, vol. 4, no. 2, pp. 37–44, 2016, doi: 10.1109/MELE.2016.2544238.

[58] R. L. Dohn, "The business case for microgrids." Siemens, White papers, pp. 1-9, 2011.

[59] J. Carvallo, D. Schnitzer, D. Lounsbury, R. Deshmukh, J. Apt, and D. Kammen, "Microgrids for rural electrification: A critical review of best practices based on seven case studies," UC Berkeley, pp. 1-122, Feb. 2014. doi: 10.13140/RG.2.1.1399.9600.

[60] "Fraunhofer ISE: Photovoltaics report," Fraunhofer Institute for Solar Energy Systems, ISE with support of PSE Projects GmbH, Jul. 2021.

[61] Jäger-Waldau, Arnulf, "Snapshot of photovoltaics - March 2021," EPJ Photovolt., vol. 12, p. 2, 2021, doi: 10.1051/epjpv/2021002.

[62] IEA, "Technology roadmap - Solar photovoltaic energy," Paris, 2014.

[63] "Bloomberg New Energy Finance (BNEF). Electric Vehicle Outlook 2021; BNEF: New York, NY, USA, 2021."

[64] M. S. Ismail, M. Moghavvemi, and T. M. I. Mahlia, "Techno-economic analysis of an optimized photovoltaic and diesel generator hybrid power system for remote houses in a tropical climate.," Energy Conversion and Management, vol. 69, pp. 163–173, 2013.

[65] N. Williams, P. Jaramillo, J. Taneja, and T. S. Ustun, "Enabling private sector investment in microgrid-based rural electrification in developing countries: A review," Renewable and Sustainable Energy Reviews, vol. 52, pp. 1268–1281, Dec. 2015, doi: 10.1016/j.rser.2015.07.153.

[66] ARE, "Hybrid power systems based on renewable energies: A suitable and cost-competitive solution for rural electrification." 2008.

[67] J. D. Lara, D. E. Olivares, and C. A. Cañizares, "Robust energy management of isolated microgrids," IEEE Systems Journal, vol. 13, no. 1, pp. 680–691, 2019, doi: 10.1109/JSYST.2018.2828838.

[68] B. Asare-Bediako, W. L. Kling, and P. F. Ribeiro, "Home energy management systems: evolution, trends and frameworks," 2012 47th International Universities Power Engineering Conference (UPEC), pp. 1–5, 2012.

[69] M. Bortolini, M. Gamberi, A. Graziani, and F. Pilati, "Economic and environmental bi-objective design of an off-grid photovoltaic–battery–diesel generator hybrid energy system," Energy Conversion and Management, vol. 106, pp. 1024–1038, Dec. 2015, doi: 10.1016/j.enconman.2015.10.051.

[70] R. W. Wies, R. A. Johnson, A. N. Agrawal, and T. J. Chubb, "Simulink model for economic analysis and environmental impacts of a PV with diesel-battery system for remote villages," IEEE Transactions on Power Systems, vol. 20, no. 2, pp. 692–700, 2005, doi: 10.1109/TPWRS.2005.846084.

[71] B. Zhao, X. Zhang, P. Li, K. Wang, M. Xue, and C. Wang, "Optimal sizing, operating strategy and operational experience of a stand-alone microgrid on Dongfushan Island," Applied Energy, vol. 113, pp. 1656–1666, Jan. 2014, doi: 10.1016/j.apenergy.2013.09.015.

[72] Y. B. Aemro, P. Moura, and A. T. de Almeida, "Design and modeling of a standalone DC-microgrid for off-grid schools in rural areas of developing countries," Energies (Basel), vol. 13, no. 6379, p. 6379, 2020.

[73] T. Theubou, R. Wamkeue, and I. Kamwa, "Dynamic model of diesel generator set for hybrid wind-diesel small grids applications," in 25th IEEE Canadian Conference on Electrical and Computer Engineering (CCECE), 2012, pp. 1–4. doi: 10.1109/CCECE.2012.6334849.

[74] Á. Herraiz-Cañete, D. Ribó-Pérez, P. Bastida-Molina, and T. Gómez-Navarro, "Forecasting energy demand in isolated rural communities: A comparison between deterministic and stochastic approaches," Energy for Sustainable Development, vol. 66, pp. 101–116, 2022, doi: https://doi.org/10.1016/j.esd.2021.11.007.

[75] G. Prinsloo, R. Dobson, and A. A. Mammoli, "Smart village load planning simulations in support of digital energy management for off-grid rural community microgrids," Current Alternative Energy, vol. 2, no. 1, pp. 1–18, 2018.

[76] A. Arif, Z. Wang, J. Wang, B. Mather, H. Bashualdo and D. Zhao, "Load modeling—A review," in IEEE Transactions on Smart Grid, vol. 9, no. 6, pp. 5986–5999, Nov. 2018.

[77] D. Nilsson and A. Sannino, "Load modelling for steady-state and transient analysis of low-voltage dc systems," in Conference Record of the 2004 IEEE Industry Applications Conference, 2004. 39th IAS Annual Meeting., 2004, vol. 2, pp. 774–780. doi: 10.1109/IAS.2004.1348502.

[78] S. Phrakhonkham, J.-Y. Lechenadec, D. Diallo, and C. Marchand, "Optimisation software tool review and the need of alternative means for handling the problems of excess energy and mini-grid configuration: A case study from Laos," in ASEAN Symposium on Power and Energy Systems, Sep. 2009, pp. 53–58.

[79] S. Sinha and S. S. Chandel, "Review of software tools for hybrid renewable energy systems," Renewable and Sustainable Energy Reviews, vol. 32, pp. 192–205, Apr. 2014, doi: 10.1016/j.rser.2014.01.035.

[80] IEA, "World-wide overview of design and simulation tools for hybrid PV systems," International Energy Agency, IEA PVPS Task 11, pp. 1–29, 2011.

[81] S. Bahramara, M. P. Moghaddam, and M. R. Haghifam, "Optimal planning of hybrid renewable energy systems using HOMER: A review," Renewable and Sustainable Energy Reviews, vol. 62, pp. 609–620, Sep. 2016, doi: 10.1016/j.rser.2016.05.039.

[82] A. Lyden, R. Pepper, and P. G. Tuohy, "A modelling tool selection process for planning of community scale energy systems including storage and demand side management," Sustainable Cities and Society, vol. 39, pp. 674–688, May 2018, doi: 10.1016/j.scs.2018.02.003.

[83] J. Philip et al., "Control and implementation of a standalone solar photovoltaic hybrid system," IEEE Transactions on Industry Applications, vol. 52, no. 4, pp. 3472–3479, 2016, doi: 10.1109/TIA.2016.2553639.

[84] A. D. A. Bidram, "Hierarchical structure of microgrids control system," IEEE Transactions on Smart Grid, vol. 3, no. 4, pp. 1963–1976, 2012, doi: 10.1109/TSG.2012.2197425.

[85] A. M. Ameen, J. Pasupuleti, and T. Khatib, "Simplified performance models of photovoltaic/diesel generator/battery system considering typical control strategies," Energy Conversion and Management, vol. 99, pp. 313–325, Jul. 2015, doi: 10.1016/j.enconman.2015.04.024.

[86] K. Kusakana, "Operation cost minimization of photovoltaic–diesel–battery hybrid systems," Energy, vol. 85, pp. 645–653, Jun. 2015, doi: 10.1016/j.energy.2015.04.002.

[87] L. Meng, E. R. Sanseverino, A. Luna, T. Dragicevic, J. C. Vasquez, and J. M. Guerrero, "Microgrid supervisory controllers and energy management systems: A literature review," Renewable and Sustainable Energy Reviews, vol. 60, pp. 1263–1273, 2016, doi: https://doi.org/10.1016/j.rser.2016.03.003.

[88] F. Perez, "Control of AC/DC microgrids with renewables in the context of smart grids: including ancillary services and electric mobility," Université Paris-Saclay, Ph.D. Dissertation, 2020.

[89] J. Kumar, A. Agarwal, and V. Agarwal, "A review on overall control of DC microgrids," Journal of Energy Storage, vol. 21, pp. 113–138, 2019, doi: https://doi.org/10.1016/j.est.2018.11.013.

[90] C. Yin, H. Wu, M. Sechilariu, and F. Locment, "Power management strategy for an autonomous DC microgrid," Applied Sciences, vol. 8, no. 11, 2018, doi: 10.3390/app8112202.

[91] M. F. Zia, E. Elbouchikhi, and M. Benbouzid, "Microgrids energy management systems: A critical review on methods, solutions, and prospects," Applied Energy, vol. 222, pp. 1033–1055, Jul. 2018, doi: 10.1016/j.apenergy.2018.04.103.

[92] M. Tucci, L. Meng, J. M. Guerrero, and G. Ferrari-Trecate, "Stable current sharing and voltage balancing in DC microgrids: A consensus-based secondary control layer," Automatica, vol. 95, pp. 1–13, Sep. 2018, doi: 10.1016/j.automatica.2018.04.017.

[93] S. Sinha and P. Bajpai, "Power management of hybrid energy storage system in a standalone DC microgrid," Journal of Energy Storage, vol. 30, 101523, pp. 1–12, 2020.

[94] H. Mahmood and J. Jiang, "Decentralized power management of multiple PV, battery, and droop units in an islanded microgrid," IEEE Transactions on Smart Grid, vol. 10, no. 2, pp. 1898–1906, 2019, doi: 10.1109/TSG.2017.2781468.

CHAPTER-II: RURAL MICROGRID DESIGN CONSIDERATIONS

KEY TERMS

DC microgrid architecture, PV-diesel-battery hybrid, sizing, SIMPOWERSYSTEMS™, energy system modeling, parametric tuning, system constraints, energy management.

ACRONYMS

DG	Diesel generator
DoD	Depth-of-discharge
EMS	Energy management system
kW	kilowatt
LF	Load factor
LCOE	Levelized cost of energy
LMSE	Least mean square estimator
MLC	Microgrid lifetime cost ($)
MPP	Maximum power point
RES	Renewable energy source
SHS	Solar home system
SoC	State-of-charge
SoH	State-of-health
STC	Standard test conditions
V_{oc}	Open-circuit voltage

CHAPTER HIGHLIGHTS

This chapter provides the modeling steps of a microgrid with a technological state of the current art. We first present the different analytical approaches for the modeling of microgrid energy sources and loads. In parallel, we provide the electrical and mathematical representation of the proposed models and their working. Then, we describe the energy cost modeling and system configuration for the energy flow and resource sharing. The chapter concludes with a description of the operational strategy and energy flow model of the proposed system.

CONTENTS

CHAPTER 2

RURAL MICROGRID DESIGN CONSIDERATIONS

The trending use of renewable energy sources (RES) tremendously changed the traditional grid, but the microgrids are also going through this transition [1]. Microgrid structures are rapidly evolving with the consumer energy demand, local conditions, available finances, and socio-economic benefits. These architectures are designed to split and feed the local load in a distributed manner to maximize the benefits of utilizing indigenous resources. The ultimate goal is to decrease the energy cost, remove technological barriers, define success factors, increase social acceptance of the energy technologies, formulate standards, and provide solutions for the rapid commercial growth of utility-scale microgrids in the underdeveloped world [2], [3].

In this chapter, we entered into a more detailed discussion on modeling aspects of the microgrid components. This chapter provides a technical description of the system (physical layout and features), design steps, and system constraints. The developed framework will provide a basis for the simulation of a typical rural microgrid.

2.1 Architecture of the Proposed System

The system feasibility, choice of energy sources, financial benefits, and a decision on the system architecture is the first and most crucial step for designers and microgrid managers. The local electrification systems must be flexible to be adapted more closely to the local conditions, load profile, safe voltage level, and efficient utilization of the available energy resources [4]. The system designers choose many possible options to balance cost and performance [5]. Though other renewables such as wind and biomass have attracted attention from the system planners, they may not suit small-scale rural electrification. The wind power is too site-specific and suits only large-scale microgrids.

On the other hand, biomass has environmental impacts and cannot be sized close to the community load of a few kilowatts (kW). Biomass plants are primarily preferred for combined heat and cooking power, which is not a requirement for basic electricity access. Undeniably, with many advantages, these technologies may not best fit the village-scale microgrids in the underdeveloped world. As the affordable energy access issues concern the population in SOUTH ASIA and SUB-SAHARAN AFRICA, all with considerable irradiance power and less electrification rate, such as our study site in the village GOGMA, BURKINA FASO. Therefore, a low-budget standalone PV-hybrid is feasible and economical [6].

2.1.1 System Configuration

(1) Description: Photovoltaics (PV), with lower prices and subsidies, is the first choice as an energy source in community-scale microgrids. In off-grid communities, utilization of the already in use batteries, diesel generators (DGs), and PV panels in small SHS is a challenge but also an opportunity. It is possible to integrate these locally available energy sources to design a community microgrid with the minimum installation cost. It can also increase consumer participation and favor the environment as the legacy equipment may not go obsolete.

(2) System Schematic: The most feasible system schematic for our proposed microgrid was detailed in SECTION 1.4 by using Figure 1.14. It can be easily adapted to the geographic distribution of rural households. The proposed configuration is more suitable for rural household conditions as people live in the form of clusters in a typical village. In addition, it is easier to accommodate more consumers and energy sources using the scalability feature of the microgrid. For more clarity, key features of the system architecture are listed in Table 2.6. The proposed system consists of a standalone PV system, acting as the primary RES. The low bus voltage requires less protection against direct contact, so it is more practical for rural systems, where less technically skilled people or technicians are supposed to operate and maintain the system. The battery power packs consist of weak and fresh batteries. The 12V 100Ah lead-acid batteries are easily available in the local market and on-site solar home systems (SHS). Therefore, other type of storage options is ignored. We have optimized and simulated an average microgrid model. It is the designer's choice to allocate a specific number of PV panels, batteries, and DG in the system. The average consumption of 4kWh/day/household accumulates to total daily consumption of 500kWh for 125 households by 1100 inhabitants.

Table 2.6— Description and specifications of the system

Microgrid components	Specifications and functions
PV	Utilization on highest priority, fixed (non-tracking) mounts
Batteries	
Type	Lead-acid/ *VRLA
Ah rating	100Ah
DG	Minimum 30kW to take load and charge batteries Utilization with lowest priority to minimize cost
Load	Yearly load profile
Total households/ inhabitants	125/1100
Daily energy consumption	500kWh
Control and Energy Management	Based on local measurements
System optimization	Hybrid PSO-GA
Energy dispatch strategy	Rule-based

*VRLA: Valve-regulated lead-acid

2.1.2 Comparison of Modeling and Simulation Tools

The four main stages of a microgrid design project include pre-feasibility, energy sources selection and their sizing, simulations, and performance testing using different dispatch strategies and scenarios. Among the design steps, simulation is the most critical stage to see a global view of the system performance under particular cost and source constraints. For further reading, a classic comparison of different software tools for sizing and designing can be found in publications [7]–[9]. It is worth noting that the pre-feasibility, system configuration, and sizing tools are usually simple and used by the system installers and planners in the first phase of a microgrid project. The scientists and engineers use the more involved and complex software tools for the system performance evaluation, control, dispatch strategies, and optimum operation [10].

In Table 2.7 (inspired from the related work in [9], [11]), we provide summary information, desired features, capabilities, target applications, and end-users of the existing tools for microgrid design and planning at the industry or academic level.

Table 2.7— Desired features of the software tools for microgrid designing

Target Applications	Tool Features	Users
Pre-feasibility	Automates the initial calculations and provides a rough sizing, financial analysis, energy cost, and a global view of the system layout and net cost. Available as a spreadsheet or integrated apps with a simple code.	Consultants, planners, vendors
Sizing or dimensioning	Determine the size of energy components based on the desired energy requirement, scenarios, and location. Such tools give different system configurations and roughly calculate system size and cost. These packages come with their component library. However, they are usually fixed and pre-defined and not easy to modify.	Installers, dealers, technologists, and technicians
Simulations	Determine the system's behavior based on the size and capabilities of the sources and loads. Scientists in universities or research centers usually develop such tools. Some are free, but the majority of them are paid.	Developers, researchers
Open architecture	Allows users to create and modify the algorithms, change default parameters, design their own models, dispatch strategies, and simulation time-steps for better accuracy such as MATLAB®/Simulink®, with plenty of library components. These are usually the tools of choice for research units and Universities. They are relatively too complex to use and paid/licensed. However, researchers can confidently evaluate the impact of components and scenarios or a new methodology and concept with whatever strategy they choose for a target application.	Researchers, engineers, developers

The pre-feasibility and sizing tools are usually small packages, user-friendly, quick, and easy to use. Also, the open architecture and simulations tools are more flexible, adaptable, and configurable and have vast modifiable library components, but require heavy computational resources. The computational burden is due to the intensive sensitivity analysis of many parameters and the level of model complexity. On the other hand, the pre-feasibility spreadsheets can give only one result. A comparison becomes challenging to distinguish the technical and economic advantages. Therefore, even if technicians and installers can use a comparison table to analyze pre-feasibility, it is still time-consuming and cumbersome. Some of these advantages and concerns leave the final choice to the researcher for the best tool selection.

The commonly used software tools were briefly discussed in CHAPTER-I, SUBSECTION 1.5.2. In this subsection, the authors select only the tools used in this study.

(1) MATLAB®: Provides a flexible environment to build models of the system components and determine their interaction within the system. It provides a user-friendly interface to model the dynamic performance of microgrid components using theoretical equations or experimental data. The developed models can conveniently simulate linear, centralized, or distributed microgrid systems. Linear architecture is the simplest form of a microgrid when it directly powers a single facility from dedicated energy sources. In addition, it is easier to implement different optimization and control strategies with or without constraints and determine system performance. Some of the great modeling examples of microgrid components in SIMPOWER/ SIMULINK® are detailed in [12].

(2) HOMER PRO®: A tool for '*easy to learn, design, and quickly evaluate'* is a well-known hourly simulation and assessment tool for designing hybrid energy microgrids [13]. The tool has the flexibility of a robust sensitivity analysis allowing users to compare hundreds of possibilities in a single run. With its easy and user-friendly interface, one can quickly evaluate a small-scale rural microgrid to a large-scale grid-connected system. These features enable the designers to see the impact of a scenario, constraint, or parameter evolution. In addition, HOMER® can capture system dynamics faster and in a more convenient way. Figure 2.21 (adapted from [13]) illustrates the hourly variation of PV power, load demand, and battery state-of-charge (SoC) for a sample week. This plot depicts the rise and drop of the battery SoC as a function of the available PV power and load. HOMER® records these constraints when the final results are compared at the end of the yearly simulations. However, it is possible to get the same kind of results with more flexibility in modeling the average microgrid system in MATLAB®. We, therefore, used HOMER® only to model the yearly load for the study location.

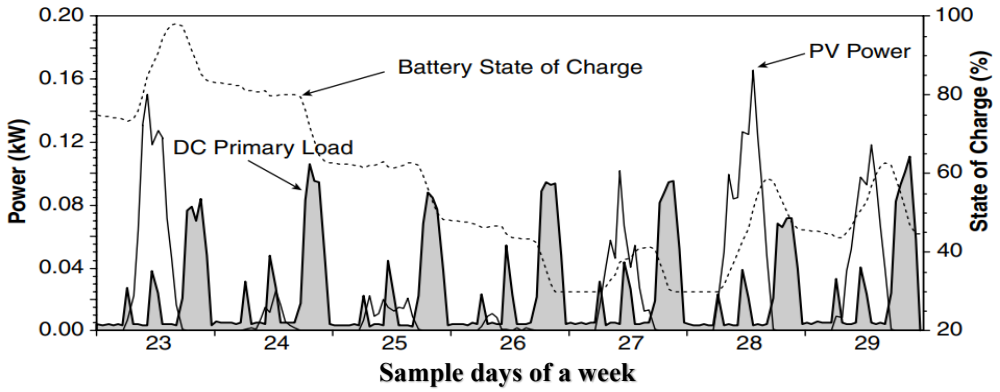

Figure 2.21 – Sample simulation results of a PV-battery system using HOMER® [13]

Though, MATLAB® software is primarily used as a numeric computational tool with its technical programming environment. It is paired with SIMULINK® to design systems from thousands of library components. The graphical interface allows the designer to configure any arrangement of the PV, converters, batteries, and load. We have developed some of the models in MATLAB® R2021b SIMPOWERSYSTEMS™ toolbox. It allows users to choose among many options such as energy sources, loads, and power electronic switches to model a physical system. The flexibility of design and control make SIMULINK® SIMPOWERSYSTEMS™ a standard platform for designing and simulating electrical energy systems. Conclusively, MATLAB® outclasses all other available options as a high-standard research tool based on the different performance parameters of which the most prominent one is control, optimization, and a vast library [14], [15], [16]. We use this tool to model and optimize the average microgrid model and analyze the energy flow within the system components.

2.2 Analytical and Physical Modeling of System Components

This section describes the physical and analytical models of PV, DG, battery, and loads in order to simulate a typical rural microgrid. The operational characteristics of each system component are greatly discussed in their relevant subsections. The system size is affected by several factors such as type of energy sources, rated power and voltage level, load, usage hour, consumer income, willingness to pay for the services, capital expenditures, and operational cost. Among many, load determines the efficient way of utilizing microgrid energy resources. Serving loads is the reason for the existence of an electrification system, so we start with the load modeling.

2.2.1 Load Modeling

Rural load modeling is considered the first step in designing a local microgrid. The overall component sizing and power rating of the energy sources and battery storage are based on system load profile. The load profile also significantly impacts the design and performance as each household has a unique and random energy consumption pattern.

Although the rural load is merely an energy demand for lighting, low-power appliances, small entertainment devices, and a few kW of community loads, the design may be relatively complex due to load evolution, highly unpredictable lifestyle, electricity-dependent culture, consumer behavior, the local conditions, and available finances [16]. Therefore, designing a local microgrid is relatively challenging due to these

technical limitations. In addition, the household load changes depending on many factors such as time, weather, population growth, and the economic condition of consumers. Considering all these factors, designers and engineers use small computer-based model approaches to design loads [17]. Practically, we can eliminate the industrial load in a rural context and only consider domestic and small-scale commercial load. Generally, the load profile could be split into the following categories,

- Load that remains constant throughout the year;
- Load that depends on the season, *i.e.*, summer or winter;
- Time-dependent load (specific to day or night);
- Critical load, like a refrigerator in a small community hospital; and
- Other community loads like street lighting for public safety.

A typical hourly load profile is depicted in Figure 2.22. The 24-hours consumption hypothesis is split into five distinct periods. The load profile shows two peaks in the morning (06h30-11h00) and the evening (17h00-22h00). It is assumed that there is no seasonal variation to simplify our initial analysis. It is then designer's choice to choose the best combination if the load is handled by PV only, PV-DG only, or PV-DG-battery hybrid with minimal costs [18], [19]. In addition, a load consumption hypothesis is enlisted in Table 2.8 [20], which is based on the load profile depicted in Figure 2.22[11]. The peak consumption during the evening is attributed to lighting and entertainment only in the period 17h00 to late evening 22h00.

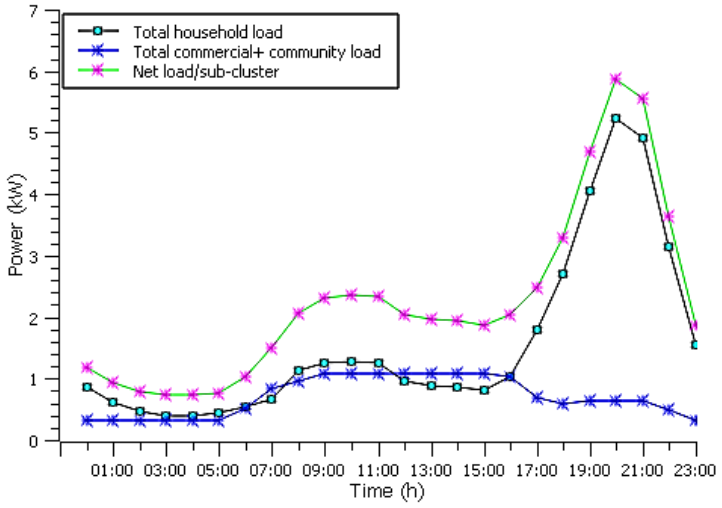

Figure 2.22 – Load profile of rural household for a typical day [20]

[11] Plotting tool: SciDAVis® , plot data from NREL [20].

Table 2.8— Load consumption hypothesis for a typical day [20]

Time	Scenario
00h00-06h00	Low-load period (late night)
06h00-09h00	Morning peak (average load demand)
09h00-17h00	Low household load, high community load
17h00-22h00	Evening peak (high household demand)
22h00-00h00	Low-load period (midnight)

The community load has a relatively flat load profile compared to household consumption. In an energy deficit, the DG is used to supply the system and charge batteries. However, improper load design may lead to voltage collapse, stress on batteries, fluctuations, and failure of the electrification system if the DG operation is restricted to minimize the overall system cost. In our simulation, we compromise a portion of the load for reduction of DG operational cost. It is done using a load cut in the event of a shortfall.

2.2.2 PV Modeling and Design Considerations

PV is an attractive RES due to its low-cost, universal availability, and noiseless operation. The technology has gained prominence due to its negligible environmental impact and long life. The PV module prices are getting lower. Their availability in the local market is now much more accessible. As a small-scale business case, the local availability of PV modules also stimulates the local economy and the development of local businesses. Therefore, PV power production is considered the most suitable and economical renewable generation technology in rural sites [21]. One of the superior advantages of PV is that more modules could be easily paired in series or parallel in case of load evolution. A few more advantages of the inclusion of PV in a local electricity system include but are not limited to the following:

- Unlike a DG, PV could be sized very close to the required power;
- Portable, easy to move to far-flung zones, and easy installation;
- Not too site-specific like other renewables, such as wind and hydro;
- No moving parts, hence no technical maintenance and no noise, longer life of around 25 years;
- Natural DC coupling with battery storage and modern DC loads;
- More units can be added in series/parallel strings to cover the load evolution; and
- Easy to decommission and install at another location.

(1) Linear PV Model: It is worth noting that the PV module output voltage is highly affected by the temperature while the PV current is by the irradiance or weather condition. The linear PV model is a simple power generator source as a function of two variables, *i.e.*, solar cell temperature and irradiance. This model is also called EVANS model [22]. The extracted maximum power $P_{PV,MPP}$ as a function of temperature and irradiance could be represented by,

$$P_{PV,MPP} = P_{MPP}\frac{G}{1000}[1 + \gamma(\theta_c - 298.15)] \times N_{c,PV} \qquad (2.1)$$

Where P_{MPP} is PV maximum power at standard test conditions (STC), G the solar global in-plane irradiance, γ is the power temperature coefficient at maximum power point (MPP), and θ_c is the individual PV cell temperature in °K, and $N_{c,PV}$ the total number of PV cells. This model does not need particular numerical computations if the γ is determined from experiments. The model is simple to use, but significant errors can occur due to the dependency of the model on weather conditions. Therefore, the correct use of this model requires accurate mapping of the γ values for different temperatures and irradiances.

(2) Single-Diode PV Model: The PV model can be represented by combining a few circuit elements, such as the single-diode model. PV cells are commonly modeled as circuits to extract the five parameters of the single-diode model from the experimental curves [23]. The PV model can be represented by combining a few circuit elements. An electrical representation of the single-diode PV cell is shown in Figure 2.23. A PV cell can be modeled as a light-generated current source I_{ph} parallel to a diode and shunt/series resistors [23], [24]. Unlike the linear PV model, this model has non-linear characteristics of a PV cell, and it is not only limited to the MPP but the entire I-V and P-V curves.

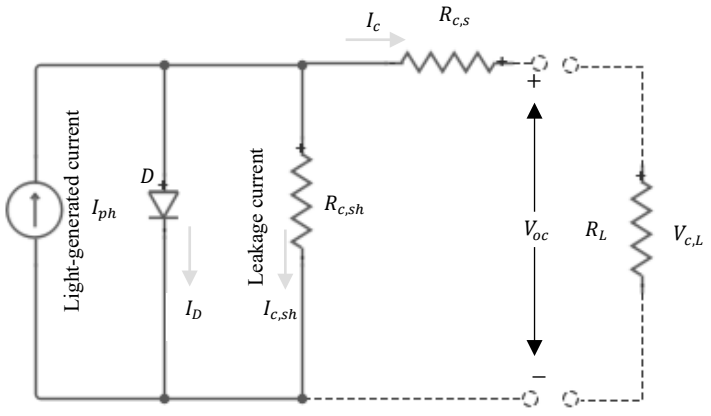

Figure 2.23 – Electrical equivalent-circuit representation of a PV cell [23], [24]

In this model, the sunlight with an appropriate energy level generates electron-hole pairs, which are drifted to the external circuit via junction potential. The losses are modeled using series and shunt resistances. A fraction of the leakage current across the junction can be modeled with a shunt resistance $R_{c,sh}$. In an ideal solar cell, the shunt resistance $R_{c,sh} = \infty$ and series resistance $R_{c,s} = 0$, indicating no leakage to the ground and no series drops, respectively. This PV cell model is susceptible to the parameter variation of $R_{c,s}$ where a slight increase can cause a rapid drop in solar cell efficiency. The relation for solar cell voltage $V_{oc,c}$ can be written as:

$$V_{oc,c} = V_{c,L} + I_c R_{c,s} \tag{2.2}$$

The load current I_c, which is also solar cell output current, can be represented by subtracting the diode leakage current I_D and the shunt leakage current $I_{c,sh}$ from the PV current I_{ph} and is expressed as:

$$I_c = I_{ph} - I_D - I_{c,sh} \tag{2.3}$$

Where I_D could be represented by the classical relation:

$$I_D = I_{0,D}\left[exp\left(\frac{qV_{oc,c}}{n_D K_B \theta_c}\right) - 1\right] \tag{2.4}$$

Finally, the total output current of the solar cell by substitution becomes,

$$I_c = I_{ph} - I_{0,D}\left\{exp\left[\frac{qV_{oc,c}}{n_D K_B \theta_c}\right] - 1\right\} - \frac{V_{oc,c}}{R_{c,sh}} \tag{2.5}$$

Where I_{ph} could be represented as,

$$I_{ph} = \frac{G}{1000}[I_{SC} + K_I(\theta_c - 298.15)] \tag{2.6}$$

and,

$$I_{0,D} = I_{or}\left(\frac{\theta_c}{\theta_r}\right)^3 exp\left[\frac{qE_{GO}}{n_D K_B}\left(\frac{1}{\theta_r} - \frac{1}{\theta_c}\right)\right] \tag{2.7}$$

The parameters used from Eq. (2.3)–(2.7) represent:

q is the electron charge, which equals 1.6×10^{-19}C;

n_D ideality factor of the diode, a curve fitting constant and unit less, [$n \in 1; 2$];

K_B Boltzmann constant equals 1.38×10^{-31}JK^{-1};

θ_c is the cell temperature in °K;

θ_r represents the reference temperature and equals 298.15°K;

$R_{c,s}$ series resistance of the solar cell;

$V_{oc,c}$ the solar cell voltage at open-circuit in volts;

$V_{c,L}$ the load voltage of PV cell;

I_D diode leakage current;

I_c represents solar cell output current;

K_I is the short-circuit current temperature coefficient at I_{SC}, the equivalent of γ;

$I_{0,D}$ equals reverse saturation current of the cell;

I_{SC} represents the short-circuit current at STC;

I_{ph} the light-generated current from the incident photons at a certain energy level;

I_{or} the cell saturation current at θ_r (reference temperature);

E_{GO} the bandgap energy ≈1.12eV for polycrystalline silicon at θ_r; and

G is the solar global in-plane irradiation in W⁄m^2 at STC.

Further, the term $(K_B\ \theta_c)/q$ in Eq.(2.5) is denoted as V_T, the solar cell's thermal voltage. The complete governing equation of a single diode PV cell current I_c is written as,

$$I_c = I_{ph} - I_{0,D}\left[exp\left(\frac{V_c + I_c R_{c,s}}{n_D V_T}\right) - 1\right] - \frac{V_c + I_c R_{c,s}}{R_{c,sh}} \tag{2.8}$$

Where $I_{0,D}$ is a strong function of θ_c and V_c, where V_c is the individual cell's voltage. In addition, Eq. (2.8) can be used to extract the five parameters $(I_{ph}, I_0, R_{c,s}, R_{c,sh}, n_D)$ of the equivalent-circuit model.

Like PV cells in series-parallel combination, multiple PV modules can be grouped in series-parallel strings to get the desirable PV power. This grouped illustration is merely a scaled version of Figure 2.23. The same equations represent a cell, a module, and a PV system. Lastly, the steady-state PV power could be expressed with the total installed PV surface times efficiency times irradiance power. Mathematically, the available PV power P_{PV} gets the following relation:

$$P_{PV} = \eta_{PV}\ \eta_{MPP}\ N_{PV}\ A_{s,PV}\ G \tag{2.9}$$

Where η_{PV}, η_{MPP} represent the PV panel array and converter efficiency at maximum power point (MPP), respectively. Also, N_{PV} is the number of PV modules to constitute the array and $A_{s,PV}$ is the module surface in m^2. The value of G can change significantly at different global locations. At STC, the η_{PV} is ~17%-19.7% (for silicon solar cells) and is very specific to the technology used. As the solar panel power fades over time due to the reduction in the module efficiency. For a given year $y\ \forall\ [y \in 1; 20]$, the output power $P_{PV,y}$ is expressed by:

$$P_{PV,y} = P_{PV,0}\left(1 - \sigma_{PV,y}\right)^{y}/1000 \quad (2.10)$$

Where $P_{PV,0}$ in (kW) is the initially calculated PV array power at STC during the installation and commissioning. The factor $\sigma_{PV,y}$ is the PV yearly degradation rate. While considering a degradation rate of 0.495% per year, the PV array could be capable of giving ~90% of the commissioned power after a PV lifetime (25 years). More accurate models also consider the recombination phenomenon, such as the double-diode model that provides better PV cell characterization [25]. The interested readers can find further literature on the circuit models of PV cells in [26], [27]. In conclusion, the Evans single-diode model [22], can be used with acceptable error tolerance. The PV manufacturers do not provide all of these parameters in the module datasheet, but only a few, for *e.g.*, I_{SC}, I_{MPP}, V_{MPP}, and V_{oc} on the back label of a PV panel.

2.2.3 Battery Modeling

The battery is considered as an energy reservoir for strategic situations [28], [29]. It is an essential microgrid component that can significantly help optimize the power flow and save the microgrid from voltage collapse [30]. It can quickly respond to cover the energy loss due to intermittent PV sources or load variations [31]. Electrochemical batteries are considered a good and economical choice for low-power microgrids due to ease of maintenance, simple design, operational flexibility, universal availability, and modularity [32], [33]. Power quality, reliability, absorbing excess PV power, and uninterruptable service are a few more advantages. They store energy directly in the electrolytic solution.

Lead-acid batteries are considered the first choice for system planners in low-power stationary applications due to their low cost. Figure 2.24a [33] shows the storage categories as a function of energy needs, which give various choices for the proper selection of energy storage in different applications. The critical selection parameters include cost and energy storage capacity to reach a particular power level. The importance of storage in utility-scale RES management for power quality and reliability is depicted in Figure 2.24b [34]. Batteries can also help the DG to run at optimal operation. They can utilize the excess PV power and avoid PV shedding during days of good sunshine. From the design point of view, batteries can fit any voltage level by proper series-parallel strings for the proper converter operation [32]. More detailed literature on the usefulness and utilization of battery storage can be found in [35], [36].

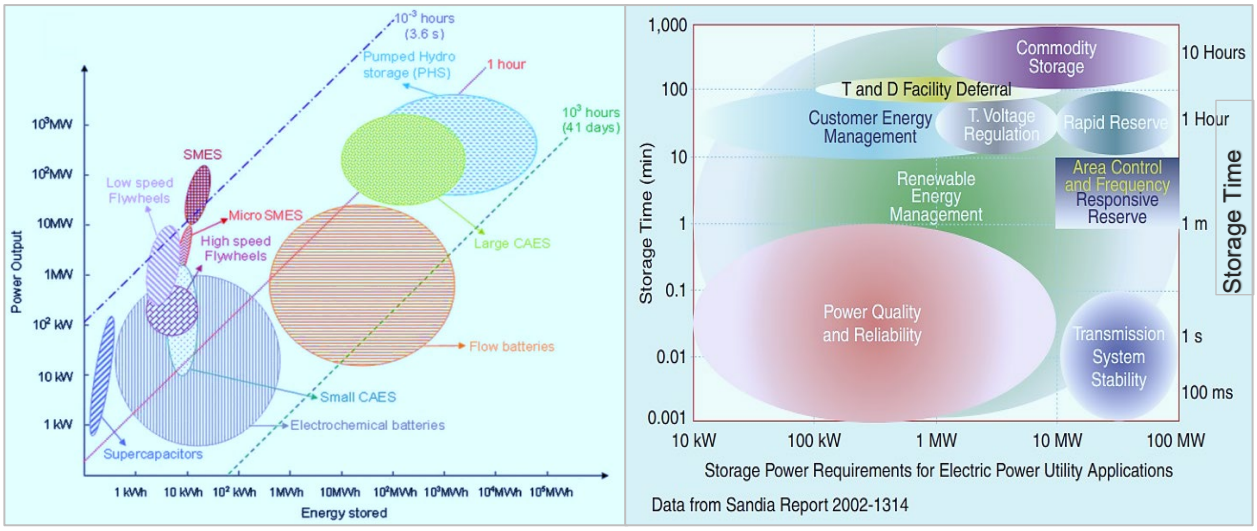

(a) energy needs [33] (b) application areas [34]

Figure 2.24 – Selection of right storage system for right application

Like PV panels, batteries also have modularity, *i.e.*, with identical characteristics, they can be grouped to design storage banks ranging from a few hundred watts to several hundred kW. This feature allows the batteries to match any required DC bus voltage with reasonable converter efficiency. The analysis and effectiveness of some of these advantages require a certain level of physical and analytical modeling [37], [38]. Now, we switch to battery modeling in the following subsections.

2.2.3.1 Electrical and analytical modeling of battery

This study does not consider temperature or electrolyte chemical kinetics [39]. Therefore, simple electrical representation is sufficient for the desirable battery discharge behavior, which considers the charge immediately available, not chemically bound [39]. Many battery models have been proposed in the prior art, but electrical models have always remained a focus of researchers [40].

The work in this subsection mainly focuses on electrical equivalent-circuit models as the electrochemical models are less practical for system-level control. These parametric models can be tailored for any application by adequately selecting the number of required circuit elements and their parameter values. The circuit elements can be tuned to match the battery response from field measurements. The battery could be represented as an ideal voltage source in series with a resistance. This circuit representation is depicted in Figure 2.25. The given circuit shows that the battery terminal voltage V_{bat} is a function of the battery current I_{bat} considering the two other parameters V_{int} and R_{int} as constant. In this model, R_{int} shows the losses associated with the battery plate and

electrolyte resistance and models the internal voltage drop. From now onwards, $V_B = V_{bat}$ and $I_B = I_{bat}$ to simplify writing all equations relating battery voltages and currents.

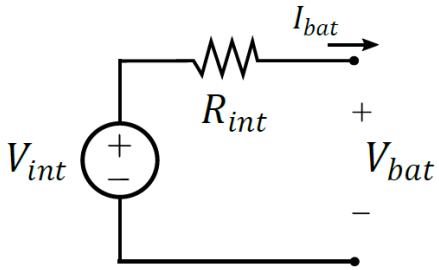

Figure 2.25 – Thevenin's equivalent battery model

For the series-connected battery cells $n_{B,c}$, the following mathematical expression represents the circuit.

$$V_B = n_{B,c}V_{int} - n_{B,c}I_B R_{int} \tag{2.11}$$

Where V_{int} is a strong function of the battery SoC. As the model only represents a linear relationship, it cannot model any discharge or voltage recovery exponentials. The classic SoC equation can be represented by the Coulomb counting method, which is given as,

$$SoC = \frac{C_{B,r}}{C_{B,t}} = \left[1 - \frac{1}{C_{B,t}}\int_0^t -I_B(t)\,dt\right] \tag{2.12}$$

Where $SoC \in [0; 1]$, $C_{B,r}$ and $C_{B,t}$ are battery remaining and total capacities in Ah. Some of the limitations of the simplest battery model include:

- The battery self-discharge is not considered;
- Battery capacity is not affected by the magnitude of discharge current I_B;
- Practically, the charge-discharge phenomena are different. There is no explicit change in parameters for the charge and discharge models [41]; and
- The internal resistance is not affected by the current variation.

Modeling Approach: Electrical modeling is preferred for large system-level development, such as microgrids, due to its simplicity and ease of control. Each element is more intuitive, manageable, and easy to handle in such a component and mathematical-based modeling. In this way, it can provide an excellent foundation to model the behavior of any fresh or aged battery. This work thus focuses only on the mathematical and physical elements-based modeling using SIMULINK® [42]. The presented work in this section is an inspiration from [43]. Different battery models have been used to determine the dynamic response and performance parameters [44]. Interestingly, the RC equivalent-

circuit-based models can be used to accurately model the charge-discharge processes in the frequency or time domain. Batteries are highly non-linear, especially in their second life. Though simple equivalent-circuit models, such as first-order (1RC) or second-order (2RC), cannot accurately represent the natural dynamic response; however, they can provide a foundation to model the behavior of a genuine battery using parameter estimation and model parameterization. This section models the battery dynamics that can behave like an actual 12V battery. It is possible to correlate the model with the experimental data using curve fitting/ parameter optimization [45]. In this way, the model with its estimated parameters could be as realistic as a genuine battery, and the performance impact could be simulated quite close to reality.

2.2.3.2 Modeling of the battery dynamics

This subsection is based on the results from the three different simulation models of a lead-acid battery cell, namely; 1) the physical elements-based model using electrical equivalent-circuits, 2) the mathematical equations-based models using MATLAB® function blocks, and 3) the built-in library components-based model using SIMSCAPE™. The same equations are used to build a more controlled and accurate model using the SIMSCAPE™ library components, and the results are compared.

(1) Equivalent-Circuit Models: Electrical equivalent-circuit models use a voltage source (E_m), battery terminal resistance (R_0) and plate and electrolyte resistance (R_2) which are collectively the same as R_{int} of the battery circuit in Figure 2.25, and RC branch resistance/ capacitance (R_1C_1). In Figure 2.26, these physical elements are used to simulate the 1RC model of a battery cell in the SIMSCAPE™ interface. Where R_0 and R_2 represent the instantaneous response, R_1C_1 constitute the exponential response, E_m is the battery cell voltage representing the open-circuit potential.

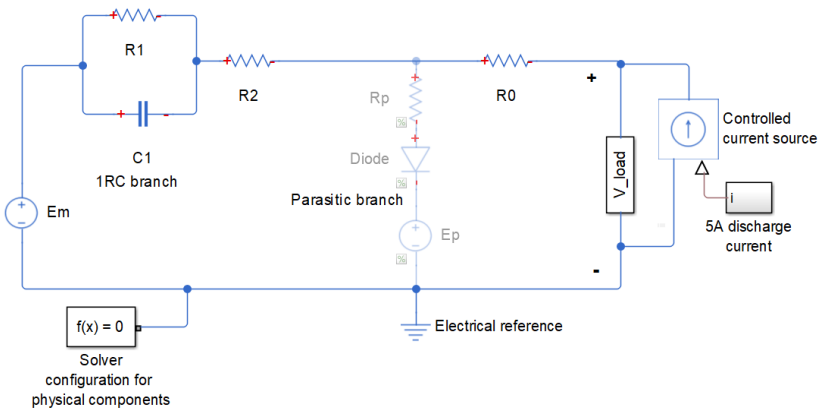

Figure 2.26 – Simulation model of a single battery cell using 1RC electrical equivalent-circuit

A discharge current pulse repeated each hour is used to simulate the circuit. The controlled current source is driven by a 5A pulse of width 300s (7.692% duty cycle) with a repetition period of 3900s (one-hour rest time for the voltage recovery). The obtained simulation results with and without an RC branch are plotted in Figure 2.27. The respective single-cell simulation parameters are listed in Table 2.9. These parameters are based on the assumptions in [43].

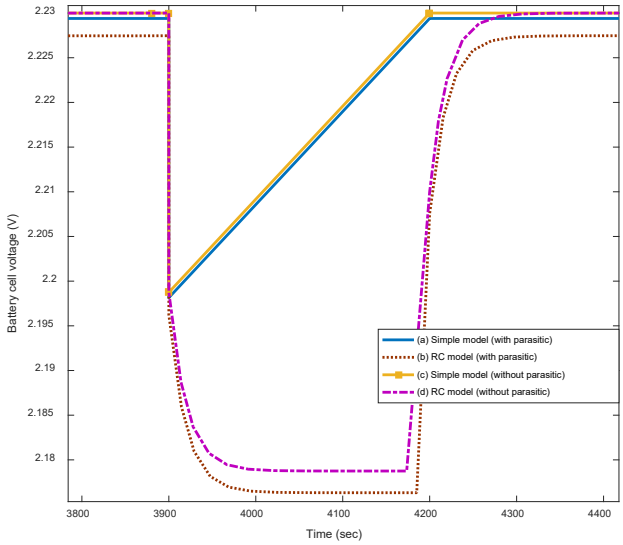

Figure 2.27 – The 5A discharge dynamics of a single battery cell: a closer view with and without parasitic branch

Table 2.9— Simulation parameters for a single battery cell

Cell-type	*Cell voltage* (E_m)	*Terminal resistance* (R_0)	*Internal plate resistance* (R_2)
Lead-acid	2.23V	5mΩ	1.25mΩ
Discharge source (Pulsed current)	*Branch resistance* (R_1)	*Branch capacitance* (C_1)	*Pulse period/ Pulse duration*
5A	4mΩ	τ_1/R_1, where τ is the circuit time-constant	3900s /300s

The two plots (Figure 2.27a,c) represent a Thevenin's equivalent-circuit for the simple battery model of Figure 2.25. Whereas the plot figures (b,d) represent the 1RC equivalent-circuit model in Figure 2.26. In this plot, the 1RC branch contributed to the discharge and recovery exponentials. The response from recovery exponentials resembles a real battery's response, but the battery voltage stays at the same level each time it recovered, which may not be the case. The parasitic branch effect due to E_p and R_p was also

evaluated for this model to simulate self-discharge. There was as such no significant self-discharge, which shows some of the limitations of this basic battery model. All other performance parameters, such as SoC, remaining capacity in Ah, depth-of-discharge (DoD), and the recovery slope, could not be determined from these simulations. These battery parameters are closely linked in the following mathematical relationship.

$$E_m = E_{m0} - K_E(T_B + 273.15)(1 - SoC) \tag{2.13}$$

$$R_0 = R_{00}[1 + A_0(1 - SoC)] \tag{2.14}$$

$$R_1 = -R_{10}\, ln(DoD) \tag{2.15}$$

$$C_1 = \tau_1 / R_1 \tag{2.16}$$

$$R_2 = R_{20} \frac{exp[A_{21}(1 - SoC)]}{exp(A_{22} I_m / I_B^*) + 1} \tag{2.17}$$

In Eq. (2.13), E_m is the battery cell voltage, E_{m0} is the cell V_{oc} at full charge, K_E is a constant in volts/°C, T_B is the internal battery temperature in °C . In Eq. (2.14), R_{00} is the value of R_0 at $SoC = 1$, A_0 is a constant. In Eq. (2.16), τ_1 is the time-constant of the R_1C_1 branch. In Eq. (2.17), R_{20}, A_{21}, and A_{22} are constants, I_m is the single RC branch current, and I_B^* is the nominal battery current which is related to the nominal battery capacity $C_{B,n}$ at a discharge rate of C_{10}.

The results in Figure 2.27 show that the physical element-based modeling is much simpler for analysis. However, the non-realistic discharge exponentials and voltage recovery limit the model for accurate simulations. The recovery voltage permanently settled at 2.23V, which may not truly reflect the battery discharge behavior. It is due to the ideal voltage source at the input of a battery cell. The same methodology is used in the equation-based simulations for comparison.

(2) Equation-based Battery Modeling: Batteries can also be modeled with simple numerical descriptions [46]. The battery Eqs. (2.13)−(2.17) are used with MATLAB® functions to model a battery cell in SIMULINK®. The elementary accumulator is scaled with six identical cells to form a 12V battery. The terms relating to parasitic branch also ignored due to its negligible impact in this case. In these simulations, the total battery terminal voltage V_B and extracted charge $Q_{B,e}(t)$ are based on the following two relations,

$$V_B = 6 * E_m - V_{R1||C1} - I_B(R_0 + R_2) \tag{2.18}$$

$$Q_{B,e}(t) = Q_{B,init} + \int_0^t -I_m\,(\tau)\,d\tau \qquad (2.19)$$

Where $Q_{B,init}$ is the initial stored charge in the battery. The corresponding mathematical Eqs. $(2.13)-(2.17)$, representing a circuit element are coded in MATLAB®. The battery performance parameters such as SoC, rated capacity in Ampere-hour (Ah), temperature, power loss, and DoD are based on the assumptions in [43], [46]. The obtained simulation results are plotted in Figure 2.28.

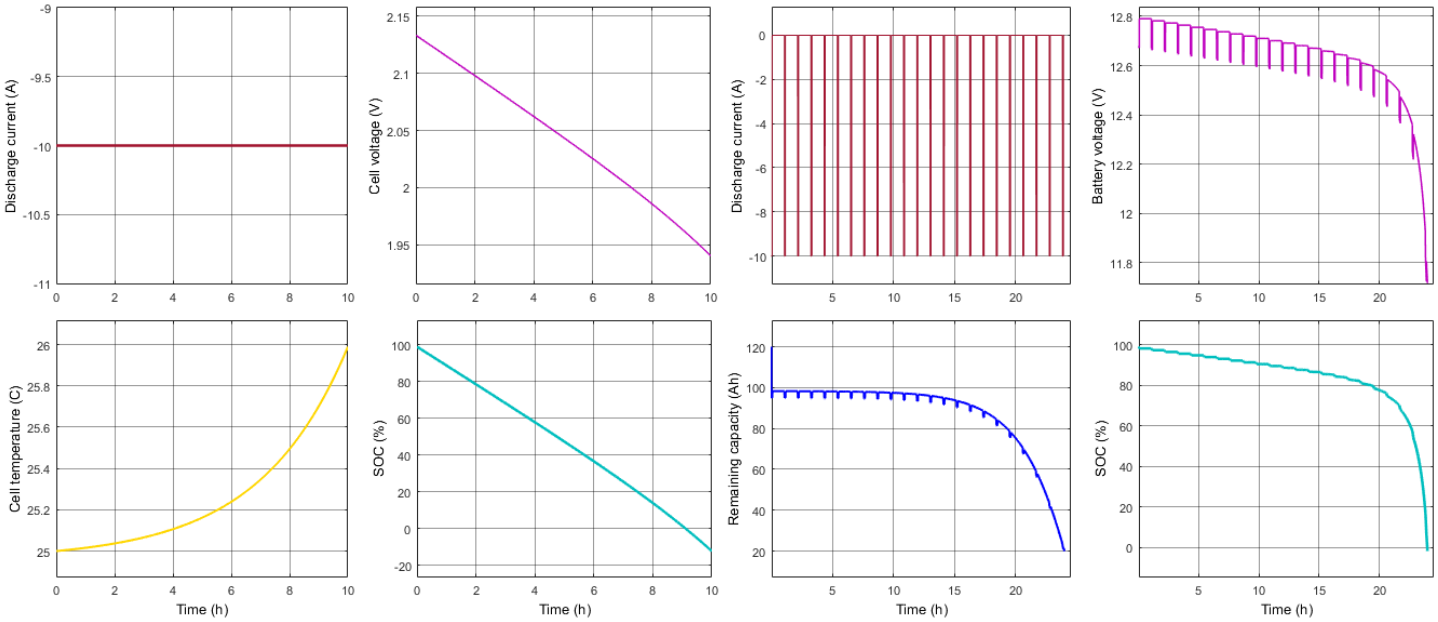

(a) 10A constant current discharge (b) 10A pulsed discharge

Figure 2.28 – Battery dynamics using equation-based models

In Figure 2.28a, a 10A constant discharge current is used to obtain individual cell discharge behavior with an optional subplot for cell temperature. In this plot, the rise in internal cell temperature and the corresponding drop in SoC, cell voltages are very close to the behavior of a real battery. In Figure 2.28b, the battery is discharged using a 10A pulsed current to simulate the dynamic response. The obtained simulation results are close to an actual 12V battery representing the non-linearity and recovery response. The battery temperature was assumed to be the same and uniform, so it is excluded from the figure plot and replaced by the battery capacity. At 20% SoC, the battery is considered as fully discharged. The value of remaining capacity at this point is only 40Ah. This model also has a drawback. It may not accurately capture the different cell dynamics as the battery is merely a scaled version of the single-cell response, which may not be the case for a 12V battery response in the real conditions.

(3) Component-based Modeling: The encountered accuracy problems with physical circuit elements and mathematical equation-based models can be addressed using component-based modeling. This section uses more controlled built-in SIMSCAPE® library components to model a typical battery cell. This modeling approach provides the flexibility to consider all the non-linearity and inter-dependency of battery parameters. Any kind of first or higher-order electrical equivalent-circuits can be modeled and parameterized using these components. These dedicated library components also provide the flexibility to program a component to the desired model response. The modeled battery cell from physical components is shown in Figure 2.29.

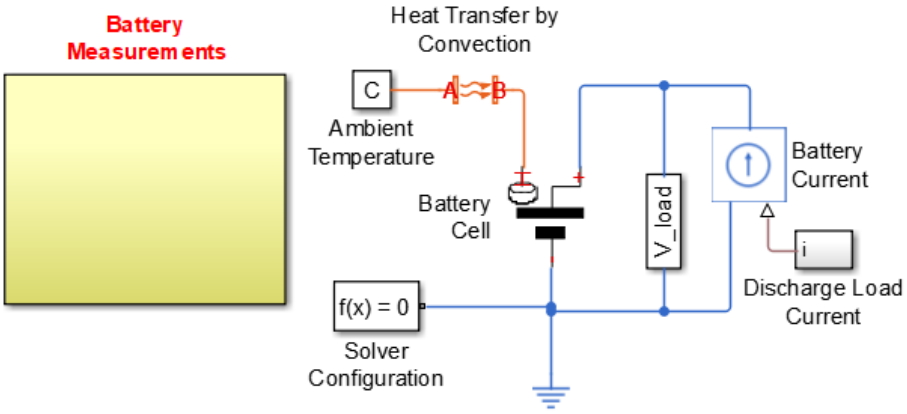

Figure 2.29 – Component-based modeling: a single battery cell model

Designing battery equivalent-circuits using the built-in library components need additional settings like the physical system to SIMULINK® or vice versa (PS-S OR S-PS)[12]. A reasonable battery response can be obtained by adequately selecting the number of series RC branches. The dynamic response of the three different RC combinations is shown in Figure 2.30. It can be observed that the source voltage changes with the battery parameters and remaining capacity. Additionally, some notable responses, such as voltage recovery, voltage dips, and recovery exponentials, change with the number of RC branches. The effect of self-discharge is bypassed until a comparable response is observed and a specific RC combination be qualified for further analysis.

[12] PS-S: Physical system to SIMULINK®, S-PS: SIMULINK® to physical system.

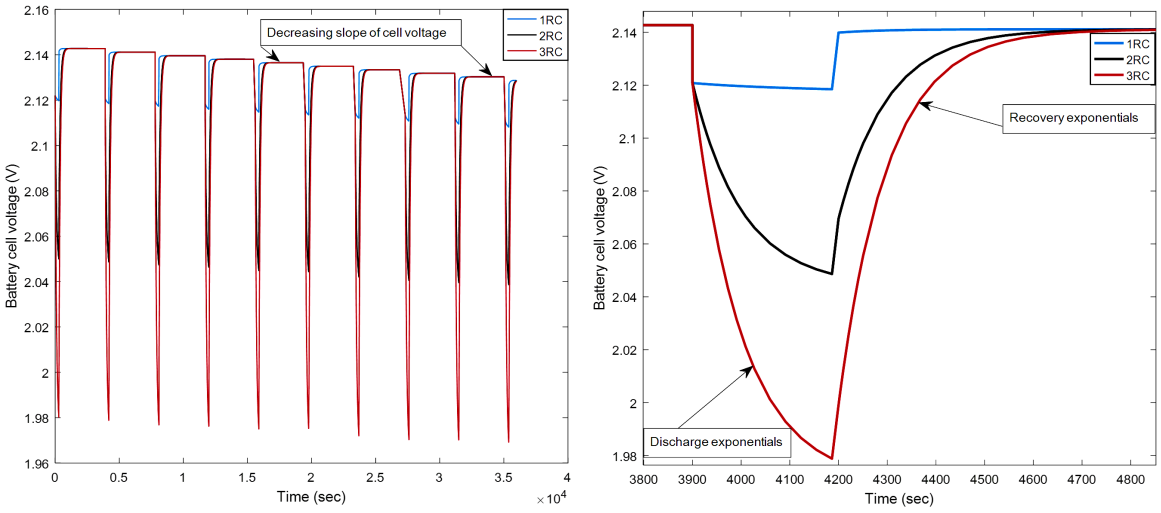

(a) repeated pulsed discharge

(b) closer view of a single discharge pulse behavior

Figure 2.30 – Dynamic response of 1RC, 2RC, 3RC models

It is observed from the obtained results that a single RC branch does not represent the actual dynamics of a battery cell during pulsed discharge. The discharge and recovery exponentials for 1RC are pretty linear. The model is not able to generate a realistic battery response. The model is then scaled up to 2RC and 3RC branch elements to know their impact on the exponentials. The 2RC and 3RC models genuinely represent the actual battery dynamics. It is observed that the exponential response of a more complex 3RC with additional elements is not much different from the relatively simple 2RC model, except for an increase in circuit complexity, computational burden, and roughly 3.65% more voltage drop. Therefore, we chose the 2RC model, which generated a well-matched response of the battery cell to that of a real battery. The 2RC model also provides a good compromise between complexity and accuracy [47]. The schematics of an equivalent-circuit with a pair of RC branches are depicted in Figure 2.31.

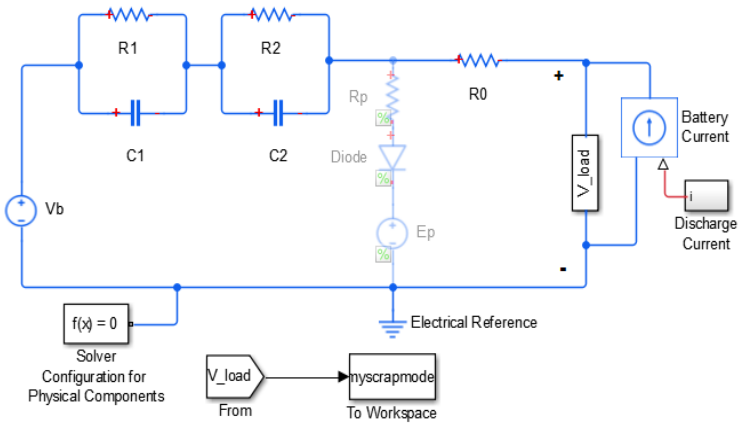

Figure 2.31 – Schematic diagram of a 2RC equivalent-circuit model

(4) Presence of the Parasitic Branch: Since the simulated model represents fresh batteries and does not account for any parameter evolution due to aging, the self-discharge effect is negligible and ignored. The effect of self-discharge become dominant when the model is adapted to the parameter degradation [48]–[50].

The purpose of the battery simulations was to find an accurate equivalent-circuit model that represents the discharge dynamics of a typical 12V lead-acid battery. These simulations were conducted with no aging in the models. It is noted that the physical element-based model is best as a foundation step due to its simplicity. However, the parameter values on the initial guesses resulted in a meaningless battery response. The voltage recovery was not too realistic due to an uncontrolled ideal voltage. In the second step, though with a few minor limitations, the equation-based model was quite good for validating the fundamental battery Eqs. (2.13)-(2.17). Finally, we observed that the built-in library component-based modeling was more accurate and easier to handle. Among various RC combinations, the equivalent-circuit with 2RC branches was found adequate to model the battery dynamics, which is also a perfect compromise between complexity and accuracy.

2.2.3.3 Battery parameter extraction

The battery parameter extraction could be determined using pulsed discharge experiments [45] or the analytical procedures for computing parameters of equivalent-circuit models [51]. Now considering the 2RC branch model in Figure 2.31a, with elements (R_1C_1 and R_2C_2), battery terminal and electrolyte accumulated series resistance (R_0), and the battery open-circuit voltage (V_{oc}) where V_{oc} is a strong function of the battery SoC. The battery dynamics can be modeled using the following representation,

$$\begin{bmatrix} \frac{dv_1(t)}{dt} \\ \frac{dv_2(t)}{dt} \\ \frac{dSoC(t)}{dt} \end{bmatrix} = X \begin{bmatrix} V_1(t) \\ V_2(t) \\ SoC(t) \end{bmatrix} + YI_B(t) \tag{2.20}$$

$$V_B = V_{oc}(SoC) - V_1(t) - V_2(t) - R_0 I_B(t) \tag{2.21}$$

and the coefficients X, Y as,

$$X = \begin{bmatrix} \frac{-1}{R_1 C_1} & 0 & 0 \\ 0 & \frac{-1}{R_2 C_2} & 0 \\ 0 & 0 & 0 \end{bmatrix}, \qquad Y = \begin{bmatrix} \frac{1}{C_1} \\ \frac{1}{C_2} \\ \frac{-\eta_c}{C_{B,n}} \end{bmatrix}$$

By substitution, the values of X and Y in Eq. (2.20), the following relations are found for the state variables.

$$\begin{cases} \frac{dv_1(t)}{dt} \\ \frac{dv_2(t)}{dt} \\ \frac{dSoC(t)}{dt} \end{cases} = \begin{cases} \frac{-1}{R_1 C_1} V_1(t) + \frac{1}{C_1} I_B(t) \\ \frac{-1}{R_2 C_2} V_2(t) + \frac{1}{C_2} I_B(t) \\ \frac{-\eta_c}{C_{B,n}} I_B(t) \end{cases} \tag{2.22}$$

Where η_c is the Coulombic efficiency, $C_{B,n}$ is the battery nominal capacity, $I_B(t)$ is the battery discharge current, $V_1(t)$, $V_2(t)$ are the voltage drops across capacitors, $v_1(t), v_2(t),$ and SoC are the three states and $v_B(t)$ is an output variable. In contrast, Eq. (2.20) could be used for the battery parameter extraction in its discretized form. The extracted battery parameters are important as they can be used to parameterize the simulation models [52]. Further, Eq. (2.20) can be used to write a discrete-time model, where k is the discrete-time index, T_s the sampling period, and V_{oc} is held constant between two sampling periods.

$$\begin{bmatrix} v_1(k+1) \\ v_2(k+1) \\ SoC(k+1) \end{bmatrix} = A \begin{bmatrix} V_1(k) \\ V_2(k) \\ SoC(k) \end{bmatrix} + B I_B(k) \tag{2.23}$$

$$V_B(k) = V_{oc}(SoC) - V_1(k) - V_2(k) - R_0 I_B(k) \tag{2.24}$$

$$A = \begin{bmatrix} \frac{-T_s}{e^{R_1C_1}} & 0 & 0 \\ 0 & \frac{-T_s}{e^{R_2C_2}} & 0 \\ 0 & 0 & 1 \end{bmatrix}, \qquad B = \begin{bmatrix} R_1(1 - \frac{-T_s}{e^{R_1C_1}}) \\ R_2(1 - \frac{-T_s}{e^{R_2C_2}}) \\ \frac{-\eta_c T_s}{C_{B,n}} \end{bmatrix}$$

Furthermore, the parameter identification and V_{oc} estimation can be computed with the classical recursive least mean square estimation (LMSE) algorithm. The V_{oc} is assumed as a constant term to simplify the analysis.

$$\begin{cases} \begin{bmatrix} V_1(k+1) \\ V_2(k+1) \end{bmatrix} = A \begin{bmatrix} V_1(k) \\ V_2(k) \end{bmatrix} + BI_B(k) \\ V_B(k) - V_{oc} = C \begin{bmatrix} V_1(k) \\ V_2(k) \end{bmatrix} + DI_B(k) \end{cases} \tag{2.25}$$

Where A, B, C, and D are scalars and could be calculated as follows.

$$A = \begin{bmatrix} \frac{-T_s}{e^{R_1C_1}} & 0 \\ 0 & \frac{-T_s}{e^{R_2C_2}} \end{bmatrix} = \begin{bmatrix} a_1 & 0 \\ 0 & a_2 \end{bmatrix} \quad B = \begin{bmatrix} R_1(1 - \frac{-T_s}{e^{R_1C_1}}) \\ R_2(1 - \frac{-T_s}{e^{R_2C_2}}) \end{bmatrix} = \begin{bmatrix} b_1 \\ b_2 \end{bmatrix},$$

$$C = [-1, -1\,], \quad D = R_0$$

For the regression-based method, the z-transform pairs of Eq. (2.25) can be rewritten using the following expressions.

$$\frac{Y(z)}{U(z)} = [C(zI - A)^{-1}B + D] \tag{2.26}$$

$$\frac{V_B(z) - V_{oc}}{I_B(z)} = \left[\frac{b_1(a_2 - z) + b_2(a_1 - z)}{(z - a_1)(z - a_2)} - R_0\right] \tag{2.27}$$

The recurrent equation of $V_B(t)$ can be derived using the method in [53]. By applying the inverse z-transform using Eq. (2.27), the expression for $V_B(t)$ becomes,

$$\begin{aligned} V_B(k) &= (a_1 + a_2)V_B(k-1) \\ &- a_1a_2V_B(k-2) - R_0I_B(k-1) \\ &+ (R_0a_1 + R_0a_2 - b_1 - b_2)I_B(k-1) \end{aligned} \tag{2.28}$$

$$+ (b_1a_2 + b_2a_1 - R_0a_1a_2)\, I_B(k-2)$$
$$+ (1 - a_1 - a_2 + a_1a_2)V_{oc}$$

Which may be represented in a more generalized form as follows,

$$V_B(k) = \varphi'(k)\theta_p \tag{2.29}$$

Where $\varphi'(k) = [V_B(k-1)\ V_B(k-2)\ I_B(k)\ \ I_B(k-1)\ I_B(k-2)\ 1]$, and

$\theta_p = \begin{bmatrix} \theta_1 \\ \theta_2 \\ \theta_3 \\ \theta_4 \\ \theta_5 \\ \theta_6 \end{bmatrix}$ is a parameter vector.

Where the vector $\varphi(k)$ is called Regressors, the known variables can be easily determined from the battery voltage and current measurements. The vector consists of V_B and I_B and their previous samples. Also, for θ_p, each of the six battery parameters could be represented with the following relations,

$$\theta_{p1} = a_1 + a_2$$
$$\theta_{p2} = -a_1a_2$$
$$\theta_{p3} = -R_0$$
$$\theta_{p4} = R_0a_1 + R_0a_2 - b_1 - b_2 \tag{2.30}$$
$$\theta_{p5} = b_1a_2 + b_2a_1 - R_0a_1a_2$$
$$\theta_{p6} = (1 - a_1 - a_2 + a_1a_2)V_{oc}$$

Using the values from Eq. (2.30) and substituting in Eq. (2.28), we get the final relation of battery V_{oc}, which is written as,

$$V_{oc} = \frac{\theta_{p6}}{(1 - a_1 - a_2 + a_1a_2)} = \frac{\theta_{p6}}{(1 - \theta_{p1} - \theta_{p2})} \tag{2.31}$$

The LMSE algorithm can be implemented in MATLAB® SIMULINK® (Figure 2.32). The presented Regressors analysis is quite efficient in parameter retrieval from the battery measurements. In addition, it is possible to model each type of battery from its voltage and current response.

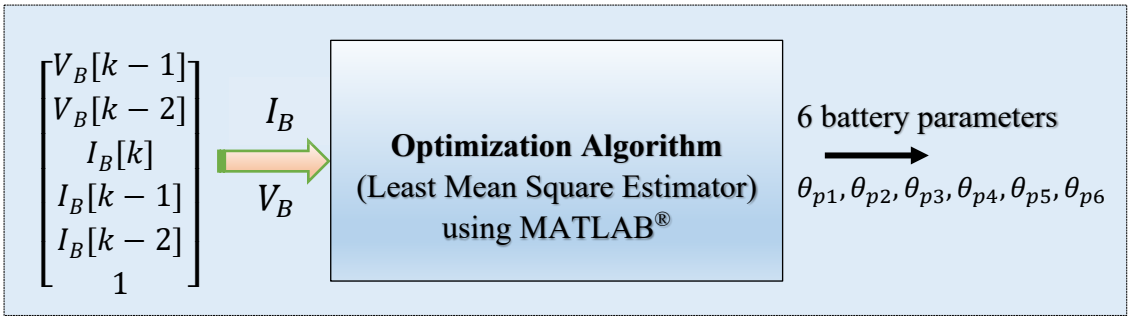

Figure 2.32 – Procedure for battery parameter extraction

The ease of the LMSE technique is its dependence on just two inputs (V_B, I_B). Therefore, the procedure can be quickly and easily done for the battery model parameterization with different health conditions, such as fresh, average, and weak batteries. The parameter extraction could be interesting in tracking the battery evolution and adaptive energy management system (EMS) to properly manage the energy flow in the system.

Further, it may be noted that the identification of battery model's parameters will help to understand the aging impact. The parameters are not used for the simulation of the average microgrid to test the EMS where only the battery performance is determined from the SoC. In a similar way, the parameters are not experimentally validated using the battery models.

2.2.3.4 Parameter evolution and aging

Nevertheless, like PV panels, batteries also suffer from time and cyclic aging, which could be represented with the same expression as Eq. (2.10). For a given year $y \; \forall \; [y \in 1; 10]$, and under normal temperature and room storage, the battery's remaining capacity in years $C_{B,r(y)}$ could be computed using the relation,

$$C_{B,r(y)} = C_{B,n(0)} \left(1 - \sigma_{B,y}\right)^{y} \tag{2.32}$$

Where $C_{B,n(0)}$ is the battery's initial rated capacity (Ah) during the installation and commissioning phase. The factor $\sigma_{B,y}$ is the battery yearly degradation rate with time and throughput energy. Considering a yearly degradation rate of 0.495%, the battery could be capable of giving ~60% of the commissioned capacity after a reasonable lifetime of 10 years as specified by the manufacturers in the battery datasheet. The battery power flow evolution, capacity degradation, and state-of-health (SoH) are shown in Figure 2.33 and Figure 2.34 (figure plots adapted from [54], [55]). Practically, a battery's SoH is 100% at installation time and will decrease proportionally, reaching below 70% within the ten years of use in their safe operational limits.

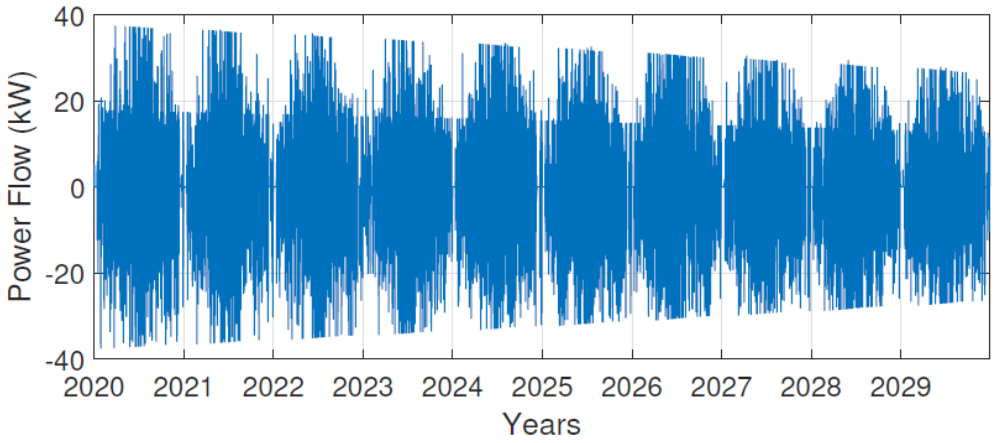

Figure 2.33 – Battery power flow evolution in ten years [54], [55]

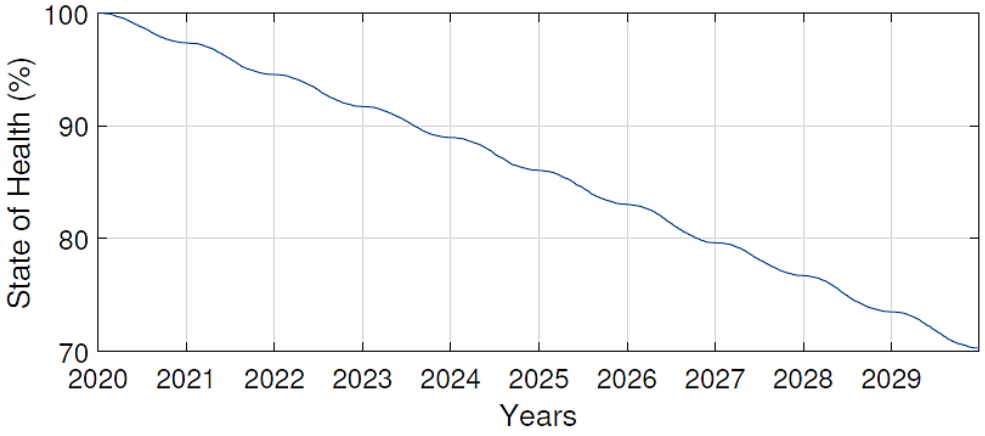

Figure 2.34 – Battery SoH evolution and capacity degradation in its ten years lifetime [54], [55]

These plots show that the battery power delivering capacity and SoH are closely linked. The battery degradation evolves in the same pattern over the ten years. The battery SoH drops from 100% to ~70%, close to the lower SoH limit at 60%. After this limit, the batteries are discarded or repurposed in another application. For the interested readers, a lot more literature about battery modeling can be found in [56]–[58]. The literature provides a good foundation of models, which are more dynamic with different levels of complexity and simulation quality. Some of these are derived from extensive lab tests and measurements.

2.2.4 Modeling and Design Considerations of DG

(1) Working Principle: A DG is a fully controlled electromechanical system that considers a disturbance such as a change in the output electrical load, which is sensed as a change in the engine speed. A governor perceives any change in the coupling shaft's speed by continuously comparing the DG speed to a reference signal. The speed controller processes the difference between the reference and shaft speeds [59]. The controller sends

a proportional signal to the fuel injection system that adjusts the fuel flow within the admissible limits. This way, the speed is regained and adapted to the nominal speed of the synchronous machine. The speed adjustment thus saves fuels and increases the efficiency of both mechanical and electrical parts.

(2) DG Modeling: A DG can be represented by a synchronous generator coupled with an internal combustion engine. The remaining auxiliary components include DC excitation, sensors, fuel tank, command panel, automatic transfer switch (ATS), and digital signal processors. The ATS and circuit breakers connect and disconnect the DG supply from the mains. As depicted in Figure 2.35, a DG consists of five essential blocks: speed governor, fuel injection, diesel engine, coupling shaft, and synchronous machine [60].

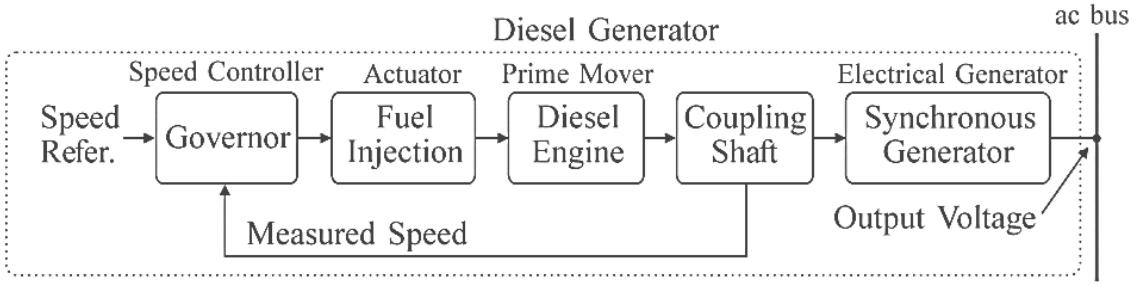

Figure 2.35 – Components of a typical diesel generator [60]

The DG model is depicted in Figure 2.36 [60]. The automatic voltage regulator (AVR) and governor are closed-loop control systems seeking a signal disturbance and thus maintaining voltage and speed regulation, respectively. These two control units keep the DG to operate at fixed voltages irrespective of the variations in the load current or speed. A detailed description of this model and parameter description is available in [60].

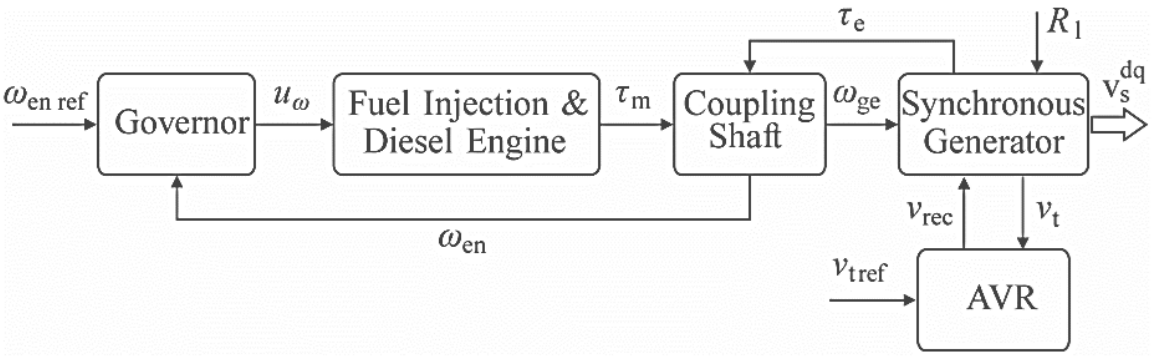

Figure 2.36 – DG model [60]

A more illustrative representation of the same model is represented in Figure 2.37. In this model, the diesel engine governor and excitation system are the two main inputs to the synchronous machine.

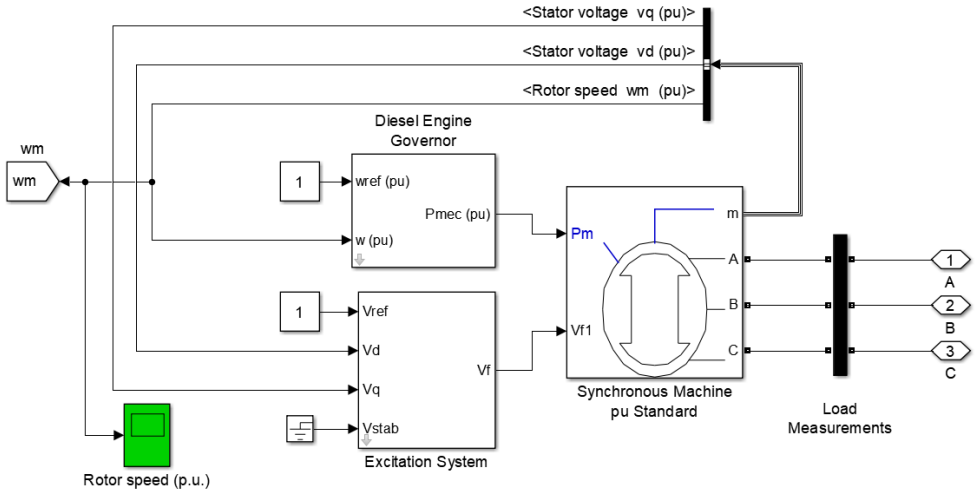

Figure 2.37 – Simulink model of a DG

The DG slow-startup can be compensated by a flywheel or supercapacitors to allow additional degree of freedom to manage the DC bus voltage until the availability of a stable DG power. Figure 2.38 (both plots adapted from [61]) shows the experimental response of a DG, which takes at least 5 to 6 seconds to deliver a stable power.

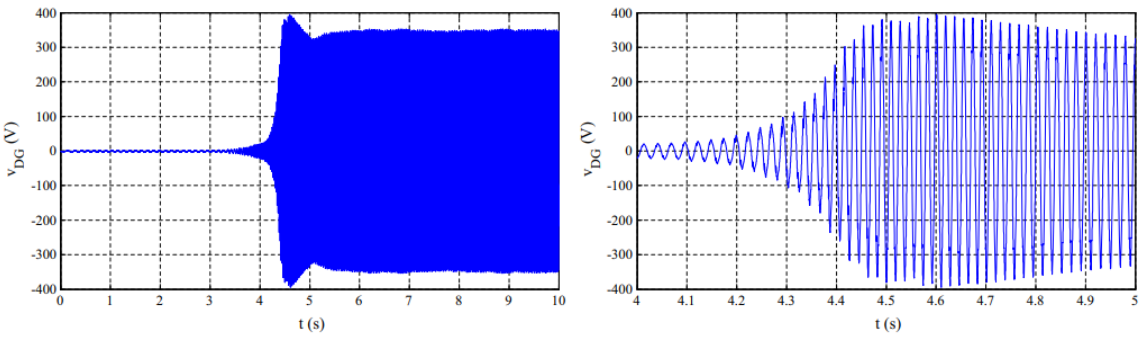

(a) (b)

Figure 2.38 – DG startup characteristics without load: (a) voltage curve (b) closer view [61]

The startup characteristics depicted in Figure 2.38 could be represented with a SIMULINK® model already depicted in Figure 2.36. Thus, a DG may be considered as an independent voltage source coupled with the AVR and speed regulator units. The modeling steps mainly include:

- A second-order model to represent the fuel injection and diesel engine;
- A time delay function to reach and stabilize the output voltage; and
- An independent voltage source to represent the synchronous generator.

Further, the model in Figure 2.36 could be represented with a parametric relation. The model is described by the following differential equation [60].

$$\frac{d\tau_m}{dt} = \frac{1}{t_e}\tau_m + \frac{k_e}{t_e}u_\omega(t - t_d) \quad (2.33)$$

Where τ_m is the developed mechanical torque by the engine, u_ω the control signal from the governor, and τ_d transport delay for the generator voltage to reach the stabilized regime from the initial transient. The value of τ_d may range from a few seconds to ten or fifteen seconds to deliver a stable output voltage and power. The developed torque directly relates to the signal u_ω from the speed governor in the range $[u_\omega \in 0; 1]$ and considering other parameters constant. More information about these parameters from an experimental setup is available in [62] and the IEEE Standards [63].

(3) DG Fuel Consumption: In order to minimize the system costs, increase fuel efficiency, reduce diesel maintenance and emission, the power sourced by the DG is limited to the following range,

$$P_{DG,min} \leq P_{DG} \leq P_{DG,max} \quad (2.34)$$

Where $P_{DG,min}$ represents the lower permissible power limit to run the DG at the best load factor (LF) and $P_{DG,max}$ is the maximum rated power a DG can source to the microgrid without compromising the wear to engine and winding. If $P_{L,peak} = P_L + P_B$ defines the combined maximum household load and the power to charge batteries, then the boundaries of DG operation can be rewritten as,

$$P_{DG,min} \leq P_{DG,r} \leq P_{L,peak} \quad (2.35)$$

Where $P_{DG,r}$ is now the peak rated power of the DG in kW. In this case, the hourly fuel consumption can be described by the linear relation between the $P_{DG,r}$, fuel consumption function $F(t)$ in US$/liter/hour, and the instantaneous power $P_{DG}(t)$ of the DG [59].

$$F(t) = (0.246P_{DG}(t) + 0.08415P_{DG,r}) \quad (2.36)$$

and the annual fuel cost (AFC) by,

$$AFC = \sum_{t=1}^{8760}\sum_{DG=1}^{N_{DG}} F(t) \quad (2.37)$$

Where N_{DG} is the total number of DGs. All the power values in these calculations are expressed in kW. The fuel cost function can also be represented in its quadratic form [64] or through approximated fuel consumption charts [65]. The DG's fixed cost of energy $M_{DG,fix}$ can be represented with the relation [13], which also takes into account the DG lifetime, running, and replacement costs.

$$M_{DG,fix} = M_{DG,o\&m} + \frac{M_{DG,rep}}{L_{DG}} + F_0\, P_{DG,r} M_{fuel,eff} \quad (2.38)$$

Where the operation and maintenance expenses are denoted by $M_{DG,o\&m}$ in ($/hour), $M_{DG,rep}$ is the DG replacement cost in $, L_{DG} is the total lifetime of the DG in hours, F_0 is the fuel curve intercept of the fuel function $F(t)$ in Eq. (2.36), and $M_{fuel,eff}$ the effective cost of fuel in $/liter. In Eq. (2.36), the fuel consumption has a dominant linear relation with the DG instantaneous power $P_{DG}(t)$. Therefore, the DG cannot be operated below or above the bounded range expressed in Eq. (2.35).

We present a configuration in which the DG is put to operation in the best conditions by choosing the lower threshold for LF at 40% of the rated power. This condition allows the DG to run at the best possible efficiency. The optimal operation also gives added advantages such as reduced carbon emissions, a longer lifetime, and lower fuel consumption and maintenance costs.

2.2.5 Energy Cost Modeling

The cost projection is one of the key modeling steps in standalone microgrid systems. As microgrids are composed of several energy sources, the least-cost combination becomes essential for the installers. In the worst conditions, a microgrid may fail if the system costs hike unexpectedly or reliability decline below the minimum acceptable thresholds. The Levelized cost of energy (LCOE) is a performance indicator that gives indices that can be used for critical decisions on sizing, choice of components, economic viability of the project, and tariffs [66]. The generalized equation for LCOE is represented with a simple relation of the microgrid lifetime cost (MLC) to the total energy production [13], [67].

$$LCOE = \frac{MLC\ (\$)}{GE_t\ (kWh)} \quad (2.39)$$

$$LCOE = \frac{CC_0 + \sum_{y=0}^{l_a} y\, M_{t,o\&m(y)}\, (1+r)^{-y}}{\sum_{y=0}^{n} y\, GE_t\, (1+r)^{-y}} \quad (2.40)$$

Where CC_0 is the cumulative initial capital cost of PV, DG, and batteries (material, manufacturing, transportation, and installation costs), $M_{t,o\&m(y)}$ is the yearly operational and maintenance cost, GE_t is the net produced energy by the microgrid system, y represents each year, n an integer, and l_a the asset lifetime. In addition, a devaluation rate r in the range ~8-8.5% needs to be included to account for the depreciation of component and energy production costs. The expression for cost influencing factors in Eq. (2.40)

can be graphically represented by Figure 2.39 [67]. Where CC_0 and are GE_t equivalent of I_0 and E_t, respectively. The plot shows a strong influence of the CC_0 on the LCOE of a system. A reduction of 75% of CC_0 can reduce the electricity cost to a quarter [67]. The microgrid component cost is usually around two-thirds of the total initial investment CC_0, which can be significantly reduced by repurposing the second-life DG and batteries.

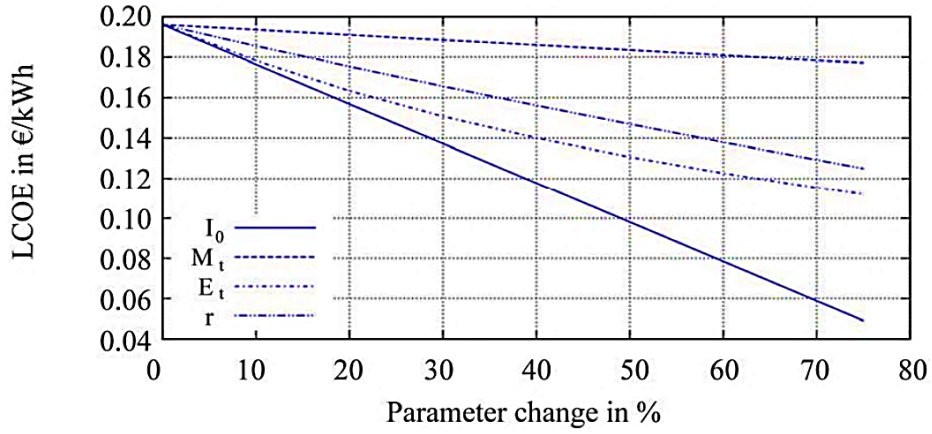

Figure 2.39 – Parameter impact on LCOE [67]

The expression in Eq. (2.40) is universal to individual LCOE of PV, DG, and other microgrid components. In other words, it is the linear sum of individual LCOE to find system LCOE. Generally, the central portion of the overall system cost comes from premature battery wear and early replacements. The LCOE for batteries ($LCOE_B$) may be calculated with the minor addition of battery roundtrip efficiency, energy cost on battery charging, and charging efficiency [68]. Considering these factors, the expression for the battery wear cost $M_{B,w}$ could be represented by the expression,

$$M_{B,w} = M_{B,rep} N_B \, L_{B,th} \sqrt{\eta_{B,rt}} \tag{2.41}$$

Where $M_{B,w}$ in \$/kWh is a function of the capital invested in battery bank replacement due to wear, $M_{B,rep}$ is the battery replacement cost in \$, N_B is the total number of batteries, $\eta_{B,rt}$ is the round trip efficiency, and $L_{B,th}$ is the battery lifetime throughput in kWh.

The model in Eq. (2.40) can be enriched by including capacity fade impact for PV power production. Considering N_{PV} as the total number of PV panels, the modified relation in Eq. (2.40) for $LCOE_{PV}$ becomes:

$$LCOE_{PV} = \frac{N_{PV} \, CC_{0,PV} + \sum_{y=0}^{l_a} N_{PV} \, M_{PV,o\&m(y)} \, (1+r)^{-y}}{\sum_{y=0}^{l_a} \left(1 - \sigma_{PV,y}\right)^{y} \, y \, GE_{PV} \, (1+r)^{-y}} \tag{2.42}$$

Where $M_{PV,o\&m(y)}$ is held fixed each year as there are no operational or fuel costs associated with PV. The factor $M_{PV,o\&m(y)}$ mainly include the annual costs of cleaning, land rent, equipment repair, taxes, and insurance. $CC_{0,PV}$ includes the total cost of PV

panels, structure, concrete foundations, planning, transport, survey, and installations. The inclusion of annual degradation factor $\sigma_{PV,y}$ (0.495%, 25 years lifetime) reduces total PV energy production and slightly increases $LCOE_{PV}$. In the simulations, we have assumed no PV degradation by considering its useful lifetime for 20 years. This assumption is based on the 20 years project lifetime. All other factors, such as PV energy used directly or retrieved from batteries and the unutilized excess PV power during low load, increases the system LCOE. The interested readers can find further detailed analysis in [68].

2.3 Design Goals and System Constraints

The only goal is to satisfy load requirement at affordable cost under the given constraints for PV, DG, and batteries. The generation and consumption within the microgrid are presented in their generalized form using Eqs. (2.47)-(2.51). Some of the design goals and constraints are briefly discussed as follows.

(1) PV: We design our microgrid to provide the required load demand, mainly covered by PV or batteries, and in extreme operational situations to be backed up by DGs. For a full day, the PV array can be sized as,

$$\int_{T_{1ss}}^{T_{2ss}} P_{PV}\,dt \geq \int_{T_{1ss}}^{T_{2ss}} P_L\,dt\,;\, where\ P_{PV} \leq N_{PV} * A_{s,PV} * G \qquad (2.43)$$

Where T_{1ss} and T_{2ss} denote the time slots with a burst of sunshine, P_{PV} and P_L are the total PV power and load power for a typical day, respectively. The output power is limited by the total number of PV panels (N_{PV}) and average maximal irradiance (G). However, it is not possible to continuously feed the entire load without the support of other energy sources due to intermittent solar power. Therefore, batteries or a DG can be added as a backup source to contribute to the power demand in unavoidable weather conditions.

(2) DG: The DG saves the DC bus from voltage collapse and the overall system from loss of electricity in the event of an emergency or a shortfall. It also reduces the pressure on batteries in harsh conditions (peak load, no sunshine, unplanned load evolution) and provides the power that could not be sourced the other way. However, the DG is on low-priority to support the microgrid due to cost and environmental issues.

$$\int_{0}^{T_3} P_{DG}\,dt \geq \left(\int_{0}^{T_3} \Delta P_{PV} + \Delta P_L - \Delta P_B - \Delta P_{L,lp} \right) \qquad (2.44)$$

Where ΔP_{PV} and ΔP_L are the worst-case variation of PV and load power (power deficit), ΔP_B is the maximum admissible variation of battery power (to source), and $\Delta P_{L,lp}$ is the required load cut with low priority. The DG is operated under limited use due to cost and environmental issues under the constraints $0 \leq P_{DG} \leq P_{DG,max}$. For interested readers, a nice literature about PV and DG sizing is suggested for further reading [69], [70].

(3) Battery: In order to make the system more reliable, additional power is sourced from the batteries for a specific duration T_1, which is represented as,

$$\int_0^{T_1} P_B dt \geq \int_0^{T_1} P_L dt \tag{2.45}$$

$$\int_0^{T_{2(tr)}} P_B dt \geq \int_0^{T_{2(tr)}} \Delta P_L dt + \int_0^{T_{2(tr)}} \Delta P_{PV} dt \tag{2.46}$$

Where, $T_{2(tr)}$ is the transient variation period for intermittency or load changes and batteries operate in their operational limits $Soc_{min} \leq SoC \leq SoC_{max}$.

2.4 Energy Flow in the System

Although, most of the work in this chapter is dedicated to the sizing and design of the microgrid system components. It is equally important to present the strategies for energy dispatch and power flow balance. Power management in DC microgrids with storage and intermittent sources has always been tricky for controllers [71]. Proper sizing and techno-economic selection of energy sources (PV, DG, and battery) are essential for optimal energy dispatch and flow balance [72]. There have been many proposed approaches to coordinate the operation of PV, DG, and batteries to meet loads [73].

2.4.1 Power Management and Energy Flow Balance

An energy storage unit is the most critical component whose primary duty is to keep an energy balance in the system and avoid the unnecessary starting of a DG or load cuts. Given the sources and loads characteristics and constraints [57], the power balance can be represented as the following generalized relation,

$$\sum P_{Gen} + P_{Con} = 0 \tag{2.47}$$

$$P_{PV} + P_{DG} \pm P_B - P_L = 0 \; ; or \; P_{PV} + P_{DG} \pm P_B = P_L \tag{2.48}$$

In Eq. (2.47), P_{Gen} is the total generated power, P_{Con} is the total consumed power within the microgrid, $P_{PV} + P_B$ (PV power deficit, batteries discharging), and $P_{PV} - P_B$ (a

condition with excess PV power, batteries charging). In addition, Eq. (2.48) defines the only goal to satisfy the load requirements under the given constraints expressed using Eqs. (2.43), (2.44), and (2.46). If the batteries are charging and load is served, then the combined expression for P_{PV} and P_{DG} is expressed as,

$$P_{PV} + P_{DG} = P_B + P_L \tag{2.49}$$

Where, Eq. (2.49) explicitly shows a condition for microgrid operation during the night or extreme weather. The power losses due to degradation of batteries and DG as a function of time t are denoted as $P_{DG,d}(t)$ and $P_{B,d}(t)$. In such a condition, Eq. (2.48) can be represented as follows.

$$P_{PV} + (P_{DG} - P_{DG,d}(t)) \pm (P_B - P_{B,d}(t)) - P_L = 0 \tag{2.50}$$

We put a constraint on P_{DG} to operate above 40% LF to maximize fuel efficiency and reduce frequent maintenance. The low-priority load cut is enabled if the batteries cannot source the required power due to physical limitations. If there is less available PV power due to partial shading $P_{PV,s}$ and the low-priority load cut $P_{L,lp}$ enabled, then the expression in Eq. (2.49) becomes,

$$P_{PV} - P_{PV,s} + P_{DG} - P_{DG,d}(t) = P_B - P_{B,d}(t) + P_L - P_{L,lp} \tag{2.51}$$

Where $P_{PV} = P_{MPP}$,

A typical power flow scheme within our proposed microgrid is shown in Figure 2.40 (inspired by the work in [74]). In this configuration, loads, batteries of different health, DG, and PV sources are lumped to present the energy flow directions.

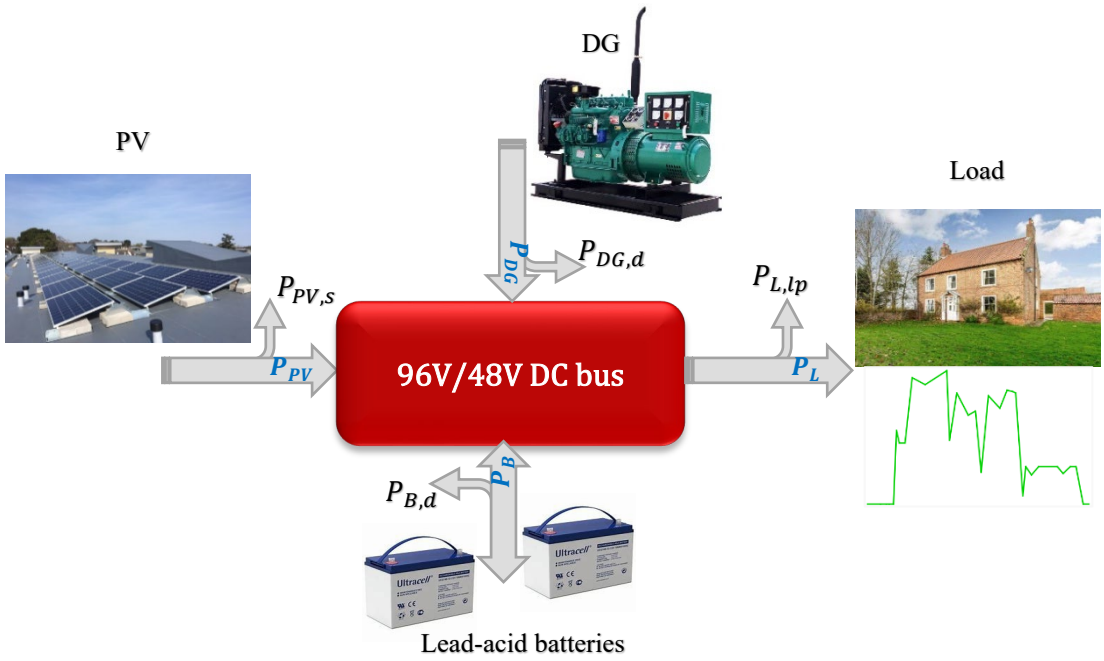

Figure 2.40 – Lumped system interconnection and power flow (source: own elaboration, inspired from [74])

The load is partially controllable by enabling a power cut during extreme situations. The number of required PV panels for the proposed microgrid is held fixed due to surface constraints. The two fully controllable sources, *i.e.*, batteries and DG, are optimized for an economical operation of the microgrid. These sources operate in proper coordination to optimally run the system and keep an energy balance. For the stable operation of a microgrid, the total power difference ΔP_t between generation ΔP_{Gen} and total consumption $\Delta P_{L,t}$ should be minimum. It is expressed as,

$$\Delta P_t = \Delta P_{L,t} - \Delta P_{Gen} \tag{2.52}$$

Where ΔP_t can be sourced by either batteries or DG or compensated by a load cut if the constraints do not allow the sources to provide the energy deficit. When the batteries cover the power deficit, it is recommended to consider other factors such as converter efficiency, self-discharge, and the remaining SoC. At any time interval t, the battery's remaining capacity is a function of SoC, which again is a function of battery cell voltage. Two different cases are presented to express the stored or discharged energy during a the one-hour time interval t.

Case-I (Battery Charging): If the total generation P_{Gen} exceeds the load demand P_L, the excess power is used to charge the batteries. It is mathematically described using the following linear relation.

$$C_B(t) = C_B(t - \Delta t)\big(1 - \sigma_{B,s}\big) + (\,\eta_{conv}(P_{Gen}(t) - P_L(t))\Delta t) \tag{2.53}$$

The power and energy values are interchangeable at one-hour time-steps. Here, $C_B(t)$ is the battery energy storage capacity (Wh) at $\Delta t = 1\text{h}$, $C_B(t-1)$ is capacity at the previous hour, $\sigma_{B,s}$ is battery self-discharge rate, and η_{conv} is the bidirectional converter efficiency. The term $\sigma_{B,s}$ is negligible when a long storage duration is not intended. It happens when the batteries are continuously being used. In this case, the stored energy remains a linear function of available power times the conversion efficiency.

Case-II (Battery Discharging): The battery storage units are discharging in the event of a power deficit when the load demand $P_L(t)$ exceeds the available PV generation $P_{PV}(t)$. The relation could be represented with the same conventions used in Eq. (2.53) but with the sign reversed for the power difference term.

$$C_B(t) = C_B(t - \Delta t)\big(1 - \sigma_{B,s}\big) - (\,\eta_{conv}(P_{Gen}(t) - P_L(t))\Delta t) \tag{2.54}$$

From the hierarchical point of view, the secondary control layer performs the power flow control within the system components and keeps the DC bus balanced [71]. As PV has a non-dispatchable and intermittent output power. Therefore, maintaining a power balance while satisfying system constraints is more challenging [57]. In such situations, batteries keep energy flow balance within their physical limits [31], [74].

2.4.2 Energy Management Controllers

In general, EMS is a system-level control to meet load demand at minimal costs and within the physical limits of each component. It can be done through power allocation using different strategies, simple to more complex [75]. For a low-power rural microgrid, simple rule-based EMS is more suitable. As a starting point, such kind of EMS has the following main advantages.

- Human experiences can be easily automated to get desired microgrid behavior;
- Requires minimal computations;
- Can be modified easily to change operational limits and constraints; and
- Easy and understandable for fine-tuning the system components. Thus, it is easy to handle by the local technicians and best suit the rural sites.

The rule-based EMS uses human knowledge and experience. It makes sense as keeping skilled persons in rural areas is relatively not easy. With the manually tuned parameters and system constraints, such as physical limits on the battery SoC, fuel consumption, and maximum DG operation hours in a day, the addition or decommissioning of any storage unit/energy source can be easily set in the EMS controllers. The beauty of rule-based EMS is in its practicality and run-time power allocation decisions while respecting the operational limits of the energy sources [76]. In situations where uncertainty arises, such as the addition of unplanned loads or degraded performance of DG and batteries, genetic algorithm-based optimized rules are used to automatically evolve the decisions with the new constraints.

2.4.3 System Operational Strategy

Some of the main points about our system operational strategy are described below. There are different scenarios in which a DG is turned ON. A low-priority load cut can reduce the DG operational hours if there is a power deficit. The load-cut in the first stage is used to reduce pressure on the batteries and delay turning ON a DG. The energy profiles of

sources and batteries are calculated and compared in kWh. As the system simulations are performed at one-hour time-steps, therefore, the PV power in kW is considered as kWh energy available in the system for each of the simulation time-step, making it easier for calculating energy balance. The modified and simple rule-based EMS is summarized in the following steps and a detailed flow is depicted in Figure 2.41.

- If the load demand $P_L(t)$ is less than the PV generated power $P_{PV}(t)$, the surplus power is used for batteries charging. If surplus power is more than the batteries capacity $C_{B,max}(t)$, the excess power dumped as surplus PV;
- If $P_L(t)$ is higher than $P_{PV}(t)$ and batteries remaining capacity $C_B(t)$ is higher than the minimum capacity threshold $C_{B,min}(t)$, the batteries supply the difference $P_L(t) - P_{PV}(t)$;
- If $P_L(t)$ is higher than the combined power $P_{PV}(t)$ and $C_B(t)$, then a low-priority cut is enabled. If the batteries are getting down beyond $C_{B,min}(t)$, the DG is turned ON at rated power to supply $P_L(t)$ and charge the batteries to $C_{B,max}(t)$; and
- If the power insufficiency is still higher than the total energy sources ($P_L(t) > P_{PV}(t) + P_{DG}(t) + C_{B,max}(t)$) the shortfalls occurs and only 25% of the high-priority load is served. The magnitude of load cut in this case is increased to 75%.

It can be noted that the implementation of a load cut in emergency conditions saves the DC bus from voltage collapse. However, 25% of the total load is served even at increased DG operation hours to cover the essential high-priority loads, such as equipment in a dispensary or public lighting during the night. The load loss is compromised by less energy tariff, which is an important consideration for increasing the social acceptance of the electrification services in rural environments.

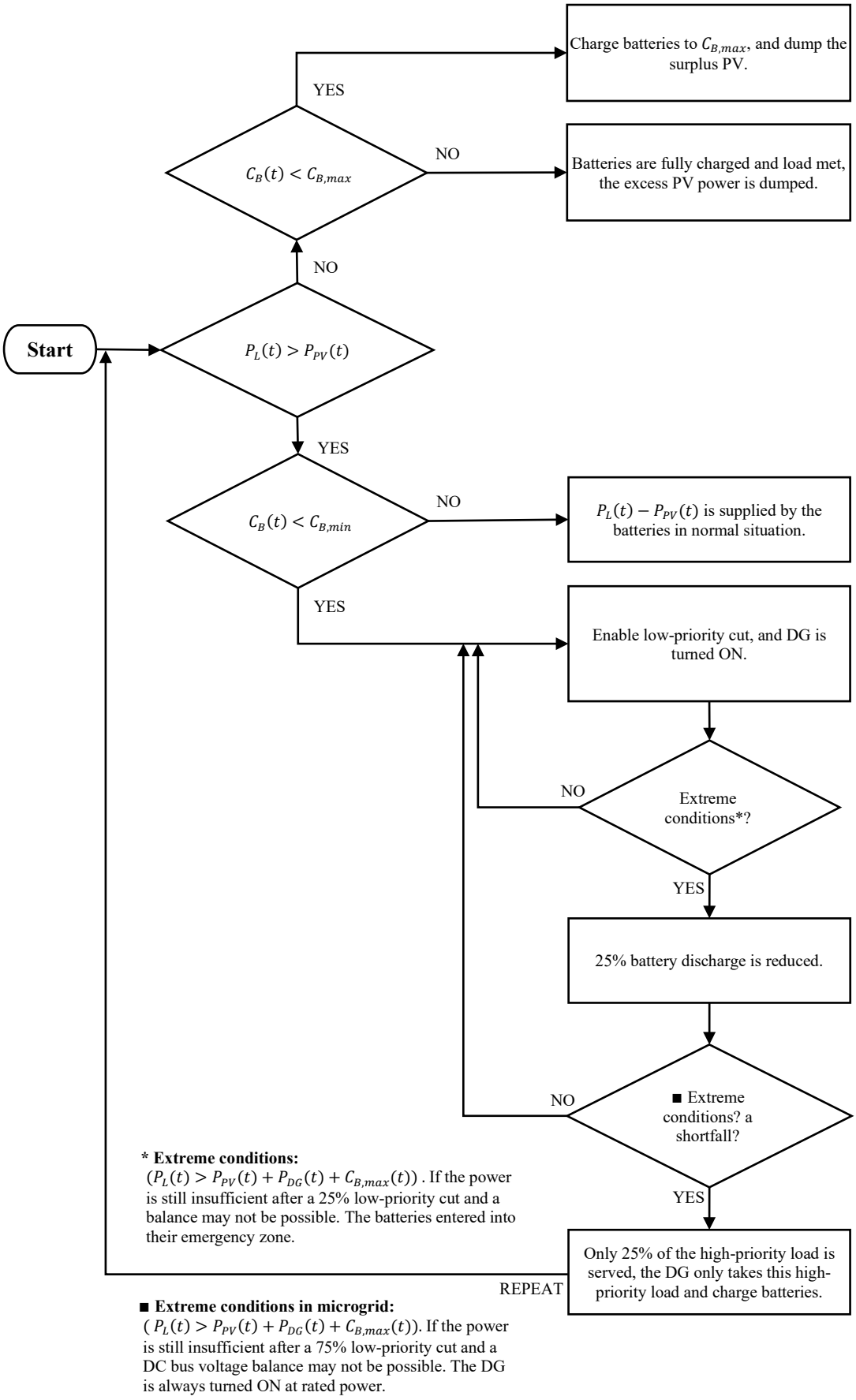

Figure 2.41 – Flow scheme of the proposed operational strategy

In the simulations part of CHAPTER-IV, an extreme condition is defined as an event at any arbitrary interval t, when the microgrid may not remain stable after this point. The DG must be turned ON to provide an energy balance and charge the batteries efficiently.

2.5 Summary

In conclusion, this chapter has provided a foundation step toward planning a low-power PV-based microgrid with batteries and a DG. The chapter covered each element of a microgrid, from theoretical equations to physical modeling. Later, electrical models were presented for ease of simulation and control. These models are parameterized to analyze the aging response in the following chapter. It will thus enable to use the models in the degraded mode operation of the microgrid in upcoming chapters. A considerable portion of the next chapter covers battery measurements and laboratory-level experimental tests.

--The end----Chapter-II--**

Bibliography Chapter-II

[1] I. Patrao, E. Figueres, G. Garcerá, and R. González-Medina, "Microgrid architectures for low voltage distributed generation," Renewable and Sustainable Energy Reviews, vol. 43, pp. 415–424, Mar. 2015, doi: 10.1016/j.rser.2014.11.054.

[2] A. T. Elsayed, A. A. Mohamed, and O. A. Mohammed, "DC microgrids and distribution systems: An overview," Electric Power Systems Research, vol. 119, pp. 407–417, Feb. 2015, doi: 10.1016/j.epsr.2014.10.017.

[3] M. Soshinskaya, W. H. J. Crijns-Graus, J. M. Guerrero, and J. C. Vasquez, "Microgrids: Experiences, barriers and success factors," Renewable and Sustainable Energy Reviews, vol. 40, pp. 659–672, Dec. 2014, doi: 10.1016/j.rser.2014.07.198.

[4] S. Qazi, "Fixed standalone PV systems for disaster relief and remote areas," in Standalone Photovoltaic (PV) Systems for Disaster Relief and Remote Areas, S. Qazi, Ed. Elsevier, 2017, pp. 139–175. doi: 10.1016/B978-0-12-803022-6.00005-8.

[5] O. Erdinc and M. Uzunoglu, "Optimum design of hybrid renewable energy systems: Overview of different approaches," Renewable and Sustainable Energy Reviews, vol. 16, no. 3, pp. 1412–1425, Apr. 2012, doi: 10.1016/j.rser.2011.11.011.

[6] P. Pal, V. Mukherjee, P. Kumar, and M. Elizabeth Makhatha, "Viability analysis of direct current (DC) standalone hybrid photovoltaic (PV)/ hydrogen fuel cell (HFC) energy system: A techno-economic approach," Materials Today: Proceedings, vol. 39, pp. 1807–1812, Jan. 2021, doi: 10.1016/j.matpr.2020.10.405.

[7] K. A. Kavadias and P. Triantafyllou, "Hybrid Renewable Energy Systems' Optimisation. A Review and Extended Comparison of the Most-Used Software Tools," Energies (Basel), vol. 14, no. 24, pp. 1-28 (8268), 2021, doi: https://doi.org/10.3390/en14248268.

[8] P. H. Shaikh, A. Shaikh, Z. A. Memon, A. A. Lashari, and Z. H. Leghari, "Microgrids: A review on optimal hybrid technologies, configurations, and applications," International journal of energy research, vol. 45, no. 9, pp. 12564–12597, 2021.

[9] D. Turcotte, M. Ross, and F. Sheriff, "Photovoltaic hybrid system sizing and simulation tools: Status and Needs," PV Horizon : Workshop on Photovoltaic Hybrid Systems, pp. 1–10, Sep. 2001.

[10] L. Arribas, G. Bopp, M. Vetter, A. Lippkau, and K. Mauch, "World-wide overview of design and simulation tools for hybrid PV systems." IEA, Report IEA-PVPS T11-01:2011, Jan. 2011.

[11] S. Phrakhonkham, J.-Y. Lechenadec, D. Diallo, and C. Marchand, "Optimisation software tool review and the need of alternative means for handling the problems of excess energy and mini-grid configuration: A case study from Laos," in ASEAN Symposium on Power and Energy Systems, Sep. 2009, pp. 53–58.

[12] W. Su, "Microgrid Modeling, Planning and Operation," Virginia Polytechnic Institute and State University, Thesis and Dissertations, 2009.

[13] T. Lambert, P. Gilman, and P. Lilienthal, "Micropower System Modeling with Homer." John Wiley & Sons, 2005.

[14] S. Phrakonkham, "Contribution to the pre-sizing and optimization of electrical energy production sites in isolated sites from renewable energies: application to the case of Laos," University Paris-Sud, France, Doctoral dissertation, 2012.

[15] D. Connolly, H. Lund, B. V. Mathiesen, and M. Leahy, "A review of computer tools for analysing the integration of renewable energy into various energy systems," Applied Energy, vol. 87, no. 4, pp. 1059–1082, Apr. 2010, doi: 10.1016/j.apenergy.2009.09.026.

[16] J. L. Bernal-Agustín, R. Dufo-López, and D. M. Rivas-Ascaso, "Design of isolated hybrid systems minimizing costs and pollutant emissions," Renewable Energy, vol. 31, no. 14, pp. 2227–2244, Nov. 2006, doi: 10.1016/j.renene.2005.11.002.

[17] G. Prinsloo, R. Dobson, and A. A. Mammoli, "Smart Village Load Planning Simulations in Support of Digital Energy Management for Off-grid Rural Community Microgrids," Current Alternative Energy, vol. 2, no. 1, pp. 1–18, 2018.

[18] H. Tazvinga, X. Xia, and J. Zhang, "Minimum cost solution of photovoltaic–diesel–battery hybrid power systems for remote consumers," Solar Energy, vol. 96, pp. 292–299, Oct. 2013, doi: 10.1016/j.solener.2013.07.030.

[19] E. C. Nnaji, D. Adgidzi, M. O. Dioha, D. R. E. Ewim, and Z. Huan, "Modelling and management of smart microgrid for rural electrification in sub-saharan Africa: The case of Nigeria," The Electricity Journal, vol. 32, no. 10, p. 106672, Dec. 2019, doi: 10.1016/j.tej.2019.106672.

[20] X. Li, J. Salasovich, and T. Reber, "Microgrid Load and LCOE Modelling Results https://data.nrel.gov/submissions/79." National Renewable Energy Laboratory (NREL), 2018.

[21] M. Sechilariu, F. Locment, and B. Wang, "Photovoltaic Electricity for Sustainable Building. Efficiency and Energy Cost Reduction for Isolated DC Microgrid," Energies (Basel), vol. 8, no. 8, pp. 7945–7967, 2015.

[22] D. L. Evans, "Simplified method for predicting photovoltaic array output," Solar Energy, vol. 27, no. 6, pp. 555–560, 1981, doi: https://doi.org/10.1016/0038-092X(81)90051-7.

[23] M. B. H. Rhouma, A. Gastli, L. Ben Brahim, F. Touati, and M. Benammar, "A simple method for extracting the parameters of the PV cell single-diode model," Renewable Energy, vol. 113, pp. 885–894, Dec. 2017, doi: 10.1016/j.renene.2017.06.064.

[24] I. Houssamo, B. Wang, M. Sechilariu, F. Locment, and G. Friedrich, "A simple experimental prediction model of photovoltaic power for DC microgrid," in 2012 IEEE International Symposium on Industrial Electronics, 2012, pp. 963–968.

[25] F. Masmoudi, F. Ben Salem, and N. Derbel, "Single and double diode models for conventional mono-crystalline solar cell with extraction of internal parameters," in 2016 13th International Multi-Conference on Systems, Signals Devices (SSD), 2016, pp. 720–728. doi: 10.1109/SSD.2016.7473725.

[26] A. R. Jordehi, "Parameter estimation of solar photovoltaic (PV) cells: A review," Renewable & Sustainable Energy Reviews, vol. 61, pp. 354–371, 2016.

[27] H. Tian, F. Mancilla-David, K. Ellis, E. Muljadi, and P. Jenkins, "A cell-to-module-to-array detailed model for photovoltaic panels," Solar Energy, vol. 86, no. 9, pp. 2695–2706, Sep. 2012, doi: 10.1016/j.solener.2012.06.004.

[28] T. Kousksou, P. Bruel, A. Jamil, T. El Rhafiki, and Y. Zeraouli, "Energy storage: Applications and challenges," Solar Energy Materials and Solar Cells, vol. 120, pp. 59–80, Jan. 2014, doi: 10.1016/j.solmat.2013.08.015.

[29] V. A. Boicea, "Energy Storage Technologies: The Past and the Present," Proceedings of the IEEE, vol. 102, no. 11, pp. 1777–1794, 2014, doi: 10.1109/JPROC.2014.2359545.

[30] A. A. Eajal, A. H. Yazdavar, E. F. El-Saadany, and K. Ponnambalam, "On the Existence of Voltage Collapse in Islanded Microgrid," in 2018 IEEE Electrical Power and Energy Conference (EPEC), 2018, pp. 1–6. doi: 10.1109/EPEC.2018.8598349.

[31] F. Locment, M. Sechilariu, and I. Houssamo, "DC Load and Batteries Control Limitations for Photovoltaic Systems. Experimental Validation," IEEE Transactions on Power Electronics, vol. 27, no. 9, pp. 4030–4038, 2012, doi: 10.1109/TPEL.2012.2189134.

[32] M. Aneke and M. Wang, "Energy storage technologies and real life applications – A state of the art review," Applied Energy, vol. 179, pp. 350–377, Oct. 2016, doi: 10.1016/j.apenergy.2016.06.097.

[33] H. Ibrahim, A. Ilinca, and J. Perron, "Energy storage systems—Characteristics and comparisons," Renewable & sustainable energy reviews, vol. 12, no. 5, pp. 1221–1250, 2008.

[34] P. Butler, J. L. Miller, and P. A. Taylor, "Energy storage opportunities analysis phase II Final Report: A study for the DOE energy storage systems program," Sandia report, SAND2002-1314, May 2002.

[35] K. R. Bullock, "Lead/acid batteries," Journal of power sources, vol. 51, no. 1–2, pp. 1–17, 1994.

[36] "IEEE Guide for selecting, charging, testing, and evaluating lead-acid batteries used in stand-alone photovoltaic (PV) systems," in IEEE Std 1361-2014 (Revision of IEEE Std 1361-2003), pp. 1–39, Jun. 2014.

[37] S. X. Chen, H. B. Gooi, and M. Q. Wang, "Sizing of Energy Storage for Microgrids," IEEE Transactions on Smart Grid, vol. 3, no. 1, pp. 142–151, 2012, doi: 10.1109/TSG.2011.2160745.

[38] "IEEE Recommended Practice for Sizing Lead-Acid Batteries for Stationary Applications," IEEE Std 485-2010 (Revision of IEEE Std 485-1997), pp. 1–90, 2011, doi: 10.1109/IEEESTD.2011.5751584.

[39] J. F. Manwell and J. G. McGowan, "Lead acid battery storage model for hybrid energy systems," Solar Energy, vol. 50, no. 5, pp. 399–405, May 1993, doi: 10.1016/0038-092X(93)90060-2.

[40] S. M. Mousavi G. and M. Nikdel, "Various battery models for various simulation studies and applications," Renewable and Sustainable Energy Reviews, vol. 32, pp. 477–485, Apr. 2014, doi: 10.1016/j.rser.2014.01.048.

[41] S. Lavety, R. Keshri, S. Ghosh, and M. A. Chaudhari, "Non-Linear Model and Parameter Extraction for Charge/Discharge Behavior of Valve Regulated Lead-Acid Battery," IEEE Transactions on Energy Conversion, vol. 36, no. 4, pp. 2600–2611, 2021, doi: 10.1109/TEC.2021.3062087.

[42] M. A. Fouad, M. A. Badr, and M. M. Ibrahim, "Modeling of micro-grid system components using MATLAB/Simulink," GSJ Scientific Journals, vol. 5, no. 5, pp. 1–15, 2017.

[43] R. A. Jackey, "A simple, effective lead-acid battery modeling process for electrical system component selection," in SAE World Congress & Exhibition, Apr. 2007, vol. 116, pp. 219–227. doi: https://doi.org/10.4271/2007-01-0778.

[44] O. Gergaud, G. Robin, B. Multon, and H. Ben Ahmed, "Energy Modeling of a Lead-Acid Battery within Hybrid Wind/Photovoltaic Systems," EPE 2003 - Toulouse, pp. 1–10, Sep. 2003.

[45] A. Hentunen, T. Lehmuspelto, and J. Suomela, "Time-Domain Parameter Extraction Method for Thévenin-Equivalent Circuit Battery Models," IEEE Transactions on Energy Conversion, vol. 29, no. 3, pp. 558–566, 2014, doi: 10.1109/TEC.2014.2318205.

[46] T. Hu, B. Zanchi, and J. Zhao, "Simple Analytical Method for Determining Parameters of Discharging Batteries," IEEE Transactions on Energy Conversion, vol. 26, no. 3, pp. 787–798, Sep. 2011, doi: 10.1109/TEC.2011.2129594.

[47] X. Lin et al., "A lumped-parameter electro-thermal model for cylindrical batteries," Journal of Power Sources, vol. 257, pp. 1–11, Jul. 2014, doi: 10.1016/j.jpowsour.2014.01.097.

[48] N. Barnel and M. Cordonnier, "Predicting valve regulated lead-acid battery sensitivity to ageing processes," in CIRED 2021 - The 26th International Conference and Exhibition on Electricity Distribution, 2021, pp. 167–171. doi: 10.1049/icp.2021.2023.

[49] M. Mohsin, A. Picot, and P. Maussion, "Lead-acid battery modelling in perspective of ageing: a review," in 2019 IEEE 12th International Symposium on Diagnostics for Electrical Machines, Power Electronics and Drives (SDEMPED), 2019, pp. 425–431. doi: 10.1109/DEMPED.2019.8864849.

[50] M. Alramlawi, Y. Souidi, and P. Li, "Optimal design of PV-Battery Microgrid Incorporating Lead-acid Battery Aging Model," in 2019 IEEE International Conference on Environment and Electrical Engineering and 2019 IEEE Industrial and Commercial Power Systems Europe (EEEIC / I CPS Europe), 2019, pp. 1–6. doi: 10.1109/EEEIC.2019.8783927.

[51] T. Hu, B. Zanchi, and J. Zhao, "Simple Analytical Method for Determining Parameters of Discharging Batteries," IEEE Transactions on Energy Conversion, vol. 26, no. 3, pp. 787–798, 2011, doi: 10.1109/TEC.2011.2129594.

[52] T. Kim and W. Qiao, "A Hybrid Battery Model Capable of Capturing Dynamic Circuit Characteristics and Nonlinear Capacity Effects," IEEE Transactions on Energy Conversion, vol. 26, no. 4, pp. 1172–1180, 2011, doi: 10.1109/TEC.2011.2167014.

[53] J. Meng, M. Boukhnifer, and D. Diallo, "Comparative study of lithium‐ion battery open‐circuit‐voltage online estimation methods," IET Electrical Systems in Transportation, vol. 10, no. 2, pp. 162–169, 2020, doi: 10.1049/iet-est.2019.0026.

[54] R. Vincent, M. Ait-Ahmed, A. Houari, and M. F. Benkhoris, "Residential microgrid energy management considering flexibility services opportunities and forecast uncertainties," International Journal of Electrical Power & Energy Systems, vol. 120, p. 105981, 2020.

[55] R. Vincent, "Energy management strategies applied to photovoltaic-based residential microgrids for flexibility services purposes," PhD Thesis, University Bretagne Loire, 2020. doi: 10.13140/RG.2.2.16075.41769/1.

[56] M. Ceraolo, "New dynamical models of lead-acid batteries," IEEE Transactions on Power Systems, vol. 15, no. 4, pp. 1184–1190, 2000, doi: 10.1109/59.898088.

[57] I. A. Azzollini et al., "Lead-Acid Battery Modeling Over Full State of Charge and Discharge Range," IEEE Transactions on Power Systems, vol. 33, no. 6, pp. 6422–6429, 2018, doi: 10.1109/TPWRS.2018.2850049.

[58] S. Barsali and M. Ceraolo, "Dynamical models of lead-acid batteries: implementation issues," IEEE Transactions on Energy Conversion, vol. 17, no. 1, pp. 16–23, 2002, doi: 10.1109/60.986432.

[59] G. Iwanski, Ł. Bigorajski, and W. Koczara, "Speed control with incremental algorithm of minimum fuel consumption tracking for variable speed diesel generator," Energy Conversion and Management, vol. 161, pp. 182–192, Apr. 2018, doi: 10.1016/j.enconman.2018.01.053.

[60] M. Torres and L. A. C. Lopes, "Inverter-Based Diesel Generator Emulator for the Study of Frequency Variations in a Laboratory-Scale Autonomous Power System," Energy and Power Engineering, vol. 5, no. 3, pp. 274–283, 2013, doi: 10.4236/epe.2013.53027.

[61] C. Yin, H. Wu, F. Locment, and M. Sechilariu, "Energy management of DC microgrid based on photovoltaic combined with diesel generator and supercapacitor," Energy Conversion and Management, vol. 132, pp. 14–27, Jan. 2017, doi: 10.1016/j.enconman.2016.11.018.

[62] H. Nikkhajoei and R. H. Lasseter, "Distributed Generation Interface to the CERTS Microgrid," IEEE Transactions on Power Delivery, vol. 24, no. 3, pp. 1598–1608, 2009, doi: 10.1109/TPWRD.2009.2021040.

[63] "IEEE Guide for Synchronous Generator Modeling Practices and Applications," IEEE Std. 1110-2002, pp. 1–80, 2003, doi: 10.1109/IEEESTD.2003.94408.

[64] X. Zhang, "Power Control of Diesel Engine-Generator Set Subject to Emission Constraints." Electronic Theses and Dissertations, University of Windsor 5357, 2012.

[65] "Approximate Diesel Fuel Consumption Chart 2013," Diesel Service and Supply. https://www.generatorsource.com/Diesel_Fuel_Consumption.aspx (accessed Mar. 03, 2022).

[66] C. S. Lai and M. D. McCulloch, "Levelized cost of electricity for solar photovoltaic and electrical energy storage," Applied Energy, vol. 190, pp. 191–203, Mar. 2017, doi: 10.1016/j.apenergy.2016.12.153.

[67] R. Knorr, "Design criteria and levelized costs of electricity for photovoltaic power plants at different global locations," in International Multi-Conference on Systems, Signals Devices, 2012, pp. 1–6. doi: 10.1109/SSD.2012.6197972.

[68] C. S. Lai et al., "Levelized cost of electricity for photovoltaic/biogas power plant hybrid system with electrical energy storage degradation costs," Energy Conversion and Management, vol. 153, pp. 34–47, Dec. 2017, doi: 10.1016/j.enconman.2017.09.076.

[69] S. H. El-Hefnawi, "Photovoltaic diesel-generator hybrid power system sizing," Renewable energy, vol. 13, no. 1, pp. 33–40, 1998.

[70] P. Arun, R. Banerjee, and S. Bandyopadhyay, "Optimum sizing of battery-integrated diesel generator for remote electrification through design-space approach," Energy, vol. 33, no. 7, pp. 1155–1168, Jul. 2008, doi: 10.1016/j.energy.2008.02.008.

[71] A. Iovine, T. Rigaut, G. Damm, E. De Santis, and M. D. Di Benedetto, "Power management for a DC MicroGrid integrating renewables and storages," Control Engineering Practice, vol. 85, pp. 59–79, Apr. 2019, doi: 10.1016/j.conengprac.2019.01.009.

[72] V. V. S. N. Murty and A. Kumar, "Multi-objective energy management in microgrids with hybrid energy sources and battery energy storage systems," Protection and control of modern power systems, vol. 5, no. 1, pp. 1–20, 2020.

[73] H. Mahmood and J. Jiang, "Decentralized Power Management of Multiple PV, Battery, and Droop Units in an Islanded Microgrid," IEEE Transactions on Smart Grid, vol. 10, no. 2, pp. 1898–1906, 2019, doi: 10.1109/TSG.2017.2781468.

[74] H. Tazvinga, B. Zhu, and X. Xia, "Optimal power flow management for distributed energy resources with batteries," Energy Conversion and Management, vol. 102, pp. 104–110, Sep. 2015, doi: 10.1016/j.enconman.2015.01.015.

[75] Y.-K. Chen, Y.-C. Wu, C.-C. Song, and Y.-S. Chen, "Design and Implementation of Energy Management System With Fuzzy Control for DC Microgrid Systems," IEEE transactions on power electronics, vol. 28, no. 4, pp. 1563–1570, 2013.

[76] M. Ashari and C. V. Nayar, "An optimum dispatch strategy using set points for a photovoltaic (PV)–diesel–battery hybrid power system," Solar Energy, vol. 66, no. 1, pp. 1–9, May 1999, doi: 10.1016/S0038-092X(99)00016-X.

Chapter-III: Modeling of the Aging Dynamics

Key Terms

Legacy batteries, battery characterization, battery capacity tests, battery aging, aging dynamics, model parameterization, pulsed discharge, staggered discharge.

Acronyms

AGM Absorbed glass mate
Ah Ampere-hour
C_{10} Discharge rate at 10A (C-rate)
CCCV Constant current constant voltage
DoD Depth-of-discharge
EoL End-of-life
EVs Electric vehicles
IEC International electrotechnical commission
V_{oc} Open-circuit voltage
PV Photovoltaic
SC Supercapacitor
SoC State-of-charge

Chapter Highlights

This chapter analyzes battery characterization and aging dynamics using simulations and experiments. Physical and capacity recovery tests are conducted to identify recoverable batteries and repurpose them by extending their lifecycle, which is an eco-friendly contribution. Two tests are conducted to determine the battery's remaining capacity and group them into three different health categories. During these tests, the battery discharge is periodically stopped in a controlled manner. Among many other battery behaviors, the discharge and recovery exponentials were of great interest for health characterization and parameter extraction. The study does not consider battery thermal dynamics, physics-based models, and degradation due to charge controllers. The diesel generator (DG) performance degradation and starting failures are presented before concluding the chapter.

Contents

CHAPTER 3

MODELING OF THE AGING DYNAMICS

Aging leads to performance degradation and irreversible changes in the battery chemistry. The battery aging mechanism such as corrosion, sulfation, reduction of active material, loss of electrolyte, sludging, and the inner short-circuits are often inter-dependent. Controlling one of them can break the chain and stop accelerated degradation. Though lead-acid batteries are the most accessible and low-cost option for electrification services, the literature on aging behavior is barely available. We try to cover this gap by finding ways to deal with discarded batteries that might operate as if they were at the end of their life. It is done through simulations and experimental tests on batteries with different discharge behaviors. These tests enabled us to analyze the performance impact of battery aging in a microgrid system.

3.1 Battery Aging and Performance Degradation

3.1.1 Parameter Evolution and Capacity Fade

This subsection covers the electrical and mathematical representation of battery models and their parameterization. In this work, we have studied lead-acid technology for the system-level implementation in microgrids as a primary energy storage component. Therefore, the electrochemical kinetics, acid concentration, or any inner physio-chemical processes are out of the scope of this work. A general arrangement of the electrodes, separators, and current collectors of a lead-acid cell is shown in Figure 3.42a,b [1]. It mainly consists of an electrolyte, a negative electrode (Pb), a positive electrode (PbO_2), current collecting grids, and a porous separator.

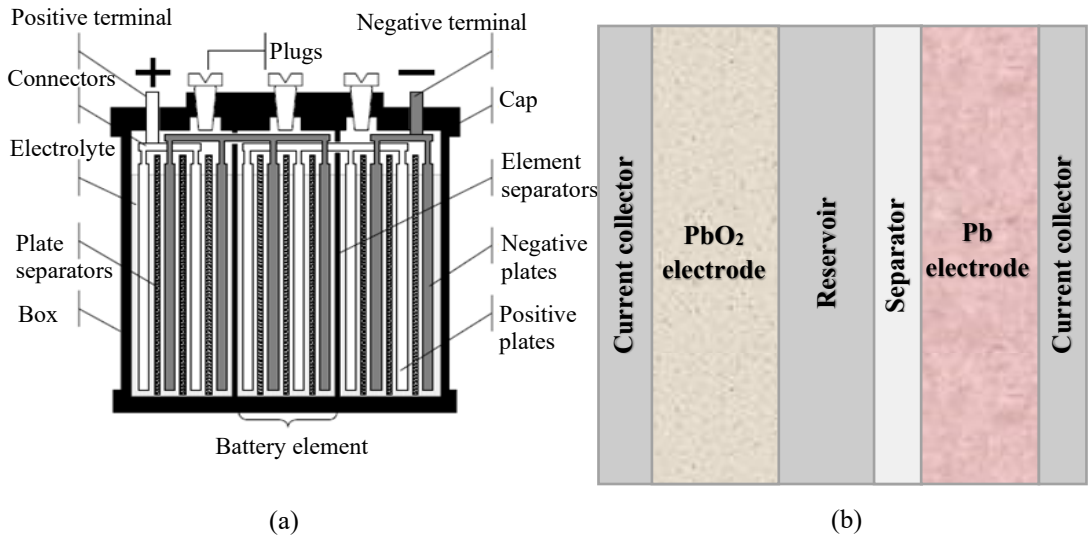

Figure 3.42 – Lead-acid battery: (a) cross-sectional view (b) physical arrangement of a cell [1]

(1) Battery Aging: The aging evolution depends on cycling, use history, and calendar life. In some cases, the premature capacity loss is due to the high-power cycling and internal short-circuits [2]. Many physical models help explain this physical phenomenon and its consequences under laboratory conditions [3], [4]. The remaining battery capacity directly impacts the maximum power delivery [5]. The primary aging processes include the time evolution of internal parameters, such as inner plate and electrolyte resistance. Some of these mechanisms are linear inter-dependent, while others are complex and could be represented with non-linear expressions [6]. Only a few of these influencing factors are listed as follows.

- Increased depth-of-discharge (DoD) and low state-of-charge (SoC);
- The charge/discharge current magnitude (both low and high);
- Acid stratification;
- Corrosion and degradation of the active material;
- Sulfation and growth of acid crystals;
- Time since the last full charge; and
- The time for which a battery is kept idle since the previous full discharge.

Aging is a strong function of SoC, DoD, temperature T_B, battery current I_B (by both charging/or discharging cases), and calendar aging time interval Δt. The aging could be represented as a function of these influencing parameters as follows.

$$C_{B,f}(t) = f(SoC, DoD, T_B, I_B, t) \tag{3.55}$$

Where $C_{B,f}(t)$ is the battery capacity fade linked in a non-linear relationship with the sudden drift in the battery SoC. The dependency of battery SoC on the remaining capacity and current drift is expressed using the following relationship.

$$SoC(t) = -\frac{1}{C_{B,n}}\int_0^t I_B(t)\,dt + SoC_0 \tag{3.56}$$

Where $C_{B,n}$ is the nominal battery capacity in Ampere-hour (Ah), and SoC_0 is the initial SoC at $t = 0$. In the event of discrete time-step k, the expression becomes,

$$SoC(k) = SoC(k-1) - \frac{I_B \Delta k}{C_{B,n}} \tag{3.57}$$

Where Δk is discharge interval in hours, and I_B is the constant discharge current during a time-step. In our case, two 100Ah batteries with different state of aging are tested for the discharge response at C_2 (50A pulse, $C_{B,n} = 100Ah$). So, Eq. (3.57) becomes,

$$SoC(k) = SoC(k-1) - 50 \times \left(\frac{1}{12}\right).\frac{1}{100} \tag{3.58}$$

Where 1/12 represents five minutes. The corresponding battery behaviors are plotted in Figure 3.43. As the battery voltage is a function of SoC and remaining health, the average health battery quickly touches the lower cutoff compared to the fresh battery.

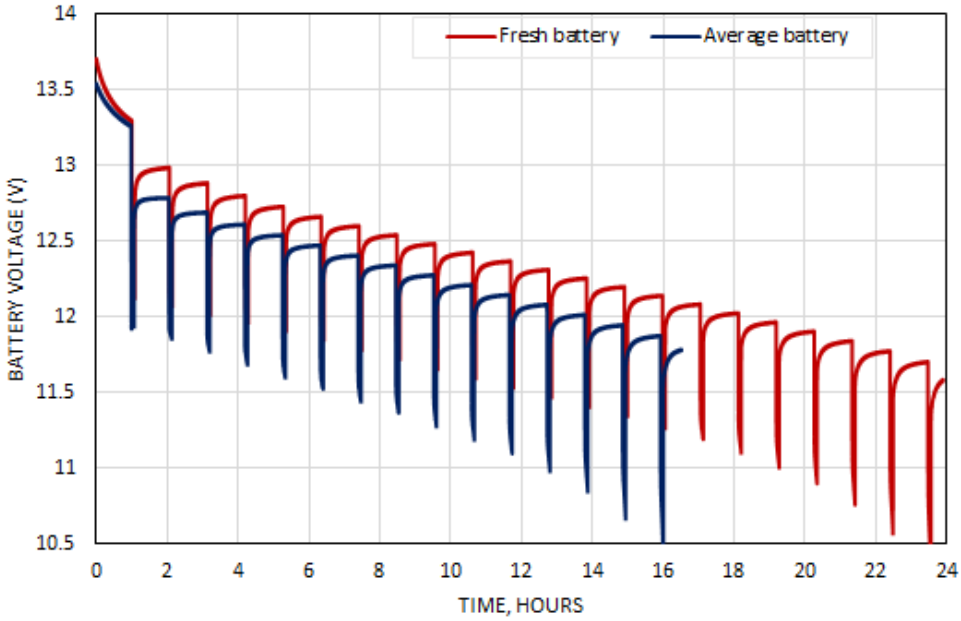

Figure 3.43 – Pulsed discharge response: two batteries with different stages of aging

The battery DoD is a function of the battery discharge current that drift over the intervals t_i to t_f and the battery initial capacity $C_{B,n}$. It is mathematically represented as,

$$DoD = \int_{t_i}^{t_f} \frac{I_B(t)\,dt}{C_{B,n}} \tag{3.59}$$

Unlike SoC, which is expressed as the battery charge regarding total capacity, DoD refers to the discharged capacity as a fraction of the total initial capacity [7]. Undeniably, the battery voltage becomes non-linear with DoD less than 70%, SoC below 30%. The non-linearity effect is also stronger at higher discharge currents. This battery behavior become dominant at colder temperatures due to slow electrochemical conversion. As calendar aging is steady, minor, and linear with time, the charge loss may be represented as,

$$Q_{B,f}(t) = C_{B,r}\, t \tag{3.60}$$

Where $C_{B,r}$ is the remaining battery capacity and $Q_{B,f}$ is the battery charge loss due to capacity fade, which can be approximated as a straight line for any arbitrary time interval denoted as t [8]. An important assumption here is to consider $C_{B,r}$ independent of capacity loss. It means that at each SoC level, the value of $C_{B,r}$ can be found independently.

(2) Mathematical Analysis of Battery Degradation: We assume that aging is directly related to the Ah-throughput [9], which is the extracted capacity in extreme conditions. The degradation factors are interrelated using Eq. (3.61). The impact of battery lifecycles could be modeled using Eq. (3.62) [9]–[12].

$$C_{B,r}(t) = C_{B,n(0)} - \left[C_{B,corr}(t) + C_{B,deg}(t)\right] \tag{3.61}$$

$$C_{B,deg}(t) = C_{B,deg(limit)} \times e^{-\sigma_{B,z}\left(1-\left(\frac{Z_W(t)}{1.6Z_{IEC}}\right)\right)} \tag{3.62}$$

Where $C_{B,n(0)}$ is the battery capacity during commissioning and $C_{B,corr}(t)$, $C_{B,deg}(t)$ are the capacity loss due to corrosion and degradation, respectively. In Eq. (3.62), $C_{B,deg(limit)}$ is the battery retirement limit at 80% remaining capacity due to cycling, $\sigma_{B,z}$ is a constant equals 5, Z_W is the weighted number of cycles without corrosion, and Z_{IEC} is provided on the datasheets and denotes the expected number of cycles up to the end of battery life. As battery aging is a combination of cycling and corrosion, the battery lifecycle is reached when Z_W equals $1.6Z_{IEC}$. In this case, Eq. (3.62) becomes,

$$C_{B,deg}(t) = C_{B,deg(limit)} \tag{3.63}$$

Further, the impact of SoC, discharge current, and acid stratification could be modeled with the expression of $Z_W(t)$.

$$Z_W(t + \Delta t) = Z_W(t) + \frac{|I_B(t)|\, f_{SoC}(t)\, f_{acid}(t)\, \Delta t}{C_{B,n}} \tag{3.64}$$

Where $|I_B(t)|$ denotes the charge-discharge current irrespective of the current direction. Whereas $f_{SoC}(t)$ and $f_{acid}(t)$ are the impacts of SoC and stratification, and $C_{B,n}$ is the nominal battery capacity at C_{10}. Additionally, the low level of SoC significantly reduces the battery capacity, which is more dangerous at considerable time intervals. It may increase the thickness of acid crystals on top of the active material, which resists charge acceptance.

(3) Impact of the Low SoC: This impact is modeled using the factor $f_{SoC}(t)$. At each full charge, its value is 1 indicating no net impact, but the factor gradually increases with time. The expression can be represented as,

$$f_{SoC}(t) = 1 + \left[K_{SoC,0} + K_{SoC,min}\left(1 - SoC_{min}(t)|_{t_0}^{t}\right) f_1(I_B, n_{bc})\,(t - t_0)\right] \quad (3.65)$$

Where t_0 is the time of the last fully charged condition of the battery. At $t = t_0$, the term to the right becomes zero. If more time passes, the effect becomes more dominant, and the term becomes considerable. The battery may not serve longer if the charge acceptance rate is either too slow or negligible. Also, $f_1(I_B, n_{bc})$ is the factor representing current, $K_{SoC,0}$ and $K_{SoC,min}$ are the constants, which relate SoC_{min} to SoC_0. Also, $SoC_{min}(t)$ is the minimum SoC at which the charging stopped in the preceding cycle. The factor $f_1(I_B, n_{bc})$ could be mathematically represented using the following expression,

$$f_1(I_B, n_{bc}) = \sqrt{\frac{I_{B,10}}{I_B(t)}}\ \sqrt[3]{exp\left(\frac{n_{bc}(t)}{3.6}\right)} \quad (3.66)$$

Where $I_{B,10}$ is the battery charge-discharge at a 10-hour rate and n_{bc} is the number of bad charges beyond 90% SoC. This factor may also reduce the battery performance.

(4) Corrosion Layer: The corrosion can be expressed as a function of the effective layer thickness $\Delta W(t)$ at a time interval t. It can be mathematically described as follows.

$$C_{B,corr}(t) = C_{corr,limit}\frac{\Delta W(t)}{\Delta W_{limit}} \quad (3.67)$$

Where $\Delta W(t)$ is the formation of the layer at any interval t and ΔW_{limit} is the absolute limit of corrosion layer thickness that gives maximum internal resistance and loss of active material. The resistance of the corrosion layer $\rho_{corr}(t)$ at any arbitrary time t, follows the same relation with $\Delta W(t)$. Therefore, $\rho_{corr}(t)$ could be expressed as:

$$\rho_{corr}(t) = \rho_{corr,limit}\frac{\Delta W(t)}{\Delta W_{limit}} \quad (3.68)$$

The battery is considered to reach its end-of-life (EoL) at ΔW_{limit}. It occurs at the battery float lifetime $F_{B,life}$. If the battery remains in a harsh operational situation, ΔW_{limit} may reach soon. It can be mathematically described as a linear function as follows.

$$\Delta W_{limit} = F_{B,life}\, S_{B,limit} \tag{3.69}$$

Where $S_{B,limit}$ is the speed factor that accelerates the capacity loss. The loss of capacity factor $C_{B,corr}(t)$ reaches its absolute limit when the growing layer ΔW equals the maximum limit of the thickness of the corrosion layer. Since the impact of corrosion is negligible on the negative electrode, we ignore its analysis.

(5) Acid Stratification: Finally, the degradation due to acid stratification $f_{acid}(t)$ could be obtained with the relation,

$$f_{acid}(t) = 1 + f_{str}(t)\sqrt{\frac{I_{B,10}}{|\, I_B(t)|}} \tag{3.70}$$

Undeniably, the low currents have a much more substantial impact as they can build up a thick formation of acid crystal layer that degrades the active mass. The stratification function $f_{str}(t)$ increases or decreases with the factor $\sqrt{\frac{I_{B,10}}{|\, I_B(t)|}}$ but cannot be zero in any case. Therefore, batteries degrade over time with this degradation factor. While considering a typical low-load consumption in a household for one year, and according to the battery datasheets as per international electrotechnical commission (IEC) standards, batteries are expected to last for ten years at nominal discharge currents. Due to the seasonal variations and the availability of photovoltaic (PV) power for charging batteries, the small charging currents may cause $f_{acid}(t)$ to be much more dominant. The batteries also accept and deliver low currents at cold temperatures. If the batteries are heavily sulfated, the stratification can be quickly diffused by slightly overcharging and outgassing using a custom-made rectifier-based charger. We refer to our published work for a complete description [13].

The batteries hardly find a rest time in our proposed microgrid, so calendar aging is void. This is the opposite of electric vehicles (EVs), where the cars are mostly parked, and batteries may undergo calendar aging. The readers are referred to many good papers for more details on capacity fade and degradation analysis, *e.g.*, [8], [10], [14]. Furthermore, an interesting article is recommended to learn more about battery degradation and degraded battery parameterization using measured data [9].

3.1.2 Battery Physical Tests and Capacity Restoration

This subsection is based on our experimental work on battery capacity restoration [13]. In this work, a rapid and low-cost battery test procedure for quick sorting and capacity restoration without a use history is proposed. For the sake of brevity, only work highlights are presented. Our published work can provide a complete description of the methodology and obtained results [13]. The related methodologies and experimental tests on second-life batteries could be further explored in the articles [15], [16], and remaining capacity recovery in [17]. The physical battery tests are conducted for quick sorting and to facilitate a decision on recycling or repurposing. Some of these tests include:

- ***Physical/ visual inspection:*** Battery and cell voltages, terminal condition, the color of the plates and vent plugs (for flooded cells), cell fluid/acid level, and specific gravity.
- ***Low load/ high load test:*** Open, shorted, and hard sulfated cells are identified using these tests. If the voltage drops by more than 1V with a rated discharge current, one or more battery cells are damaged.
- ***Charge acceptance test:*** Batteries with hard sulfation do not readily accept any charge, especially from intelligent chargers.
- ***Capacity recovery:*** It is done using heavy cycling at least for three times.
- ***Assembling:*** Batteries can then be assembled in different power packs.

3.1.2.1 Capacity recovery using heavy cycling

All the batteries, which pass the physical inspection, are subjected to heavy cycling process. The flow scheme in Figure 3.44 provides a global view of the methodology and description of the proposed capacity restoration technique. In this method, a weak battery is slightly overcharged and then deeply discharged using an ordinary battery charger with no intelligence. These custom-designed ordinary rectifier-based charger with no microprocessor control have the ability to slightly overcharge the batteries. In this way, the charger keeps pushing the current with a relatively higher voltage. It allows the battery plates to breath during the overcharge intervals that results in acid crystals detached from the plates allowing batteries to accept current for storing energy. In the event of really hard sulfation, the battery may not recover using this method.

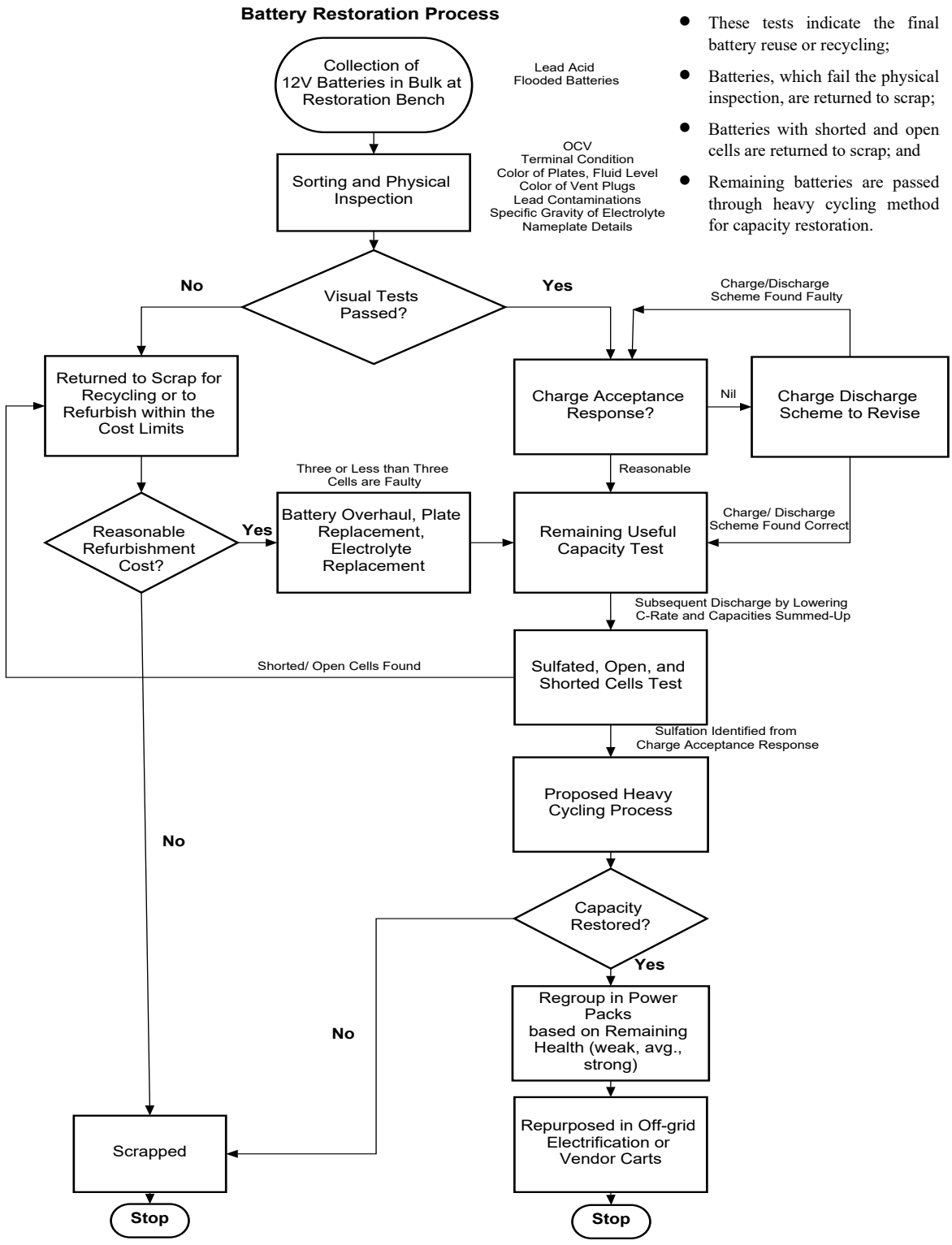

Figure 3.44 – Experimental methodology of the physical battery tests and capacity restoration

The recovered battery capacity and their charge acceptance response are detailed using Table 3.10. The battery performance before and after recovery is plotted in Figure 3.45. The recovered batteries with reasonable capacity are more economical, generate more revenues, and contribute to the green environment by delaying toxic recycling [18].

Table 3.10— Heavy cycling and charge acceptance response

100Ah Lead-acid Battery	Specs. of the Custom-made Charger	Connected Load Through a Cheap Inverter	Initial Current Acceptance (A)	Charging Time (hrs.)	Discharge Time @ 20A (mins)	Percentage Capacity Recovery (%)
Cycle 1	16V/6A	200W	0.1	24	10	3.30
Cycle 2	16V/6A	200W	1.2	24	30	10.0
Cycle 3	16V/6A	200W	2.5	24	50	16.7
Cycle 4	16V/6A	200W	3.3	24	90	30.0

- ☐ For at least four cycles, overcharge and deep discharge using a load of amperage of at least twice the battery C_{10} discharge current.
- ☐ A custom-made charger with no intelligence can be used. It consists of a transformer and rectifier that rely slightly on overcharge.
- ☐ The battery initial charge acceptance response is quite low, but increases from cycle to cycle.
- ☐ The battery can be discharged using a normal low-power inverter with a load or the car headlights.

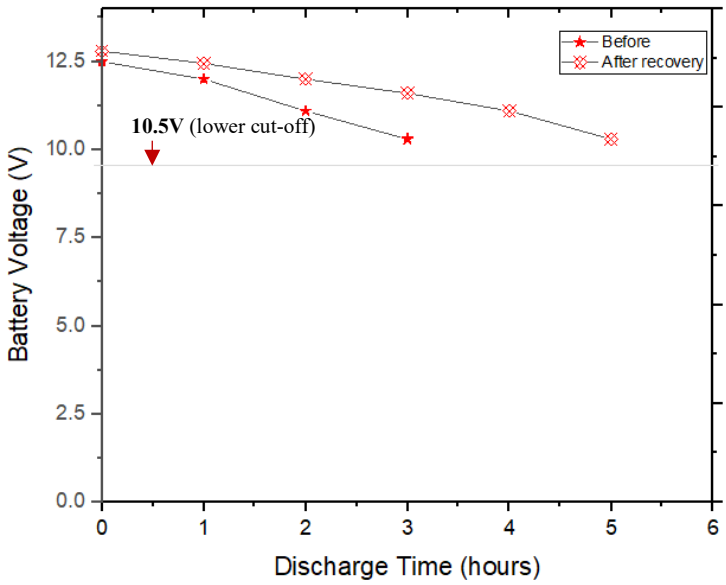

Figure 3.45 – Battery discharge response before and after capacity recovery

3.1.2.2 Experimental outcomes

Some of the leading experimental observations using the methodology in Figure 3.44 in the preceding SUBSECTION 3.1.2.1 include the following.

- Lead-acid batteries are mostly recoverable;
- Batteries that refuse to accept charge are heavily sulfated;
- Smart chargers cannot restore sulfated batteries, but transformer-based traditional chargers can do so with a slight overcharge;
- Acid crystals can be cracked down and dissolved using heavy cycling;
- The battery plates breath, and the crystals break down during the heavy cycling;
- The capacity recovery after four cycles is negligible. The test may be stopped and the recovered battery is repurposed;

- A battery with a shorted cell cannot be recovered;
- The change in charge acceptance time in each cycle is a fair indication of the battery recovery;
- The battery electrolyte gets boiled and outgassed, therefore, vent plugs to remain open; and
- Aspirin, baking soda, or Epsom salts reduces the battery's remaining life. They work in a pinch but also cause accelerated self-discharge and plate corrosion.

The experimental study was conducted for the flooded lead-acid batteries and may be extended to other battery chemistries with necessary modifications.

3.2 Battery Aging Analysis

The battery performance degradation directly impacts the system sizing, cost, and performance. This section covers simulations of a few battery models with and without aging. The model-based approach and its quick analysis had made it simple to parameterize different battery models. The models are based on the experimental outcomes from the battery test bench. The model parameters can be obtained using battery voltage and current measurements.

3.2.1 Test Bench and Experimental Protocol

This section describes the dynamics of genuine batteries with unknown use history and remaining health using two different experimental tests. A measurement platform is set up for the experiments to record the battery discharge behavior. The discharge current periodically stops to know the recovery exponentials for different battery groups. In this work, a one-hour battery rest is used to allow sufficient thermal equilibrium and voltage recovery time. The recovery slopes and battery rest voltages determine the battery health and their grouping. This information could also be used for the model parameterization.

(a) Experimental Bench: We have set up an experimental bench in the laboratory for the battery characterization and physical tests. As shown in Figure 3.46, a PC equipped with the LABVIEW® is used as a supervisor to control the experiment. The bench is capable of recording battery dynamics in a controlled manner. It is configured to automate data collection and test supervision thus speeds up reproducible measurements. All the samples are recorded for each second to precisely analyze the battery dynamics.

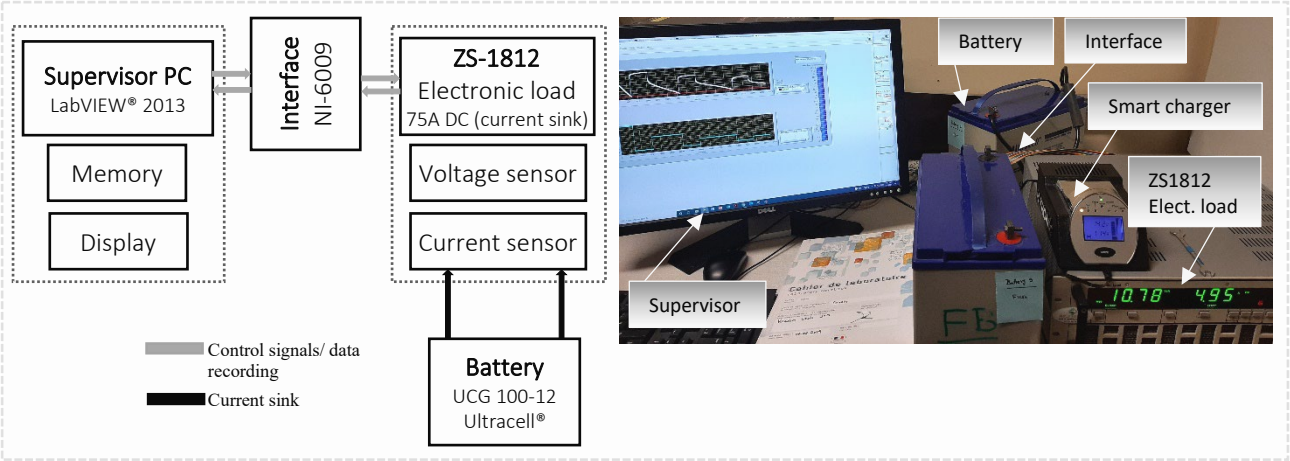

Figure 3.46 – Battery experimental bench

The H&H ZS-1812 electronic load is configured in constant current (CC) mode to act as a load or sink. The equipment initialization and settings are detailed as follows.

(b) Control Settings of the Electronic Load: The electronic load is configured in the external mode via different commands. These settings are configured in LABVIEW®. The control settings were verified for a range of discharge currents before starting the actual measurements. The bench can charge one battery with a constant current constant voltage (CCCV) charging profile and a discharge experiment with the CC mode at the same time. The plot in Figure 3.47 shows a 5A charging profile and a C_{10} rate discharge of the battery. The plot was recorded during the initialization phase to verify accuracy of the measurement. The equipment resolution is adjusted to a 50A discharge current without compromising measurement accuracy. However, the readers can choose the most appropriate procedure of the test equipment for their relevant application.

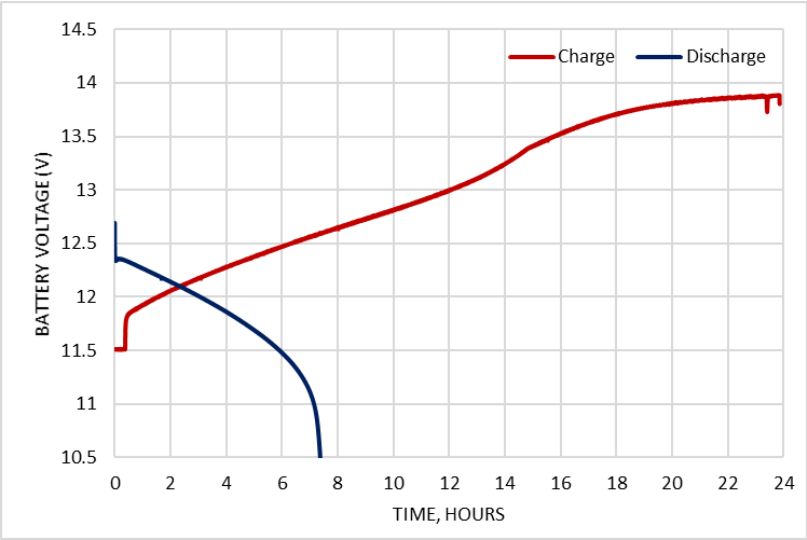

Figure 3.47 – Charge (5A) and discharge (10A) characteristics of the 12V battery

(c) Forced or Accelerated Aging: The proposed technique is used for the time and cycle aging of batteries at the laboratory level. The process is depicted in Figure 3.48.

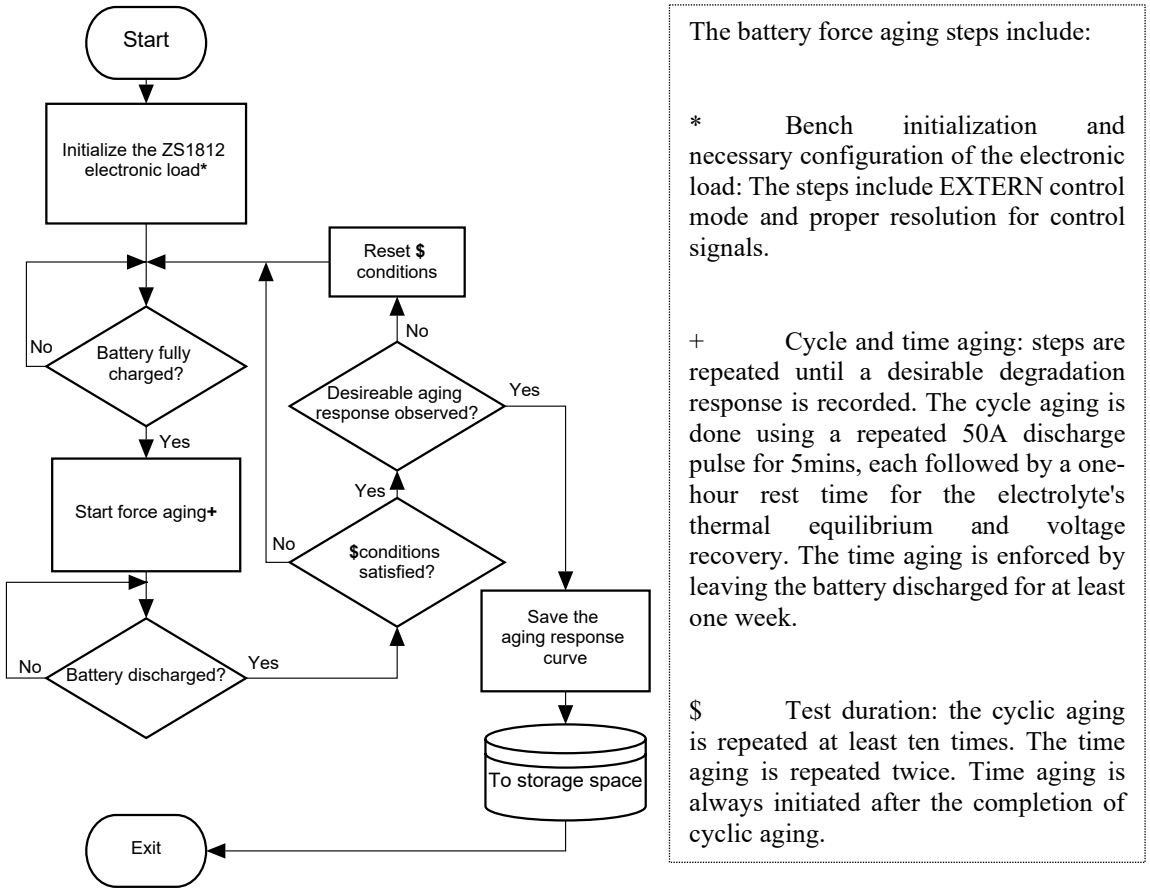

Figure 3.48 – Bench initialization and battery force aging procedure

3.2.2 Experimental Evaluation of the Battery Remaining Capacity

In this subsection, we cover the experimental evaluation of the actual remaining capacity of lead-acid batteries using two different discharge tests. The outcomes are based on our published work about the exact measurements of the remaining battery capacity [19]. This experimental work highlights the importance of an altered discharge sequence to avoid discarding a good battery. The outcome of these experiments provides the basis to identify fresh and weak batteries and size the battery banks more efficiently and economically. For the sake of brevity, only essential work highlights are presented.

(a) Methodology: The experimental test protocol is depicted in Figure 3.49. First, all the batteries are fully charged using the CCCV charging profile. The electronic load H&H ZS-1812 is initialized and discharge parameters are configured in LABVIEW®. A one-hour

relaxation is set for the electrolyte equilibrium and the open-circuit voltage (V_{oc}) recovery. It ensures to start the discharge experiment from the same test condition to avoid any measurement errors. All the system parameters for the experimental bench are enlisted in Table 3.11.

Table 3.11— System parameters for battery experiments

		Electronic load		
Load type	Range/ resolution	Device interface	Control mode	Measurement accuracy
H&H ZS-1812 current sink	75A DC	NI-6009 to Analog I/O	EXTERN/ remote	± 0.2% of measured value
		Batteries		
Capacity at C_{10}	Nominal voltage	Battery type	Cut-off threshold	Fully charge voltage
100Ah	12V	UCG 100-12 lead-gel	10.50V	14.30V
		Control supervisory system and battery chargers		
Smart charger	Charge/ discharge	Temp. control	Supervisor PC	Relaxation/ recovery
H-Tronic HTDC5000	CCCV/ CC	Ambient	LabVIEW® 2013	1 hour

Battery under test: UCG-100/12 absorbed glass mat (AGM) with gelled electrolyte commonly known as valve-regulated lead-acid (VRLA) batteries [20]. The battery datasheet is annexed as *A-V Battery Datasheet*.

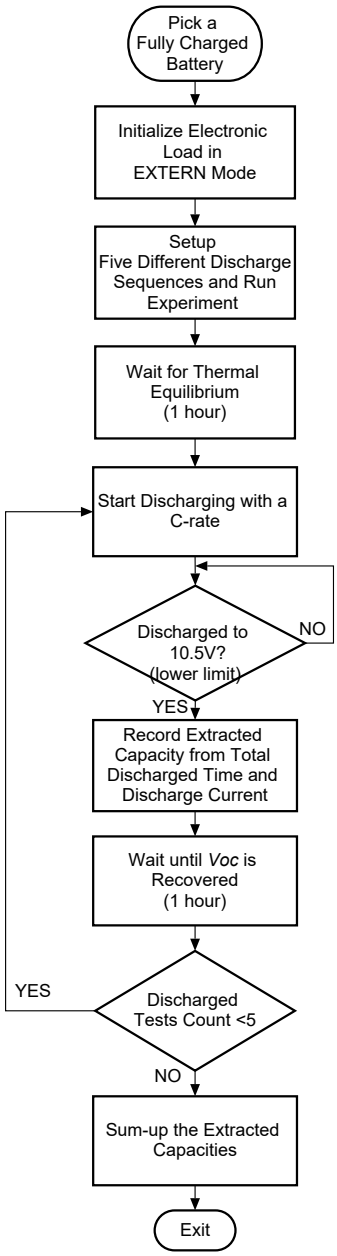

Figure 3.49 – Flow scheme of the experimental procedure (source: self-elaboration)

(b) Results: The following known datasheet C-rates are used in two different sequences to extract the residual capacity of a fully charged battery.

C_3	C_5	C_{10}	C_{20}	C_{40}	(fresh battery)
$C_{2.5}$	C_5	C_{10}	C_{20}	C_{40}	(fresh battery)
C_3	C_5	C_{20}	C_{10}	C_{40}	(weak battery)
$C_{2.5}$	$C_{2.5}$	C_{10}	C_{20}	C_{40}	(weak battery)

However, the readers can choose the most appropriate procedure of the test equipment for their relevant application. The measured battery capacity in each discharge cycle is enlisted in Table 3.12, and separately plotted in Figure 3.50.

Table 3.12— Extracted battery capacities in Ah during each discharge

Battery A (fresh)					Battery B (weak)				
Discharge sequence (Test 1) C = C_{10}= 100Ah									
C_3	C_5	C_{10}	C_{20}	C_{40}	C_3	C_5	C_{20}	C_{10}	C_{40}
83.2	6.6	5.0	2.9	2.4	66.6	9.3	8.9	0.8	3.7
100.2Ah (Total extracted capacity)					89.4Ah (Total extracted capacity)				
Altered discharge sequence (Test 2) C = C_{10}= 100Ah									
$C_{2.5}$	C_5	C_{10}	C_{20}	C_{40}	$C_{2.5}$	$C_{2.5}$	C_{10}	C_{20}	C_{40}
74.6	11.3	6.0	4.1	4.6	64.6	4.6	5.5	2.2	1.8
100.7Ah (Total extracted capacity)					78.9Ah (Total extracted capacity)				
Negligible capacity loss					Significant capacity loss				

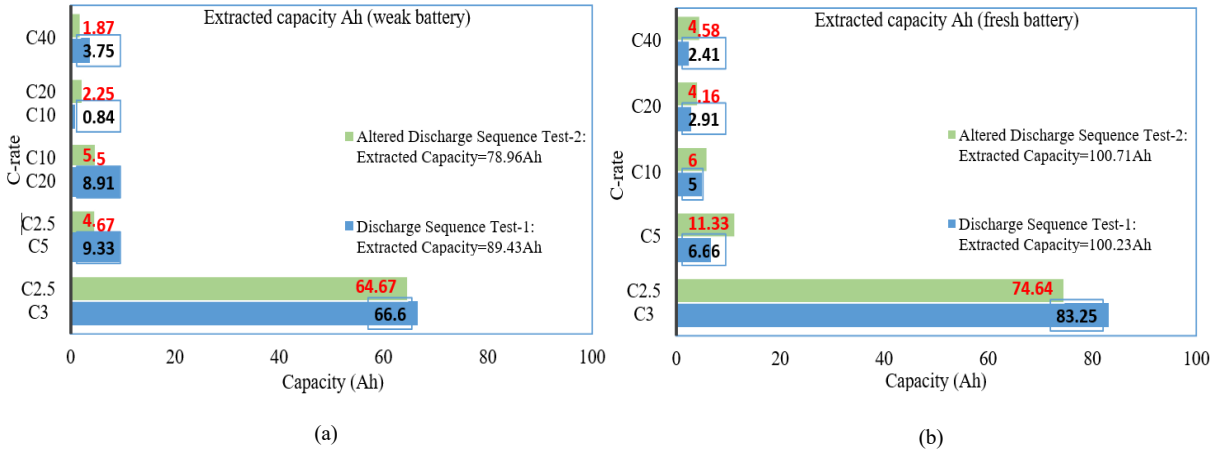

Figure 3.50 – Measured battery capacity in Ah (a) weak battery (b) fresh battery [19]

It is observed that the extracted capacities have a significant deviation in altering the discharge sequence for the weak battery, which indicates aging and capacity loss due to parameter evolution. Some of the key experimental observations include:

- ☐ A simple repeated discharge test could determine the battery's remaining capacity as a health indicator;
- ☐ Aging can be enforced at the laboratory level;
- ☐ The impact of altered discharge sequence is negligible for fresh batteries as their internal resistance is much lower. No significant capacity is lost due to the high discharge current;

- ☐ The altered discharge sequence has a dominant impact on the aged battery; and
- ☐ The aged battery significantly deviates from the initially extracted capacities by changing the discharge sequence. It is mainly due to increased internal drop.

This method of characterizing legacy batteries is particularly interesting for battery grouping in different power packs, where the corresponding weak battery group can be discharged in light load conditions.

3.2.3 Pulsed Discharge and Staggered Discharge Experiments

This subsection presents two classic experimental battery health identification and capacity determination techniques. The work is based on extending the experimental outcomes in our published work [19]. A detailed flow scheme of the two tests is included to understand the experimental methodology and test outcomes.

(a) Problem Formulation: When batteries start to degrade, the terminal voltages and residual capacities drift down quickly. The effect becomes dominant at high C-rates. Such a complex nature of the batteries is usually misinterpreted for capacity calculations. Figure 3.51 (adapted from [20]) shows the discharge characteristics of a 12V 100Ah battery. It can be noted that the battery discharge curves at different C-rates are misunderstood when the useful capacity is confused with the battery's actual residual capacity. Other problems include *e.g.,* misinterpretation of Peukert's law [21], [22], and the inaccurate battery sizing. Therefore, any miscalculation of the capacity may lead to high initial capital cost for microgrid installations [23].

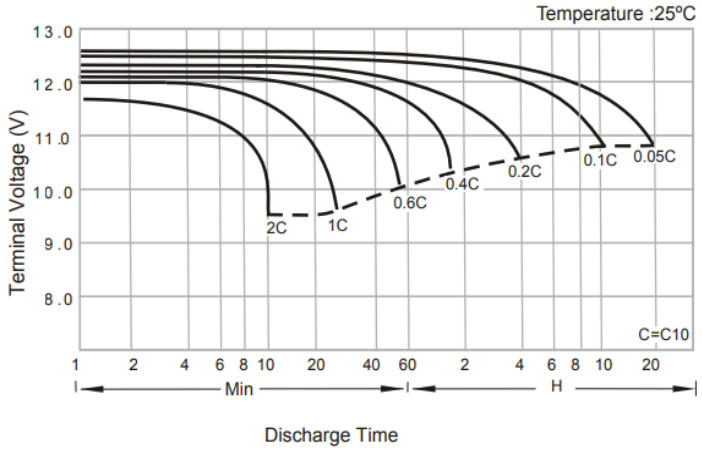

Figure 3.51 – Impact of different C-rates on the functional battery capacity [20]

In this plot, C_{10} is represented as 0.1C, which is also another way of representing C-rates in some battery datasheets. However, we use the first notation to present some of the battery measurement results.

(b) Proposed Methodology: The proposed system utilizes current, voltage measurements, and recovery slopes to determine battery capacity and aging. More precisely, this work covers battery health identification using a pulsed discharge test and capacity determination using the staggered discharge. All batteries are returned to a fully charged state before restarting an experiment. In this way, measurements can be recorded from the same test conditions. The experiment is conducted with five randomly selected batteries, all with unknown use history and health information. Two of these batteries give the same charging profile as others. Therefore, the CCCV charging response of the three batteries is considered interesting as they behave entirely different from each other and may fall in three different battery groups. The charging response is plotted in Figure 3.52. It can be observed that Battery 3 follows a slightly different charging trajectory than Battery 1 and Battery 5. It is mainly due to the increased internal battery resistance, which forces the charger to stay at a relatively higher voltage than the other two batteries. The Battery 3 behavior also indicates a low charge acceptance, which will result in less energy being stored and relatively low performance during discharge.

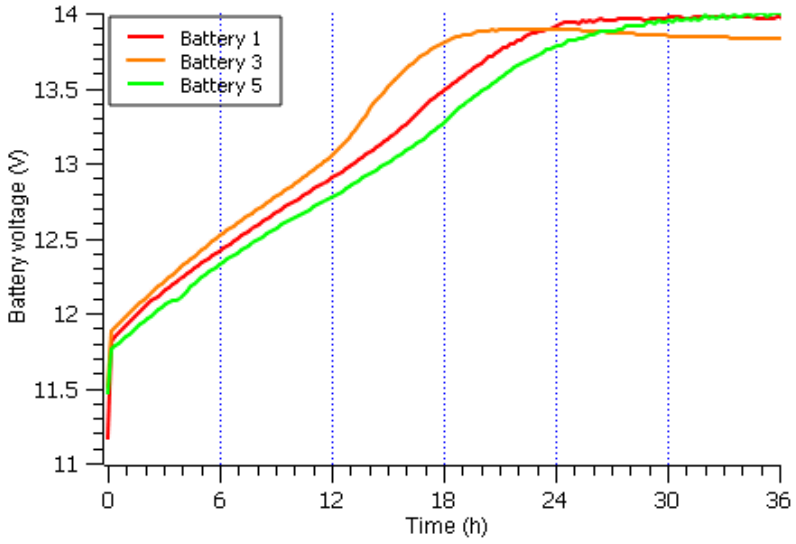

Figure 3.52 – Measured charging profiles of the three different battery groups

3.2.3.1 Measurement results

The measurement results are presented in the following sequence. A descriptive flow of the two experimental tests is given in Figure 3.53, which greatly details the process. It can be noted that Test 1 terminates on the battery lower cut-off at 10.5V, while Test 2 terminates on the two stop conditions, lower cut-off plus the number of staggered discharge sequences.

$I_{array(n)}$	$\Delta t_{array(n)}$
I_0	Δt_0
I_1	Δt_1
I_2	Δt_2
I_3	Δt_3
I_4	Δt_4

$n \in [0;4]$

0: VRLA 12V battery charged with CCCV mode.

1: Current sink (CC discharge).

2: Pulsed discharge test. Cut-off 10.5V, pulse duration 5mins, relaxation 60mins.

3: Staggered discharge test. $I_0 = C_{2.5\,(40A)}$, $I_1 = C_{5\,(20A)}$, $I_2 = C_{10\,(10A)}$, $I_3 = C_{20\,(5A)}$, $I_4 = C_{40\,(2.5A)}$.

4: From the array. Battery discharging with a pattern.

5: Data conversion via NI-6009 to I/O interface.

6: Δt in hours, array updated.

7: Pulse count 'n_i' save to array.

8: Test completed. Voltage recovery response after a full discharge.

9: Net Ah determined; no. of pulses measured. Further data analysis for both tests.

10: Charge battery for the next test.

11: Pulse duration: 5mins.

12: System in long rest. Test 2 stops at $V_B < 10.5V$ and pulse count equals 5.

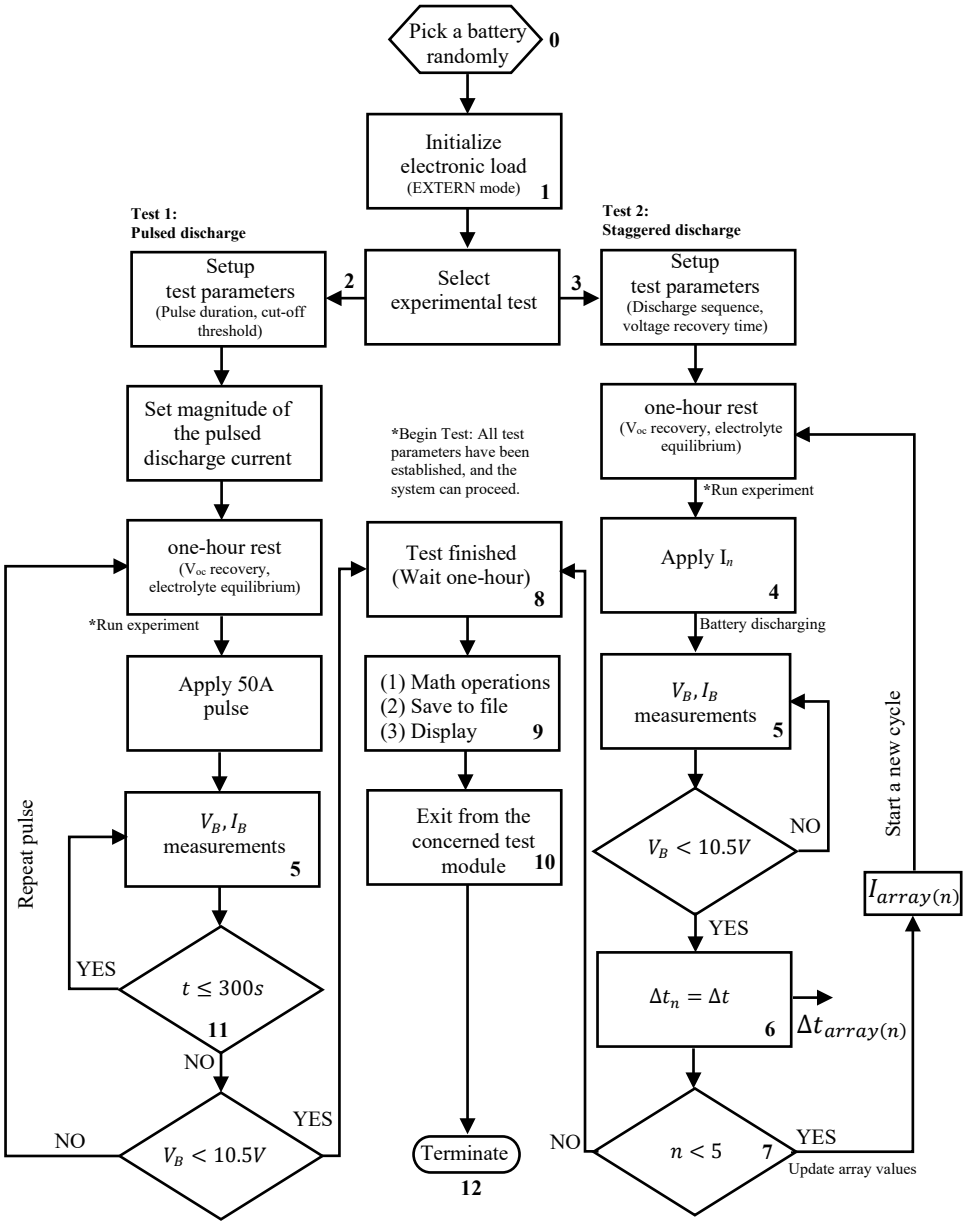

$$C_{B,e}\,(Ah) = C_0 + C_1 + C_2 + C_3 + C_4 = \sum_{n=0}^{4} \left(I_{array(n)} \times \Delta t_{array(n)}\right) \quad (3.71)$$

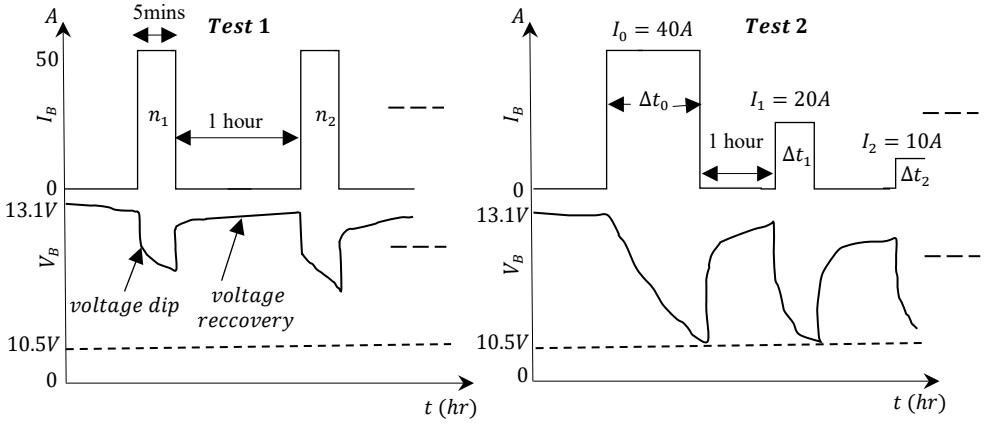

Figure 3.53 – Descriptive flow of the two experimental tests

A. Test 1: Pulsed discharge

The measurement results from Test 1 are plotted in Figure 3.54. The following essential battery dynamics can be obtained from the experimental observations.

- Voltage dips and voltage recovery slopes;
- Discharge and recovery exponentials; and
- The number of discharge pulses for test completion at 10.5V cut-off.

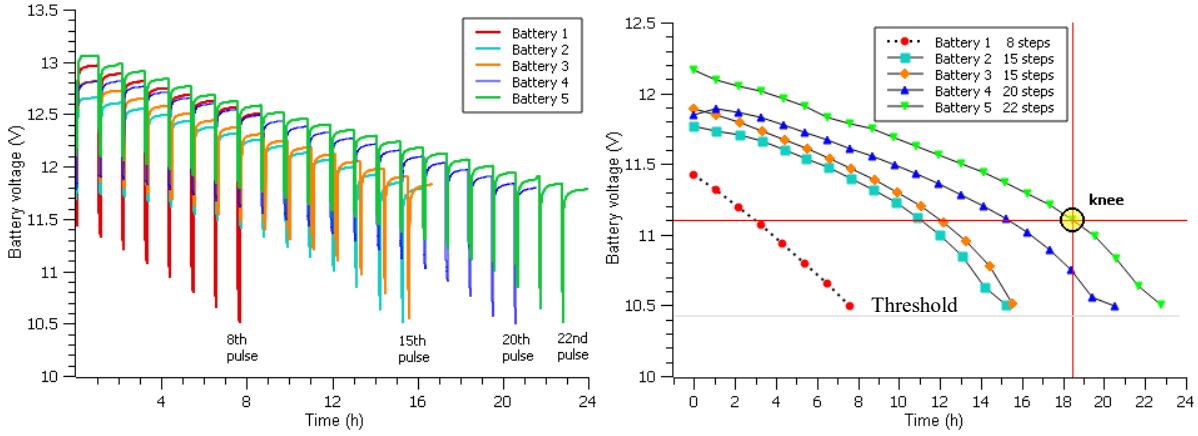

Figure 3.54 – Test 1 measurement results: (a) 50A pulsed discharge (b) discharge trajectory

(a) Knee point: It can be observed from Figure 3.54b that the progression of the voltage dips is quite linear and fast for Battery 1 as compared to a stable response of other four batteries. The knee point[13] approaches quickly for Battery 1, Battery 2, and Battery 3 as compared to Battery 4 and Battery 5. For the ease of analysis, we are more interested to analyze only three batteries that exhibit three distinct health conditions *i.e.*, weak, average, and fresh batteries.

(b) Voltage Dips and Recovery Exponentials: A notable response of the batteries in their respective groups are the voltage dips and recovery slopes, especially in the first few discharge cycles. Voltage dip is the sudden drop in battery voltage from the respective V_{oc} at rest when a discharge pulse is enabled. The battery voltage instantly sags down at this point. Therefore, it is calculated as the difference between two voltage points. These dynamics are plotted in Figure 3.55. These distinct responses are a fair indication of the different health conditions.

[13] Knee point: a point on the discharge progression curve at which the linear line slightly bends.

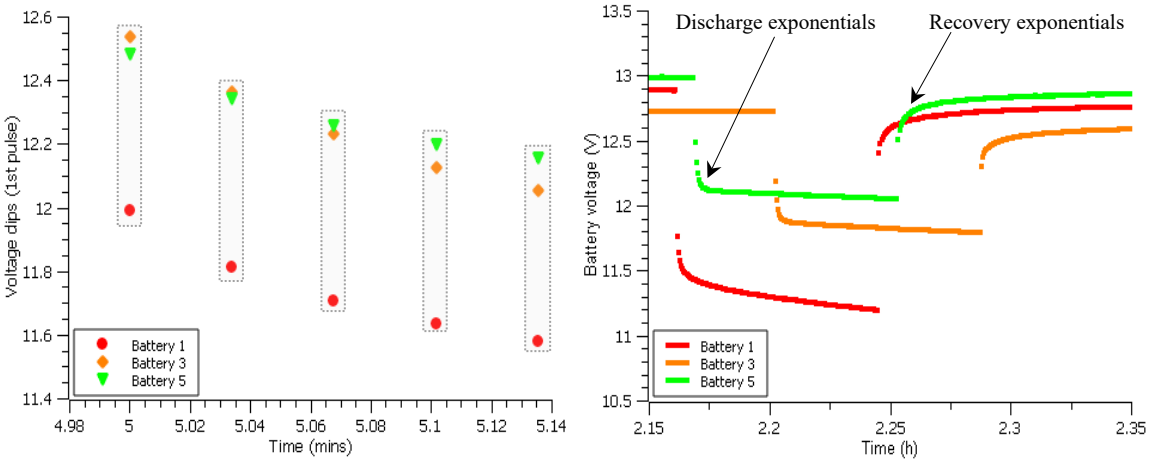

(a) (b)

Figure 3.55 – Measured results during Test 1: a closer view of the (a) voltage dips (b) recovery exponentials

B. Test 2: Staggered discharge

In this experiment, a fully charged battery is repeatedly discharged with five different C-rates, each with a one-hour relaxation. All the C-rates are the commonly used datasheet currents. The relaxation interval is sufficient to bring back a battery to its normal condition and be ready for the subsequent discharge in the next test. A full description of the C-rates for the battery under test can be found in [20] and is annexed. The battery cut-off at the lower threshold (10.5V) is carefully controlled by the electronic load to avoid any deep discharge or fatal damage to the battery. The system monitors the battery condition and disconnect it from the electronic load if any of the stop conditions is met. The experimental results are plotted in Figure 3.56a-f.

3.2.3.2 Comparative analysis of Test 1 and Test 2

(1) Performance Comparison: The proposed tests are briefly summarized as follows.

— ***Pulsed Discharge (Test 1):*** This test is mainly used to determine important battery dynamics. One of the plus points of this test is the ability to retrieve battery parameters from the dynamic response. These parameters could be used to tune the simulation models that could predict the performance of any battery.

— ***Staggered Discharge (Test 2):*** This test is primarily used for, ***(i)*** calculation of the total extracted remaining capacity ($C_{B,e}$) and ***(ii)*** to validate the battery characterization/ experimental response in Test 1. This accurate testing method classifies batteries in different groups and provides the exact value of the remaining utilizable capacity.

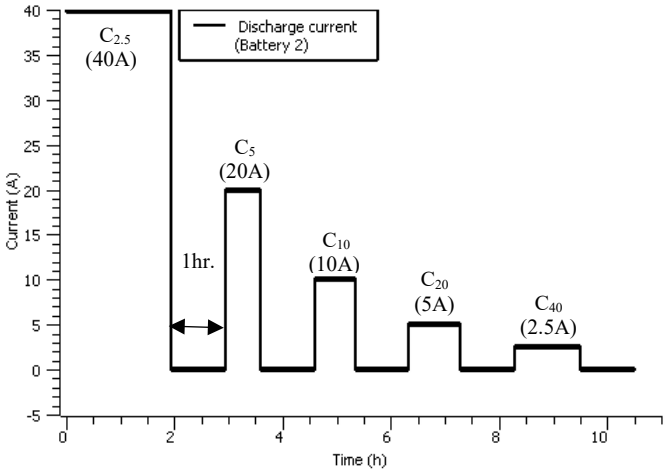

(a)

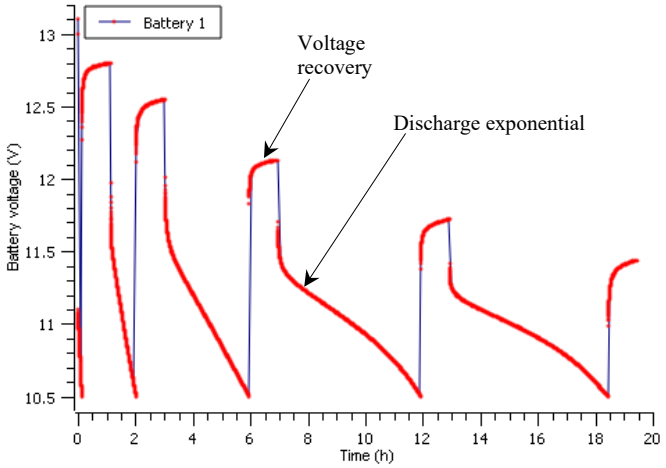

(b) $C_{B,e}$ = 91.13Ah

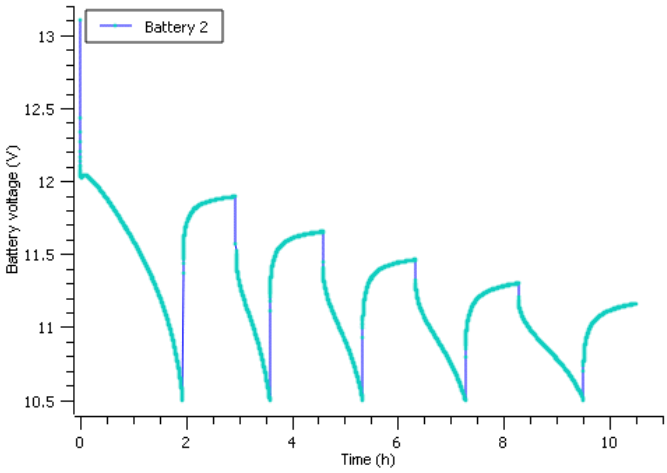

(c) $C_{B,e}$ = 105.83Ah

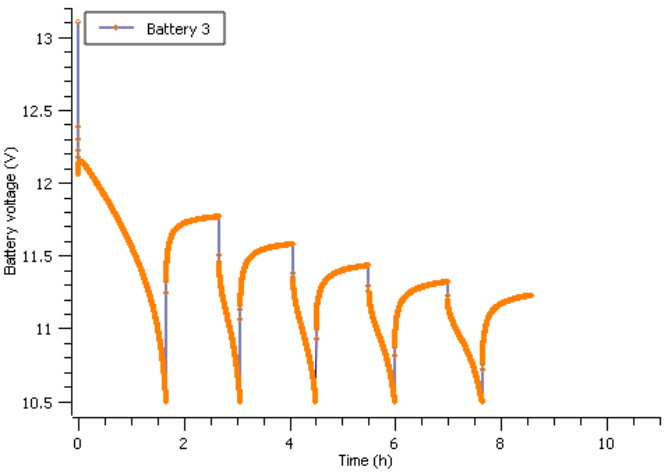

(d) $C_{B,e}$ = 83.06Ah

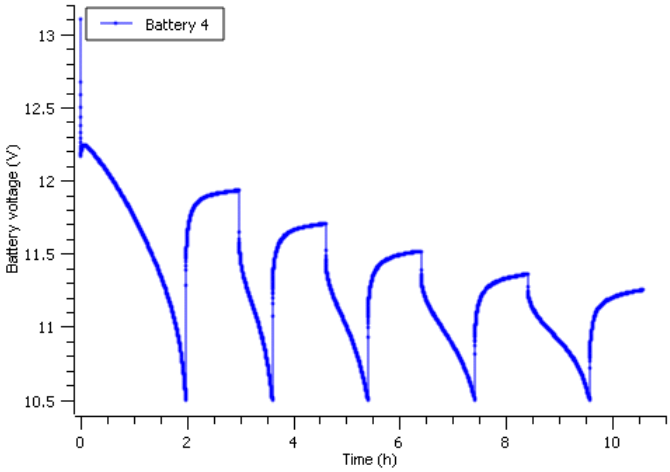

(e) $C_{B,e}$ = 107.80Ah

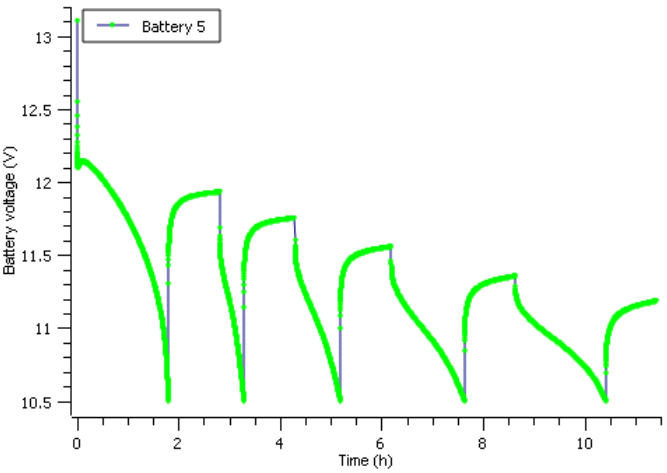

(f) $C_{B,e}$ = 103.82Ah

Figure 3.56 – Experimental results for Test 2: (a) C-rate sequence (b-f) discharge response of individual battery

(2) Quantitative Analysis of Test 1 and Test 2: In SUBSECTION 3.2.2, we found the net accumulated battery capacities using staggered discharge. The experimental results in both tests are now compared to distinguish weak, average, and fresh batteries. For better illustration and comparison, the individual capacity information is plotted in Figure 3.57. Additionally, all the performance parameters for the selected three batteries are listed in Table 3.13 and Table 3.14. In Table 3.14, the extracted capacity is the net sum of individually measured capacities in the five discharge cycles with different C-rates.

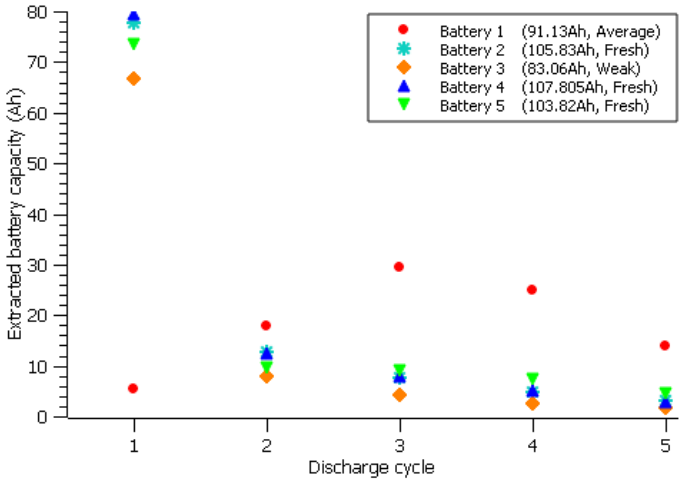

Figure 3.57 – Comparison of the individually extracted battery capacity

Table 3.13— Key performance parameters in Test 1

	Pulsed discharge				
Battery No.	*No. of 50A pulses*	*Voltage dip at 1st pulse*	*Voltage dip at 2nd pulse*	*Recovery voltage (1st exponential)*	*Knee point (h)*
Battery 1	8	− 1.53V	− 1.37V	12.96V	6
Battery 3	15	− 1.05V	− 0.86V	12.81V	10
Battery 5	22	− 0.95V	− 0.85V	13.06V	18

Table 3.14— Key performance parameters in Test 2

	Staggered discharge		
Battery No.	*Similar response*	*Extracted capacity, $C_{B,e}$ (Ah)*	*Capacity loss*
Battery 1	None	91.15	~ 10%
Battery 3	None	83.09	~ 20%
Battery 5	Battery 2, Battery 4	103.82	< 1%

The number of discharge pulses and knee points, discharge duration, extracted capacity using staggered discharge, and magnitude of the voltage dips are a few critical performance parameters for battery sorting and grouping. The tabulated data and figure

plots indicate the relevant dynamics of each battery in their respective groups, exceptions to Battery 1, which behaves entirely differently. With the lowest extracted capacity in cycle 1, the remaining net capacity is higher than Battery 3 for each of the remaining four cycles. It indicates that a battery may not be considered weak until the test is completed and the accumulated capacity sum is compared.

(3) Discussion on Outcomes of Test 1 and Test 2: The proposed system uses an experimental platform to characterize fresh and used lead-acid batteries without their use history and mission profile. The pulsed discharge method (Test 1) had effectively identified fresh batteries. However, the testing method was not accurate in determining the difference between a weak and an average battery. However, the test was convenient for the recovery exponentials and other essential battery dynamics. The ease and usefulness of Test 1 is in its rapid identification of the battery behavior in a single pulse. The test dynamics such as recovery exponentials can be used for battery parameter extraction. It could be helpful in the adaptive tuning of the battery models for microgrid simulations and battery health monitoring. In doing so, the energy management system (EMS) could evolve with the degraded performance of the aged batteries and change controls to utilize each battery pack based on their remaining capabilities.

The second method (Test 2) best characterizes the battery based on the actual remaining capacity. For the large collection of batteries, if the response differences are not much deviated, they belong to the same group and have the same use history. Therefore, Test 1 and Test 2 could be used concurrently to quickly sort a huge collection of discarded batteries. The tests also provide fair use of the battery aging behavior to avoid a good battery being junked, which may still serve longer in different power packs. Now, we are moving to the next subsection to analyze the battery performance using simulations.

3.2.4 Aging Analysis with Simulations

In this section, a generic 12V battery model is parameterized in SIMULINK® [24]. The parameters such as remaining capacity, internal battery resistance (R_0), SoC, and discharge currents strongly impact the model dynamics [25]. The parameters are chosen such that the model behaves like a genuine battery in the experimental part of SUBSECTION 3.2.2. These parameters are used as an initial condition for the simulations. The model assumptions are based on the experimental outcomes. In the experimental analysis,

temperature, Peukert's effect [21], [22], self-discharge, and the impact of discharge current amplitude on the battery resistance were ignored. Likewise, the exact impact is simulated, and results are compared. The model simulates batteries with three different remaining health categories (fresh, average, and weak). The response to a 50A pulse current is plotted and compared using Figure 3.58. Each battery model is tuned using the listed parameters in Table 3.15. These parameters are adapted from the experimental outcomes discussed in SUBSECTION 3.2.3. The simulated model discharge dynamics are in a close approximation with the experimental response described in Test 1 Figure 3.54a.

Table 3.15— Battery model parameters and their comparison

Parameters	Fresh	Average	Weak
Rated capacity (Ah)	100	89	78
Nominal voltage (V)	12	12	12
SoC (%)	100	91	80
Battery cut-off (V)	10.5	10.5	10.5
Internal resistance, R_0 (Ω)	0.0012	0.0015	0.0018

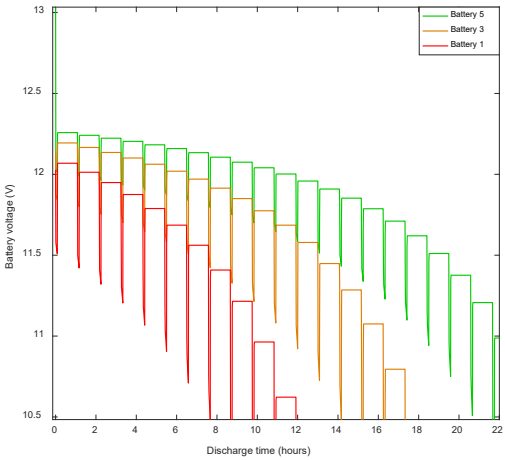

Figure 3.58 – Simulation results: 50A pulsed discharge response

The aging phenomenon is modeled by a 10% capacity loss and 25% increase in the internal resistance for the average battery and a 20% capacity loss and 50% increase in internal resistance for the weak battery. The assumption of 20% capacity loss at the end of life has been used by Sauer [3] and Schiffer [9]. Now, we consider a generic battery model in SIMULINK® to explain different parts of the battery response curve. The model is configured with parameters tuned from measurements. A discharge curve with the fresh battery parameters is shown in Figure 3.59. The first figure (Figure 3.59a) represents the discharge curve at C_{10} (nominal discharge current, $I_{B,n}$). The second figure (Figure 3.59b) represents the total discharge time for the known datasheet C-rates. The currents are selected of the same values used in Test 2, *i.e.*, 2.5A, 5A, 10A, 20A, and 40A.

In Figure 3.59a, the first portion of the discharge curve is a small section with a rapid exponential drop, called linear zone. The starting nominal voltage ($V_{B,n}$) represents the endpoint of the linear zone. The shaded segment represents the battery nominal operating region. The third part shows discharge trajectory until the lower cut-off. At this point, the battery is empty and remain no more useful for further discharge.

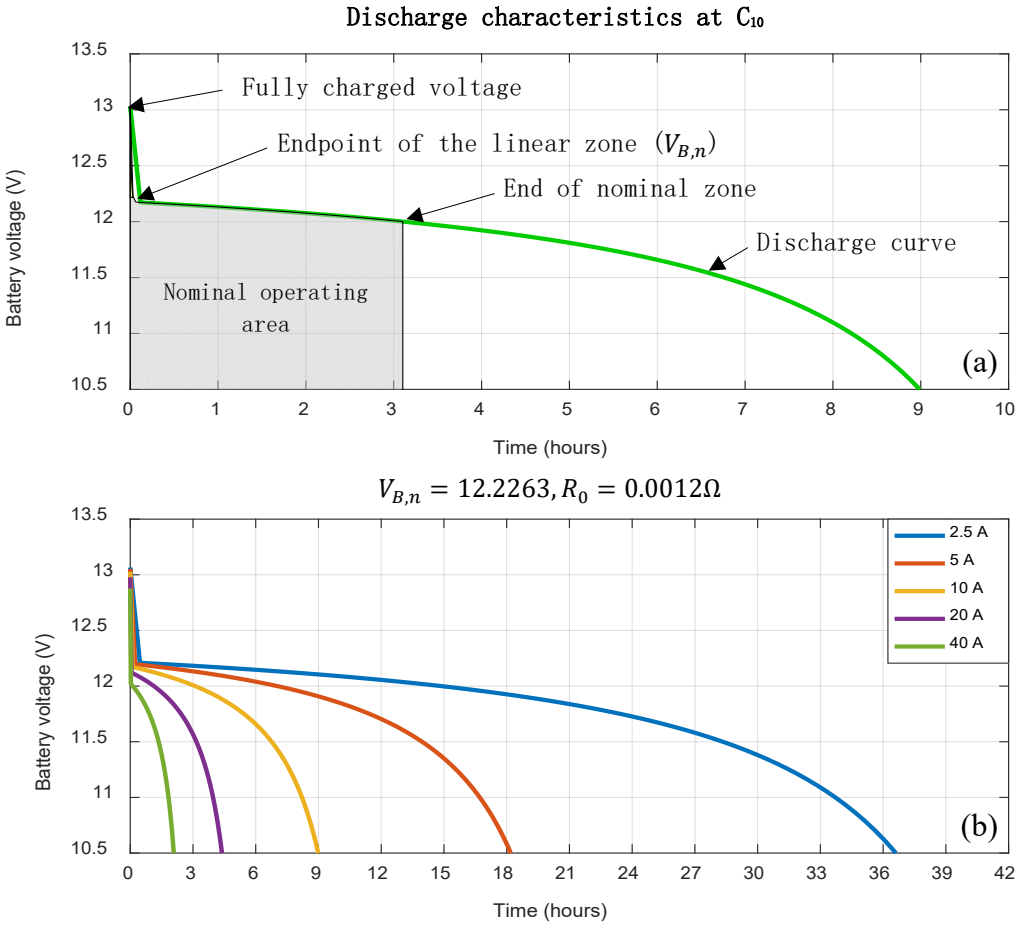

Figure 3.59 – Fresh battery: (a) nominal discharge curve (b) discharge duration at selected C-rates

In a similar way, the dynamics of an average battery are plotted in Figure 3.60. Compared to the characteristics of fresh battery in Figure 3.59a, the proportional shift in the nominal operating area is a result of the battery parameter evolution. There is a proportional shift in the discharge curves at selected C-rates (Figure 3.60b). As indicated in Table 3.16, there is also a gradual decrease in the extracted capacity within the nominal area. These values are determined from the nominal parameters of the generic battery model in SIMULINK®.

Table 3.16— Battery characteristics in the nominal operating area

Battery Parameters	Fresh	Average	Weak
Fully charged voltage (V)	13.0658	13.0458	13.0058
Maximum extracted capacity (Ah)	104	90.7	78
Extracted capacity at the nominal voltage (Ah)	31.0278	24.6147	18.2017

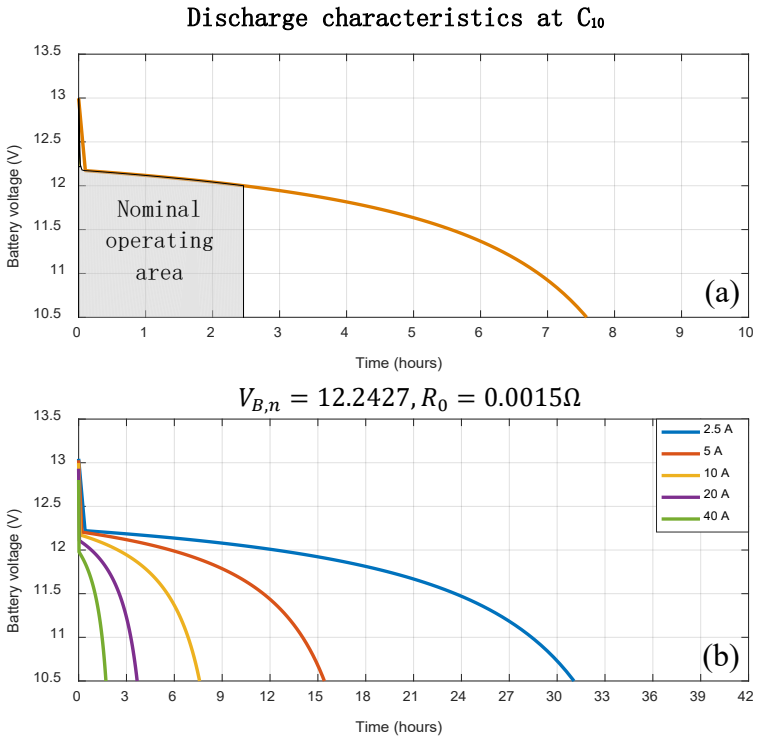

Figure 3.60 – Average battery: (a) nominal discharge curve (b) discharge duration

The lower cut-off quickly approaches, indicating a gradual battery health reduction. Finally, the simulation results of a weak battery are plotted and compared in Figure 3.61. The growth in battery resistance and low charge acceptance (low SoC) has shown considerable shrinkage of the operating curves and resulted in a much more capacity loss.

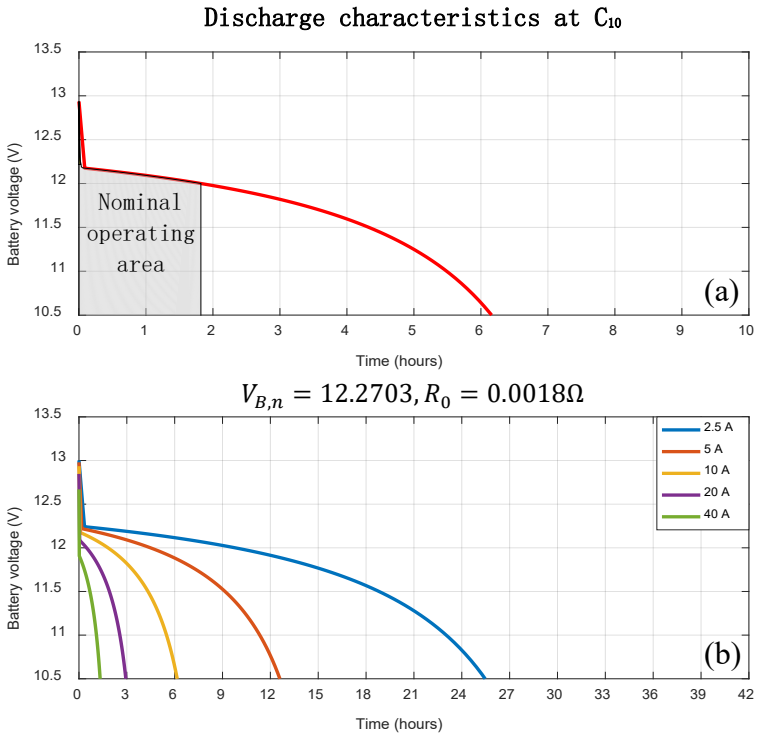

Figure 3.61 – Weak battery: (a) nominal discharge curve (b) discharge duration

It is also observed in these figures that beyond the nominal area, the remaining battery capacity strongly influences the discharge curve. Likewise, the rapid decline in battery voltage strongly impacts the SoC slope. The same battery generic model is used to plot SoC at the set values found during measurements. The corresponding shift in battery SoC for all three categories is depicted in Figure 3.62. The SoC slope of a weak battery is steep than those of average and fresh batteries.

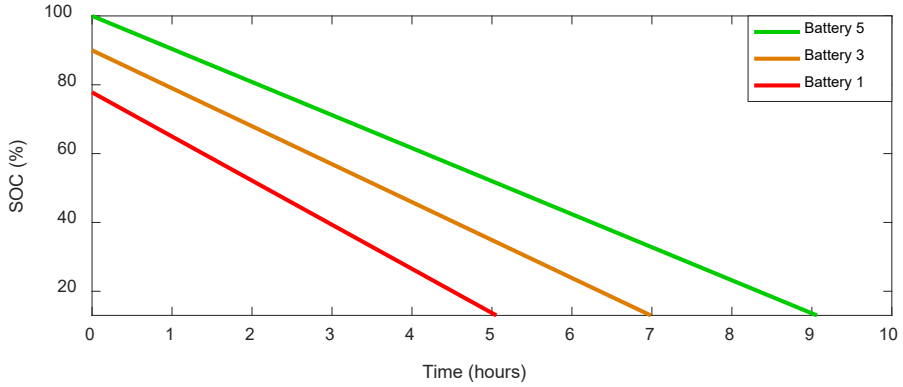

Figure 3.62 – SoC comparison of the three different battery groups

These plots give a fair indication of the corresponding change in operational characteristics due to parameter evolution. In conclusion, the nominal operating area is vital for the battery to deliver more capacity [24]. After this point, the battery voltage decreases non-linearly and faster.

3.3 DG Performance Degradation

All electrical machines have an optimum point to run efficiently. Any deviation from the rated specifications causes suboptimum operation and degradation, which increases the risk of generator tripping. It may result in an unrecoverable system voltage. Some of the DG dynamics and aging impacts are detailed in the following subsections.

(a) Factors Contributing to DG Degradation

The DG power degradation and increased fuel consumption are related to the engine wear. Factors that mainly indicate the performance degradation are listed as follows.

- Reduction in the generated power;
- Increased consumption of lubrication/engine oil;
- Increased engine noise;
- Leakage of engine oil into the combustion chamber, wet stacking, and sludge;

- Parts wear: such as bearing, crankshaft, and pistons;
- Impurities in engine oil: These impurities indicate the degree of wear;
- Increased fuel consumption; and
- Increased smoke through the exhaust pipe.

(b) DG Start-up Failure

Other factors that mainly contribute to the generator starting failures include,

- ☐ ***Environmental conditions:*** essential for the proper ignition.
- ☐ ***Air level:*** air is infused with the fuels for combustion inside the pistons. The bad air-fuel mix may lead to start-up failures. Altitude, temperature, and humidity can affect the air level and thus contribute to performance degradation.
- ☐ ***Low temperatures:*** causes diesel gelling, which creates ignition and generator start-up problems in cold seasons.

Undeniably, fuel is the main factor contributing to the high energy tariffs due to operational costs. It is usually recommended to operate a generator at the admissible load factor to optimize the fuel consumption and prolong the engine lifetime [26]. The DG can also be forced to run at 100% rated power in emergencies but for limited operating hours. Because of these limitations, a DG is started only if the load and battery charging power is above the 40% minimum load factor. For further reading, fuel chart statistics are available online [27], and a detailed experimental analysis of the diesel consumption in [28]. In addition, these operational range definitions are graphically depicted in Figure 3.63 (adapted from [29]).

The red (overload) and yellow (underload) regions indicate suboptimum operations. The generator underload/overload conditions are permissible for a certain period but not recommended. In particular, the yellow operating region will require more frequent maintenance due to unburnt fuel particles when operating below the load factor. In Figure 3.64a, the fuel consumption (liter/ hour) as a generator power (kW) function is plotted. The corresponding linear fit in Figure 3.64b can be used to derive a general linear expression for the fuel consumption (figure data from [27] and figure plots adapted from [30], [31]).

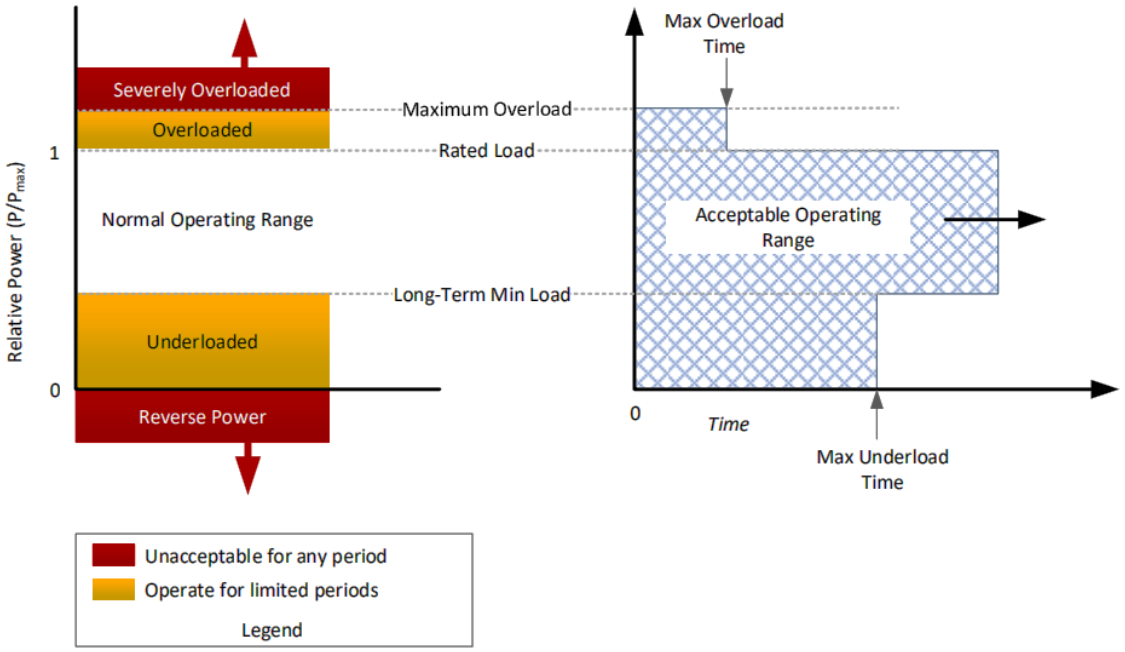

Figure 3.63 – DG operating regions [29]

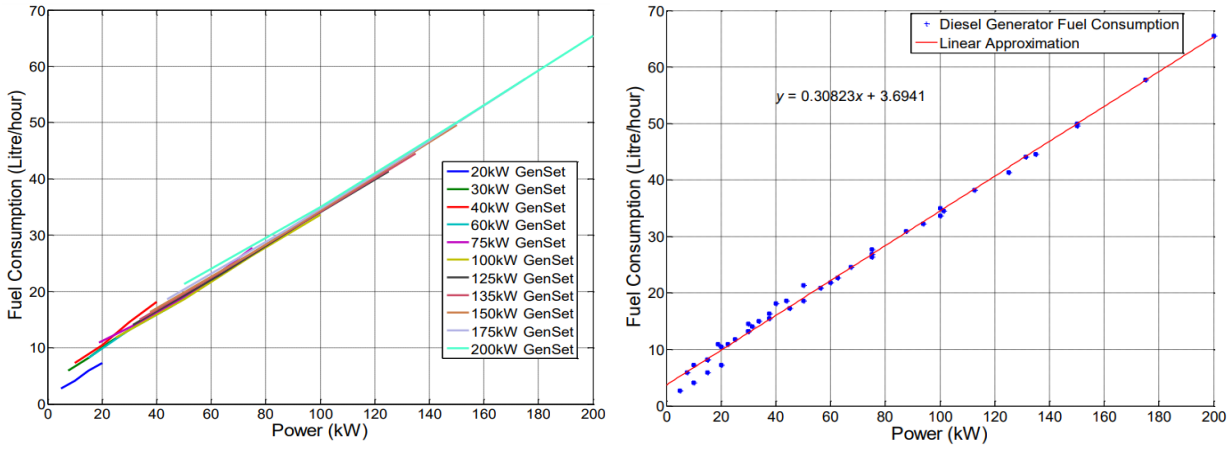

(a) (b)

Figure 3.64 – DG fuel consumption: (a) for various DG capacities [30] (b) linear fit [31]

(c) Impact of System Parameters on DG Dynamics

In a DG system, the complex engine model can be approximated as a simple model providing engine torque τ_{en} to the coupling shaft [32]. It is expressed as,

$$\tau_{en} = f(n_{en}, r_{ff}) \tag{3.72}$$

Where n_{en} is the engine speed in rad/sec and r_{ff} is the fuel flow rate in g/sec. The average engine torque $\tau_{en,avg}$ is represented with the relation,

$$\tau_{en,avg} = 2\pi\, \eta_T . F_{h,l} . r_{ff} \tag{3.73}$$

Where η_T is the thermal efficiency and $F_{h,l}$ is the lower heating value of fuels, which equals 42.9MJ. The mechanical torque equation could be written using the following relationship,

$$\tau_m = \tau_l + B\omega_m + J\frac{d\omega_m}{dt} \quad (3.74)$$

Where B and J represent the damping coefficient of the engine generator set and rotational inertia, respectively. The term J can filter out large disturbances and noise. For the generator part, the electrical torque component $\tau_{g,e}$ could be written as,

$$\tau_{g,e} = \frac{3}{2} n_p \lambda_m i_{\tau,e} \quad (3.75)$$

Where λ_m is the machine field flux, $i_{\tau,e}$ is the current producing electrical torque, and n_p is the total number of poles in the machine. The DG degradation is a combination of the engine and synchronous machine aging. A torque balance equation could represent the combined DG system dynamics. Considering $\tau_{g,e}$ as an electrical torque component and substituting for the load torque τ_l in Eq. (3.74), where $\tau_l = \tau_{g,e}$, and equating to Eq. (3.73). The combined expression for the balanced torque becomes as follows [33].

$$2\pi\, \eta_T . F_{h,l} . r_{ff} - \tau_{g,e} - B\omega_m = J d\omega_m dt \quad (3.76)$$

Where the term $J\frac{d\omega_m}{dt} = J\dot{\omega_m}$ is the dynamic torque of the diesel engine and generator system [34]. In this model, the engine is controlled through fuel injection. This combined model could be sufficient for the system-level observation of the DG dynamics. It also greatly details the impact of the parameter variation on the overall system dynamics. CHAPTER-IV will describe the optimum DG utilization within a microgrid with PV and batteries. The control algorithms will be developed to utilize the available PV resources and reduce the DG operation and maintenance hours.

3.4 Summary

In this chapter the battery physical tests and aging dynamics were greatly detailed using simulations and experiments. We proposed two experimental tests to determine the battery's remaining capacity and health. The quantitative analysis and performance comparison was carried out to support the arguments in our proposition. The chapter concluded with a mathematical analysis of the DG degradation. The key parameters were identified for the DG dynamics and performance degradation. In CHAPTER-IV, these simulations will serve as a foundation step in the design and performance validation of our proposed microgrid system due to component aging. In the following chapter, we simulate a PV-diesel-battery microgrid with and without aging and provide a comparative techno-economic analysis of the second-life proposition.

---The end------Chapter-III---***

Bibliography Chapter-III

[1] UNEP, "Technical guidelines for the environmentally sound management of waste lead-acid batteries," Basel Convention series/SBC No. 2003/9, Switzerland, 2003.

[2] J. H. Yan, W. S. Li, and Q. Y. Zhan, "Failure mechanism of valve-regulated lead–acid batteries under high-power cycling," Journal of Power Sources, vol. 133, no. 1, pp. 135–140, May 2004, doi: 10.1016/j.jpowsour.2003.11.075.

[3] D. U. Sauer and H. Wenzl, "Comparison of different approaches for lifetime prediction of electrochemical systems—Using lead-acid batteries as example," Journal of Power Sources, vol. 176, no. 2, pp. 534–546, Feb. 2008, doi: 10.1016/j.jpowsour.2007.08.057.

[4] U. S. Kim, C. B. Shin, S. M. Chung, S. T. Kim, and B. W. Cho, "Modeling of the capacity loss of a 12V automotive lead-acid battery due to ageing and comparison with measurement data," Journal of Power Sources, vol. 190, no. 1, pp. 184–188, May 2009, doi: 10.1016/j.jpowsour.2008.12.091.

[5] M. Sufyan, N. Abd Rahim, C. Tan, M. A. Muhammad, and S. R. Sheikh Raihan, "Optimal sizing and energy scheduling of isolated microgrid considering the battery lifetime degradation.," PLoS One, vol. 14, no. 2, p. e0211642, 2019, doi: 10.1371/journal.pone.0211642.

[6] J. Zhang, S. Ci, H. Sharif, and M. Alahmad, "Modeling Discharge Behavior of Multicell Battery," IEEE Transactions on Energy Conversion, vol. 25, no. 4, pp. 1133–1141, 2010, doi: 10.1109/TEC.2010.2048904.

[7] N. Narayan et al., "Estimating battery lifetimes in Solar Home System design using a practical modelling methodology," Applied Energy, vol. 228, pp. 1629–1639, Oct. 2018, doi: 10.1016/j.apenergy.2018.06.152.

[8] E. Redondo-Iglesias, P. Venet, and S. Pelissier, "Modelling Lithium-Ion Battery Ageing in Electric Vehicle Applications—Calendar and Cycling Ageing Combination Effects," Batteries, vol. 6, no. 14, pp. 1–18, Feb. 2020, doi: 10.3390/batteries6010014.

[9] J. Schiffer, D. U. Sauer, H. Bindner, T. Cronin, P. Lundsager, and R. Kaiser, "Model prediction for ranking lead-acid batteries according to expected lifetime in renewable energy systems and autonomous power-supply systems," Journal of Power Sources, vol. 168, no. 1, pp. 66–78, May 2007, doi: 10.1016/j.jpowsour.2006.11.092.

[10] R. Dufo-López, J. M. Lujano-Rojas, and J. L. Bernal-Agustín, "Comparison of different lead–acid battery lifetime prediction models for use in simulation of stand-alone photovoltaic systems," Applied Energy, vol. 115, pp. 242–253, Feb. 2014, doi: 10.1016/j.apenergy.2013.11.021.

[11] H. Bindner, T. Cronin, P. Lundsager, J. Manwell, U. Abdulwahid, and I. Baring-Gould, "Lifetime Modelling of Lead Acid Batteries," Risø National Laboratory, Risø-R-1515(EN), pp. 1–82, Jan. 2005.

[12] H. Wenzl et al., "Life prediction of batteries for selecting the technically most suitable and cost effective battery," Journal of Power Sources, vol. 144, no. 2, pp. 373–384, Jun. 2005, doi: 10.1016/j.jpowsour.2004.11.045.

[13] K. U. Jan, A. M. Dubois, D. Diallo, W. Uddin, M. Nasir, and I. Khan, "Reuse Legacy to Repower the Microgrids–An Affordable Solution for Test and Restoration of Repurposed Lead Acid Batteries," in 2020 2nd International Conference on Smart Power Internet Energy Systems (SPIES), 2020, pp. 463–468. doi: 10.1109/SPIES48661.2020.9243053.

[14] S. Obukhov, I. Plotnikov, and V. Masolov, "Service life tests for storage batteries used in islanded power systems with renewable energy sources," Proceedings of Irkutsk State Technical University, vol. 25, pp. 463–477, Sep. 2021, doi: 10.21285/1814-3520-2021-4-463-477.

[15] J. Dulout and L. F. L. Villa, "Working towards greener golf carts – A study on the second life of lead-acid batteries," in 2019 Fourteenth International Conference on Ecological Vehicles and Renewable Energies (EVER), 2019, pp. 1–5. doi: 10.1109/EVER.2019.8813658.

[16] M. Mohsin, A. Picot, and P. Maussion, "Lead-acid battery modelling in perspective of ageing: a review," in 2019 IEEE 12th International Symposium on Diagnostics for Electrical Machines, Power Electronics and Drives (SDEMPED), 2019, pp. 425–431. doi: 10.1109/DEMPED.2019.8864849.

[17] I. Mizumoto, Y. Yoshii, K. Yamamoto, and H. Oguma, "Lead-acid storage battery recovery system using on–off constant current charge and short–large discharge pulses," Electronics letters, vol. 54, no. 12, pp. 777–779, 2018.

[18] M. Bortolini, M. Gamberi, A. Graziani, and F. Pilati, "Economic and environmental bi-objective design of an off-grid photovoltaic–battery–diesel generator hybrid energy system," Energy Conversion and Management, vol. 106, pp. 1024–1038, Dec. 2015, doi: 10.1016/j.enconman.2015.10.051.

[19] K. U. Jan, A. B. Oudot, A. M. Dubois, and D. Diallo, "Experimental Evaluation of the True Remaining Capacity of Legacy Lead-Acid Batteries," in 2021 9th International Conference on Smart Grid (icSmartGrid), 2021, pp. 92–96. doi: 10.1109/icSmartGrid52357.2021.9551263.

[20] "Ultracell batteries 'UCG 100-12.'" Accessed: May 05, 2021. [Online]. Available: https://allo.solar/amfile/file/download/file/1128/product/438/

[21] W. Peukert, "Über die Abhängigkeit der Kapazität von der Entladestromstärke bei Bleiakkumulatoren," Elektrotechnische Zeitschrift/Electrotech. Journal, vol. 20, pp. 287-288 (In German), 1897.

[22] D. Doerffel and S. A. Sharkh, "A critical review of using the Peukert equation for determining the remaining capacity of lead-acid and lithium-ion batteries," Journal of Power Sources, vol. 155, no. 2, pp. 395–400, Apr. 2006, doi: 10.1016/j.jpowsour.2005.04.030.

[23] M. Alramlawi and P. Li, "Design Optimization of a Residential PV-Battery Microgrid With a Detailed Battery Lifetime Estimation Model," IEEE Transactions on Industry Applications, vol. 56, no. 2, pp. 2020–2030, 2020, doi: 10.1109/TIA.2020.2965894.

[24] O. Tremblay and L.-A. Dessaint, "Experimental validation of a battery dynamic model," World Electr Veh J, vol. 3, pp. 1–10, Jun. 2009, doi: 10.3390/wevj3020289.

[25] R. Rynkiewicz, "Discharge and charge modeling of lead acid batteries," in APEC '99. Fourteenth Annual Applied Power Electronics Conference and Exposition. 1999 Conference Proceedings (Cat. No.99CH36285), 1999, vol. 2, pp. 707–710. doi: 10.1109/APEC.1999.750438.

[26] S. Dufrane, "Optimization of daytime fuel consumption for a hybrid diesel and photovoltaic industrial micro-grid," Colorado State University, Thesis and Dissertations, 2017.

[27] "Approximate Diesel Fuel Consumption Chart 2013," Diesel Service and Supply. https://www.generatorsource.com/Diesel_Fuel_Consumption.aspx (accessed Mar. 03, 2022).

[28] C. Yin, H. Wu, F. Locment, and M. Sechilariu, "Energy management of DC microgrid based on photovoltaic combined with diesel generator and supercapacitor," Energy Conversion and Management, vol. 132, pp. 14–27, Jan. 2017, doi: 10.1016/j.enconman.2016.11.018.

[29] D. Zimmerle and J. Duggan, "Theory of Operation: High Penetration, Hybrid PV-Diesel Supervisory Control System Version V1," Colorado State University, Thesis and Dissertations, 2016.

[30] L. K. Gan, J. K. H. Shek, and M. A. Mueller, "Hybrid wind–photovoltaic–diesel–battery system sizing tool development using empirical approach, life-cycle cost and performance analysis: A case study in Scotland," Energy Conversion and Management, vol. 106, pp. 479–494, Dec. 2015, doi: 10.1016/j.enconman.2015.09.029.

[31] L. K. Gan, J. K. H. Shek, and M. A. Mueller, "Optimised operation of an off-grid hybrid wind-diesel-battery system using genetic algorithm," Energy Conversion and Management, vol. 126, pp. 446–462, Oct. 2016, doi: 10.1016/j.enconman.2016.07.062.

[32] S. Benhamed et al., "Dynamic modeling of diesel generator based on electrical and mechanical aspects," in 2016 IEEE Electrical Power and Energy Conference (EPEC), 2016, pp. 1–6. doi: 10.1109/EPEC.2016.7771756.

[33] X. Zhang, "Power Control of Diesel Engine-Generator Set Subject to Emission Constraints." Electronic Theses and Dissertations, University of Windsor 5357, 2012.

[34] J. Leuchter, P. Bauer, V. Rerucha, and V. Hajek, "Dynamic Behavior Modeling and Verification of Advanced Electrical-Generator Set Concept," IEEE Transactions on Industrial Electronics, vol. 56, no. 1, pp. 266–279, 2009, doi: 10.1109/TIE.2008.2009517.

Chapter-IV: Control, Energy Management, and Aging Impact Analysis

Key Terms

Energy flow, energy management, dispatch strategies, power flow balance, optimum operation, economic dispatch, reliability evaluation.

Acronyms

DG	Diesel generator
DoD	Depth-of-discharge
GHG	Greenhouse gases
LCOE	Levelized cost of energy
MAC	Microgrid annualized cost ($)
NGO	Non-governmental organization
NLPP	Non-linear programming problem
O&M	Operation and maintenance
PSO-GA	Particle swarm optimization-genetic algorithm
PVGIS	Photovoltaic geographical information system
REF	Renewable energy fraction
SoC	State-of-charge
STC	Standard test conditions
$	United States dollar

Highlights

This chapter presents simulation results of a PV-diesel-battery rural microgrid with and without the diesel generator (DG) and battery aging. The hypothesis that a second-life microgrid with retired batteries and DG could be realized with a certain level of energy management is implemented using an average DC microgrid model. The idea is to operate the system within the physical constraints of degraded batteries and DG but at a certain level of reliability. The simulations are conducted to satisfy the electrical needs of Gogma village, a remote community in Burkina Faso, a developing country in West Africa. First, we simulate a base case (no degradation) of the microgrid with fresh batteries and DG. The feasibility of the proposition is analyzed by comparing the performance impact of aging to the base case. The overall system is optimized for the least-cost operation and controlled using rule-based energy management. The simulations and quantified comparison enable us to test the second-life hypothesis and present it as a base case for further investigation and practical realization in electrifying rural areas.

Contents

CHAPTER 4

CONTROL, ENERGY MANAGEMENT, AND AGING IMPACT ANALYSIS

The feasibility, choice of energy sources, and a decision on their dispatch and energy management significantly impact the microgrid cost and reliability. The modeling task becomes complicated and tricky when using degraded system components such as retired batteries and already-in-use diesel generators (DGs). Such a low-cost solution may get high social acceptance in low-income rural areas. For this purpose, we have chosen our study site in BURKINA FASO due to the off-grid context and its geographic and economic conditions. The current electricity access rate in rural areas of BURKINA FASO is less than 5% [1], [2], which is a motivation to study the viability of our study in the region.

This chapter details a two-step methodology to optimize and analyze a PV-diesel-battery hybrid with and without the aging impact of DG and batteries. In this chapter, we optimize the performance of DG and battery without compromising supply reliability. The microgrid performance is optimized on the least average annualized cost. An intelligent hybrid optimization technique called particle swarm optimization genetic algorithm (hybrid PSO-GA) is used to determine optimal sizing and least cost operation [3]. The optimization algorithm best suits our requirement as it is robust to find the optimum size and search for local minima to find the best system cost. The PSO algorithm is also computationally efficient, easy to implement, robust, and very effective in rule-based energy management system (EMS) [4]. The PV-diesel-battery hybrid is modeled using mathematical formulas to accelerate the yearly simulations. As a result, fuel consumption, operation & maintenance (O&M) cost, and the capital costs of PV, DG, and batteries is minimized. A systematic representation of the work done toward achieving the study objectives is depicted in Figure 4.65. The theoretical background of Steps 2-3 was covered in CHAPTER-II and CHAPTER-III. Now, we combine all steps from the implementation perspective to achieve the thesis goals.

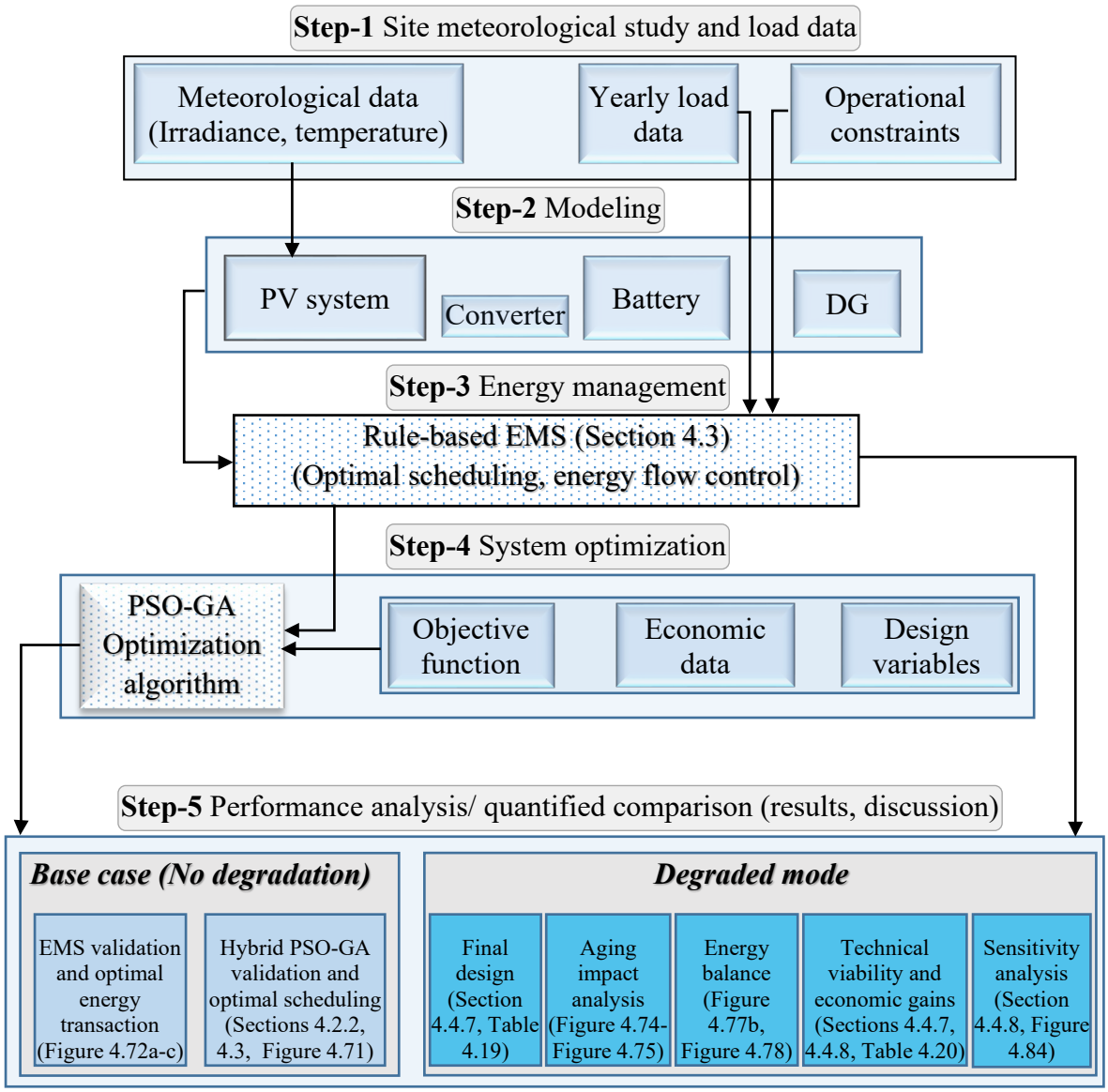

Figure 4.65 – Systematic flow of the overall work towards achieving the study objectives

4.1 Study Site and Meteorological Data

4.1.1 Study Location

The average model of a PV-diesel-battery microgrid is simulated for the GOGMA village in BURKINA FASO (GPS coordinates: *Latitude 11.73°; Longitude - 0.58°*). This rural site is remarkably detailed by S. Meunier [4], who proposed water pumping project for the site. We propose electrification for the same village by considering feasibility of the project to the local climatic and economic conditions, which is the main motivation for selection of the same site for our case study. The proposed site has a range of climatic variations to test the microgrid performance in harsh conditions. The average monthly high and low temperatures in the nearest location of OUAGADOUGOU capital city to our proposed site are shown in Figure 4.66 [5]. The study location has two distinct seasons;

hot and cold, which are highlighted in the plot. The hot season lasts for 2.3 months, from March 8 to May 16, with an average daily high temperature above 38°C. The hottest month of the year is April. The cool season lasts for the same period, from July 9 to September 18, with an average daily high temperature below 32°C. The coldest month of the year is January, with an average low of 18°C and a high of 33°C in mid-April. According to [5], the cloudier part of the year begins around March 11 and lasts for 7.5 months, ending around October 26. In this period, the PV power generation is low, specifically during the hot season (Mar-May). We analyze the proposed microgrid performance in three distinct seasonal conditions. The remaining meteorological information on BURKINA FASO'S weather and availability of sunshine could be further researched in [5].

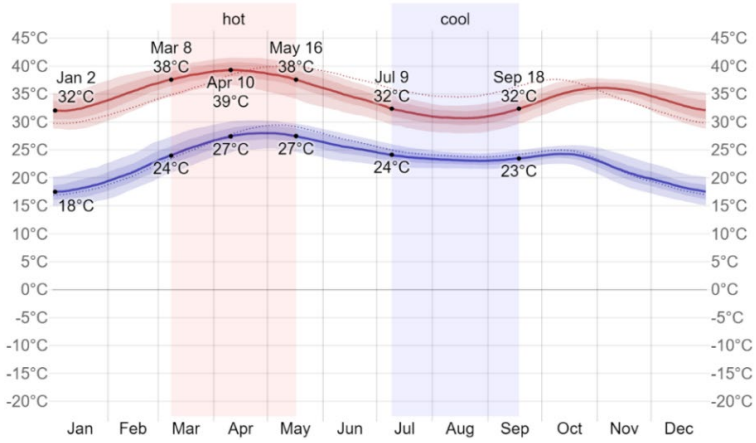

Figure 4.66 – Monthly averaged temperatures in Burkina Faso © WeatherSpark.com [5]

4.1.2 Meteorological Data

The irradiation and temperature data are obtained from the PVGIS [6], [7] for the position, *Latitude 11.73° and Longitude -0.58°*, at an elevation of 303m using the PVGIS-SARAH2 radiation database for the year 2019, which is the same year of case study as in [4], [8]. The hourly irradiance and temperature data for an entire year are depicted in time-series plots using Figure 4.67a. The corresponding PV-generated energy for the study location is shown in Figure 4.67b. The second plot is for the optimized number of PV panels and corresponds to the two simulated cases in SECTION 4.4. It is evident from these plots that the target site has good availability of solar resources throughout the year, except for a few months in the middle. Interestingly, a high-load demand in this period enabled us to analyze our microgrid in harsh conditions. The profile is suitable for testing the microgrid performance in energy surplus and deficit. The optimization algorithm uses the meteorological information to optimally choose the required number of PV, DG, and batteries with the required power/energy rating to take the load.

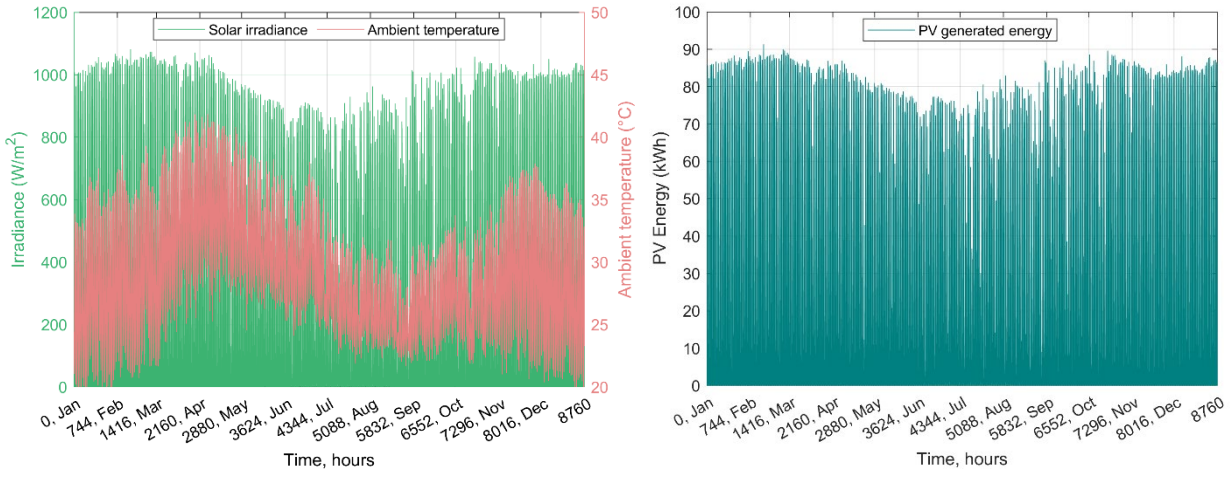

(a) Temperature and irradiance

(b) PV-generated energy

Figure 4.67 – Meteorological data of the study location

4.1.3 Electrical Load Assessment

Based on the geographic conditions and population in GOGMA, a total of 125 households of 1100 inhabitants are considered in this study [4]. It is assumed that each household consumes uniform energy of 4kWh/day. The load is considered irrespective of its nature, AC or DC. The proposed hybrid system is modeled for a 30kW load, which assumes a 25kW average load for households and 5kW for the community loads (street lights and community shops). The yearly energy demand with an hourly variation is depicted in Figure 4.68a. The corresponding daily load on the first day of each quarter is then plotted using Figure 4.68b. The daily averaged load for the whole year is depicted using Figure 4.68c. This figure also shows an average base load of 20.8kW, which corresponds to an average energy consumption of 500kWh/day by the entire load demand. The load has a reasonably large degree of variation during the whole year.

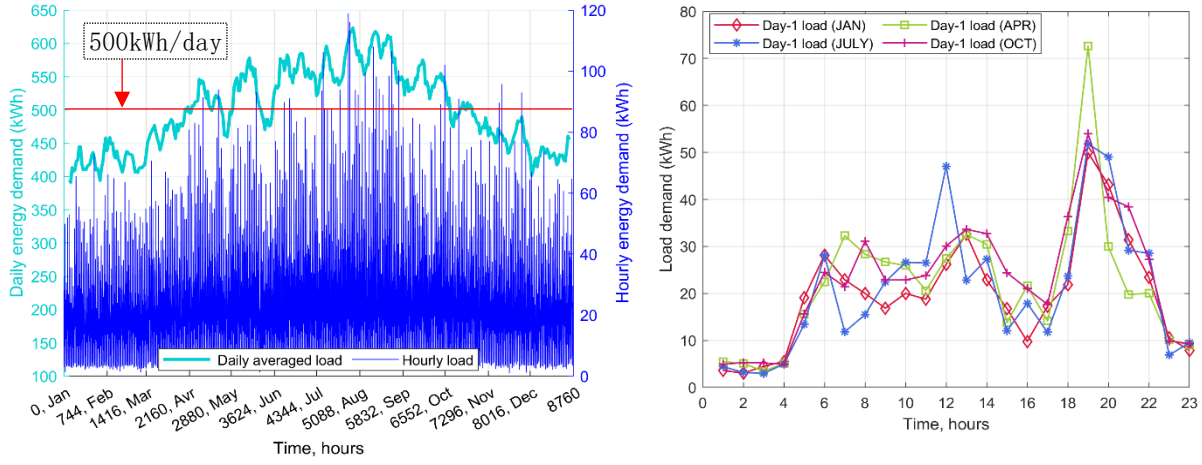

(a) Hourly variation of the annual load

(b) Day-1 load in each quarter

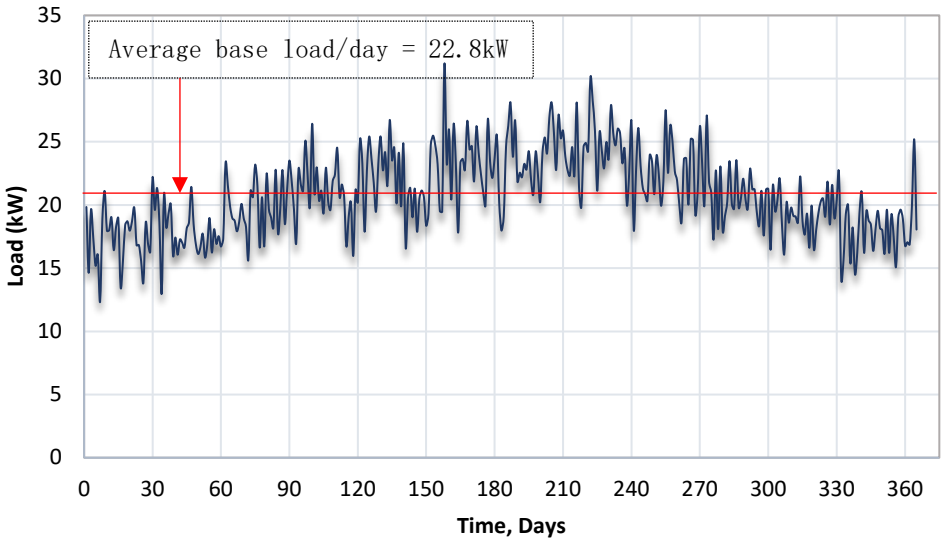

(c) Daily averaged load in kW

Figure 4.68 – Assumed yearly load profile for the study site

The assumption of this load profile can be justified by a total consumption of 500kWh/day by 125 households, each with an average consumption of 200Wp, to cover basic electrification needs as described before in Table 1.2. However, the system can be scaled with additional cost to accommodate more users with time. The average monthly bill is approximately 120kWh/month/household, which is assumed the average bill for a typical household with a low to moderate income. The average monthly load variation is listed in Table 4.17. It can be noted that the average load in the middle of the year is very high, which is also a period of less PV power due to warm weather and clouds. This period could be interesting to simulate the optimum energy transaction and stability of our proposed system in its degraded mode operation.

Table 4.17— Average monthly load variation for the proposed study location

Month	**Average load/month (kW)**
January	17.5
February	17.7
March	19.7
April	21.0
May	21.9
June	23.4
July	23.8
August	24.2
September	22.7
October	20.6
November	19.1
December	18.2
Monthly average power demand (kW)	20.8

Month	Average load/month (kW)
No. of households in study site	125
Average consumption per household/day (kWh)	4
Average consumption per household/month (kWh)	120
Daily total energy demand of the study site (kWh)	500
Yearly energy demand (without load evolution) (kWh)	182,500
Yearly energy demand (with a 2.5% increase per quarter) (kWh)	189,570
Permissible load cut in degraded mode operation (10% of the total demand in kWh/year)	18,957

The 200W_p/household is adequate to test our proposition for low-power applications in rural areas. Therefore, the assessment of the proposed microgrid is feasible for the study location with the given load information.

4.1.4 Microgrid Performance Projection

As a starting point, we use the interactive tool [6] to model a simple PV-battery off-grid system for the energy demand of 500kWh considering the load requirement for the case study of 125 households. The provided randomly chosen input parameters for randomly chosen PV power and battery capacity and simulation output of the tool are listed in Table 4.18. The 35° default slope angle and the 0° south orientation angle is chosen for the PV modules in the fixed (non-tracking) mounts. However, the tool has the flexibility to calculate optimal slope and orientation for the given conditions.

Table 4.18— Performance summary of an off-grid simulated system

Provided inputs	Parametric values
Location (Lat. /Lon.)	Lat. 11.73° and Lon. -0.58°
Horizon:	Default
The database used:	PVGIS-SARAH2
Installed PV (kWp)	30
Battery storage (kWh)	30
Battery cut-off limit (%)	30
Energy demand per day (kWh)	500
Slope angle (°):	35
Azimuth angle (°):	0
Simulation outputs	
Percentage days with a full battery (%)	50.87
Percentage of days with an empty battery (%)	100
Average energy not captured due to a full battery (kWh)	12.69

The available energy in the system is estimated by the modeling tool using the input parameters. The battery performance in the stated meteorological conditions in [5] is plotted using Figure 4.69 [6]. This plot provides an average monthly available and deficient energy in the PV-battery system in islanded mode. The green and red bars denote the percentage of days in the whole month in which the batteries get fully charged or completely discharged. These fluctuations strongly depend on the storage capacity and the number of PV modules.

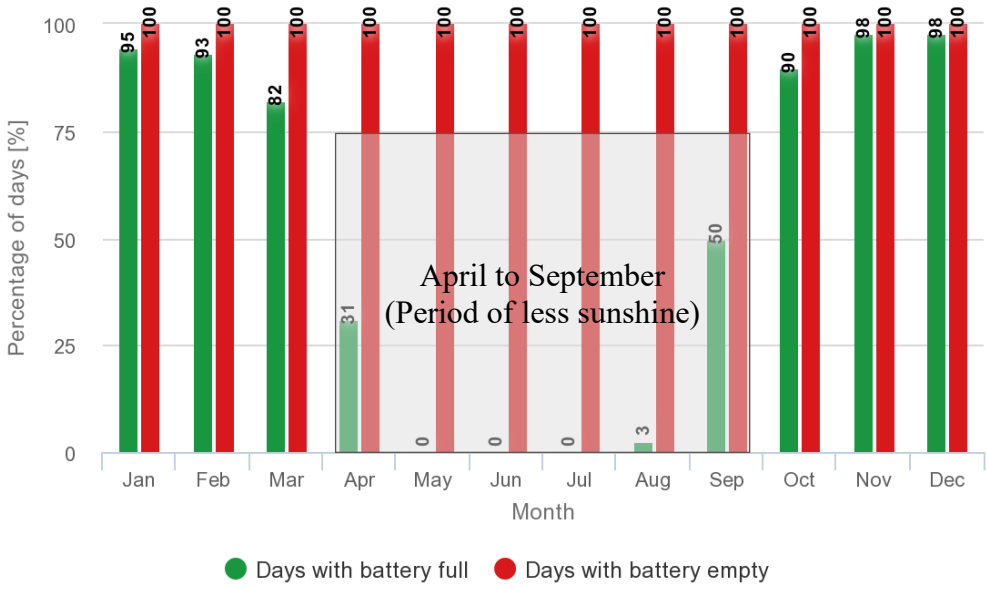

Figure 4.69 – Battery performance for a hypothetical off-grid system in Burkina Faso [6]

The tool is used only for demonstration with randomly chosen values for PV and battery without using a DG. The idea is to see the periods of high pressure on batteries in different months of the year in a PV-battery system. It is obvious in the plot that the batteries remained undercharged from April to September as the number of PV modules are not enough or the storage capacity is too small or the load is high. Also, the batteries touch their lower cut-off each day during the whole year due to insufficient power. It can be noted in this plot that the load may not be met due to an empty battery for quite a reasonable time during the year, in particular from April to September, a high load period with less sunshine. Therefore, a PV-battery system could be unreliable and unstable for our assumed yearly load and study location. Consequently, it will be interesting to include a DG in the system to minimize the '%' of days with an empty battery. The inclusion of a DG increases the operational cost of the system. However, the readily available, low-cost legacy lead-acid batteries can offset the cost.

4.2 Proposed Simulation Plan

The average microgrid model is simulated using MATLAB® R2021b using M-file scripts. All the system components are modeled using the modeling equations presented in CHAPTER-II and CHAPTER-III. The simulations are conducted to find the optimum size and lowest Levelized cost of energy (LCOE) while meeting system operational constraints and physical boundaries, especially in the degraded conditions. LCOE is the key parameter to evaluate a system with a comparable per unit electricity cost [9]. Apart from the technical viability of the system, this economic side is vital for the social acceptance of the microgrid.

The overall system performance is evaluated with the real temperature and irradiation data for the study site using [6] and an assumed 1-year load data generated by HOMER® [10]. The simulations are conducted for fresh and degraded cases. The simulations are then compared on the basis of components feasibility, system economics, and performance reliability, such as the frequency of shortfalls and '%' of the deficient energy compared to the total energy requirement. The load loss thresholds are assumed at 5% of the total demand for the base case (no degradation) and 10% for the degraded condition of batteries and DG. The analysis is carried out annually for a project lifetime of 20 years with DG and batteries replacement. In the event of a violation of performance reliability, a penalty cost is included using the set thresholds.

4.2.1 Simulation Parameters

Although some data comes from the real measurement such as temperature and irradiation, the number of other assumptions, constraints, and choice of numerical values for the two simulated cases are chosen and scaled suitable to apply to this study. The following are considered in the set of simulations for the base case and degraded mode operation of the microgrid. Later, in SUBSECTION 4.4.7, we also provide a comprehensive table of the final design that compare both cases with additional simulation parameters.

(1) Battery

1. The optimization selects 592 batteries as an optimum size to fulfill the load demand. Each battery is 12V/100Ah and of the type lead-acid. There are eight batteries in a string to get 96V DC bus voltage.

2. Weak battery life is assumed to be 2.5 years (degraded mode) instead of 10 years (base case).

3. The weak battery prices are reduced to one fourth of a fresh battery.

4. In the aging simulations, the degraded batteries have already lost 20% of their initial rated capacity.

5. The depth-of-discharge (DoD) is set at 0.8 and 0.7 for the base case and degraded condition, respectively. As SoC should never be lower than the DoD, the safe operating limits are set at SoC above 30% for the base case and 40% for the degraded condition. The lower cut-off thresholds are set at 20% and 30%, respectively. The region in between these limits is assumed to be an emergency condition in which the DG must come online to support the load and charge batteries.

6. The simulation in both cases starts with similar conditions, *e.g.*, initial SoC at 50%.

(2) Aging Evolution

1. There is no degradation in the first set of simulations in the base case for fresh batteries and DG. The degradation evolution is included for each quarter. The aging factor denotes '%' decline of the rated capacity or DG power. The assumed aging factors for this study are: (i) weak batteries (2.5%), (ii) DG (1.25%), and (iii) load evolution (2.5%) [11], [12].

2. For batteries, the 2.5% quarterly increase in the degradation is considered adequate as it accumulates to 25% degradation at the end of 2.5 years (end of the second life for weak batteries).

3. The load evolution is considered at an annual growth factor of 10% in an incremental change of 2.5% of the load in each quarter.

4. Due to the degradation factor, the SoC of degraded batteries never reaches 100% at the end of the yearly simulations.

(3) Operational Constraints

1. The 25% high-priority load is considered in both cases. In a harsh operational situation or during a shortfall, 75% of the load cut is allowed. In the event of a shortfall, even in the base case, 25% load is served all the time, which is assumed to be important equipment in a municipality's dispensary.

2. The EMS is changed according to the physical limitations of the degraded batteries. It includes the selection of a safe operating region and lower cut-off, as stated above.

3. Shortfall occurs if the batteries and DG cannot meet the load demand. In this case, 25% of the high-priority load is ensured to keep from DG. The DG is always operated at rated power for fuel efficiency and to charge the batteries.

(4) System Economics

1. The O&M cost is considered per battery, per PV panel, and DG size in kW. A 50% increase in O&M for batteries and DG is considered due to degradation, which needs frequent maintenance. However, no increase in O&M is considered for PV as they remain the same as in the base case.

2. There are replacements for DG and weak batteries at the end of their useful remaining life. The DG life is considered five years instead of 20 years.

3. Initial capital cost for DG is 25% less than that of a fresh DG. However, due to degradation, 10% more fuel consumption and emissions are included in the calculations.

4. The interest rate is reduced by 50% due to expected subsidies from the government/ non-government organizations (NGOs) for using second-life components.

5. The total microgrid life is considered the same as the useful life of PV panels, which is assumed 20 years. Therefore, no additional replacement costs are associated with PV.

The simulations are conducted for one year (8760h) using one-hour time-steps. The hourly time-step notably allowed us to reduce the computing time for the optimization and conveniently analyze the results for various operational scenarios. Also, it is more convenient to interpret energy and power units, kWh consumptions, and other parameters such as hourly DG consumption with one-hour time-steps. However, the time-step could be adjusted to lower values in simulating a real system.

4.2.2 Microgrid Optimization using hybrid PSO-GA Algorithms

In simulations, a hybrid method combining two heuristic optimization algorithms, PSO and GA is used to evaluate the optimal proposal of a number of possible systems using collaborative search by the two algorithms. The hybrid of PSO-GA reaches the optimal solution faster, accurately, and get better results as we are dealing with a fragile microgrid system with legacy equipment. Therefore, combining the best features of the searching abilities of both algorithms is logical for legacy systems.

A. Formulation of the Optimization Problem: The non-linear programming problem (NLPP) with constraints can be mathematically formulated as:

$NLPP$: $\min f(\bar{x})$; given the three decision variables $\{N_{PV}, P_{DG,r}, N_B\}$ at best microgrid annualized cost (MAC). Where, N_{PV} → the number of PV panels, $P_{DG,r}$ →the rated capacity of DG in kW, and N_B → the number of batteries:

$$\mathbb{F} = \{\bar{x} \in \mathbb{D}^n | g_i(\bar{x})\} \leq 0, \quad i = 1, 2, \dots, m\},$$

$$\mathbb{S} = \{\bar{x} \in \mathbb{D}^n | l_b(x_j) \leq x_j \leq u_b(x_j),\ j = 1, 2, \ldots, n\}$$

Where $f(\bar{x}) = MAC\ (\$)$ is a real-valued objective function to minimize; $\bar{x} \in \mathbb{F} \subseteq \mathbb{S}$; $g_i(\bar{x})$ is set of constraints given in Eqs. (2.43), (2.44), and (2.46); and x_j is the decision variable. The set $\mathbb{S} \subseteq \mathbb{D}^n$ is called the rectangular search space in $\mathbb{D}^n$ and the set $\mathbb{F} \subseteq \mathbb{S}$ defines the feasible part of the search space, $\mathbb{S}$. In addition, $\mathbb{S}$ is defined as a *n*-dimensional rectangle in $\mathbb{D}^n$ domain defined by the lower (l_b) and upper (u_b) bounds. A general formulation of the optimization steps is outlined as follows. The particles are randomly repositioned in the search space $\mathbb{S}$ according to the given two equations.

$$v_i^{k+1} = w \times v_i^k + c_1 \times r_1 \times (p_{best} - x_i^k) + c_2 \times r_2 \times (g_{best} - x_i^k), \quad (4.77)$$

$$x_i^{k+1} = x_i^k + v_i^{k+1} \quad (4.78)$$

Where v_i^{k+1} is the i^{th}particle new velocity attained during each iteration; w is the inertia weight; v_i^k is particle's velocity; c_1, c_2 are two constants called cognitive and social parameters, respectively. Also, r_1 and r_2 are the uniformly distributed numbers within the range [0 1]; g_{best} is the global best particle; p_{best} is the best previous position of i^{th}particle; x_i^k is the current position; x_i^{k+1} is the new position of the i^{th} particle; and k in the superscripts which denotes the iterations count. It is clear that the new position x_i^{k+1} of the i^{th} particle depends on the obtained new velocity v_i^{k+1}. The following pseudo-code helps understanding the working of the hybrid PSO-GA algorithms and a related optimization flow chart is depicted in Figure 4.70.

Pseudo codes of PSO-GA algorithms

A. Apply GA over the initial population
Pseudo code for GA algorithm
Initialize:
1) Initialize the search space $\mathbb{S}$;
2) Generate initial population in $\mathbb{S}$ with P particles; initial guesses of $(N_{PV}, P_{DG,r}, N_B)$
begin
Do
1. Select parent from the population;
2. Recombine (crossover and mutation operators);
3. Produce offspring;
4. Evaluate fitness of the offspring;
5. Replace some or all of the population by the offspring;

While maximum iterations or evolution not completed.
end
B. Apply PSO over the GA proposals to find cost-optimal solution
Pseudo code for PSO algorithm
Initialize:
1) Set parameters bounds and define constraints $(50 \leq N_{PV} \leq 300,\ P_{DG} \geq 30kW,\ N_B \geq P_L)$;
2) Load real meteorological data (irradiance G, temperature T) and assumed yearly load profile $P_{L,y}$;

3) Load economic data; set c_1, c_1 and r_1, $r_1 \in [0\ 1]$;
4) Get GA-generated particles;
5) Randomly initialize current positions x_i^k and velocities v_i^k of all particles P;
Evaluate:
begin
for each particle, $i = 1 \rightarrow P$
Do
1. Set initial local best (p_{best}) and global best (g_{best});
2. Update position $x_i^{k+1}$and velocities v_i^{k+1} using Eqs. (4.77), (4.78);
3. Evaluate fitness values for each i^{th} particle;
4. Find the current best solution for each i^{th}particle and update p_{best} , g_{best};
5. $i = i + 1$;

While maximum iterations or stopping criteria is not attained. The reach criteria is set as the optimal configuration of $N_{PV}, P_{DG,r}, N_B$ at minimum annualized cost.
end
Output: Minimum annualized cost $\{min\, f(\bar{x})$ in the base case and degraded mode at the given constraints$\}$. The final fitness function values $(300, 50kW, 360$: Base case) and $(300, 60kW, 592$: Degraded mode) at minimum annualized cost \$46,672 and \$32,832, respectively.

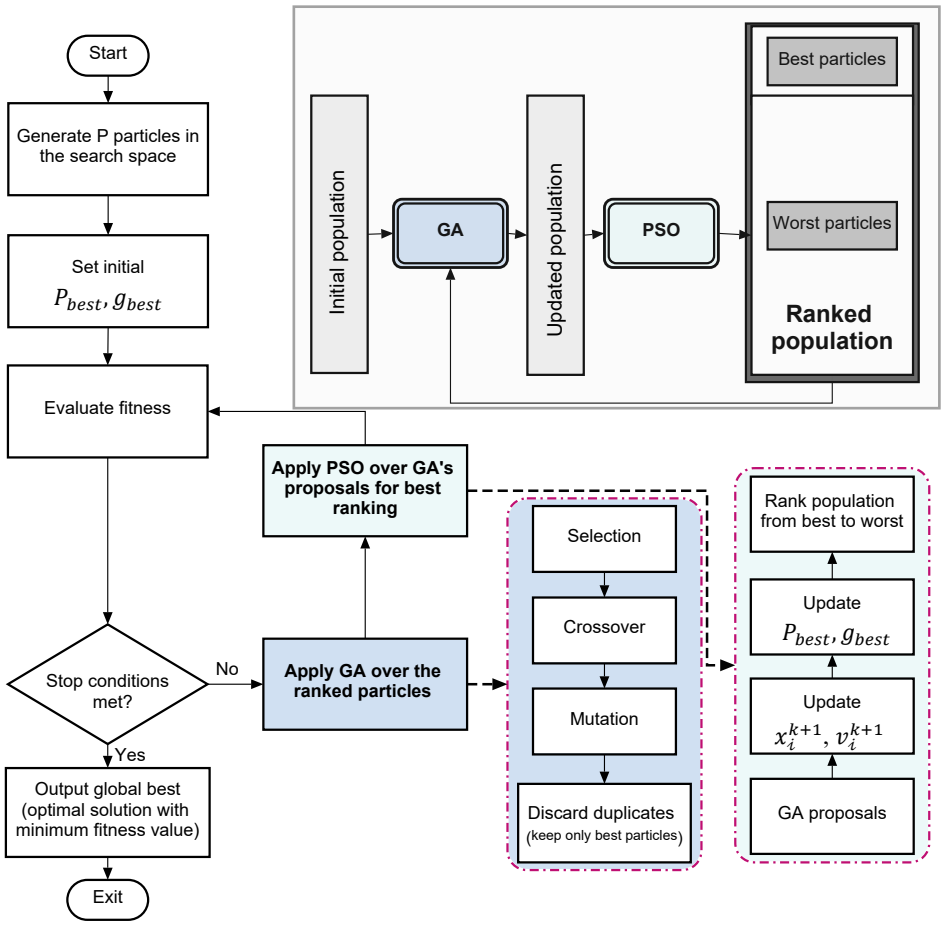

Figure 4.70 – Optimization chart

The above-mentioned optimization procedure is used to formulate our proposed system. We have used GA to guide PSO not to converge to the false minimum to improve results. The GA algorithm creates and evolve individual particles with their own intelligence which are then self-improved in the PSO phase. The input to the optimization algorithm

is solar irradiance data, temperature, load, and economic data (component prices and O&M cost). The output of the algorithm is an optimized system with the required number of PV panels, size of the DG, and required number of batteries. The optimization scheme is implemented as a MATLAB® code in SIMULINK®. The optimization outputs the total number of required equipment and power ratings of each component for the given constraints. The optimization takes all the system variables to provide an optimal solution with best cost. It is then the designer's choice to divide and arrange the required system components in sub-power ratings. The system is optimized for the best annual cost without compromising a certain level of reliability in the base case and degraded mode.

B. Selection of Design Variables for Optimum Solution: The proposed optimization aims to find an optimal system that fulfills energy demand at minimum LCOE. The analysis is conducted with different variable bounds and operational conditions. Three decision variables (PV, DG, and battery) are input for optimization. The lower and upper bounds on these variables and system constraints are used to avoid undesired results from the optimization. The lower bound is set to achieve a minimum level of supply reliability to avoid load shed and penalty cost. The upper bound is chosen to limit the system cost and impose restrictions on using the maximum number of PV panels and batteries. The optimization searches for all least-cost solutions within the search space in the region defined by these boundaries. For PV and batteries, different possibilities are analyzed to meet the feasibility requirement of the available surface for housing equipment, like PV rooftop and storage room for the batteries. The initial lower bound values are set at (50 50 30), which means at least 50 PV panels, 50 batteries, and a DG of size 30kW. The upper bound is chosen as constraint on the total number of PV panels, batteries, or DG rating. These lower and upper bound values are based on our initial guesses, which are used as a starting point to achieve the required reliability and system cost.

C. Convergence Curve: The convergence response of the optimization algorithm is depicted in Figure 4.71. The algorithm runs over the search space for 60 iterations to search the optimum system size and operation point at the lowest annual cost in $/year. This population size is a good compromise between accuracy and computing time. In the beginning, the cost is relatively high, which tends to go down afterward and settles at $46,672/year at the 30^{th} iteration. The same optimization procedure finds the best cost solution at the 38^{th} iteration and settles at $32,832/year for the set of aging simulations. It indicates that the algorithm minimizes the system cost, which is the fitness function, by moving toward the promising regions of the search space.

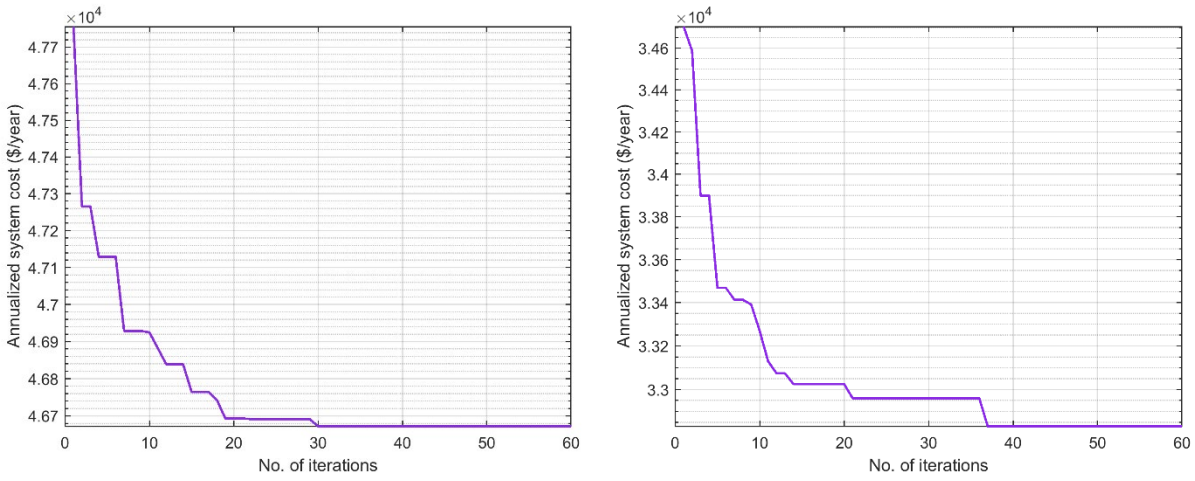

Figure 4.71 – Convergence curve to find best cost solution (a) base case (b) degraded condition

4.3 Scheduling, Operation, and Control

4.3.1 Optimal Scheduling

(1) PV and Renewable Energy Fraction (REF): The optimization puts PV on the highest priority as it contributes to significant cost reduction. The optimization chooses 300 PV panels as an optimum solution to meet the load. In both cases, this number is assumed to be 300 to determine the performance impact of batteries and DG degradation and to maintain nearly the same REF.

(2) DG Priority: We propose to operate DG only at its rated power to supply load and charge the batteries. The batteries and DG collectively cover load peaks in the evening. However, the optimization puts DG on the least priority to minimize the operational cost and get the minimum annualized cost and LCOE.

(3) Aggregate Capacity of Battery Bank: The parameters obtained through simulations and measurements in the preceding chapter are used to tune the performance parameters of batteries and determine their net impact due to aging. The aggregate capacity of the battery bank is calculated using the following relationship.

$$C_{B,bank} = \frac{N_{B,opt}}{N_{B,s}} C_B \tag{4.79}$$

Where $C_{B,bank}$ is the total aggregated battery bank capacity in the microgrid in Ah, $N_{B,opt}$ is the total number of batteries that we get from optimization, $N_{B,s} = 8$ is the number of batteries in series to get the desired bus voltage of 96V, and $C_B = 100$Ah is the individual battery capacity. The net energy storage capacity in (kWh) is calculated by multiplying

the aggregated battery capacity by the bus voltage and division by 1000. The simulations start with an initial SoC set at 50%. It is recalled that the net battery capacity in the degraded conditions is 20% less than those simulated in the base case. Also, the two important battery constraints, SoC_{min} and SoC_{max}, restrict the already degraded batteries within their operational limits. In our simulations, if the batteries absorb energy, it is denoted as negative, and if sourced to the system, it is considered positive.

4.3.2 Operation and Control in the Base Case (No degradation)

The microgrid system is first simulated with no degradation, which is, from now onwards, called a *base case*. The technical specifications of the simulated design are greatly detailed in Table 4.19. The same optimization procedure is used to find optimum size and best annual cost. In the base case, the optimization chooses 300 PV panels, 360 batteries, and a 50kW DG to meet the annual load demand. The proposed control scheme is a rule-based EMS modeled in MATLAB® using a mathematical representation of the system. Various system conditions are linked to the if-else descriptions according to the component limitations to coordinate the energy flow in the given priority and in a certain pre-defined rule. Energy flow control is critical because it determines the priority of each component in the system to achieve multiple economic objectives. The operational strategy from SUBSECTION 2.4.3 is recalled, which controls the energy flow in the following operating modes.

- *Operating mode 1: The solar power $P_{PV}(t)$ is adequate, the load $P_L(t)$ is supplied, and the remaining power is used to charge the batteries;*
- *Operating mode 2: If $P_{PV}(t)$ is insufficient, batteries source the power difference to keep the energy balance;*
- *Operating mode 3: The first load cut is initiated if the batteries SoC goes below the safe operating limits; and*
- *Operating mode 4: If both solar and batteries are not enough, and batteries SoC starts to go below 20% and 30% in the base case and degraded mode, a 25% and 75% load cut is implemented, respectively. Also, DG is turned ON to ensure system reliability, take the load, and charge batteries.*

In the proposed control scheme, DG is set to operate at rated capacity for fuel consumption efficiency. However, the optimization puts DG in the lowest priority to

minimize LCOE. The DG only supplies the system if it is cost-optimal and the batteries can no longer take the load.

4.3.3 System Operation and Control in Degraded Conditions

The system operates in the degraded mode with parameters discussed in SUBSECTION 4.2.1. When the system operates in such a condition, the reliability is compromised within acceptable limits. The same optimization process is used to find best cost. However, the operation strategy is slightly modified for the load cut and DG operation due to the physical limitations of degraded batteries. The optimization now chooses 300 PV panels (no change), 592 weak batteries, and a 60kW DG to meet the annual load in the degraded-mode operation. The operation strategy mentioned in the SUBSECTION 4.3.3 is used to coordinate the energy flow in the system. The admissible net load cut of less than 10% of the total yearly energy requirement (189,570kWh) is respected for the degraded conditions. In case of violation, a penalty cost is included in the system economics.

4.4 Results and Discussions

This section details the performance and cost-benefit analysis using simulation results. The load evolution for a year is used to demonstrate the microgrid performance in the given meteorological condition for the proposed site. The one-year simulation examines EMS over a substantially long period to ascertain that the system constraints are not violated, especially for the degraded batteries during the harsh operational condition. A *harsh condition* is defined as a situation where the batteries may not usefully discharge further or there is an energy shortfall.

First, we present the simulation results for the reference microgrid model with no degradation. The system performance and energy flow are presented on a weekly basis for three different climatic conditions in January (cold, 1st month of quarter-1), April (hot, 1st month of quarter-2), and September (cloudy, last month of quarter-3). In particular, September will be interesting to analyze the microgrid performance in low-light conditions. The yearly results for optimal battery operation are presented at the end of this subsection. Then we present the results for the degraded mode operation in the same sequence. Finally, the net energy flow balance and energy mix are presented for both cases to get a global view of the system performance for the simulation period. Ultimately, a techno-economic analysis of both cases is carried out to determine their viability in support of the second-life hypothesis.

4.4.1 Simulation Results for the Base Case

The system performance to a variable load demand is presented in Figure 4.72a-c. These results correspond to the first week of a month, each in the first three quarters to cover three different meteorological and load conditions. In these plots, Figure 4.72a represents the first week of January, the coldest month, but with plenty of sunshine, hence more PV power. The batteries discharged energy (E_{Bo}) starts to take the load at the beginning of the simulation period. The battery SoC sags down from the preset value of 50% to 30%, the lower safe limit. The load in this period is moderate. There is no deficient energy (E_D) during this period. As a result, batteries remain fully charged and return to 100% SoC during the daytime. We can observe no load cuts during the week due the good coordination of PV and batteries. Therefore, as expected, the excess PV energy is absorbed by the batteries (E_{Bi}) and a reasonable surplus PV is available for deferrable or community loads. Interestingly, the surplus PV could be separately stored and used for lighting local business markets and shops during the early evening in wintertime.

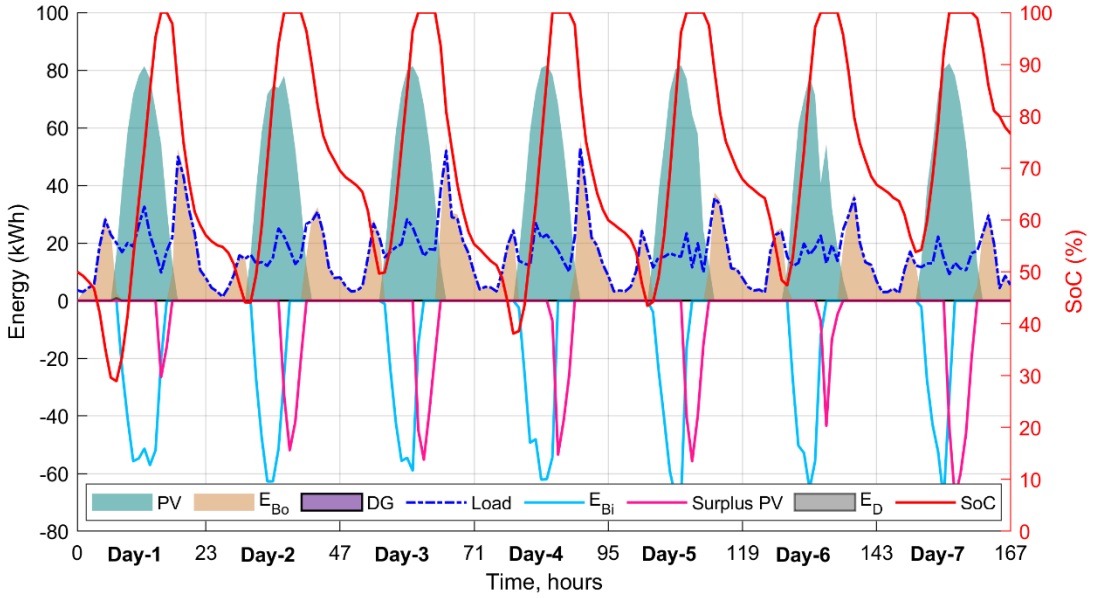

(a) Optimal operation in the base case during the first week of January (quarter-1, cold)

Figure 4.72b represents results for the first week of April, the hottest month with relatively high loads. Although April is a period of good sunshine, the PV power is slightly reduced due to the temperature rise. It can also be noted that the available PV power is still sufficient to bring the batteries from the nearly discharged status to a reasonable charged condition in the middle of each day. Compared to Figure 4.72a, the batteries relatively discharge more and enter into harsh conditions for four times during the week. The DG is turned ON twice in the morning to save batteries from further

discharge and keep serving the load until the availability of PV power. In this condition, most of the time, the batteries never returned to 100% SoC. It can also be noted that the available PV power is sufficient to bring the batteries from fully discharged status to fully charged condition in the middle of each day.

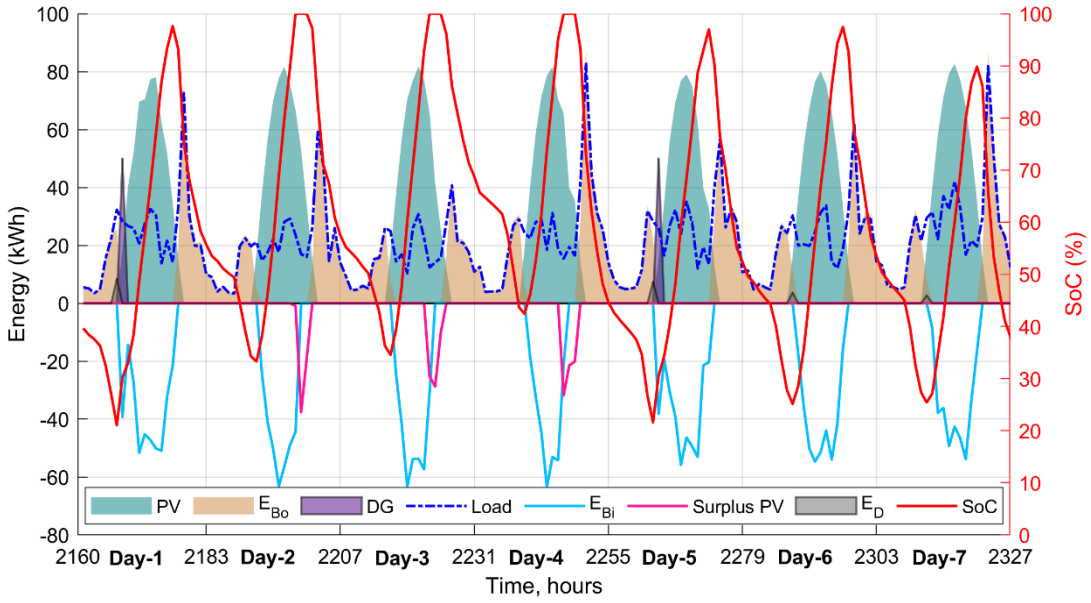

(b) Optimal operation in the base case during the first week of April (quarter-2, high temperatures)

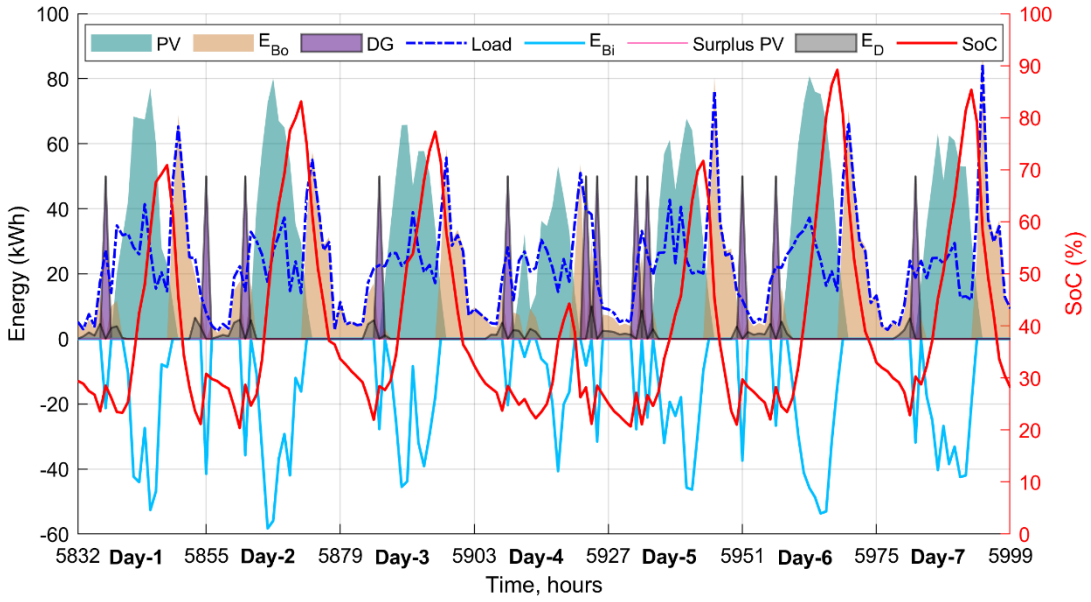

(c) Optimal operation in the base case during the first week of September (quarter-3, cloudier)

Figure 4.72 – Optimal energy transaction in the base case

Finally, Figure 4.72c depicts the weekly results for the cloudier part of the year, *i.e.*, September. The PV power is insufficient to take the load and charge batteries on an average of less than 80% SoC. In this period, more power is drawn from batteries. As a result, they stay undercharged and in extreme conditions throughout the period despite

the frequent load cuts. The middle of this week is the hardest as DG is turned ON four times to ensure reliability and avoid batteries to operate beyond their safe operating limits.

4.4.2 Optimal Battery Operation in the Base Case

The proposed system satisfies the varying load demand in a range of climatic conditions using an optimal energy transaction in which PV is on the highest priority. Figure 4.73 demonstrates the hourly SoC variation for the entire simulation period. The plot demonstrates that the batteries remained fully charged in half the simulation period (on the two sides) and the remaining half (the middle portion) in the undercharged condition. However, they have not discharged below 20% SoC. It can be noted that the batteries have remained remarkably consistent with the required load demand. The "zoom-in" analysis of the yearly results are presented in SUBSECTIONS 4.4.1, 4.4.3 for clarity.

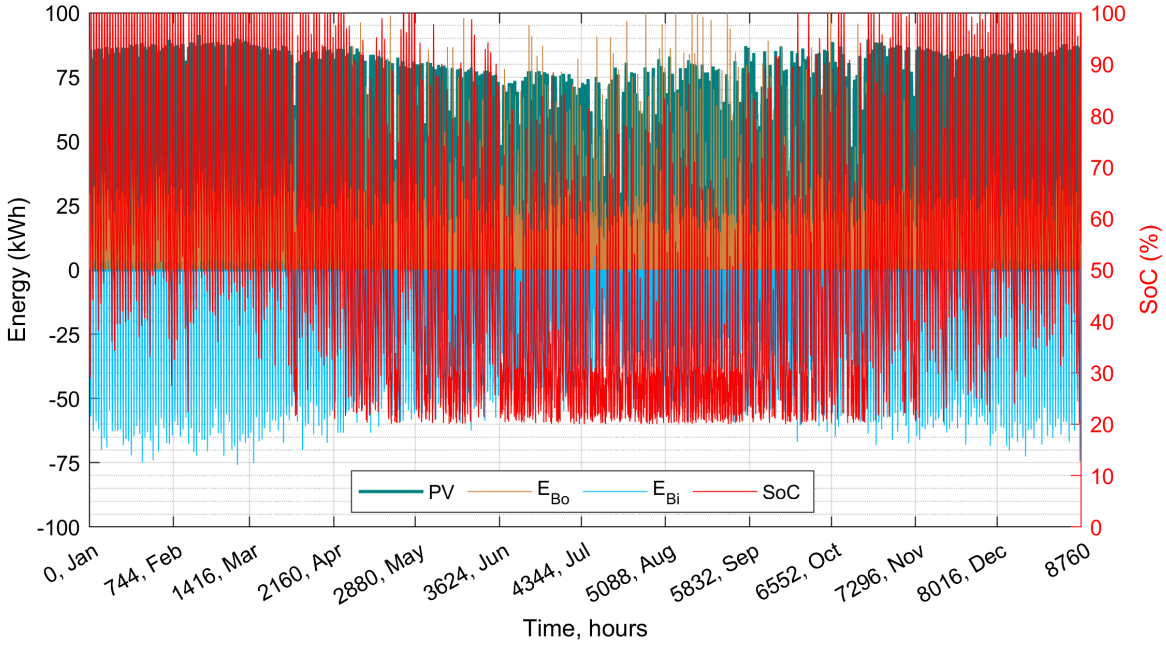

Figure 4.73 – Optimal battery operation in the base case

4.4.3 Simulation Results for the Degraded Mode Operation

In this subsection, we analyze the aging impact on the overall microgrid performance for the same period. The results are presented and discussed in the same sequence. Figure 4.74a-c demonstrates the generated and required power variations in three distinct periods covering cold, warm, and cloudier weeks. Figure 4.74a represents the first week of January, clear, shiny, and with considerable PV power. The conditions are ideal, so the performance difference compared to the base case is not considerable. As the optimized system utilizes almost double the storage size of the base case, the SoC changes with a

greater slope and slow speed. It can be observed that SoC touches the safe operating limit at 40% on the first day. There is a 25% load cut for a very short duration as the PV power is again available, and the batteries start to charge, which increases the SoC. No load cuts are observed during the rest of the week due to the proper energy dispatch in the system.

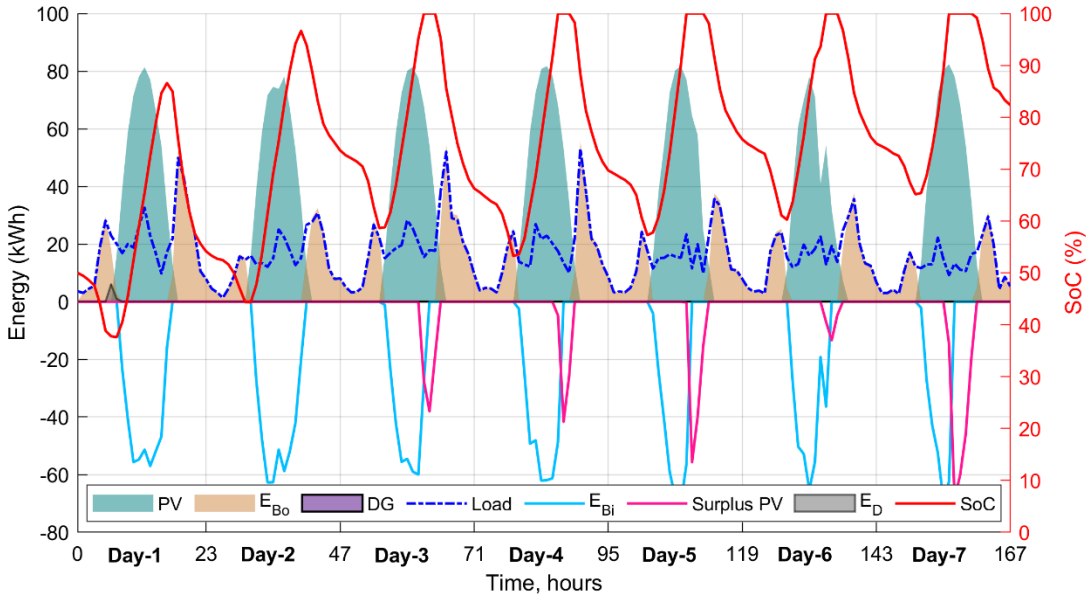

(a) Degraded mode operation during the first week of January (quarter-1, cold)

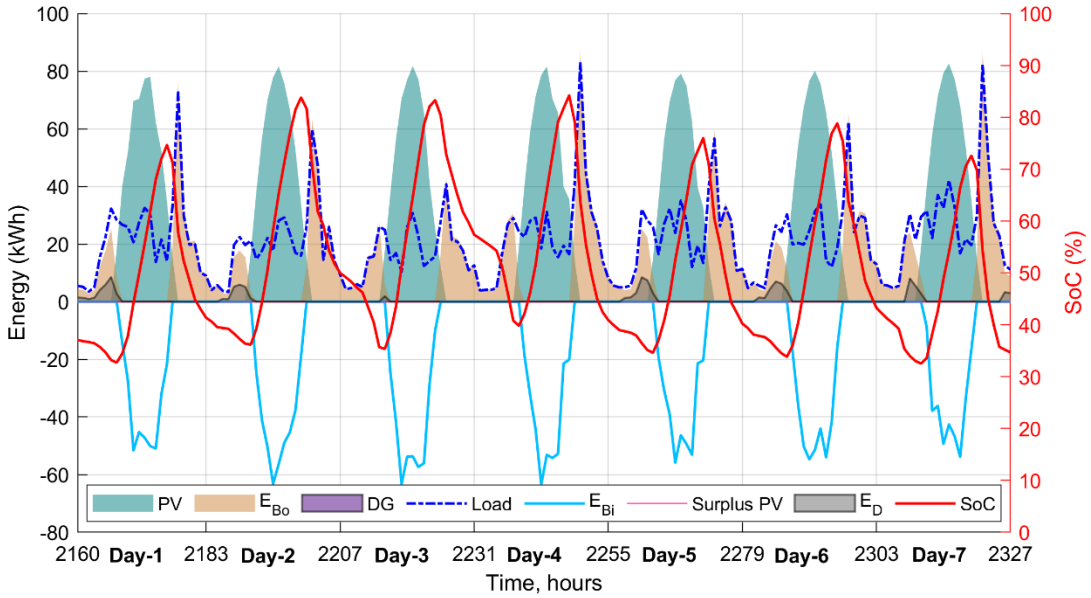

(b) Degraded mode operation during the first week of April (quarter-2, high temperatures)

Figure 4.74b represents the degraded battery operation in hot conditions. As expected, the batteries remained in harsh operating conditions during the week and never returned fully charged. Compared to the EMS in the base case, the DG has not turned ON at the lower safe limits of 40% SoC, as it will significantly increase the number of DG operation hours and its maintenance cost. However, there are frequent load cuts within the

acceptable margins. In the same way, Figure 4.74c is used to conclude the comparison for the cloudier part of the year during the first week of September. First, the DG operation is reduced by 50% but operated in the rated power mode. When a DG comes online it serves the load and the remaining power is used to charge the batteries. The DG operation cost saving is compromised for decrease in reliability due to frequent load cuts. As September is the third quarter, in which batteries degrade by 7.5% of its remaining life, the SoC tends to stay lower than the base case during the whole week.

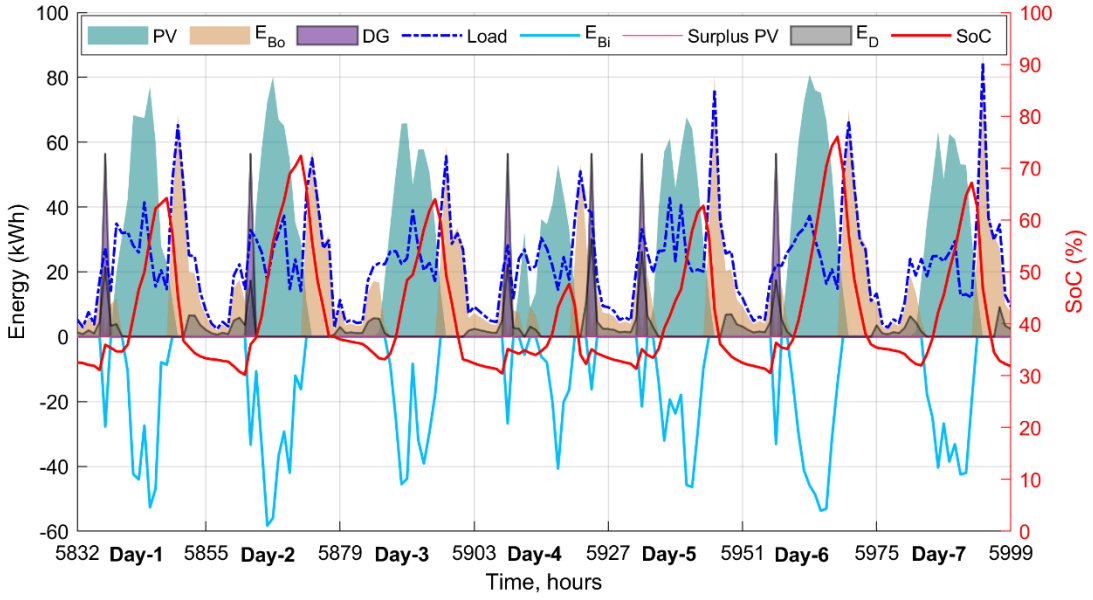

(c) Degraded mode operation during the first week of September (quarter-3, cloudier)

Figure 4.74 – Optimal energy transaction in the degraded mode

4.4.4 Optimal Battery Operation in Degraded Mode

The plot for degraded mode operation during the whole year is depicted in Figure 4.75. It can be noted that the batteries in their degraded condition still remained consistent with the available PV power and load demand for the whole year. The batteries are forced to operate in their safe region by the EMS. However, it is obvious that the batteries greatly discharge during the middle of the year. A comparison of the SoC variation in both cases is also plotted in Figure 4.76. It can be observed that the batteries performed well to absorb or deliver energy in the system. However, they never returned back their fully charged status during the last three quarters, which could significantly impact the remaining useful life due to undercharged condition. The degraded batteries are limited to operating above 30% SoC to avoid any fatal damage to the batteries and failure or frequent replacement of the storage unit.

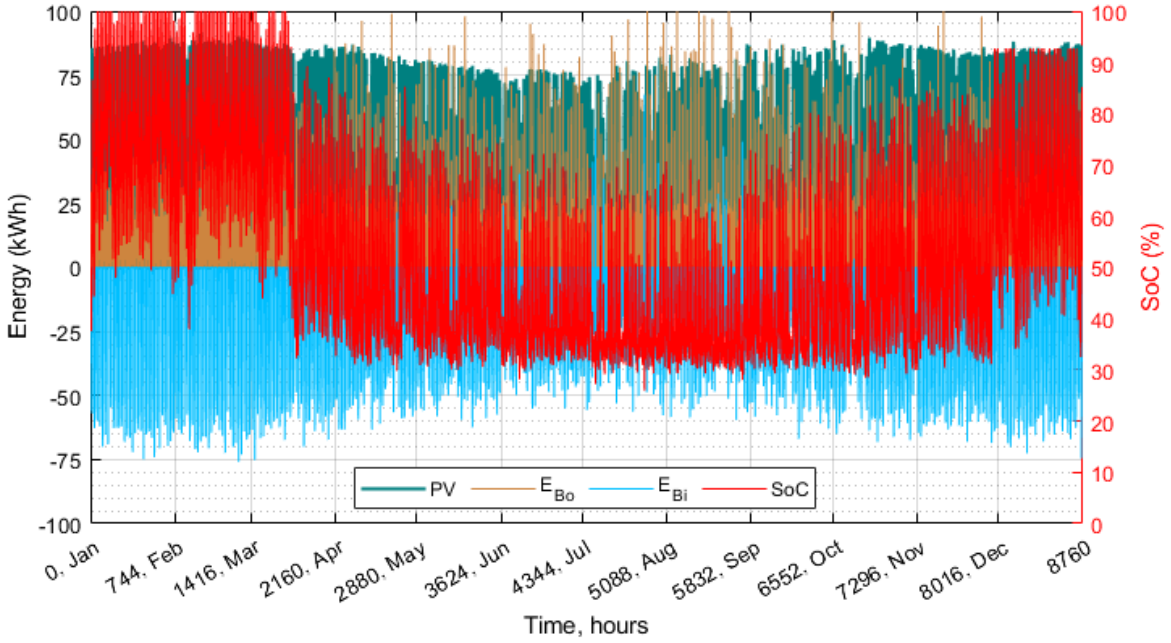

Figure 4.75 – Battery operation in the degraded mode during one year

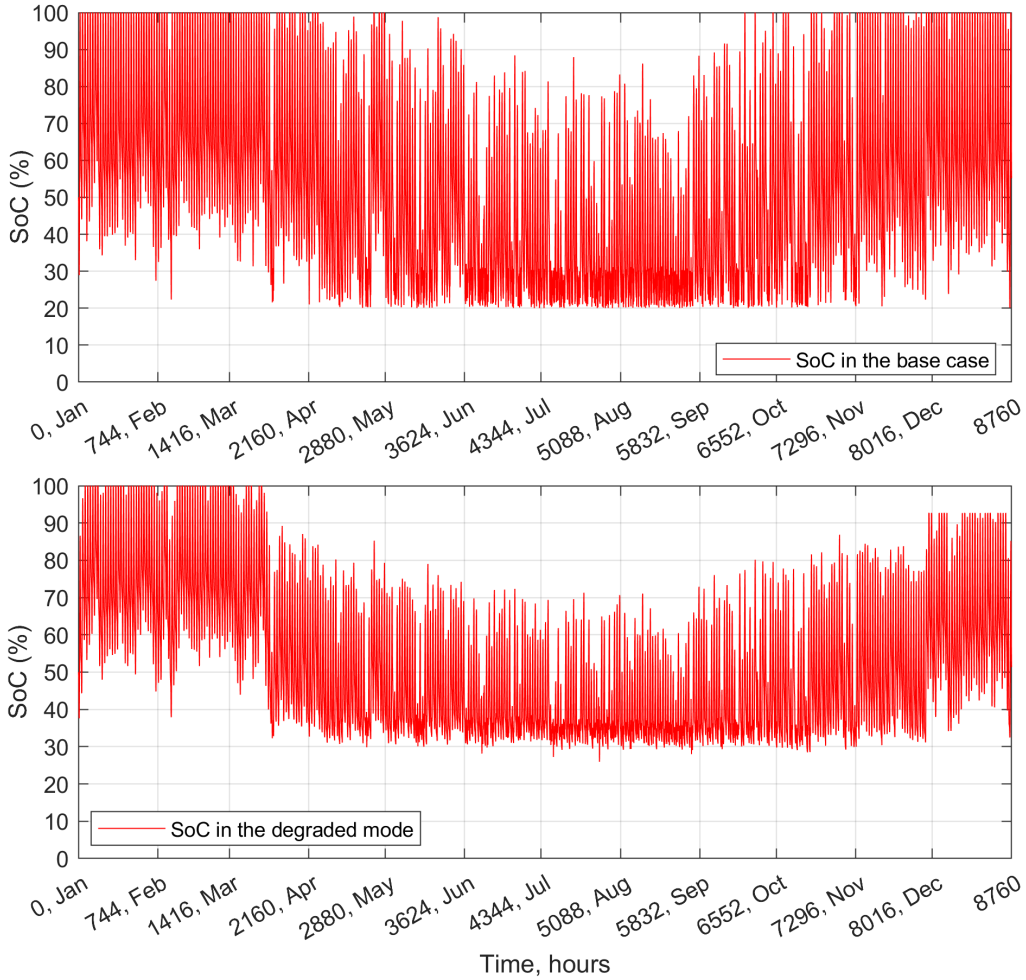

Figure 4.76 – Yearly SoC profile for the base case (fresh batteries) and degraded mode (weak batteries)

4.4.5 Energy Balance in the System

The net energy balance for the base case and degraded mode is shown in Figure 4.77. In these plots, PV and load remain unchanged, while surplus PV, E_D, and net energy imbalance vary considerably. It can be noted from the bar plots that PV is a critical component contributing to the primary source of energy in the system. The accumulated load with a 2.5% evolution per quarter requires 189,570kWh/year of energy in the system. This energy demand is met by coordination of PV and DG followed by a load cut in emergency conditions. Furthermore, the load loss (13,181.3kWh) is below 10% of the total energy demand (189,570kWh), which is acceptable as per our initial assumption.

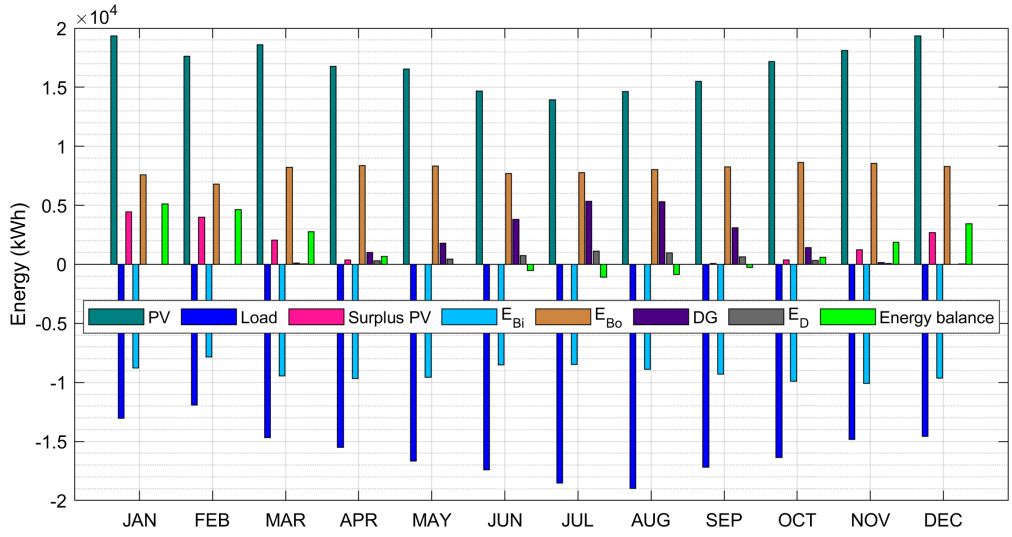

(a) Base case

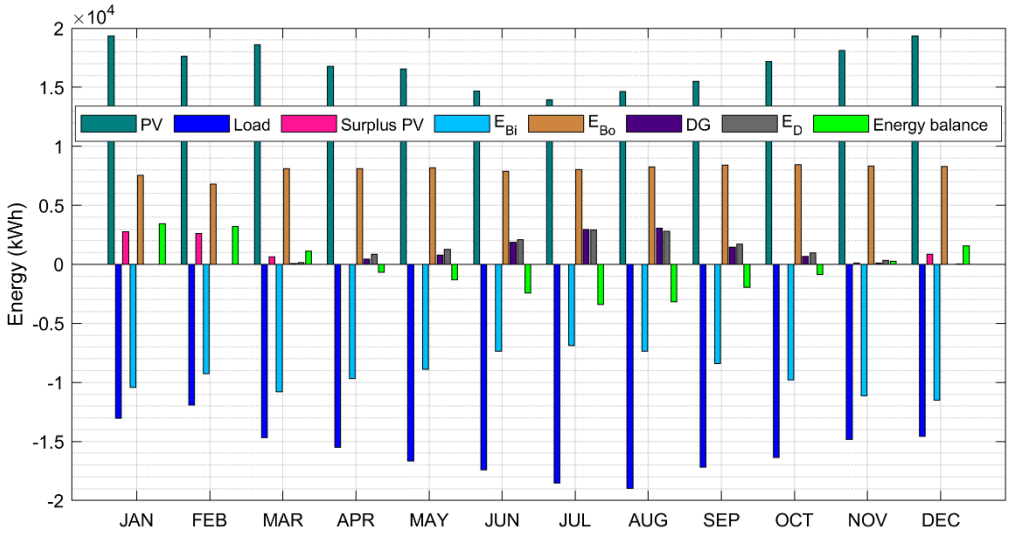

(b) Degraded mode

Figure 4.77 – Energy balance in the two simulated cases

It can be observed in both plots that April to October is the low-light period with more pressure on batteries. The energy balance is ensured by turning ON a DG or load cut. For the base case in Figure 4.77a, the excess PV energy (15,244.5kWh) during the whole year could be allocated to the community load, such as street lights and community shops in the form of dumped energy. Also, the energy imbalance in Figure 4.77b, is compensated by an increase in the load shedding for the degraded mode.

The average monthly energy mix of the final design is depicted in Figure 4.78. It is observed that the degraded batteries stayed below 50% SoC by 30% more time in the whole year than the batteries with no degradation. However, this undercharged condition may not be a risk as the remaining useful life for degraded batteries is four times less than the fresh batteries. The two SoC curves also indicate that the fresh batteries are deeply discharged compared to the degraded batteries during harsh conditions (April-October). It is because of the robust control over the lower operating limits of the degraded batteries to keep them safe from fatal damage due to deep discharge.

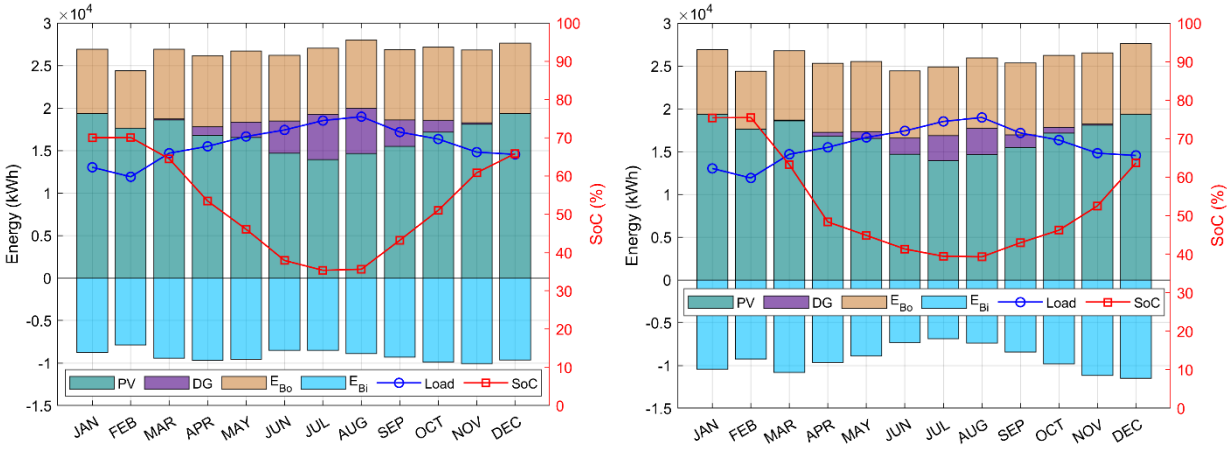

(a) Base case

(b) Degraded mode

Figure 4.78 – Accumulated monthly energy mix and battery SoC variation

4.4.6 Degradation Impact and System Performance

It is worth noting that the battery degradation is incorporated for each quarter at a 2.5% reduction in their aggregated capacity. Because of this evolution, the old batteries mostly stay undercharged and stressed compared to their counterpart in the base case.

(1) Battery Performance: It is recalled that the fresh and degraded batteries operate in their safe SoC limits above 30% and 40%, respectively. The region below these thresholds is defined as an emergency zone for the batteries. The battery SoC_{min} is the lowest charge level beyond which it is no more useful to discharge a battery. Therefore,

a proportional load is shed, or a DG is turned ON to cover the loss, maintain reliability, and protect batteries. First, the battery performance and its SoC variation for the base case and degraded conditions are detailed using Figure 4.79. The plot shows hourly SoC variation and the corresponding yearly load demand. For the base case in Figure 4.79a, it can be noted that the SoC is fairly good throughout the year, except in a few instances when the load is high. As mentioned in SUBSECTION 4.1.4, the PV generation is low, and the load is high at this particular time. Therefore, this window is considered the harsh operational period for the batteries. The fresh batteries returned to their fully charged status in the first and last quarters, indicating good PV injected power into the system. In the middle of the year, the daily average SoC is above 60%, which is reasonably good. It is further observed that the weak batteries, though with cut-off at 30%, never returned their full charge after the first quarter.

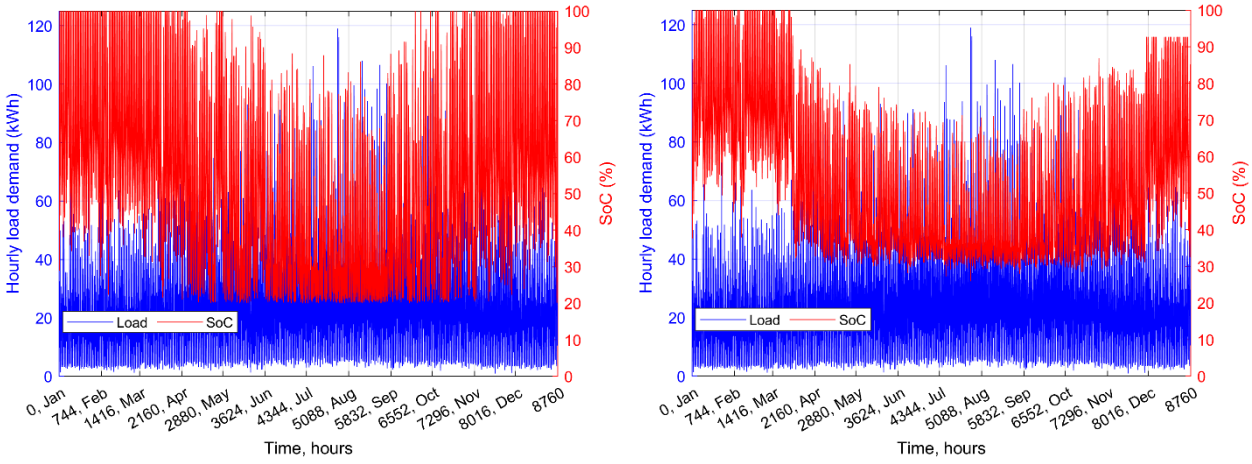

Figure 4.79 – Battery performance to meet yearly load demand

The battery performance and the need for a load cut in harsh conditions is analyzed using Figure 4.80. In this plot, the large magnitudes of the load loss are during the window of harsh operation for batteries. In Figure 4.80a, the load loss, its low magnitude, and low occurrence indicate the excellent performance of fresh batteries in the base case. The load loss magnitude and frequency in the degraded mode are comparatively higher than the base case. However, this load loss is compromised by the less energy tariff. The cost saving comes from the unmet load, which on the other hand could have been met by a DG. Conclusively, the satisfactory battery operation in the degraded condition indicates reliable microgrid operation at lower costs, which are indicators of the social acceptance of the proposed microgrid.

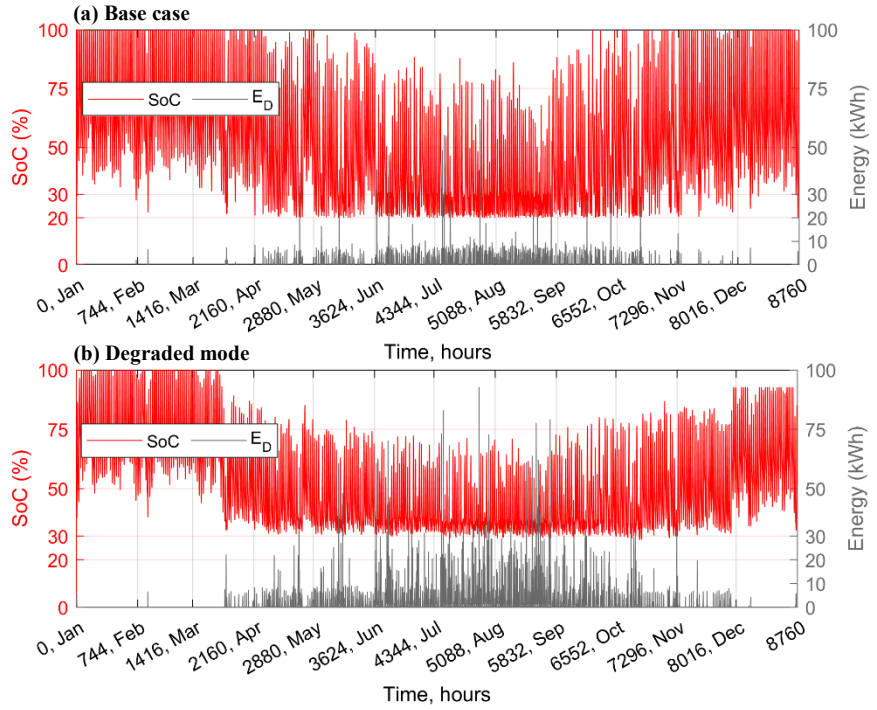

Figure 4.80 – Low-priority load cut in extreme conditions

(2) The Two-stage Load Loss Strategy and DG Performance: The two-stage load loss strategy and the DG operation is plotted using Figure 4.81. In our control strategy, we initiate the first part of the load cut in the region between safe limits and the lower cut-off (20% for fresh and 30% for degraded batteries). In this part, we only cut 25% of the load. The battery discharge is reduced by 25%. The second load cut is initiated if the SoC crosses the lower cut-off or in the event of a sudden shortfall. The load cut can never be more than 75%, as 25% of the load is to be served what we call a high-priority load. In Figure 4.82, in an emergency condition, the DG comes online to protect the system from collapse. Therefore, DG is forced to turn ON in shortfalls as well as SoC below the safe operating limits.

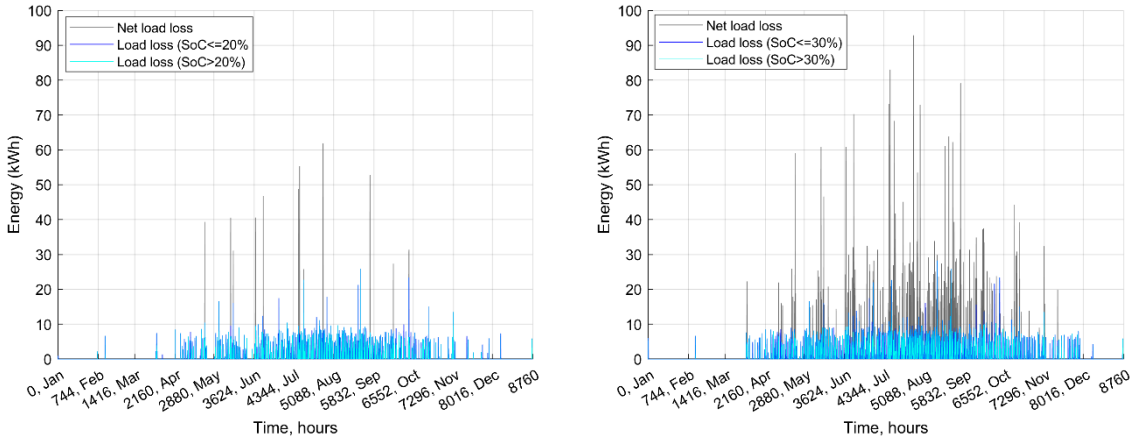

(a) Base case (b) Degraded mode

Figure 4.81 – Comparison of the two-stage load loss, its magnitude and frequency of occurrence

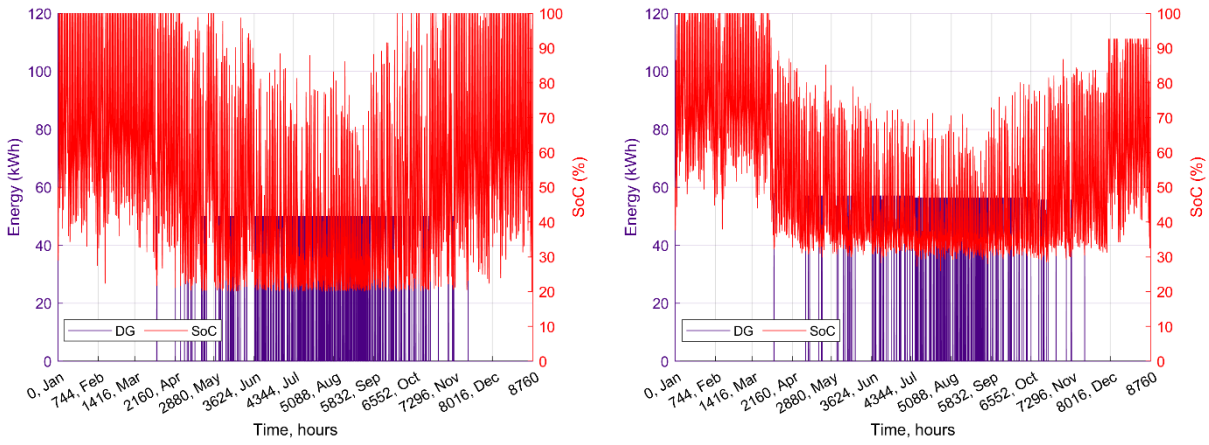

(a) DG operation in the base case (b) DG operation in the degraded mode

Figure 4.82 – DG operation in emergency condition

It can be noted in Figure 4.82a, that the DG operates at the rated power of 50kW and 60kW in its fresh and degraded conditions, respectively. The DG tends to operate at the degraded condition with a 1.25% power loss after each quarter. In the implemented EMS, the DG operation hours in the degraded condition is 54% less than the base case but at the cost of compromising reliability.

(3) Yearly Performance: Finally, a global view of the E_{Bo}, E_{Bi}, PV power, surplus PV, and E_D is plotted using Figure 4.83 for the two cases. The plot better supports the discussion in SUBSECTIONS 4.3.1, 4.3.3 on the battery performance in different climatic conditions. It is observed that the charge and discharge patterns and their magnitude in both cases resemble pretty close to each other, which is an indication of the good utilization of the battery energy. It can also be noted that comparatively less surplus PV is available in the degraded condition as the PV system has to charge relatively more weak batteries than the base case.

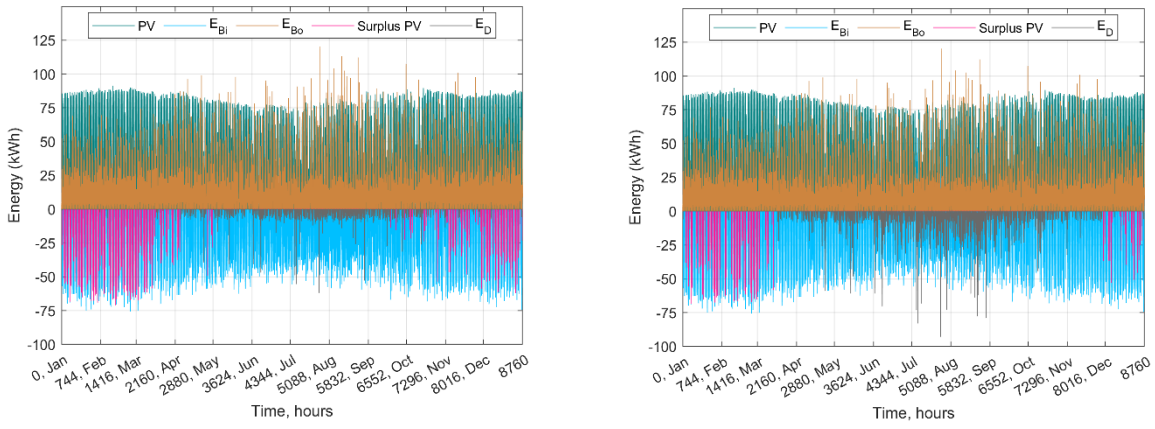

(a) Base case (b) Degraded mode

Figure 4.83 – Battery sourced and absorbed power during one year

4.4.7 Techno-Economic Analysis of the Final Design: Quantified Comparisons

(1) Technical Data of the Final Design: In this subsection, we summarize the technical and economic information of the optimal system in the base case and degraded condition. The technical specifications of the final design are summarized in Table 4.19. In this table, we had mainly summarized the component specifications, energy balance, and other technical parameters. It is interesting that the system, in its degraded condition, still performs better to meet the load demand.

Table 4.19— Specifications of the final design

	Description	Unit	Design values/obtained data	
			Base case	**Degraded mode**
Component specifications	PV	Wp/ panel at STC	325	325
	DG	kW	50	60
	DG degradation	% per quarter	-	1.25
	Battery	V/Ah/Ns	12/100/8	12/80/8
	Maximum DoD	%	80	70%
	Battery degradation	% per quarter	-	2.5
	Converter	kW	33	33
	Converter efficiency	%	95	95
Energy balance	PV	kWh/year	202,248.0	202,248
	Surplus PV	kWh/year	15,244.5	7,0035
	DG	kWh/year	22,012.9	11,4317
	Total generated energy	kWh/year	224,260.9	213,679.7
	Absorbed energy by batteries	kWh/year	110,179.6	111,449.7
	Sourced energy by batteries	kWh/year	96,534.3	96,294.8
	Consumed energy	kWh/year	184,900	176,388.8
	Total load demand	kWh/year	189,570	189,570
	Deficient energy (E_D)	kWh	4,669.1	13,181.3
	REF	%	89	93.7
Annual system and operation cost	Total annual cost	$/year	46,672.4	32,832.3
	Fuel consumption	liter/year	6,647	3,384.4
	Total emissions	g/kWh	15,358.8	8,773.7
	DG operational hours	hours	440	202
Other system parameters	Battery roundtrip efficiency	%	85	70
	SoC_{min}	%	20	30
	Battery safe operating limits	%	above 30	above 40

Description	Unit	Design values/obtained data	
		Base case	Degraded mode
Low-priority load cut	%	25	75
Load evolution	% per quarter	2.5	2.5
Fuel consumption	liters	normal	10% more
Diesel cost	$/liter	1.104	1.104
DG emissions	g/kWh	normal	10% more
Microgrid lifespan	equal to the lifespan of PV panels (years)	20	20
Optimization algorithm	-	PSO-GA	PSO-GA
Problem dimension	no. of variables	3 (PV, DG, battery)	3 (PV, DG, battery)
No. of iterations for optimum solution	-	30 out of 60	36 out of 60
Population size in the search space	-	50	50
Total shortfalls	-	12	197
Shortfall threshold	% of the net load	5	10

The size of DG in the degradation mode is 10kW more than the base case to be able to charge more batteries and feed the load. The DG operation hours and fuel costs are significantly reduced by including nearly twice the readily available low-cost second-life lead batteries and increasing the level of load cut. The 54% reduction in DG operation hours also resulted in a 43% reduction in total greenhouse gases (GHG) emissions. The size of the converter is selected based on the total peak load demand. In the average model, the converter is considered equal to the sum of the average converters used in the system. A 33kW converter is simulated for a peak system load of 30kW. A 5% safe margin for load fluctuation at 95% converter efficiency is considered. However, the size of the converter is not a decision variable for the optimization problem as its price is negligible compared to other system components. Also, the REF is slightly improved from 89% to 93.7%. As PV energy and load requirements are the same, this factor improved due to less DG participation and the increasing magnitude of load cut, which resulted in more than three times deficient energy in the system. The number of shortfalls in the base case is 12, on average, once a month. However, the number of shortfalls in the degraded case is 197, nearly every alternate day. Nevertheless, the partial loss of supply during these short falls is acceptable for a rural microgrid with the level of reliability of shedding less than 10% of the total demand.

(2) Financial Data: In addition, the annualized cost summary and energy tariff for the two scenarios are described in Table 4.20. The financial outcomes for the final design include initial capital cost, O&M cost, replacement cost, and lifetime of the components compared to the entire project life. The DG O&M and fuel consumption is a function of its size and operation hours. As a result, the hourly consumption rate is different. The annual interest rate is assumed to be half of the actual interest rate in the base case. This reduction is not much of a contributing factor to the net annual system cost; however, it slightly changed the PV prices in the degraded mode. It would be appealing to include this factor due to expected subsidies on such environment-friendly projects in poor regions. While considering the economic results summarized in Table 4.20, the average monthly electricity bill is only $21.5 compared to $28.0 in the base case. It is also observed that the reasonable replacement cost comes from replacing batteries with an interval of 10 years in the base case and 2.5 years in the degraded condition.

Table 4.20— Annualized cost summary of the proposed system in ($/year)

Microgrid component	Total units	Capital cost ($/unit)	O&M ($/unit)	Total fuel price ($)/operation hours	Lifetime in years	Net cost ($/year)
Base case with no degradation						
PV	300	250	2	-	20	6,365.7
DG	50kW	175/kW	1	7338.6/440 @1.104$/liter	20	28,784.8
Batteries	360	250	2	-	10	11,130
Converters	-	100	1	-	20	391.9
Annual interest		4.50%		Net cost per year		46,672.4
				LCOE		$0.233/ kWh
				Average monthly electricity bill		$28.0/household
Degraded mode						
PV	300	250	2	-	20	5,298
DG	60kW	131.2/kW	1.5	4,110/202 @1.104$/liter	5	21,314.6
Batteries	592	62.5	3	-	2.5	5847.6
Converters	-	100	1	-	20	372.1
Annual interest		2.25%		Net cost per year		32,832.3
				LCOE		$0.179/ kWh
				Average monthly electricity bill		$21.5/household
				Cost saving		23.2% cheaper

The lower LCOE in our proposed design is a determining factor for economic profitability and social acceptance of the supply system in the region. The LCOE calculation include the assumption of utilization surplus PV for community load and included in the net

useful consumed energy. The resulting LCOE from the final design is \$0.18/kWh, the same as the domestic electricity tariff in BURKINA FASO in March 2022 [13]. The same grid tariff was \$0.22-\$0.25 in 2019 [1]. According to the reports, many set goals have not yet been achieved to reduce regional energy poverty [1]. Therefore, further cost reductions in grid tariff cannot be relied on without realizing rural microgrids in the region. It also makes the project competitive and a promising solution in BURKINA FASO and other SUB-SAHARAN countries. Therefore, implementing such a system can bring social and economic benefits to rural areas with similar requirements for electrification.

4.4.8 Impact of the Battery Roundtrip Efficiency on LCOE and REF

The performance impact of variations in critical parameters such as battery roundtrip efficiency is analyzed. We considered 85% and 70% efficiencies for fresh and degraded batteries for the default condition, respectively. All the presented results in this chapter are based on the default case. The converter's efficiency is held at 95%, while the system is tested for a range of roundtrip efficiencies in the base case and degraded mode. In Figure 4.84, a comparison of the impact of roundtrip efficiency on the LCOE and REF is determined from simulations. It can be observed that LCOE hikes with lower roundtrip efficiencies, which is also a determining factor in considering useful legacy batteries.

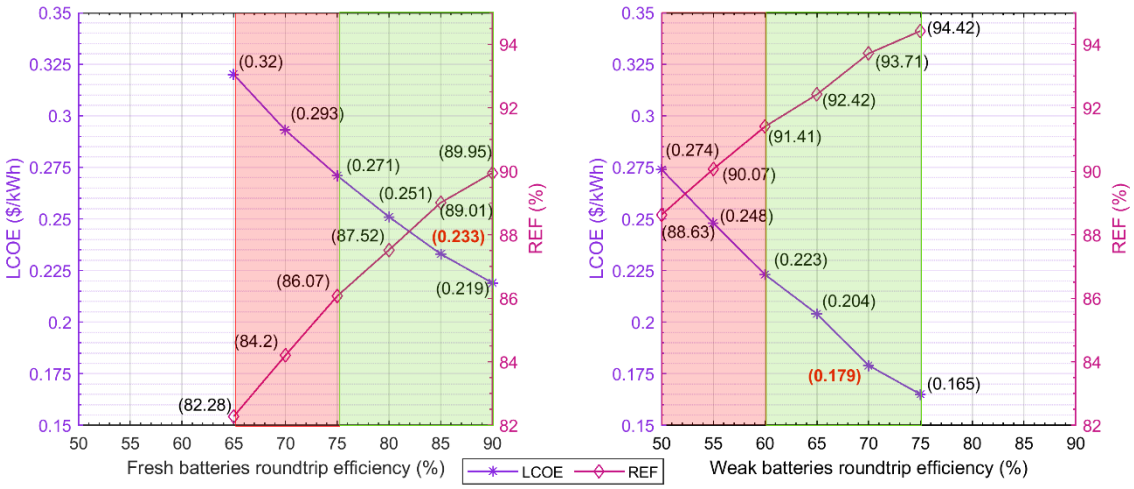

Figure 4.84 – Impact of the battery roundtrip efficiency on LCOE and REF

The green-shaded region represents an economical operating region in both cases, while the red region shows an uneconomical operation or a parameter value that might not be technically realizable. It can be noted that the roundtrip efficiencies of fresh lead-acid batteries above 85% may not be practically possible to contribute to further cost reduction. Similarly, a weak lead-acid battery cannot have efficiency above 70% to

further reduce LCOE to $0.165/kWh. The degraded batteries still serve economically up to their useful remaining life even if the efficiencies decline to the lower threshold, which is 60% from our analysis. We also found the limit of the second useful remaining capacity in the degraded mode. These values range from 80% in their first retirement life to 70% in the degraded mode, *i.e.*, another 10% of the utilizable capacity during a year. This outcome is based on the simulated degradation rate of 2.5% per quarter. Finally, the analysis enabled us to find the lower limit of battery roundtrip efficiency beyond which it could be more expensive and impractical to use weak batteries compared to their counterpart. It is concluded that the weak batteries below 60% roundtrip efficiencies are useless. At this point, the LCOE becomes more attractive for the base case with fresh batteries instead of using already degraded batteries in their second life.

4.5 Summary

This chapter has established a foundation step for testing the second-life hypothesis by simulating a 96V/30kW DC microgrid for a remote village in BURKINA FASO. A hybrid PSO-GA optimization algorithm is used to find the optimal system performance at best cost. The simulations showed that retired batteries with a 20% capacity loss can still serve better in low-power applications, but with a slightly modified EMS and an acceptable load loss. We also observed that the batteries in their degraded condition can be cost-effective up to the lower threshold of 60% roundtrip efficiencies.

We found from simulations that the LCOE is only $0.18/kWh in the degraded operation, which equals the current grid tariff in BURKINA FASO. It was also concluded from the simulations that the energy cost in degraded mode is 23.2% cheaper than the base case with no degradation. Such a reasonable electricity cost is obtained by using low-cost batteries and a compromised load loss of less than 10% of the entire load during the year. The overall assessment of the proposed scheme leads us to conclude that integrating legacy batteries into rural microgrids can effectively contribute to the low-cost operation. Therefore, the second-life hypothesis could be a potential cost-optimal solution for rural electrification in developing regions. If such a system is realized, it could be attractive to consumers, microgrid planners, and public bodies/NGOs working on the climate theme (mainly to reduce the early recycling of lead batteries). It could also facilitate decision-makers and microgrid installers to use legacy equipment and extending their lifecycle, which is an eco-friendly contribution.

****----The end----****----Chapter-IV----****

Bibliography Chapter-IV

[1] "BURKINA FASO Power Africa Fact Sheet-USAID." Accessed: Jun. 16, 2022. [Online]. Available: https://www.usaid.gov/powerafrica/burkina-faso

[2] M. Moner-Girona, K. Bódis, T. Huld, I. Kougias, and S. Szabó, "Universal access to electricity in Burkina Faso: scaling-up renewable energy technologies," Environmental Research Letters, vol. 11, no. 8, p. 084010, Aug. 2016, doi: 10.1088/1748-9326/11/8/084010.

[3] S. Twaha and M. A. M. Ramli, "A review of optimization approaches for hybrid distributed energy generation systems: Off-grid and grid-connected systems," Sustainable Cities and Society, vol. 41, pp. 320–331, 2018, doi: https://doi.org/10.1016/j.scs.2018.05.027.

[4] S. Meunier, "Optimal design of photovoltaic water pumping systems for rural communities – a technical, economic and social approach," Université Paris Saclay, France, Ph.D. Dissertation, 2019.

[5] "Average High and Low Temperature in Ouagadougou," © WeatherSpark.com. Accessed: Sep. 28, 2022. [Online]. Available: https://weatherspark.com/y/40160/Average-Weather-in-Ouagadougou-Burkina-Faso-Year-Round#Figures-Temperature

[6] "PVGIS Interactive Tool." https://re.jrc.ec.europa.eu/pvg_tools/en/#HR (accessed May 20, 2022).

[7] T. Huld, R. Müller, and A. Gambardella, "A new solar radiation database for estimating PV performance in Europe and Africa," Solar Energy, vol. 86, no. 6, pp. 1803–1815, Jun. 2012, doi: 10.1016/j.solener.2012.03.006.

[8] S. Meunier et al., "A validated model of a photovoltaic water pumping system for off-grid rural communities," Applied Energy, vol. 241, pp. 580–591, May 2019, doi: 10.1016/j.apenergy.2019.03.035.

[9] B. I. Ouedraogo, S. Kouame, Y. Azoumah, and D. Yamegueu, "Incentives for rural off grid electrification in Burkina Faso using LCOE," Renewable Energy, vol. 78, pp. 573–582, 2015, doi: https://doi.org/10.1016/j.renene.2015.01.044.

[10] T. Lambert, P. Gilman, and P. Lilienthal, "Micropower System Modeling with Homer." John Wiley & Sons, 2005.

[11] J.-M. Delgado-Sanchez and I. Lillo-Bravo, "Influence of Degradation Processes in Lead–Acid Batteries on the Technoeconomic Analysis of Photovoltaic Systems," Energies, vol. 13, no. 16, 2020, doi: 10.3390/en13164075.

[12] W. Merrouche, "Lead-acid Battery Degradation Mechanisms in Photovoltaic Systems PVS," Oct. 2013.

[13] "Household electricity prices/kWh in Burkina Faso." https://www.globalpetrolprices.com/Burkina-Faso/ (accessed Jun. 15, 2022).

Chapter-V: Conclusions and Perspectives

Key Terms

Work summary, key findings, research gaps, possible extensions, supplemental material.

Acronyms

Ah	Ampere-hour
ATS	Automatic transfer switch
BSP	Battery status processor
EMS	Energy management system
EoL	End-of-life
EVs	Electric vehicles
GHG	Greenhouse gases
LCOE	Levelized cost of energy
Li-ion	Lithium-ion
MPPT	Maximum power point tracking
O&M	Operation and maintenance
PV	Photovoltaic
REF	Renewable energy fraction
SHS	Solar home system

Chapter Highlights

This chapter summarizes the steps taken toward achieving the thesis goals and their contribution to the current state of the art. The chapter also connects the thesis outcomes to possible future extensions. Some of the recommended extensions could be used as grand research proposals. In addition, the supplementary material and online resources could be used to help readers as a starting reference for similar topics.

Contents

CHAPTER 5

CONCLUSIONS AND PERSPECTIVES

In this Ph.D. thesis, we studied the technical dimensions and complexities of the second-life concept as a possible new electrification trend for rural microgrids. The dissertation presents contributions to develop a problem framework and solutions to understand the impact of second-life batteries and diesel generator (DG) on the overall system economics and performance. The work is a motivation for developing energy access in isolated communities, which is directly linked to women's empowerment, job creation, safety, health, global security, and a step towards the growing recognition of climate threat. Now, we summarize this manuscript with some interesting future work and a few insightful suggestions. In the coming sections, we provide general conclusions, study limitations, and improvement areas.

5.1 General Conclusions

5.1.1 Executive Summary

New energy technologies and their social acceptance are closely linked. Therefore, any electrification services in the rural areas must be affordable. The concept of power generation close to the consumer's end is a possible solution as it best suits the geographic conditions of rural areas. However, rural microgrids are a financial risk for investors due to the lack of participation of the local people and expected less return on investment as people do not fully participate in electrification services. For example, if the microgrid is expected to serve 100 households for a certain payback period, the actual subscribers may be less than that, and the investment becomes a risk. A DC microgrid that is more suitable to the local conditions of BURKINA FASO (GOGMA village, GPS coordinates: *Latitude 11.73°; Longitude - 0.58°*) is proposed. The climatic, geographic, and economic conditions of the site and less than 5% electricity access rate in its rural areas are very suitable to test our second-life hypothesis. We provided a well-thought view of the topic

and context of linking our proposition to the energy access problems in the developing world. The presented work highlights the significance of this project to the general society and energy-deprived communities.

After introducing the topic in simple terms, we presented detailed electrical and mathematical modeling of the microgrid components. Then we discussed the technical feasibility of the microgrid components using simulations and a few experimental tests. The central portion of the experiments and measurements covered the aging dynamics of batteries. These experiments were conducted in a controlled manner using our installed battery characterization bench in the GEEPS laboratory. We proposed less labor-intensive battery tests using simple tools. We proposed two classic tests and measurement schemes for battery health characterization and determination of the actual remaining capacity. The outcomes from the measurements were used to group second-life batteries in different health categories. We also recovered the capacity using heavy cycling. In this technique, the battery capacity is recovered by overcharging and then deeply discharging it to the lower cut-off. The idea is to break the inner formed crystal layers on battery electrodes using plate breathing. We also noted that the applied technique could not be possible with intelligent microcontroller-based chargers. Therefore, a dumb rectifier-based charger was used to slightly overcharge the batteries and then discharge for at-least three cycles. The gradual acceptance of charge is an indication of the battery recovery.

Finally, we used a two-step methodology to optimize and analyze a PV-diesel-battery hybrid in the base case and degraded mode. The base case is simulated with photovoltaic (PV), DG, and batteries to develop a techno-economic optimum and sustainable design without degradation. Then we carried out comprehensive simulations and techno-economic analysis for the performance impact in the degraded condition. The technical and economic specifications of the final design were summarized in SUBSECTION 4.4.7. An intelligent hybrid optimization technique called particle swarm optimization genetic algorithm (hybrid PSO-GA) was used to determine optimal sizing and least cost operation while respecting physical constraints. The overall system is optimized for the least-cost operation at a certain level of reliability in both cases. The simulations are conducted using an average DC microgrid model with a one-hour time-step to accelerate the analysis. The battery and DG degradation are incorporated each quarter at a 2.5% and 1.25% reduction in the aggregated capacity, respectively. The microgrid life is considered that of the life of PV, which is assumed 20 years. The energy flow within the system is controlled using rule-based energy management system (EMS).

We simulated the system for the proposed study site with real meteorological data and an assumed yearly load for 125 houses with 1100 inhabitants. The simulations and related techno-economic analysis are conducted for one year. The global view of the system's energy flow balance, optimal energy transaction, and system performance was analyzed in different periods of the year on a weekly, monthly, and yearly basis. We observed an acceptable performance of the microgrid during the high load and low PV periods. This harsh operational period lies in the middle of the year.

We observed 12 shortfalls in the base case and 197 in the degraded mode. These partial blackouts occurred during the months with low light. These shortfalls mainly contributed to the % of the unmet load. The level of reliability is compromised by less initial capital. We found the limit of the second useful remaining capacity in the degraded mode. These values range from 80% in their first retirement life to 70% in the degraded mode, *i.e.*, another 10% of the remaining utilizable capacity using the assumed degradation rate of 2.5% per quarter. We also found that batteries below 60% roundtrip efficiencies could be useless, which may lead to an uneconomical and less technically viable battery operation. We found from the monthly energy mix plots that the degraded batteries stayed below 50% SoC by 30% more time in the whole year than those without degradation. However, this undercharged condition may not be risky as the remaining useful life for degraded batteries is only 2.5 years. The renewable energy fraction (REF) is slightly improved from 89% in the base case to 93.7% in degraded mode due to less DG participation. However, it comes at the cost of more than three times deficient energy in the system. The 54% reduction in DG operation hours also resulted in a 43% reduction in the total greenhouse gases (GHG) emissions.

The lower Levelized cost of energy (LCOE) in our proposed design is a determining factor for economic profitability and social acceptance of the supply system in the region. The LCOE calculation include the assumption of utilization surplus PV for community load and included in the net useful consumed energy. The resulting LCOE from the final design in the degraded mode is \$0.18/kWh, the same as the domestic electricity tariff in BURKINA FASO in March 2022. Compared to \$0.23/kWh in the base case, the LCOE in the degraded condition is 23.2% cheaper. The average electricity bill for a household is thus only \$21.5 compared to \$28.0 in the base case. There is a possibility of getting even lower LCOE as subsidies from the government could be expected for implementing such an environment-friendly project in poor regions. Ultimately, a techno-economic analysis

of both cases is carried out for comparison and to determine the technical limitations and economic gains of our second-life proposition.

5.1.2 Thesis Contributions

To the best of our knowledge, the second-life hypothesis for rural microgrid cost reduction using legacy equipment of unknown use history is unique in its nature and a timely topic to meet the dual pressures of climate and energy access. The trending use of Li-ion is decommissioning an enormous number of lead-acid batteries, which is a current challenge. There is very limited literature available on lead-acid compared to Lithium-ion (Li-ion) batteries. Therefore, the contribution to the current state of the art is in line with the climate and energy access urgency. In this dissertation, we proposed the feasibility of legacy lead-acid batteries and DG for affordable integration in rural microgrids. By using the developed aging models of batteries and DG, a cost-optimal rural microgrid is proposed for underdeveloped regions. The case study is carried out for a rural village called GOGMA, BURKINA FASO by considering the local climatic and economic conditions. The compelling simulation results confirmed *second-life* as a possible new electrification trend in developing regions. We first proposed rapid battery testing, capacity recovery techniques, and analytical models of lead-acid batteries. The parametric information is then used to simulate a typical rural microgrid in the base case and degraded mode. The simulation results are compared to propose a cost-optimal design for rural electrification.

The convincing simulation results in CHAPTER-IV enabled us to propose legacy lead-acid batteries as an exciting solution to offset the initial capital cost of low-power low-voltage rural microgrids. Now, we approach the section on general outlook and present some of the current study limitations, each with a few insightful suggestions. The following section highlights some research gaps and possible solutions.

5.2 Possible Extensions

This section covers possible extensions beyond the work presented in this manuscript that limit us due to the project's scope, timeline, and which are outside of our immediate expertise. Unfortunately, some of these are not possible to evaluate at this stage but seem interesting to us as they revolve around the topic.

The research work is partially still ongoing, and further results are expected to become available. The outcomes are expected to enable us to remove some technical

barriers and realize the full potential of legacy batteries and DG. The authors are looking into new approaches to link the modeling, simulation, and experimental outcomes to validate existing dynamic aging models of lead-acid batteries. This model could be integrated in the simulation to assess the performance of second-life batteries through dynamic scenarios. It could better represent the complex aging nature, resulting in optimum energy sharing and resource management. In doing so, the premature second-life concept will probably become a reality for rural microgrids.

5.2.1 Research Gaps

The presented work in this dissertation has opened up many research questions. The authors recommend further work on a few related and timely topics for interested researchers to continue exploring further. Some of the given promising aspects could be used as a grand proposal. The research gaps can be split into three groups: modeling, EMS, and techno-economic analysis.

The TWO relevant modeling extensions are:

1. *Aging of other battery chemistries:* Li-ion batteries have already had a tremendous entry and dominated the battery market, bringing two great opportunities. First, the availability of a considerable number of decommissioned lead-acid batteries at a much lower price, which we covered as a low-cost storage option in low-power applications. A decade after, many more powerful Li-ion batteries will be available that get retired from electric vehicles (EVs). Therefore, the inclusion of second-life Li-ion batteries in low-cost microgrids would be relevant.

2. *The second end-of-life (EoL):* There is room to thoroughly investigate the complex aging nature of lead-acid batteries beyond 80% of the remaining health, which we have partially covered with a few experimental tests and measurements. It will be interesting to explore further the exact second EoL beyond their first EoL through experimental tests and measurements. The study could be done separately for fresh, average, and weak health batteries to boost the entrance of second-life batteries and their utilization in the microgrid market. The main answer to this key challenge is to know the exact level of representation of the second-life models that could balance accuracy and computation time. It will be more convenient to know the real aging impact and get accurate results with fast computation time. The easy evaluation of these characteristics from external and low-cost measurements would be a plus. More precisely, if there could be any benchmark

publishable second-life models and datasets for different usage conditions obtained from various field measurements. If such performance degradation data and a benchmark legacy lead-acid battery model are publicly available, it will be an excellent addition to contemporary state of the art on battery aging and modeling legacy microgrids.

The FOUR energy management and control aspects include:

1. *Combining fresh and weak batteries:* The premature second-life concept in rural microgrids could be further researched to find new ways of battery grouping with different health evolution. It will be more convincing to conduct the analysis using extensive experimental tests. It will be compelling to answer questions such as, "*what proportion of second-use batteries could be able to replace a fresh battery? in which conditions? at what cost? and for how much reliable operation of the microgrid?*". There is still room to adopt good practices in making this calculation easier for the system installers during the pre-feasibility and sizing stages. As legacy batteries may have no datasheet or their use history. It will be exciting to estimate the dimension (original capacity information), the battery environment (how it was used? was it connected to a PV system? directly or through a converter), the aging (how long it has been used?), and the application (vehicle, solar home system (SHS) to deduce the battery mission profile. It will be very convincing if a way is proposed to combine fresh and legacy batteries in the same microgrid at best system economics.

2. *Parameter variability and microgrid robustness:* The parameter evolution of degraded batteries and the unpredicted consumption of the rural people could be surprising and challenging at any stage of the microgrid life. A slight variation in input parameters can completely change the overall planned management and cause a system failure anywhere in the lifetime of such legacy microgrids. This parameter variability dimension must not, therefore, be overlooked. Therefore, the impact of parameter evolution on the EMS could be explored.

3. *Fault-tolerant control:* The battery short-circuits detection and isolation could be meaningful to avoid failure of the overall power pack or a sub-storage unit. It is essential to protect the system when mixing batteries of different unknown use histories, remaining health, Ampere-hour (Ah) ratings, and strange discharge behaviors. The proposed detection scheme should classify the fault as abrupt, intermittent, or gradual. It will be interesting to investigate novel insights to capture the fault dynamics and model

parameter sensitivities. If a battery pack fails, the control scheme could still keep the grid live in the degraded mode. It will be very relevant to explore this dynamic modeling aspect and parameterization.

4. *The need for a versatile EMS:* So far, no fully developed EMS for second-life components exists that can hold promise for the complex control and management of already degraded batteries. A fully versatile EMS tailored explicitly for the degraded batteries could be developed. The EMS should know the evolution and remaining system capabilities to change its control in the runtime. The existing EMS could be enriched with advanced machine-learning techniques and prediction algorithms (load and aging evolution, weather forecasts, and changing lifestyles). Prediction algorithms for the next few days or an entire week could significantly reduce the loss of power or pressure on degraded batteries. With such an intelligent EMS in hand, one day, the second-life microgrids will be rewarded for functioning as good citizens in the electricity world.

The THREE techno-economic and social aspects to explore are:

1. *Techno-economic analysis:* Interested researchers can propose quantitative indices and a detailed techno-economic analysis of the performance, user satisfaction, environmental impact, and cost minimization of the second-life propositions in a presentable form to the grid managers. Unfortunately, this type of simulation is rather cumbersome, as it has to be carried out over long periods (years) to derive meaningful statistics.

2. *Impact of dismantled PV modules:* PV modules are installed and used up to their EoL. This work considers PV modules without being dismantled from a facility, which could be very interesting if a rural microgrid with *everything second-life* is technically and financially evaluated. There is an excellent potential for producing cheap power from decommissioned PV panels from large installations. There is a need for more research and commercial development of the term *'everything second-life'* for low-power microgrid applications.

3. *Impact of social conditions:* We have not evaluated the non-technical aspects of the project. A site-specific study of the social response, availability of other indigenous resources, the impact of local conditions on the electrification services, and people's willingness to participate and pay could be evaluated.

5.2.2 Additional Recommendations

A local microgrid for the local people with the local material must come with local solutions for the grid aftercare and maintenance. Keeping skilled technicians in rural sites is relatively difficult, especially for an indefinite period. It is highly recommended that an upkeep action plan clearly defines who is locally responsible for the operation, basic inspection, cleaning equipment, initial diagnosis of system faults, and calling the maintenance technician. A few more recommendations are enlisted to broaden the understanding and implementation of some of these plans. Some of these recommendations are considered best field practices.

(1) The feasibility of pay-as-you-go prepaid meters could be studied as an internship. In addition, the following two internships are proposed at Master's level M2.

M2 Internship Proposal-I: Affordable integration of legacy batteries for multi-tier expansion of rural microgrids.
M2 Internship Proposal-II: Characterization and integration of second-life diesel generators.

(2) The global need for basic electrification is changing. Therefore, bringing electricity to the local communities for lighting is not enough to achieve universal energy access. Other ways could be explored in finding low-cost innovations for the flexible integration of small-scale commercial loads and a more economical distribution scheme in community microgrids.

(3) The tariff paid by the consumers within their '*willingness-to-pay*' must be able to sustain at least the operation and maintenance (O&M) cost to keep the grid running. The inflows should also compensate for the component replacement and other charges. On the other hand, high tariffs can reduce consumer participation and possible loss of revenue. Therefore, a tariff decision should be based on the ground circumstances to avoid the risk of microgrid failure on the social side.

(4) Consumer education is central to the sustainable operation of a rural microgrid. It is better to describe to the villagers all the system's limitations. There are famous stories when some SHS users buy simultaneously a small PV system and an electric iron. The difference between a 500W water pumping motor and a 15W hair clipper is evident to an engineer but not to a local consumer.

(5) Adapting the rural people to the system is relatively complex. Therefore, the grid managers could adjust the system to the local conditions. After all, social acceptance is a critical element to accommodate more consumers and generate revenues. In such remote microgrid installations, psychologically, ownership by the villagers is better than ownership by a private investor. The building owners who willingly host system equipment and the PV array on their rooftops can benefit from the bonus tariffs. It could help attract more and more consumers and increase profit margins.

(6) Sooner or later, 100% rural electrification with locally built legacy microgrids is futuristic. There is a lack of rigorous standards for their regulation, which could be researched and presented as a white paper to the local and regional regulatory authorities.

Finally, technology gives fewer headaches than social issues, which should not be underestimated. Undeniably, an electrification system in rural communities is more likely to fail not because of the technical limitations but having no explicit organizational schemes, ownerships, involvement of the end consumers in decisions, and management committees (responsible for new connections/revenue collection, and enforce rules). Rural people must be appropriately informed of the system limitations and the consequences of unplanned load evolution. The disconnection policy should be apparent and enforced to protect such a low-inertia rural microgrid from collapse. It is possible to address these issues by adequately training local personnel incharge of the system.

5.2.3 Remarks on the Project Feasibility and Sustainability

Our proposed second-life concept satisfies the following four main criteria that could be used to evaluate the feasibility and sustainability of our project.

- ☐ **The urgent need:** what is necessary*; electricity access in developing regions, development of the poor communities, equal opportunities, delaying recycling.*
- ☐ **The available finances:** what is affordable; *retired batteries, utilization of indigenous resources, and equipment from existing SHS.*
- ☐ **The environment:** what is acceptable; *giving a second life to batteries as waste disposal brings environmental concerns.*
- ☐ **The technology:** what is feasible; *the use of existing methods for the optimization and energy management of legacy batteries*.

Given that electrification is a final solution for women's empowerment, primary healthcare, safety, growing concerns of climate threats, global security through job creation, and opportunities for the development of local businesses. These driving forces are key enablers for the attention of international, public, and private institutions toward the necessity of such energy-related projects. With the growing interest in renewable-based electrification projects, it is expected that more funding will be available from the developmental budget for rural microgrids. In parallel, it will also require the involvement of private investment and donor bodies to complement the government funds. The availability of funds to offset some of the capital costs is logical due to these multifold benefits of using second-life.

Whether *industrialized, middle-income, or low-income*, all countries prioritize facilitating reliable energy access to their citizens. The local political setup and community people can act as a *trigger* by providing motivation and a more secure place for installations, the private sector and investors as *enablers* to realize the actual rural microgrid system by investment, and the government sector as a *facilitator* to provide subsidies. In this way, a second-life rural microgrid will have much more social acceptance and success rate. It is hoped that there will be enough initiatives to promote the local grid-modernization with second-life components and establish an electricity market that can attract private investment. Therefore, the lights are green towards a more sustainable, inclusive, and affordable electrification system as a technically relevant and competent energy solution in the underdeveloped regions of energy-poor countries.

*****-----The end-----*****-----Chapter-V-----*****

The end

"Life is like riding a bicycle. To keep your balance, you must keep moving" - Albert Einstein

Analysis of the Performance Impact of Component Aging in a Hybrid Energy PV-Diesel-Battery Rural Microgrid: Modeling, Control, and Energy Management

Khadim Ullah Jan
University Paris-Saclay
GeePs Lab| 11 rue Joliot Curie, 91192, Gif-sur-Yvette,
Paris, France

Page intentionally left blank

A. Appendices

A-I Microgrid Tariff Assessment and Load Modeling Tools

Source: https://data.nrel.gov/submissions/79

NREL Data Catalog

Citation: Li, Xiangkun; Salasovich, James; Reber, Tim (2018): Microgrid Load and LCOE Modelling Results. National Renewable Energy Laboratory (NREL).

Data and Tools: NREL develops data sets, maps, models, and tools for the analysis of energy technologies around the microgrid load and tariff considerations.

1. Micro-grid Tariff Assessment Tool: The purpose of this tool is to display LCOE results for a microgrid serving a rural village with 100 micro-grid connected homes, two shops, and one school. Cost-based modeling of these systems was done using NREL's REopt tool. REopt is a techno-economic decision support model used to determine the optimal selection, sizing, and dispatch strategy of candidate technologies such that energy requirements are met at the minimum life-cycle cost.

The tool allows the user to see how the optimized LCOE for different microgrid configurations change with input parameters. Available toggles include geographical location, fuel prices, discount rates, level of planned reliability, load profile, technology costs, distribution system costs, and other soft costs. Furthermore, a breakdown of the LCOE is provided showing how different cost components contribute to the final LCOE. This tool allows designers for different combinations of technical and economic project assumptions in order for developers to recover system costs and attract investment.

2. Rural African Load Profile Tool: The purpose of this tool is to provide hourly electrical load profiles for various household types (i.e., high income, medium income, and low income households) and for various commercial entities (i.e., water pumping for irrigation, grain milling, small shops, schools, clinics, and street lighting) that are commonly found in rural Sub-Saharan Africa. This tool allows the user to input the number of households, types of households, and number of commercial entities in order to see how the hourly electrical load profile changes and to see how the maximum and minimum electrical load changes.

A-II Further Reading— Online Supplemental Resources

References to these online resources are not biased and are given for informational use only.

https://www.club-er.org/home.html
www.ruralelec.org
https://www.ademe.fr/
https://www.ecmwf.int/
https://asdc.larc.nasa.gov/
https://www.giss.nasa.gov/
https://solargis.com/
http://solardat.uoregon.edu/
UO Solar radiation monitoring laboratory.
https://power.larc.nasa.gov/
Provides solar and meteorological data sets from NASA.
ttps://www.esolar.co.nz/residential-off-grid-solar-systems/
https://iea-pvps.org/
IEA photovoltaic power systems programme (Task-11 hybrid minigrids).
https://ec.europa.eu/jrc/en/pvgis
https://www.irena.org/publications/2019/Apr/Global-energy-transformation-A-roadmap-to-2050-2019Edition
https://sustainabledevelopment.un.org/sdg7
https://www.footprintnetwork.org/our-work/sustainable-development/
https://www.ipcc.ch/
The intergovernmental panel on climate change.
https://www.isdb.org/ Islamic development bank.
https://www.worldbank.org
World Bank (189 member countries).
https://en.wikipedia.org/wiki/Paris_Agreement
Climate change agreement, Paris.
https://www.osti.gov/etdeweb/
World energy base (WEB) for scientific literature.
https://www.nrel.gov/solar/
National renewable energy lab, Colorado, USA.
https://www.energy.gov/
The U.S. Department of Energy (DOE).
https://www.mpoweruk.com/performance.htm
Battery consultancy based in Chester.
https://corporate.exxonmobil.com/Energy-and-innovation/Outlook-for-Energy
https://www.seforall.org/
Sustainable energy for all.
https://sdg.iisd.org/
International Institute for sustainable development.
https://about.bnef.com/new-energy-outlook/
BloombergNEF provides independent energy analysis.
https://solar.schneider-electric.com/solution/microgrids/
Solar business of Schneider Electric Inc.
https://www.iea.org/topics/world-energy-outlook

International energy agency.
https://www.ren21.net/reports/global-status-report
Global renewable energy community.
https://ec.europa.eu/clima/eu-action/climate-strategies-targets/2030-climate-energy-framework_en
http://www.renewit-project.eu/
https://www.off-grid-europe.com/
https://energystorage.org/
Energy storage association, now American clean power (https://cleanpower.org).
https://www.rte-france.com/en/eco2mix/
All of France's electricity data in real-time
https://get.solardesigntool.com/
Tool for PV system design (project summary, site plan, single-line diagram, PV safety labels, attachment plan(s), attachment details for supported racking systems, fire safety plan, equipment datasheets)
https://pvwatts.nrel.gov/
PVWATTS® calculator: estimates the energy production and cost of energy.
http://www.energyonline.com/Data/
LCG consulting.
http://climateactiontracker.org/countries/china.html
Tracking climate action since 2009.
https://www.solarpowereurope.org/
Global market outlook for solar power in Europe.
https://www.eia.gov/outlooks/ieo/
US energy information administration. International energy outlook 2021| information and projections.
https://www.worldenergy.org/
World energy council.
https://cleanenergysolutions.org/qaf
Assisting countries with clean energy policies.
https://minigrids.org/resources/tools/
Minigrid clean energy tools and resources.
https://poweringhealth.homerenergy.com/
Dimensioning tool specific to the electrification of a healthcare center.
https://www.rte-france.com/
French public transportation grid.
https://data.nrel.gov/submissions
NREL[14] open datasets catalog.
https://www.nrel.gov/grid/solar-resource/renewable-resource-data.html
https://www.iea.org/reports/energy-access-outlook-2017
IEA, "Energy Access Outlook 2017," Paris, 2017.
https://www.ecmwf.int
ECMWF - European center for medium-range weather forecasts, producing global numerical weather predictions and other data.
https://ieeexplore.ieee.org/servlet/opac?punumber=9438968
IEEE 2030.10 Standard for DC microgrids for rural and remote electricity access applications.
https://standards.ieee.org/standard/1561-2019.html
IEEE 1561 Standard for optimizing the performance and life of lead-acid batteries in remote hybrid power systems.

14 The National Renewable Energy Laboratory (NREL) is a national laboratory of the U.S. Department of Energy, office of energy efficiency and renewable energy, operated by the Alliance for Sustainable Energy LLC.

A-III List of Publications/ Scientific Activities

The scientific production of this work has been published in international peer-reviewed conferences, and national proceedings. In addition, the author got the opportunity to present his work on many forums and took an active part in scientific activities such as conference reviewer, session chair, and voluntarily assistantship in conference organization.

1. International IEEE Conferences with Proceedings

[1] **K. U. Jan**, A. Migan Dubois, D. Diallo, W. Uddin, M. Nasir, and I. Khan, "Reuse Legacy to Repower the Microgrids–An Affordable Solution for Test and Restoration of Repurposed Lead Acid Batteries," in Proc. *of IEEE 2nd International Conference on Smart Power and Internet Energy Systems—SPIES'2020*, Bangkok, Thailand, pp.463-468, Sept. 2020.
DOI: 10.1109/SPIES48661.2020.9243053 (Experimental)

[2] **K. U. Jan**, A. B. Oudot, A. Migan Dubois, and D. Diallo "Experimental Evaluation of the True Remaining Capacity of Legacy Lead-Acid Batteries," in Proc. *icSmartGrids2021*, Portugal, pp. 92-96, June 30, 2021.
DOI: 10.1109/icSmartGrid52357.2021.9551263 (Experimental), (Best paper award)

[3] **K. U. Jan**, A. Migan Dubois, D. Diallo "Hybrid Battery-SC and Battery-Battery Multistage Design and Energy Management for Power Sharing," in Proc. *IEEE IES 47th IECON*, Toronto, Canada, Oct. 2021.
DOI: 10.1109/IECON48115.2021.9589603 (Simulations)

2. French National Conferences with Proceedings

[1] **K. U. Jan,** A. Migan Dubois, D. Diallo, F. Ossart, E. Laboué, A. N. Christine, J. Badosa, and V. Bourdin, "Hybridization of Renewable and Non-Renewable Sources for Low Cost Rural Electrification," in Proc. *Journées Nationales du PhotoVoltaïque (JNPV'2019) poster*, 3rd-6th Dec. 2019, Dourdan, France. (Poster)
https://jnpv2019.geeps.centralesupelec.fr/archives/09-fiabilite_systemes_reseaux_cpv/KUJ-GeePs-Poster_Photovoltaic_Microgrid_System_level-Khadim_Ullah_Jan_GeePs_UMR8507.pdf

[2] **K. U. Jan,** A. Migan Dubois, D. Diallo, F. Ossart, E. Laboure, J. Badosa, and V. Bourdin, "Model-based Approach to Test and Validate the Performance of an Islanded Photovoltaic Plant using Simscape Power Systems," in Proc. *Journées Nationales du PhotoVoltaïque (JNPV'2020)*, 25th-28th Jan. 2021, Dourdan, France. (Poster)
https://jnpv2020.geeps.centralesupelec.fr/archives/09-fiabilite_systemes_reseaux_cpv/JNPV_Abstract-KHADIM_Poster-Khadim_Ullah_Jan_GeePs.pdf

[3] **K. U. Jan,** A. B. Oudot, A. M. Dubois, and Demba Diallo, "Modeling and Analysis of the Impact of Second-life Components on PV-Battery-Diesel Microgrids," in Proc. *Journées Nationales du PhotoVoltaïque (JNPV'2021)*, 30th Nov -3rd Dec. 2021, Dourdan, France. (Poster) https://jnpv2021.geeps.centralesupelec.fr/archives/10-aspects_industriels/JNPV_21_Abstract-KHADIM-Poster-Khadim_Ullah_Jan_GeePs.pdf

3. Ph.D. Topic Presentations

[1] **K. U. Jan**, A. Migan Dubois, and D. Diallo, "Tuning Microgrid Components Simulation Models with Real Parameters and their Energy Management," presented on July 7, 2021 in the *Summer School Energy for Climate, E4C'2021*, Inst. Polytechnique de Paris, France.

[2] **K. U. Jan**, A. Migan Dubois, and D. Diallo, "Energy Management of the Decommissioned Vehicle Batteries in Low-power Rural Microgrids," in *International Conference on Mobility Challenges***,** CentraleSupélec (Université Paris Saclay), December 9-10, 2021 (online).

[3] **Journée annuelle Des Doctorants (JDD) GeePs CentraleSupelec,**

- **JDD'20** (Présentation, 4 novembre 2020, online mode); and
- **JDD'21** (Poster, 1 juillet 2021, Amphi-Jannet CentraleSupelec).

[4] **29èmee Colloque Alain Bouyssy** at HBAR building 625, Orsay, December 16, 2021 (Poster).

[5] **K. U. Jan,** "Rencontre Doctorants-entreprises", *ThinkSmartGrids* 2022, (180 seconds pitch presentation of the Ph.D. thesis and its extensions to a large energy community), March 25, 2022.

4. Best Paper Award

[1] **K. U. Jan**, A. B. Oudot, A. M. Dubois, and D. Diallo, "Experimental Evaluation of the True Remaining Capacity of Legacy Lead-Acid Batteries," *icSmartGrid2021*, June 30 2021, Portugal.

5. Technical Program Committee Member (International)

- 1) IEEE SPIES'2020, Bangkok, Thailand, 2) SPIES'21, Shanghai, China, 3) IEEE SPIES'22, Beijing, China, 4) IEEE SPIES'2023, Shenyang, China;
- IECC'23, Osaka, Japan;
- CEEGE 2021 Green Energy Conference, Munich, Germany;
- ICCGE'23, Xiamen, China; and
- PEMD 2022, UK,
- PEMD 2023, Belgium.

6. Session Chair

(1) Session chair: *"Energy storage technology and systems"* 2022 4th International Conference on Smart Power & Internet Energy Systems held in Beijing, China during December 9-12, 2022.
(2) Session chair: *"Advanced Electronics and Control Technology"*, SPIES'2021, Sep 25-28, 2021, China.
(3) Session chair: *"Power System Engineering and Management"*, ICCGE'23, May 25-27, 2023, Xiamen, China.
(4) Volunteered Organizer/ session moderator: IEEE ECCE Europe EPE'2020, Lyon, France.

A-IV Laboratory-level Test and Measurement Equipment

MICROGRID COMPONENTS

DESCRIPTION AND SPECIFICATIONS

Note: We do not, in any way, endorse the products and their specifications or the companies featured herein, nor do they make any claims about the quality of the products or services.

S. No.	Description	Model No.	Specifications
1.	Xtender Power Pro ***Off-grid plug and play compact control cabinet for solar power management.***	AC 3500	**48VDC, PV 3.5kW,** **charge current 50A,** **AC 1-Phase 3.5kW, 230VAC/50Hz** ***Included inside:*** • **Pre-assembled all-in-one control cabinet,** • **Use of Studer Xtender inverter/chargers and Variotrack/VarioString MPPT chargers/ controllers,** • **Shunt-based battery SoC processor BSP-500** • **Central monitoring and data logging via Studer RCC-03,** • **Standard-compliant fuse and switch components,** • **Well-arranged AC and DC input/output terminals.**
2.	Xtender Inverter/ Charger ***Equipped with a transfer relay bypass function for the grid, capability of remote monitoring and control using RCC-02.***	XTM-4000-48	**0-50Adc charge current,** **3.5kVA at 40°C,** **10.5kVA surge power capacity,** **UPS switching time<15ms.**
3.	VarioTrack MPPT Solar Charge Controller ***Configurable, suitable for a hybrid system with PV and DG, control and adjust the battery parameters for better energy management.***	VT-65	**48V, 5000W, 80Adc** **PV capacities up to 5kWp, 80A charge current capacity, self-consumption < 1W.**
4.	RCC02 Remote Controller ***For on-site or remote parameter setting, data logging, equipped with an SD card for parameter recording and pre-setting. It can be used to adopt and supervise the system according to the need.***	RCC-02	**Digital display, wall-mounted, SD card support for parameter settings.**

S. No.	Description	Model No.	Specifications
5.	Battery Status Processor ***Measures the battery state of charge SoC using highly efficient algorithms.***	BSP-1200 Studer	**In combination with RCC-02 it can feed values to RCC-02 such as voltage, temperature, current, and SoC.**
6.	Data Logger and Communication Module ***Interface for SCADA control and supervision using PC, can read all the on-site data remotely.***	Xcom-232i	**Electrical interface RS-232 serial port with PC for long-distance, communication with RCC-02 using a 2m cable.**
7.	NPort Serial Device Server ***Used for serial devices in network-ready mode.***	5110-A	**RS-232 serial device server, DB-9 male, RJ45 Ethernet interface, 48V.**
8.	Modular Solar Array Simulator Mainframe ***Accept parameters V_{mp}, I_{mp}, V_{oc}, I_{sc} to provide I-V operating curve of the solar panel for different temperatures and age. Act as a DC current source, a built-in web server for remote access.***	E4360A	**1200W@220VAC, 600W@110VAC 2x600W E4362A series modules mountable (0-130V, 0-5A DC, 600W each), programmable LAN/USB/GPIB interface, remote voltage sensing, 30 storage tables in volatile memory.**
9.	DC Electronic Load ***Controllable DC load from PC supervisor,*** *source/sink,* ***can also supply power.***	NL1V80C40 H&H	**80V/40A/3200W sink, 80V/-40A/3200W source, rated power 4.4kVA, noise 75dB.**
10.	Electronic Load ***To use as a controllable load (physical mode, external mode, remote access).***	ZS1806	60V/0-150A/1800W RS-232/GPIB/USB Ah/MPP test, four modes (V, I, P, R).
11.	Temperature and Humidity Data Logger	RC-4HC Elitech	Range -30°C~+60°C, accuracy ±1°C, humidity 0~99%RH, resolution 0.1 each, USB, 1600 points max.
12.	Solar Photovoltaic Array ***1.4kWp capacity, Installed at GeePs rooftop.***	Siliken SLK60P6L	235Wp, Vmpp~29.5V_{DC}, Impp~7.97A Vcc~36.9V, Isc~8.47 at 1000W/m^2 25°C.
13.	dSPACE ***Perform test or measurement applications quickly and easily, top connectors ideal for desk use, and easy probes plug-in.***	MicroLabbox 1202/1203	Top panel variant, programmable FPGA 1 GB DRAM 128 MB flash memory 48 bidirectional digital I/O -10V…. +10V input/output.
14.	Supervisor PC ***Realize and optimize the overall energy management by controlling the overall microgrid.***	Dell Precision Tower 3620	RJ45 Ethernet, Windows® 7 Professional, GPIB cable and CAN data bus, SD card, LabVIEW®, HDMI for the Samsung LED screen.

S. No.	Description	Model No.	Specifications
15.	Agilent DC Power Supply ***Single output programmable DC power supply, rack-mountable, lockable control for parameters, can be modeled as a supply source.***	N8741A Agilent	300V/11A/3.3kW, GPIB/LAN/USB 2.0, built-in voltage and current measurements, a built-in web server for remote access.
16.	Electrolytic Capacitor ***To use as a microgrid DC bus.***	BHC Aerovox UK	47000uF/100V_{DC}, aluminum foil.
17.	Power Resistance Load Bank	Metal Deploye, FR	120V_{DC}/60A, 6x3 resistance stack 10A,5A,2A,2A,1A, trolley rack with wheels, moveable.
18.	4-Channel Oscilloscope ***Suitable for measuring the bus voltages.***	MSOX2024A Keysight	4 analog channels, 8-digital channels, integrated digital voltmeter.
19.	Lead Gel Battery Bank ***Eight (08) 6V gelled electrolyte battery band 48V, series system, sealed and maintenance-free.***	HOPPECKE 4 OPzV 6V	48V battery bank, gel electrolyte 2100 cycles at 50% DoD, 2600 at 80%, total capacity 12kWh at C_{10} rate: 250Ah, charging current 20A max.
20.	20kWh Lead-Gel Battery Bank ***Eight batteries in a string.***	Ultracell® UCG 100-12	12V/100Ah/10hrs@C_{10} Gelled electrolyte/maintenance-free VRLA slow discharge, long shelf life 1200/2400 cycles @50%/30% DoD.
21.	Uni-Solar Amorphous Solar Panels ***4kWp capacity flexible PV modules, frameless, peel & stick, unbreakable (no glass), shadow and high heat tolerant, suitable for up to 600Vdc.***	PVL-144	24V/144Wp, Vmpp~33V, Impp~4.34A Voc~46.2, Isc~5.3A, light weight/ flexible, module efficiency~6.67%
22.	Hybrid Inverter/Charger ***multi-power, multi-energy off-grid, hybrid, UPS modes 1-phase.***	WKS 5kVA	230Vac single phase, 5kVA/4000W 48V_{DC}, Peak PVin~145V 3000Wc max. 60A charge current, 80A load current, parallel operation up to 20kVA (4 inverters in parallel)
23.	H&H Electronic Load ***Multi-purpose, multi-mode (constant current, constant power), as a current sink for battery discharge tests, could be used to determine the discharge behavior of batteries.***	ZS-1812	75A/controllable DC load, air-cooled extern mode/CC, analog I/O interface, connected via NI-6009 interface to the supervisor PC
24.	Multifunctional Battery Charger ***CCCV charging profile.***	HTDC 5000	12V/5A, 3 in 1 function, lead batteries charger (for battery type: acid, gelled electrolyte)

A-V Battery Datasheet

Ultracell®
'Quality in Every Language'

TechData

UCG100-12
12V 100Ah (C_{10})
12V 115Ah (C_{100})
Solar Series

VdS
MH 29410
CE 1188
ISO9001 CERTIFIED

2

Image

Terminal Dimensions (mm)

Standard Terminal: F10

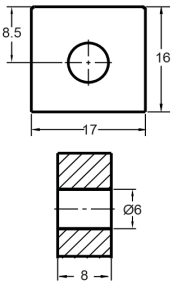

Optional Terminal: F11

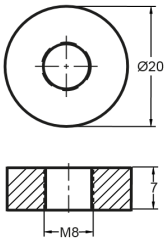

Technical Specification

Output	Nominal Voltage Nominal Capacity (10HR)	12V 100Ah
Terminal Type	Standard Terminal Optional Terminal	F10 F11
Container Material	Standard Option Flame Retardant Option (FR)	ABS ABS (UL94:VO)
Rated Capacity	(100HR 1.80V/cell, 25°C) (20HR 1.80V/cell, 25°C) (10HR 1.80V/cell, 25°C) (5HR 1.75V/cell, 25°C) (3HR 1.75V/cell, 25°C) (1HR 1.60V/cell, 25°C)	115 Ah/1.15A 103 Ah/5.15A 100 Ah/10.0A 85 Ah/17.0A 73.8 Ah/24.6A 59.7 Ah/59.7A
Max Discharge Current	1200A (5s)	
Internal Resistance	Approx 5mΩ	
Discharge Characteristics	Operating Temp Range	Discharge: -15 ~ 50°C Charge: 0 ~ 40°C Storage: -15 ~ 40°C
	Nominal Operating Temp Range	25 ± 3°C
	Cycle Use	Initial Charging Current less then 30A. Voltage 14.4V ~ 15.0V @ 25°C Temp. Coefficient -30mV/°C
	Standby Use	No limit on initial charging current. Voltage 13.5V ~ 13.8V @ 25°C Temp. Coefficient -20mV/°C
	Capacity affected by Temperature	40°C 103% 25°C 100% 0°C 86%
Design Floating Life at 20°C	15 Years	

Self Discharge

Ultracell® UCG batteries may be stored for up to 6 months at 25°C and then a refresh charge is required. For higher temperatures the time intervals will be shorter.

Constant Current Discharge / Constant Power Discharge At 25°C (Amperes & Watts/Cell)

A = Amperes W = Watts

F.V/TIME A W	5 min	10 min	15 min	20 min	30 min	45 min	60 min	2 hours	3 hours	4 hours	5 hours	6 hours	8 hours	10 hours	20 hours
1.85V/cell	161.2 297.0	126.8 235.9	107.8 202.7	90.2 171.2	71.2 136.5	54.1 104.5	44.8 86.8	28.5 55.4	22.1 43.2	18.2 35.7	15.4 30.4	13.5 26.5	11.0 21.7	9.28 18.4	5.00 9.94
1.80V/cell	213.3 389.0	159.6 293.8	128.3 238.3	105.0 196.7	82.0 155.2	61.4 117.7	49.8 96.0	30.9 59.9	23.8 46.2	19.4 37.8	16.6 32.5	14.4 28.4	11.7 23.1	10.0 19.8	5.15 10.2
1.75V/cell	245.4 437.8	179.0 324.0	143.1 262.2	115.3 213.7	87.4 164.0	64.9 123.4	52.7 101.1	32.4 62.6	24.6 47.7	20.0 38.9	17.0 33.2	14.8 29.1	11.9 23.4	10.1 20.0	5.20 10.3
1.70V/cell	273.4 473.5	197.4 348.6	154.5 278.8	122.6 225.2	92.2 171.8	68.2 128.9	55.0 105.0	34.0 65.5	25.5 49.2	20.6 40.0	17.5 34.0	15.2 29.6	12.0 23.7	10.2 20.1	5.30 10.5
1.65V/cell	298.6 508.8	210.9 368.4	162.7 290.7	129.0 234.7	96.6 178.2	70.2 131.7	57.0 108.1	34.9 66.9	26.4 50.9	21.2 41.0	17.9 34.7	15.5 30.2	12.2 24.0	10.3 20.3	5.35 10.6
1.60V/cell	332.0 552.6	230.9 394.1	175.5 308.3	138.5 249.3	102.6 187.8	74.3 138.3	59.7 112.7	36.2 69.0	27.3 52.4	21.7 41.8	18.2 35.2	15.8 30.8	12.4 24.3	10.4 20.6	5.40 10.7

Ultracell®
'Quality in Every Language'

TechData

UCG100-12
12V 100Ah (C_{10})
12V 115Ah (C_{100})
Solar Series

VdS
MH 29410
CE 1188
ISO9001 CERTIFIED

3

Discharge Characteristics

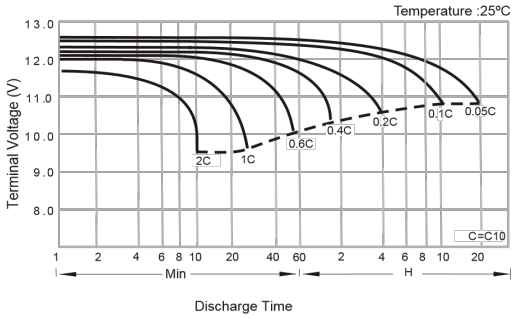

Float Charging Characteristics

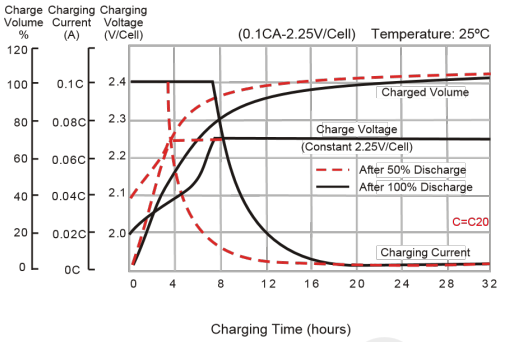

Temperature Effects in Relation to Battery Capacity

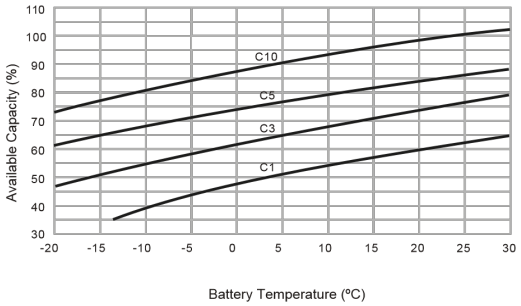

Effect of Temperature on Long Term Float Life

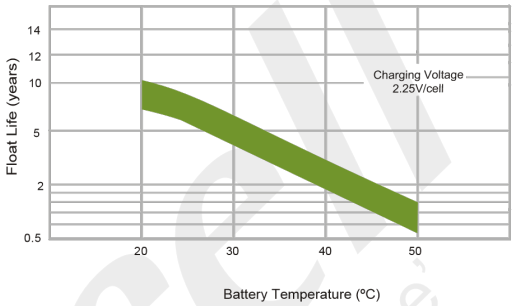

Cycle Life in Relation to Depth of Discharge

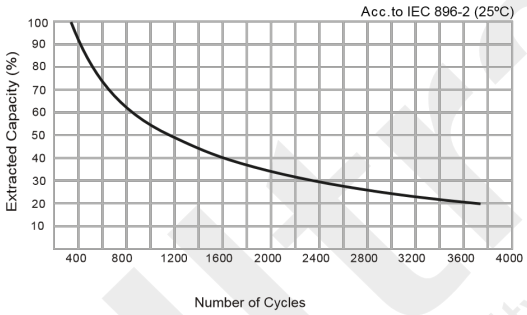

General Relation of Capacity vs. Storage Time

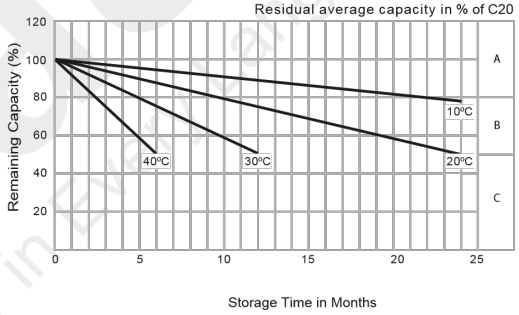

Constant Current Discharge / Constant Power Discharge At 25°C (Amperes & Watts/Cell)

A) No supplementary charge required.
(Carryout supplementary charge before use if 100% capacity is required.)

B) Supplementary charge required before use. Optional charging way as below:
1. Charged for above 3 days at limited current 0.25CA and constant voltage 2.25V/cell.
2. Charged for above 20 hours at limited current 0.25CA and constant voltage 2.25Vcell.
3. Charged for 8 ~ 10 hours at limited current 0.05 CA.

C) Supplementary charge may often fail to recover the capacity.
The battery should never be left standing till this is reached.

Page intentionally left blank

B. Résumé en Français

1. Introduction et Points Forts de la Thèse

i. Introduction générale

Ce projet consiste à proposer un micro-réseau rural à faible coût en utilisant des équipements existants. Cette thèse propose une méthodologie en trois étapes pour modéliser, optimiser, et analyser l'intégration abordable de batteries hors d'usage dans un micro-réseau rural à courant continu (CC). Un micro-réseau PV-diesel-batterie plus adapté aux conditions locales du Burkina Faso est proposé pour tester la viabilité technique et économique de notre hypothèse de deuxième vie. La température et l'irradiation sont des données réelles du site, le choix des valeurs numériques, les limites des contraintes et les hypothèses sont justifiées de manière appropriée pour cette étude.

Les objectifs de l'étude sont atteints grâce à une approche basée sur des mesures et des simulations. La partie centrale des expériences porte sur l'analyse paramétrique et le vieillissement des batteries au plomb à l'aide d'un banc d'essai développé au laboratoire. Nous proposons deux tests de batterie pour estimer la capacité restante et le tri dans différents groupes. Nous avons également appliqué une technique modifiée pour récupérer la capacité des batteries en cas de cyclage lourd.

Enfin, deux scénarios du modèle de micro-réseau moyen proposé sont simulés annuellement pour déterminer l'impact net du vieillissement des batteries et des générateurs diesel. Le flux d'énergie est contrôlé à l'aide d'une gestion de l'énergie basée sur des règles en raison de la facilité de sa mise en œuvre dans le contexte rural. Une technique d'optimisation hybride appelée optimisation par essaims de particules - algorithme génétique (PSO-GA hybride) est utilisée pour déterminer le dimensionnement optimal et le meilleur coût annuel.

Le coût nivelé de l'énergie (LCOE) du design final en mode dégradé est de 0,18 $/kWh, soit le même que le tarif domestique au Burkina Faso. Comparé à 0,23 $/kWh dans le cas de base sans dégradation, le LCOE résultant dans le mode dégradé est 23,2% moins cher et respectueux de l'environnement en raison du report du recyclage des batteries. Nous avons également constaté que les batteries dont charge-décharge est inférieure à 60 % peuvent conduire à une exploitation non rentable et moins techniquement viable des batteries dans le micro-réseau. En fin de compte, une conception technico-économique optimale du micro-réseau de seconde vie est alors proposée. Les conditions géographiques et économiques du site d'étude peuvent être utilisées pour appliquer les résultats de la thèse à des communautés similaires en manque d'énergie. La vue d'ensemble de la proposition de projet est décrite ci-dessous dans la **Figure 1**.

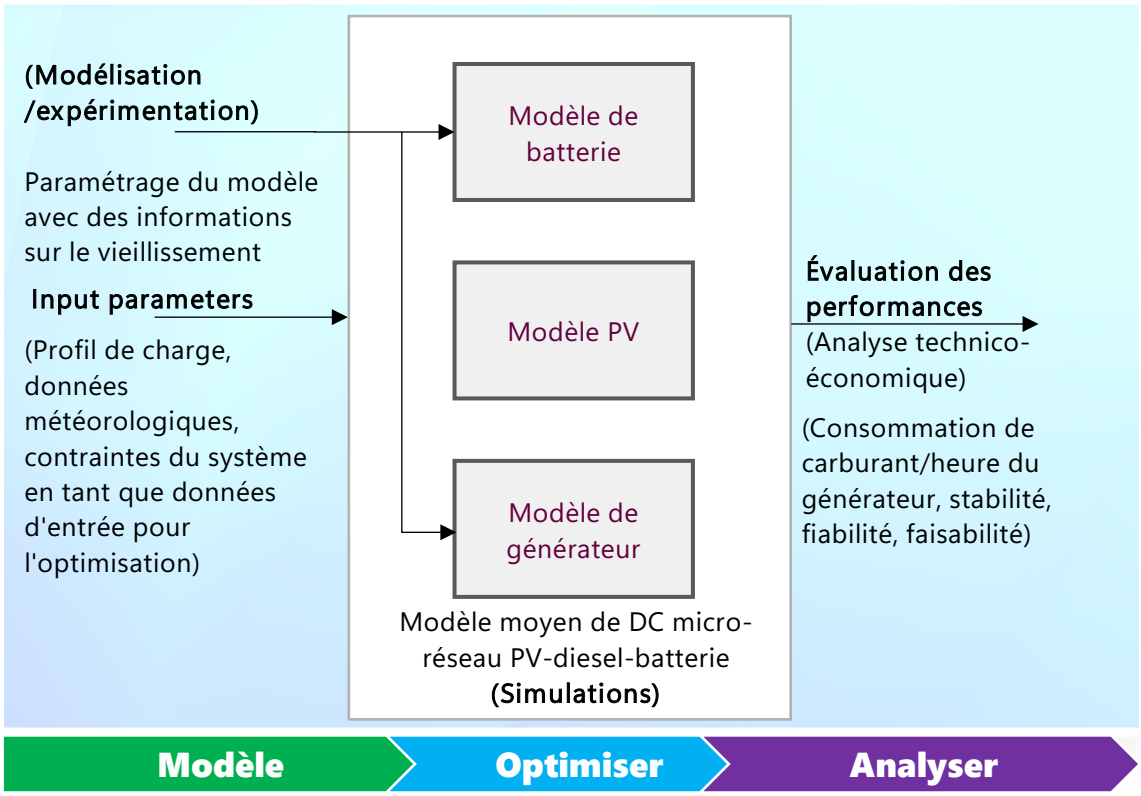

Figure 1: Vision globale du projet

Micro-réseau CC 96V_{DC}/30kW PV-diesel-batterie pour un cas de base rural de 125 ménages de 1100 habitants avec une consommation nette de 500kWh/jour à Gogma, Burkina Faso.

— **Concevoir, optimiser et simuler un micro-réseau CC de 30 kW avec un système PV-diesel-batterie comme scénario de base**[15]

— ***Simuler le système optimal en termes de coûts avec un fonctionnement en mode dégradé de la production décentralisée et des batteries***[16]

— ***Analyser l'impact net sur les performances en mode dégradé***[17]

La motivation de l'étude est de proposer une hypothèse de seconde vie pour la réduction des coûts afin d'augmenter l'acceptation sociale des micro-réseaux ruraux. Le photovoltaïque (PV) est exclu de l'impact de la dégradation car il a une durée de vie considérable par rapport aux anciennes batteries et au générateur diesel (DG). Nous avons supposé que la durée de vie utile du PV était de 20 ans, ce qui correspond également à la durée de vie du projet.

[15] L'analyse des performances annuelles est simulée à un pas de temps d'une heure. Les simulations du cas de base ne présentent aucune dégradation.
[16] L'impact de la dégradation des batteries et de la production décentralisée est pris en compte et le système est optimisé pour obtenir le meilleur coût. La dégradation du PV n'est pas prise en compte.
[17] Analyse technico-économique de la proposition de seconde vie et conclusion sur la faisabilité du projet et ses avantages économiques.

ii. Architecture du micro-réseau

L'architecture présentée à la Figure 1.14 et les spécifications énumérées au Table 1.2 peuvent répondre aux demandes d'énergie allant de la foudre élémentaire et des divertissements aux charges communautaires à petite échelle. Les micro-réseaux à CC à basse tension sont également adaptés à la sécurité et aux courtes distances. L'architecture CC, en **Figure 2**, peut alimenter la plupart des charges CC modernes de manière efficace et à un niveau de tension plus sûr, ce qui est important pour les opérateurs/techniciens locaux inexpérimentés.

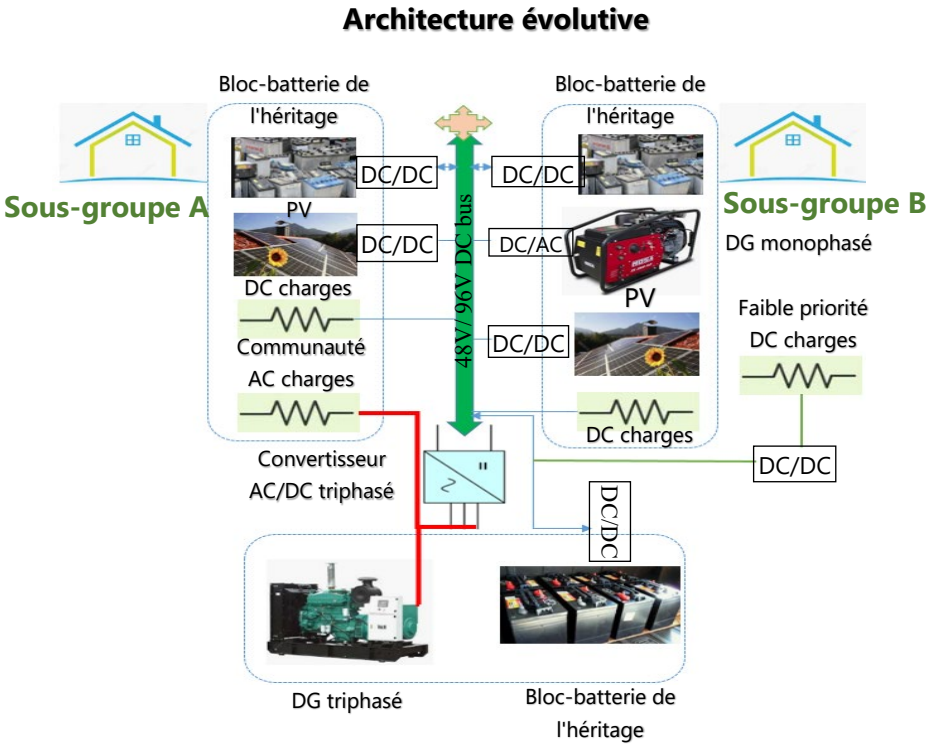

Figure 2: Architecture du micro-réseau

Cette architecture est également un choix économique intéressant car l'équipement existe déjà dans les zones locales sous la forme de petits systèmes solaires domestiques. Dans les services d'électrification à petite échelle, les DG peuvent contribuer à répondre à la demande d'énergie supplémentaire en cas de forte charge ou de conditions météorologiques extrêmes, le coût d'exploitation de ces générateurs pouvant être complété par d'anciennes batteries plomb-acide à moindre coût.

iii. Points forts du manuscrit

Cette thèse se compose de cinq chapitres dans une approche en trois étapes pour modéliser, optimiser et analyser la proposition de seconde vie. Les chapitres passent progressivement de l'introduction du sujet, de la formulation du problème, de l'approche de modélisation, à la gestion de l'énergie et à l'analyse de la dégradation des performances. La première partie de la dissertation est liée au contexte de la

recherche, y compris l'introduction, la définition du problème, les aspects sociaux du projet et quelques propositions. La deuxième partie du manuscrit est plus scientifique et concerne l'approche de la modélisation, les expérimentations, les résultats et les conclusions.

La thèse est organisée de manière à ce que chaque chapitre puisse être lu indépendamment, avec ses propres références bibliographiques, acronymes et points forts des chapitres sur les pages de titre respectives. Nous nous efforçons de traiter dans chaque chapitre les points clés et les problèmes évoqués ci-dessus. Sous une forme plus élaborée, les points saillants des chapitres sont résumés ci-dessous.

— Chapter-I: Introduction and Scope examine en termes simples les raisons de développer des systèmes d'électrification à faible coût. L'examen des principales questions liées à l'accès à l'énergie, accompagné d'une revue bibliographique de l'état de l'art.

— Chapter-II: Rural Microgrid Design Considerations fournit une vision bien pensée de la modélisation électrique et du dimensionnement optimal des composants du micro-réseau (PV, DG, batterie, et charges annuelle). L'architecture de micro-réseau proposée et ses avantages et limites techniques sont présentés.

— Chapter-III: Modeling of the Aging Dynamics porte sur la modélisation de la dynamique de vieillissement des DG et batteries. Des discussions approfondies et des simulations connexes sont incluses pour étayer la validité des modèles utilisés. La partie centrale de ce chapitre couvre les mesures de notre banc de caractérisation des batteries installé en laboratoire.

— Chapter-IV: Control, Energy Management, and Aging Impact Analysis couvre des simulations complètes sur le contrôle d'un modèle moyen d'hybride PV-DG-batterie avec et sans dégradation. En outre, nous analysons et testons la gestion globale de l'énergie et le contrôle dans diverses contraintes opérationnelles, limitations du système et conditions météorologiques.

— Chapter-V: Conclusions and Perspectives résume le cadre de la thèse et propose des extensions possibles pour l'avenir.

iv. Questions de recherche

Les questions de recherche qui motivent cette étude ont des dimensions à la fois techniques et sociales. Seuls les systèmes d'électrification qui peuvent utiliser l'héritage déjà disponible dans les foyers ruraux pour éviter le risque d'obsolescence de l'équipement existant pourraient être un succès technologique. L'idée d'utiliser les anciennes batteries et la production décentralisée est plus convaincante car elles sont déjà utilisées par les systèmes solaires domestiques (SHS) sous l'une ou l'autre forme. Sinon, la participation des consommateurs est relativement plus difficile, ce qui est la

principale cause des échecs des micro-réseaux dans les zones rurales. Cette thèse développe une approche méthodologique pour proposer des batteries patrimoniales et de la production décentralisée pour la réduction des coûts des micro-réseaux sans compromettre un certain niveau de fiabilité de l'approvisionnement. Plus précisément, nous répondons à la question suivante : **"Comment les anciennes batteries au plomb et la production décentralisée peuvent-elles constituer une solution optimale en termes de coûts pour un accès à 100 % de l'énergie dans les zones rurales des pays en développement ? "** Avec une approche approfondie pour répondre à la question principale, nous nous sommes concentrés sur les trois questions connexes en tant qu'objectifs principaux de la thèse.

(1) : " comment faire fonctionner le micro-réseau rural dans les limites physiques des batteries dégradées et de la production décentralisée à un coût optimal ? " ;

(2) : " que pourrait-on compromettre pour une performance dégradée ? " ; et

(3) : " à quelles limites opérationnelles et à quel coût de l'énergie ? ".

Dans la **Figure 3**, Les objectifs de la thèse sont atteints grâce à un processus systématique allant de la modélisation et de l'expérimentation à la simulation de différents scénarios et à la comparaison des résultats obtenus.

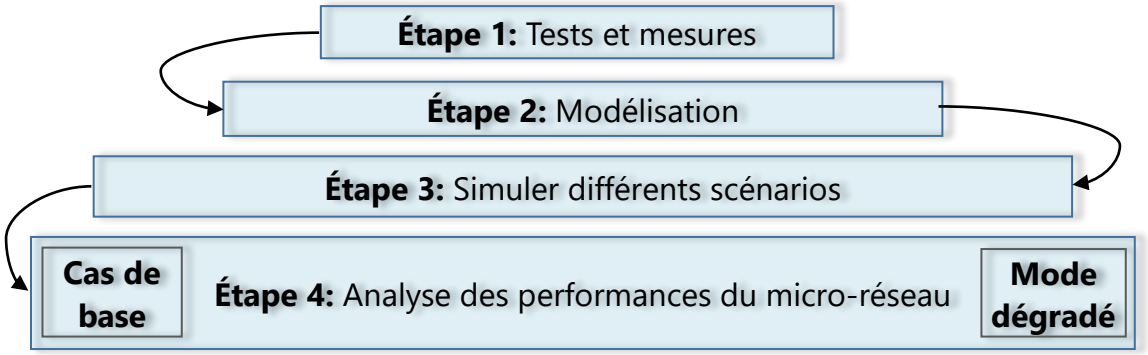

Figure 3: Flux de travail dans la thèse

La Figure 4.65, reproduite ci-dessous comme **Figure 4**, illustre le déroulement systématique de l'ensemble des travaux visant à atteindre les objectifs de l'étude. Le contexte théorique des étapes 2-3 a été couvert dans les Chapter-II and Chapter-III. Dans le Chapter-IV, toutes les étapes mentionnées ci-dessous sont combinées du point de vue de la mise en œuvre pour atteindre les objectifs de la thèse en simulant un modèle de micro-réseau moyen.

2. Contributions de la Thèse

À notre connaissance, l'hypothèse de la seconde vie pour réduire les coûts des micro-réseaux ruraux en utilisant des équipements anciens dont l'historique d'utilisation est inconnu est unique dans sa nature et constitue un sujet d'actualité pour répondre à la double pression du climat et de l'accès à l'énergie. Par conséquent, retarder de le rec-

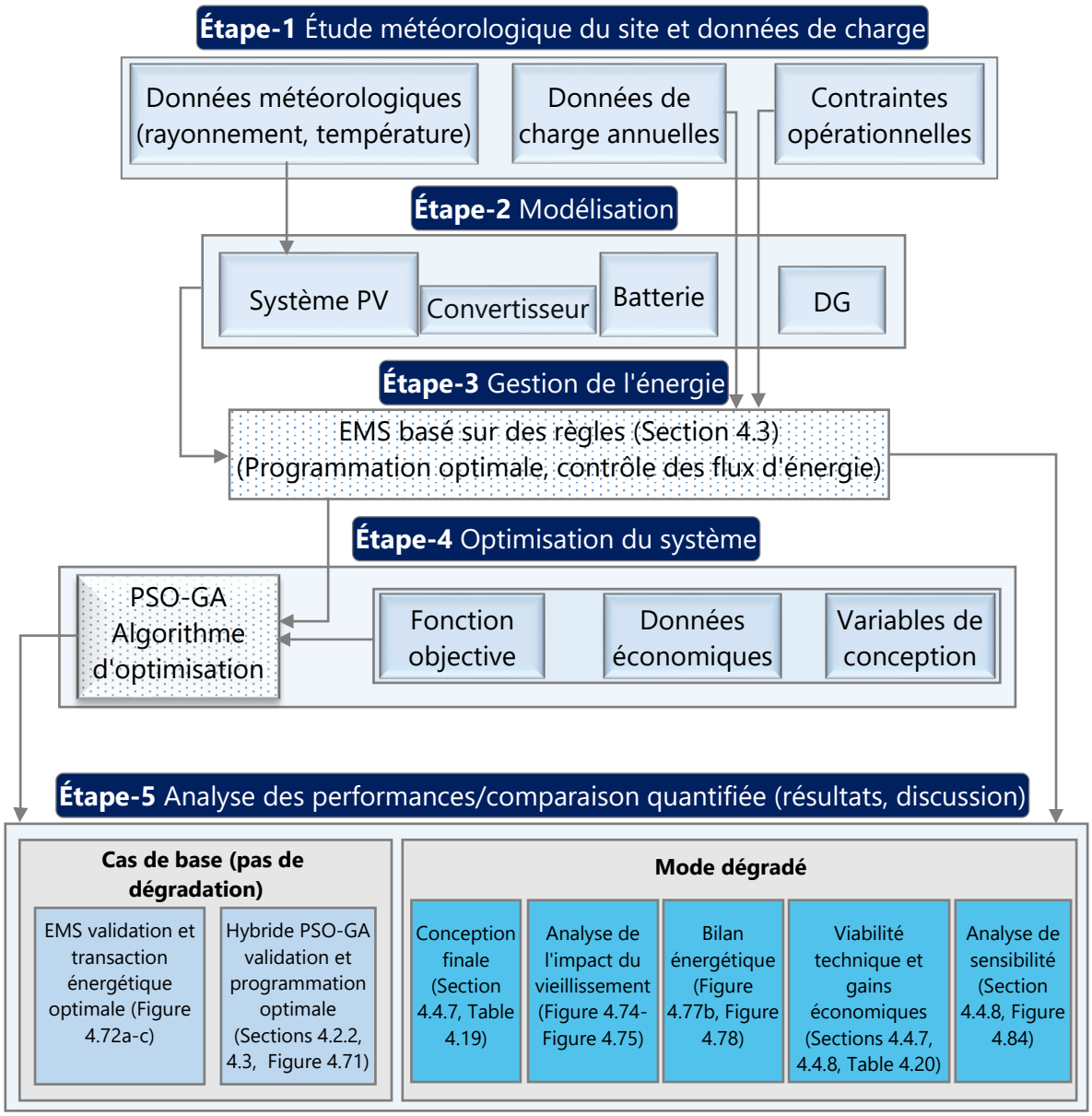

Figure 4: Structure élaborée de l'organisation du thèse et de ses flux

recyclage des batteries et les réutiliser dans des micro-réseaux ruraux de faible puissance est l'une des contributions respectueuses de l'environnement. Les principales contributions de la thèse à l'art existant sont brièvement énumérées comme suit,

- Des tests physiques de batterie modifiés et des méthodes de restauration de la capacité sont proposés ;
- Deux tests de batterie classiques et des techniques de mesure sont proposés pour la caractérisation de batterie et le calcul de la capacité restante réelle ;
- La validation de l'hypothèse de la seconde vie est effectuée en utilisant un schéma de gestion de l'énergie modifié dans un micro-réseau rural PV-DG-batterie ;

- Les gains technico-économiques des batteries de seconde vie sont évalués statistiquement ; et
- La gamme opérationnelle des batteries de seconde vie, en particulier leurs rendements économiques les plus faibles sur les trajets aller-retour, est analysée.

3. Conclusions Générales

Nous avons présenté une vision bien pensée du sujet et du contexte de l'association de notre proposition aux problèmes d'accès à l'énergie dans les pays en développement. L'étude comprend des parties d'expérimentation et de simulation, qui sont conclues comme suit.

i. Conclusions expérimentales,

— **Décharge pulsée (Test 1) :** Ce test est principalement utilisé pour déterminer les dynamiques importantes de la batterie. L'un des avantages de ce test est la possibilité d'extraire les paramètres de la batterie à partir de la réponse dynamique. Ces paramètres peuvent être utilisés pour ajuster les modèles de simulation qui peuvent prédire la performance de n'importe quelle batterie.

— **Décharge échelonnée (Test 2) :** Ce test est principalement utilisé pour (i) calculer la capacité restante totale extraite ($C_{B,e}$) et (ii) valider la caractérisation de la batterie/la réponse expérimentale dans le Test 1. Cette méthode de test précise classe les batteries en différents groupes et fournit la valeur exacte de la capacité utilisable restante.

Voici quelques-unes des principales observations expérimentales réalisées à l'aide de la méthodologie décrite à la Figure 3.44 de la sous-section 3.1.2.1 précédente.

- Les batteries qui refusent d'accepter la charge sont fortement sulfatées ;
- Les chargeurs intelligents ne peuvent pas restaurer les batteries sulfatées, mais les chargeurs traditionnels à base de transformateurs peuvent le faire avec une légère surcharge ;
- Les cristaux d'acide peuvent être décomposés et dissous par un cycle intensif;
- La récupération de la capacité après quatre cycles est négligeable. Le test peut être interrompu et la batterie récupérée est réutilisée ; et
- La variation du temps d'acceptation de la charge à chaque cycle est une bonne indication de la récupération de la batterie.

ii. Conclusions de la simulation,

Nous avons simulé le système pour le site d'étude proposé avec des données météorologiques réelles et une charge annuelle. Les simulations et l'analyse technico-économique correspondante sont effectuées pour une année. Nous avons utilisé une méthodologie en deux étapes pour optimiser et analyser un hybride PV-DG-batterie dans le cas de base et en mode dégradé. Une technique d'optimisation hybride

intelligente appelée algorithme génétique d'optimisation par essaim de particules (PSO-GA hybride) a été utilisée pour déterminer le dimensionnement optimal et le fonctionnement au moindre coût tout en respectant les contraintes physiques. Le système global est optimisé pour le fonctionnement au moindre coût à un certain niveau de fiabilité dans les deux cas. Les simulations sont réalisées à l'aide d'un modèle de micro-réseau CC moyen avec un pas de temps d'une heure pour accélérer l'analyse. La dégradation de la batterie et de la production décentralisée est incorporée chaque trimestre à raison d'une réduction de 2,5 % et de 1,25 % de la capacité agrégée. La durée de vie du micro-réseau est considérée comme celle de la durée de vie du PV, qui est supposée être de 20 ans. Le flux d'énergie au sein du système est contrôlé à l'aide d'une gestion de l'énergie basée sur des règles.

4. Résultats Principaux

Les simulations permettent d'espérer tester en temps réel un micro-réseau rural avec des équipements existants. Nous avons constaté des économies de 23,2 % en utilisant l'équipement existant, un LCOE de 0,18 $/kWh comparé à 0,233 $/kWh dans le cas de base sans dégradation. Nous avons trouvé la limite de la deuxième capacité utile restante en mode dégradé. Ces valeurs vont de 80 % dans leur première vie de retraite à 70 % dans le mode dégradé, c'est-à-dire 10 % supplémentaires de la capacité utilisable restante en utilisant le taux de dégradation supposé de 2,5 % par trimestre. La fraction d'énergie renouvelable (REF) est légèrement améliorée, passant de 89 % dans le cas de base à 93,7 % en mode dégradé, en raison d'une participation moindre de la production décentralisée. Cependant, cela se fait au prix d'une énergie plus de trois fois déficiente dans le système. La réduction de 54 % des heures de fonctionnement de la production décentralisée s'est également traduite par une réduction de 43 % des émissions totales de gaz à effet de serre (GHG).

Le flux d'énergie annuel et les performances de la batterie sont illustrés à la **Figure 5**. On peut noter que les batteries, dans leur état dégradé, sont restées cohérentes avec la charge, ce qui indique que les micro-réseaux de faible puissance sont possibles avec les anciennes batteries. L'analyse *"zoom-in"* des résultats annuels est présentée dans les sous-sections 4.4.1, 4.4.3 pour plus de clarté.

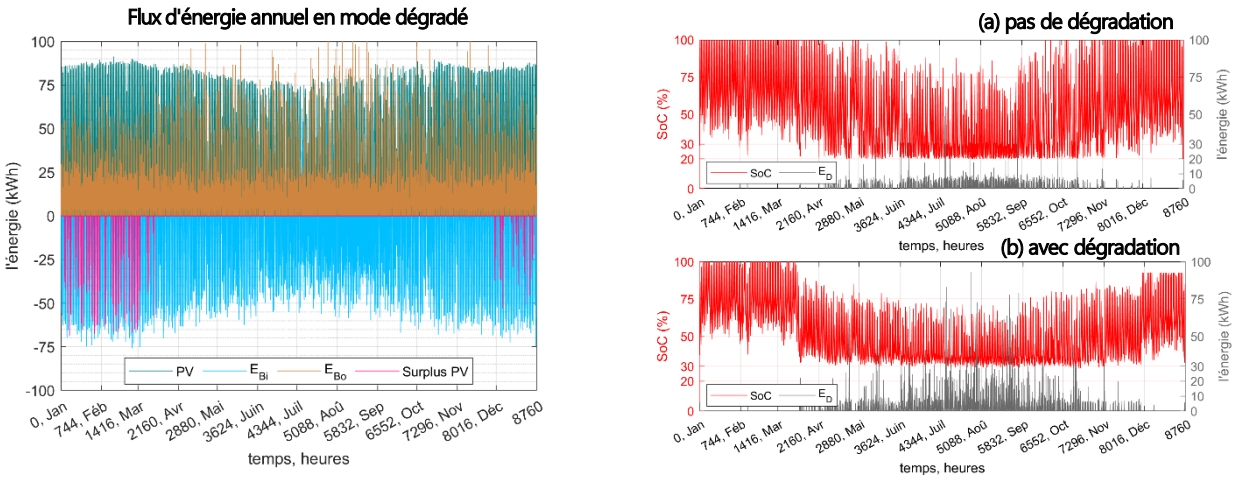

Figure 5: Structure élaborée de l'organisation du thèse et de ses flux

Enfin, l'analyse nous a permis de trouver la limite inférieure de l'efficacité de la batterie en aller-retour au-delà de laquelle il pourrait être plus coûteux et moins pratique d'utiliser des batteries faibles que leurs homologues (**Figure 6**). La conclusion est que les batteries faibles dont l'efficacité aller-retour est inférieure à 60 % sont inutiles.

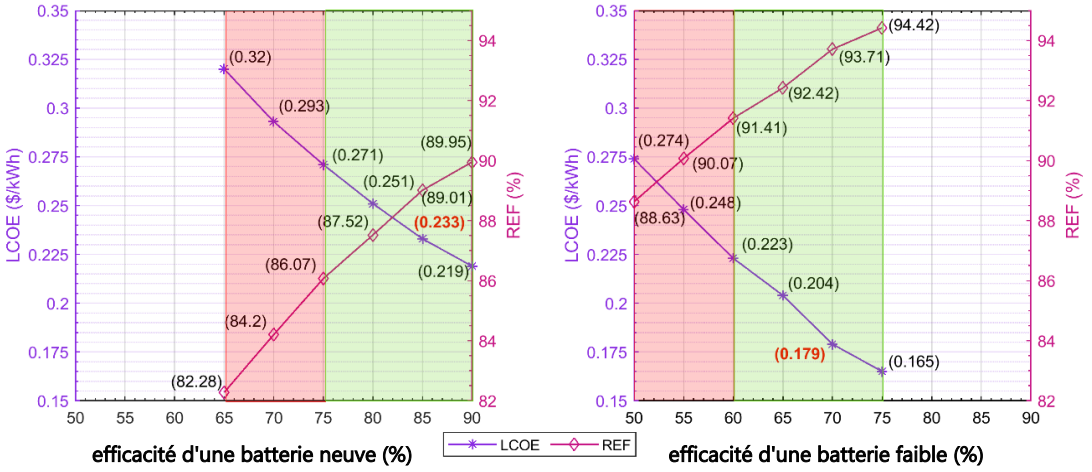

Figure 6: Efficacité d'une batteries neuves et des batteries faibles

5. Travaux Futurs

Le travail présenté dans cette thèse a ouvert de nombreuses questions de recherche. Il n'a pas été possible de répondre à ces parties intéressantes de ce travail en raison de la portée du projet actuel, du calendrier et de l'expertise immédiate du candidat. Les auteurs recommandent aux chercheurs intéressés de poursuivre leurs travaux sur quelques sujets connexes et d'actualité. Certains des aspects prometteurs cités pourraient être utilisés comme une grande proposition. Les bases de la recherche future sont établies dans quatre directions : conception et architecture, modélisation, gestion de l'énergie, et expérimentation.

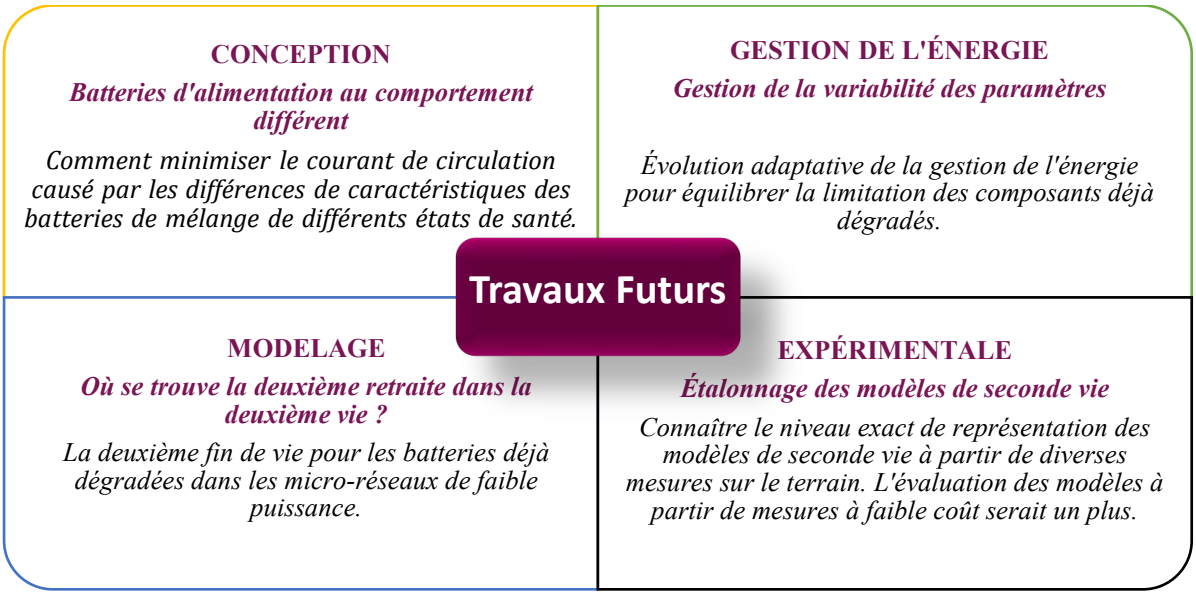

C. Bibliography

All the bibliographic references are appended at the end of the respective chapters. Click below to go to the corresponding sections.

Page intentionally left blank

Analyse de l'impact du vieillissement des composants sur les performances d'un micro-réseau rural à énergie hybride PV-diesel-batterie : modélisation, contrôle et gestion de l'énergie

Mots clés: micro-réseaux ruraux ; batteries de deuxième vie ; système optimal ; gestion de l'énergie ; impact du dégradé ; technico-économique.

Résumé: Les micro-réseaux insulaires, un système de production d'électricité au niveau local, suscitent un intérêt croissant pour électrifier le bas de la pyramide sociale. Cependant, ces systèmes sont financièrement risqués pour les gestionnaires de réseaux en raison de la baisse des revenus. Par conséquent, l'accès à une énergie abordable restera un problème pressant pour plus de 8% de la population mondiale, dont 90% sont des résidents des zones rurales. Cette thèse propose une méthodologie en trois étapes pour modéliser, optimiser et analyser l'intégration abordable de batteries hors d'usage dans un micro-réseau rural à courant continu. Un micro-réseau PV-diesel-batterie plus adapté aux conditions locales du BURKINA FASO est proposé pour tester la viabilité technique et économique de notre hypothèse de deuxième vie.

Les objectifs de l'étude sont atteints grâce à une approche basée sur des mesures et des simulations. La partie centrale des expériences porte sur l'analyse paramétrique et le vieillissement des batteries au plomb à l'aide d'un banc d'essai développé au laboratoire. Nous proposons deux tests de batterie pour estimer la capacité restante et le tri dans différents groupes. Nous avons également appliqué une technique modifiée pour récupérer la capacité des batteries en cas de cyclage lourd.

Enfin, deux scénarios du modèle de micro-réseau moyen proposé sont simulés annuellement pour déterminer l'impact net du vieillissement des batteries et des générateurs diesel. Le flux d'énergie est contrôlé à l'aide d'une gestion de l'énergie basée sur des règles en raison de la facilité de sa mise en œuvre dans le contexte rural. Une technique d'optimisation hybride appelée optimisation par essaims de particules - algorithme génétique (PSO-GA hybride) est utilisée pour déterminer le dimensionnement optimal et le meilleur coût annuel. Le LCOE du design final en mode dégradé est de 0,18 $/kWh, soit le même que le tarif domestique au BURKINA FASO. Comparé à 0,23 $/kWh dans le cas de base sans dégradation, le LCOE résultant dans le mode dégradé est 23,2% moins cher et respectueux de l'environnement en raison du report du recyclage des batteries. Nous avons également constaté que les batteries dont charge-décharge est inférieure à 60 % peuvent conduire à une exploitation non rentable et moins techniquement viable des batteries dans le micro-réseau. En fin de compte, une conception technico-économique optimale du micro-réseau de seconde vie est alors proposée. Les conditions géographiques et économiques du site d'étude peuvent être utilisées pour appliquer les résultats de la thèse à des communautés similaires en manque d'énergie.

Analysis of the performance impact of component aging in a hybrid energy PV-diesel-battery rural microgrid: modeling, control, and energy management

Keywords: rural microgrids, second-life batteries, optimal system, energy management, degradation impact, techno-economic

Abstract: Islanded microgrids, a power generation scheme at the local level, are gaining interest to electrify the bottom of the social pyramid. However, such systems are financially risky for grid managers due to less return on investment. Therefore, affordable energy access will continue to remain a pressing issue for more than 8% of the world's population, of which 90% are residents of rural areas. The thesis proposes a three-step methodology to model, optimize, and analyze the affordable integration of retired batteries in a DC rural microgrid. A PV-diesel-battery microgrid that is more suitable to the local conditions of BURKINA FASO is proposed to test the technical and economic viability of our second-life hypothesis.

The study objectives are achieved based on an approach driven by measurements and simulations. The central portion of the experiments covers the parametric analysis and aging of lead-acid batteries using a test bench developed in the laboratory. We propose two battery tests to estimate remaining capacity and sorting in different groups. We also applied a modified technique to recover battery capacity using heavy cycling.

Finally, two scenarios of the proposed average microgrid model are annually simulated to determine the net aging impact of batteries and diesel generators. The energy flow is controlled using rule-based energy management due to the ease of its implementation in the rural context. A hybrid optimization technique called particle swarm optimization-genetic algorithm (hybrid PSO-GA) is used to determine optimal sizing and best annual cost. The Levelized cost of energy (LCOE) from the final design in the degraded mode is $0.18/kWh, the same as the domestic tariff in BURKINA FASO. Compared to $0.23/kWh in the base case with no degradation, the resulting LCOE in the degraded mode is 23.2% cheaper and environment-friendly due to delaying battery recycling. We also found that batteries below 60% roundtrip efficiencies may lead to an uneconomical and less technically viable battery operation in the microgrid. Ultimately, a techno-economic optimum second-life microgrid design is then proposed. The geographic and economic conditions of the study site can be used to apply the thesis outcomes in similar energy-deprived communities.

Ph.D. is a story full of rising and fall where you're the main character to your depth and soul. The story of perseverance that initially breaks you into pieces at some stage of your studies but later brings you strength, dignity, beauty, and purposeful life.

---***---

ANALYSIS OF THE PERFORMANCE IMPACT OF COMPONENT AGING IN A HYBRID ENERGY PV-DIESEL-BATTERY RURAL MICROGRID: MODELING, CONTROL, AND ENERGY MANAGEMENT

DOCTORAL THESIS

Prepared by

Khadim Ullah Jan

University Paris-Saclay [1]
GeePs Laboratory
11 rue Joliot Curie, 91192, Gif-sur-Yvette,
Paris, France

ORCID

[1]Doctoral school: EOBE nº575
Laboratory: Group of electrical engineering Paris (GeePs),
11 rue Joliot Curie, 91192, Gif sur Yvette, Paris, France.

NNT:2022UPAST184
No. of dissertation pages: (157) of 205

The dissertation is electronically available at the French doctoral thesis database (Access URL: www.theses.fr/s223965)

Maison du Doctorat de l'Université Paris-Saclay
ENS Paris-Saclay
4 Avenue des Sciences, Moulon Plateau
91190 Gif sur Yvette,
Paris, France